HYDROXYCOUMARIN AND AZOBENZENE DERIVATIVES POLYMER COATING AS POTENTIAL PHOTOSWITCHABLE ADDITIVES WITH REVERSIBLE SURFACE POLARITY

SHAMEER BIN HISHAM

FACULTY OF SCIENCE
UNIVERSITI MALAYA
KUALA LUMPUR

2021

HYDROXYCOUMARIN AND AZOBENZENE DERIVATIVES POLYMER COATING AS POTENTIAL PHOTOSWITCHABLE ADDITIVES WITH REVERSIBLE SURFACE POLARITY

SHAMEER BIN HISHAM

THESIS SUBMITTED IN FULFILMENT OF THE REQUIREMENTS FOR THE DEGREE OF DOCTOR OF PHILOSOPHY

**DEPARTMENT OF CHEMISTRY
FACULTY OF SCIENCE
UNIVERSITI MALAYA
KUALA LUMPUR**

2021

HYDROXYCOUMARIN AND AZOBENZENE DERIVATIVES POLYMER COATING AS POTENTIAL PHOTOSWITCHABLE ADDITIVES WITH REVERSIBLE SURFACE POLARITY

ABSTRACT

Long-lasting stickers on various surfaces indicated the successful advancement of adhesive technology. Those stickers when removed often led to residues remaining on walls and surfaces which damaged and caused hideous appearance of surfaces. The main factor to the strong adhesiveness of stickers is the maximum interactions applied between the adhesive and the surface. It is proposed that surfaces with reversible polarity, particularly from the additive component, can cause the surface to gradually reduce the interactions and any stickers can peel off by itself. In this thesis, we described the formulation and the application of poly(methyl methacrylate), PMMA blends containing photoresponsive dyes as smart coatings that were capable of photoreversibly switch surface polarities. The blends contained various hydroxycoumarin dyes (**CAD1-9**), azobenzene derivatives (**AZO1-9**) and an azobenzene end-functionalized PMMA additive (**P1**), which were then applied onto clear glass substrates as coating films. It was shown that **CAD1-7** predominantly exist as hydrazone tautomers and exhibited poor photoreversible *E-/Z-* isomerization performance. Therefore, azobenzene derivatives **AZO1-9** were later applied as additives. Static water contact angle measurements conducted on the PMMA/azobenzene coating films indicated that the surface polarity is photoreversible as the azobenzene molecules undergo reversible *trans-cis* photoisomerization processes. A comparison of the contact angles obtained from PMMA/**AZO1** and PMMA/**AZO2** coating films revealed that the chromophores have random orientation in the coating matrices. Since the surface polarity can be tuned, as a proof of concept experiment, we showed that the commercial acrylic-based pressure-

sensitive stickers which adhered strongly to the PMMA/**AZO1**(13) coating film were peeled off from the coating surface after subjected to a cycle of UV light irradiation for 12 hours, followed by in the dark for another 12 hours within 14 days. This possibly indicated that the repeated changes in surface polarity disrupted the adhesive/coating interactions. In order to increase the adhesion ability of PMMA coating films onto glass substrates, an adhesion promoter, poly(methyl vinyl ether-*alt*-maleic acid monoethyl ester) (PMVEMA-ES) was blended into the coating formulations. The results have clearly indicated that PMVEMA-ES did enhance the adhesion of coating films onto glass substrates at the expense of significantly lowered proportion of *cis*-**AZO1** molecules during *trans→cis* photoisomerization processes. The restricted isomerization of azobenzene chromophores in PMMA/PMVEMA-ES matrix is due to intermolecular N=N···H-OOC hydrogen bonding interactions between PMVEMA-ES and azobenzene chromophores. The crystallization of **AZO2** in PMMA matrix at a concentration beyond 5 wt. % prompted us to synthesize **P1** to overcome the miscibility issues of **AZO2** chromophores in PMMA. It was discovered that thermal annealing of PMMA/**P1**(5) coating film above the glass transition temperature, T_g allowed the segregation of **P1** macromolecules to the surface, resulting in enhanced changes in surface polarity. In addition, the annealed PMMA/**P1**(5) coating film has shown better performance in the sticker peel-off test compared to that of the unannealed coating film. These fundamental discoveries would lead to more development of smart coatings based on simple PMMA/azobenzene blends, where they can be used as a prospective solution to retard problems associated with commercial stickers.

Keywords: Smart coatings; Surface polarity; Azobenzenes; End-functionalized PMMA; Photoisomerization.

SALUTAN POLIMER TERBITAN HIDROKSIKUMARIN DAN AZOBENZENA SEBAGAI ADITIF FOTOPENUKARAN DENGAN KEKUTUBAN PERMUKAAN BOLEH BERBALIK

ABSTRAK

Perekat yang tahan lama di pelbagai permukaan menunjukkan perkembangan teknologi perekat. Perekat tersebut apabila ditanggalkan sering meninggalkan sisa-sisa di dinding dan permukaan menyebabkan permukaan tersebut rosak dan kelihatan hodoh. Faktor utama daya tahan perekat yang kuat adalah interaksi maksimum yang berlaku di antara perekat dan permukaan. Jika ada permukaan dengan kekutuban berbalik, terutamanya dari komponen aditif, maka ia dapat menyebabkan pengurangan interaksi di antara perekat dan permukaan secara beransur dan perekat pun dapat tertanggal dengan sendirinya. Dalam tesis ini, kami menerangkan perumusan dan penerapan salutan pintar fotoresponsif berdasarkan poli(metil metakrilat) (PMMA) yang mampu menukar kekutuban permukaan secara berbalik. Campuran tersebut mengandungi pelbagai pewarna hidroksikumarin (**CAD1-9**), terbitan azobenzena (**AZO1-9**) dan aditif PMMA berfungsi akhir yang mengandungi moieti azobenzena (**P1**), yang kemudiannya digunakan sebagai salutan pada substrat kaca jernih. Telah ditunjukkan bahawa **CAD1-7** wujud sebagai tautomer hidrazon serta menunjukkan prestasi tidak memberangsangkan untuk proses pengisomeran fotoberbalik *E-*/*Z-*. Oleh itu, terbitan azobenzena **AZO1-9** kemudian digunakan sebagai bahan tambahan. Pengukuran sudut sentuhan air statik yang dilakukan pada salutan PMMA/azobenzena menunjukkan bahawa kekutuban permukaan boleh berbalik kerana molekul azobenzena mengalami fotopengisomeran *trans-cis* berbalik. Perbandingan sudut sentuhan yang diperoleh daripada salutan PMMA/**AZO1** dan PMMA/**AZO2** menunjukkan bahawa kromofor mempunyai orientasi rawak dalam matriks salutan. Oleh sebab kekutuban permukaan boleh ditala, sebagai eksperimen

pembuktian konsep, kami menunjukkan bahawa perekat peka tekanan komersial berasaskan akrilik yang melekat kuat pada lapisan salutan PMMA/**AZO1**(13) tertanggal daripada permukaan lapisan setelah dikenakan kitaran sinaran cahaya UV selama 12 jam, diikuti dengan kegelapan selama 12 jam lagi dalam masa 14 hari. Ini mungkin menunjukkan bahawa perubahan berulang dalam kekutuban permukaan mengganggu interaksi perekat/salutan. Untuk meningkatkan keupayaan lekatan salutan PMMA ke substrat kaca, penggalak lekatan, poli(metil vinil eter-*alt*-asid maleik ester monoetil) (PMVEMA-ES) dicampurkan ke dalam formulasi salutan. Hasilnya jelas menunjukkan bahawa PMVEMA-ES dapat meningkatkan lekatan salutan atas substrat kaca akan tetapi menunjukkan pengurangan signifikan perkadaran molekul *cis*-**AZO1** semasa proses fotopengisomeran *trans→cis*. Pengisomeran terhad kromofor azobenzena dalam matriks PMMA/PMVEMA-ES disebabkan oleh interaksi ikatan hidrogen intermolekul N=N···H-OOC di antara PMVEMA-ES dan kromofor azobenzena. Penghabluran **AZO2** dalam matriks PMMA pada kepekatan melebihi lima peratus berat mendorong kami untuk mensintesiskan **P1** untuk mengatasi masalah keserasian beberapa pewarna dalam PMMA. Diketahui bahawa penyepuhlindapan termal salutan PMMA/**P1**(5) melebihi suhu peralihan kaca, T_g menyebabkan pengasingan aditif **P1** ke permukaan, mengakibatkan peningkatan dalam perubahan kekutuban permukaan. Sebagai tambahan, pelapis PMMA/**P1**(5) yang tersepuh lindap menunjukkan prestasi yang lebih baik dalam ujian penanggalan perekat berbanding dengan lapisan yang tidak tersepuh lindap. Penemuan asas ini akan membawa kepada pengembangan lebih banyak salutan pintar berasaskan campuran PMMA/azobenzena, di mana ia dapat digunakan sebagai penyelesaian prospektif untuk menyelesaikan masalah yang berkaitan dengan perekat komersial.

Kata kunci: Salutan pintar; Kekutuban permukaan; Azobenzena; PMMA berfungsi akhir; Fotopengisomeran.

In loving memory of Ayah,
Hisham bin Abdullah
(July 15th 1954 – July 5th 2020)

ACKNOWLEDGEMENTS

TABLE OF CONTENTS

LIST OF FIGURES

LIST OF SCHEMES

LIST OF SYMBOLS AND ABBREVIATIONS

%	:	Percentage
&	:	Ampersand
=	:	Equals
>	:	More than
$\geq$	:	More than or equals to
<	:	Less than
μ	:	Micro
δ	:	Chemical shift
θ	:	Contact angle
λ_{max}	:	Maximum absorption wavelength
o	:	Degrees
^{o}C	:	Degrees Celsius
^{13}C NMR	:	Carbon Nuclear Magnetic Resonance
^{19}F NMR	:	Fluorine Nuclear Magnetic Resonance
^{1}H NMR	:	Proton Nuclear Magnetic Resonance
4-HC	:	4-hydroxycoumarin
Å	:	Angstrom
a. u.	:	Arbitrary units
AcOH	:	Acetic acid
ATR	:	Attenuated Total Reflectance
ATRP	:	Atom transfer radical polymerization
b	:	Broad peak
$CaCl_2$	:	Calcium chloride
CaH_2	:	Calcium hydride

CDCl$_3$	:	Deuterochloroform
CHCl$_3$	:	Chloroform
cm	:	Centimeter
CuAAC	:	Copper-catalyzed Azide Alkyne Cycloaddition
CuBr	:	Copper(I) bromide
D	:	Debye
d	:	Doublet
DCM	:	Dichloromethane
dd	:	Doublet of doublets
DME	:	1,2-dimethoxyethane
DMF	:	*N,N*-dimethylformamide
DMSO-*d$_6$*	:	Deuterated dimethyl sulfoxide
DPE	:	1,1-diphenylethylene
DPHLi	:	Diphenylhexyllithium
dq	:	Doublet of quartets
DSC	:	Differential scanning calorimetry
DSP	:	Dendrimer-like star-branched polymer
dt	:	Doublet of triplets
DTG	:	Derivative thermogravimetry
eq	:	Equivalent
EtOAc	:	Ethyl acetate
EtOH	:	Ethanol
FTIR	:	Fourier Transform Infrared
g	:	Gram
GPC	:	Gel permeation chromatography
GU	:	Gloss unit

h	:	Hour
H_2SO_4	:	Sulfuric acid
HCl	:	Hydrochloric acid
J	:	Coupling constant
J	:	Joule
K	:	Kelvin
K_2CO_3	:	Potassium carbonate
kJ	:	Kilojoule
KOH	:	Potassium hydroxide
LB	:	Langmuir-Blodgett
LiCl	:	Lithium chloride
$LiClO_4$	:	Lithium perchlorate
LiOPh	:	Lithium phenoxide
M	:	Molarity
m	:	Multiplet
MeI	:	Iodomethane
MeOH	:	Methanol
mg	:	Milligram
MHz	:	Megahertz
min	:	Minute
mL	:	Milliliter
MMA	:	Methyl methacrylate
mmol	:	Millimoles
M_n	:	Number-average molecular weight
mol	:	Moles
mp	:	Melting point

M_w	:	Molecular weight
MWD	:	Molecular weight distribution
NaCl	:	Sodium chloride
$NaNO_2$	:	Sodium nitrite
NaOH	:	Sodium hydroxide
n-BuLi	:	*n*-butyllithium
nm	:	nanometer
P(tBMA)	:	Poly(*tert*-butyl methacrylate)
PBd	:	Polybutadiene
PDI	:	Polydispersity index
PDMS	:	Poly(dimethylsiloxane)
PE	:	Polyethylene
PEO	:	Poly(ethylene oxide)
PLA	:	Poly(lactic acid)
PMMA	:	Poly(methyl methacrylate)
PMVEMA-ES	:	Poly(methyl vinyl ether-*alt*-maleic acid monoethyl ester)
PPAPE	:	Poly[2-(4-phenylazophenyl)ethyl acrylate-*co*-acrylic acid]
ppm	:	Parts per million
PPO	:	Poly(propylene oxide)
PS	:	Polystyrene
PSS	:	Photostationary state
PVP	:	Poly(*N*-vinylpyrrolidone)
q	:	Quartet
quint	:	Quintet
RAFT	:	Reversible addition-fragmentation transfer
RBS	:	Rutherford backscattering

ROP	:	Ring opening polymerization
s	:	Singlet
SAM	:	Self-assembled monolayer
SEBS	:	Styrene-ethylene-butyrene-styrene
sec	:	Second
SEC	:	Size exclusion chromatography
sec-BuLi	:	*sec*-butyllithium
T	:	Temperature
t	:	Triplet
t-BuLi	:	*tert*-butyllithium
t-BuOK	:	Potassium *tert*-butoxide
t-BuONa	:	Sodium *tert*-butoxide
td	:	Triplet of doublets
T_g	:	Glass transition temperature
TGA	:	Thermogravimetric analysis
THF	:	Tetrahydrofuran
TLC	:	Thin layer chromatography
T_m	:	Melting temperature
T_{max}	:	Maximum degradation temperature
TMEDA	:	*N,N,N',N'*-tetramethylethylenediamine
T_o	:	Onset degradation temperature
UV	:	Ultraviolet
UV-Vis	:	Ultraviolet-Visible
wt. %	:	Weight percentage
XPS	:	X-ray photoelectron spectroscopy

CHAPTER 1: INTRODUCTION

1.1 Research Background

In this era of digital and electronic media, illegal advertisement stickers still exist as a recurring problem, especially in urban areas. Mechanical forces or chemicals are usually employed to remove them from any surfaces. Cleaning or removing these stickers is often expensive and typically cause damage to the surface of substrates, including torn-off coating, contamination of chemicals and by-products such as residual adhesives permanently sticking onto the surfaces. From January to July 2015, Shah Alam City Council (Majlis Bandaraya Shah Alam, MBSA) removed 167,930 of illegal advertisements (Kerajaan Negeri Selangor, 2015). Subsequently in 2017, DBKL spent RM 3 million only to remove illegal advertisement stickers around the city ("Illegal ads an eyesore in Taman Connaught," 2018). Afterwards, DBKL has removed as much as 518,644 illegal advertisements from January to December 2020 (Azni, 2021). Additional costs are also required for applying new protective coatings on the affected surfaces.

Stemming from the necessity of needing a protective smart coating to protect surfaces from recurring problems of illegal advertisement stickers, we described work aimed at producing PMMA/chromophore blends as smart coatings where the chromophores can either be:

(i) Photoresponsive azo dyes (either hydroxycoumarin dyes or azobenzene derivatives) carrying different functional groups where the reversible *E*-/*Z*- and *Z*-/*E*- isomerization processes will bring about the changes in the polarity of coating surface necessary to reduce the adhesiveness of the advertisement sticker or

(ii) Low-molecular weight (M_w) azobenzene end-functionalized poly(methyl methacrylate), PMMA additive prepared *via* living anionic polymerization techniques where the azobenzene moiety will generate the required changes in the coating surface polarity upon *E-/Z-* (*trans→cis*) and *Z-/E-* (*cis→trans*) isomerization processes to alter the sticker/coating interactions.

1.2 Research Motivation and Objectives

Illegal advertisement stickers usually use polymer-based adhesive materials which are suitable to stick onto a wide range of substrates. Mechanical instruments or chemical materials are required when removing these illegal stickers and these processes may cause damage to the substrate surface. It will eventually add up to the additional cost of repairing the substrate surface. As mentioned in **Section 1.1**, millions of Malaysian Ringgit were spent by the city hall only for removing the illegal stickers in Kuala Lumpur.

In this work, the developed smart coatings contained PMMA, poly(methyl vinyl ether-*alt*-maleic acid monoethyl ester) (PMVEMA-ES) as an adhesion promoter and various hydroxycoumarin and azobenzene derivatives. The use of azo dyes in the coating formulations is to alter the adhesiveness of an illegal sticker by altering the sticker/coating interactions upon reversible *E-/Z-* (*trans→cis*) and *Z-/E-* (*cis→trans*) isomerization processes. Moreover, the role of PMVEMA-ES is to improve the adhesiveness of the PMMA-based smart coatings onto polar surfaces such as glass.

Firstly, hydroxycoumarin derivatives **CAD1-9** are used as a potential photoresponsive chromophores for the development of the smart coatings. Then, azobenzene derivatives **AZO1-9** are used instead since **CAD1-7** displayed poor reversible *E-/Z-* and *Z-/E-* isomerization performances. The PMMA/azobenzene coating films permitted us to observe the reversibility of *E-/Z-* (*trans→cis*) and *Z-/E-* (*cis→trans*) isomerization

processes of **AZO1-9** in PMMA media, which then give rise to changes in the surface polarity and thus, reducing the adhesiveness of commercial stickers.

Subsequently, the addition of PMVEMA-ES into the coating formulations is intended to improve the coating adhesion properties onto polar substrates. In addition, the photochemistry of azobenzene derivatives in PMMA/PMVEMA-ES matrices is also investigated. The results are then compared with the coatings without PMVEMA-ES additive.

Finally, an azobenzene end-functionalized PMMA additive, **P1** is used as an additive (**Figure 1.1**). The prepared low-M_w PMMA additive was blended into bulk PMMA coating films where further thermal annealing will drive the segregation of the additive onto the coating surface forward. Again, reversible E-/Z- (*trans→cis*) and Z-/E- (*cis→trans*) isomerization processes of the azobenzene moieties inflicted changes in the surface polarity, thus altering the sticker/coating interactions. Consequently, the ever-changing interactions caused the stickers to peel off from the coating surfaces.
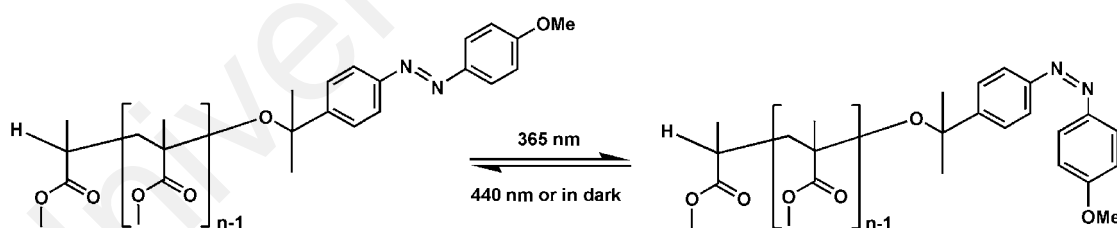
Figure 1.1: Structure of end-functionalized PMMA additive, **P1**.

The main research objective is to develop smart coatings containing photoresponsive azo derivatives that can alter the adhesiveness of stickers by repeated E-/Z- (*trans→cis*) and Z-/E- (*cis→trans*) isomerization processes. The additives will be used as a potential solution to problems associated with illegal advertisement stickers.

The research can then be divided into the following stages:

(1) Synthesizing different azo compounds as well as an azobenzene end-functionalized PMMA additive. The azo units can change their conformation when subjected to UV irradiation, changing the interactions between adhesive and coating.

(2) Characterization of the synthesized dyes and polymer additive.

(3) Investigation of the surface properties of modified coatings before and after UV irradiation.

1.3   Thesis Outline

Chapter 1 highlights some background on the problems caused by illegal advertisement stickers. Furthermore, the research motivation and objectives on solving this recurring issue are emphasized as well.

Chapter 2 firstly illustrates the literature background of photoresponsive smart surfaces and their potential properties. The most commonly used compounds for these types of surfaces are azobenzene derivatives. Hence, some background of photochemistry of azobenzene derivatives are included as well. In addition, the application of azobenzene derivatives in smart surfaces for phototunable surface polarities is also discussed.

Next, recent literature on types of polymer additives, notably end-functionalized polymer additives and their segregation behavior are reviewed. Moreover, their applications for fabricating functionalized surfaces are explored. Synthetic strategies of these types of polymers *via* living anionic polymerization reactions are explored here as well.

Chapter 3 described all experimental procedures concerning with coating formulations, synthesis and characterization of **CAD1-9**, **AZO1-9** and azobenzene end-functionalized PMMA additive, **P1**. In addition, coating preparation and characterization methods are described in detail, which include thermogravimetric analysis (TGA), differential scanning calorimetry (DSC) analysis, static contact angle measurements, gloss measurements and a unique test to examine the peel off behavior of commercial paper stickers on the prepared coating films.

Chapter 4 firstly discusses the results obtained for PMMA coatings containing **CAD1-9**, where **CAD1-7** exhibited azo-hydrazone tautomerism. The tautomerism proved to be unfavorable for our research intentions. Nevertheless, the effect of **CAD1-7** and PMVEMA-ES on the adhesion ability of PMMA coating films onto clear glass substrates is investigated. Upon the undesired results showed by **CAD1-7**, **AZO1-9** were then used as photoresponsive chromophores. The photochemistry of **AZO1** in PMMA and PMMA/PMVEMA-ES matrices is also discussed in detail. Then, the synthesis of azobenzene end-functionalized PMMA additive, **P1** is discussed in detail. The importance of thermally annealed PMMA/**P1** coating films is also highlighted here where a significant improvement in the changes in contact angle measurements is observed.

Finally, **Chapter 5** outlines concluding remarks of the research output with respect to the objectives of this thesis. The Appendices provide supplementary data related to the results and discussion of the conducted experimental work.

CHAPTER 2: LITERATURE REVIEW

2.1 Introduction to Adhesives and Adhesion

An adhesive is defined as a material, when applied to substrate surfaces, can join them together and resist separation (Kinloch, 1980). Adhesion of an adhesive to a surface or substrate is accomplished by means of adsorption of the adhesive to the substrate due to the surface force interactions between the atoms in the two contacting materials (Shaw, 1993). These interactions include Van der Waals interaction, permanent dipoles, hydrogen bonding as well as the additional presence of covalent bonds across the adhesive-adherent interface, enhancing the adhesion properties (Shaw, 1993).

2.2 Wetting Process

Wettability is defined as the ability of a liquid (or adhesive) to wet and spread spontaneously on the substrate (or adherent) surface. Wetting can be quantified in terms of θ, the contact angle a liquid form when placed in contact with a solid surface as shown in **Figure 2.1**:
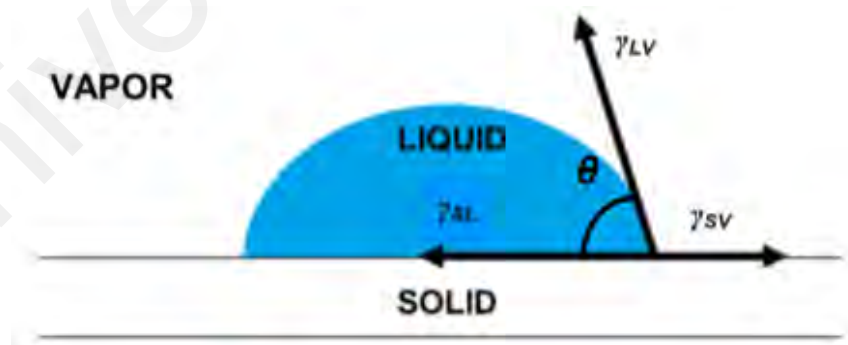
Figure 2.1: An illustration of the contact angle of a liquid on a solid surface.

The relationship between the contact angle and the surface energies of the two contacting materials is shown in equation 1.1, known as Young's equation (Young, 1805):

$$\gamma_{SV} = \gamma_{SL} + \gamma_{LV} \cos\theta \qquad (1.1)$$

Where γ_{SV} = surface free energy of substrate in contact with the vapor of the liquid

γ_{SL} = interfacial free energy

γ_{LV} = liquid surface free energy

From equation 1.1, a liquid will spontaneously spread on a substrate if:

$$\gamma_{SV} \geq \gamma_{SL} + \gamma_{LV} \qquad (1.2)$$

In other words, if the liquid exhibits low surface force energies (e.g. materials made from fluorinated and hydrocarbon-based polymers), the liquid would not be expected to wet and adhere strongly to substrates with high surface free energies (e.g. inorganic materials and metals). Conversely, liquids with high surface energies (e.g. water) will wet and adhere strongly to high surface free energy substrates.

Although metals and metal oxides are considered as materials with high surface energies, factors such as the presence of atmospheric contaminants (e.g. hydrocarbons and moisture) can convert the substrate surface from one of high surface energy to one of low surface energy (Shaw, 1993). The effect of relative humidity on the wettability of mild steel surfaces shown that the presence of atmospheric moisture was sufficient to cause a dramatic reduction in surface free energy of steel (Gledhill et al., 1977). So, the ability of the surface to allow wetting by an adhesive would depend upon the relative humidity prevalent at the time of bonding. Moreover, surface roughness can also strongly influence the contact angle values (Creton & Papon, 2003; Wenzel, 1936).

To summarize, factors affecting wetting include the chemical structure and composition (i.e. the number of interactions between contacting fluid and substrate), substrate surface properties (i.e. the roughness of substrate surface), coating thickness, mechanical properties and stresses, temperature and humidity (Zvonkina, 2016).

2.3   Smart Materials and Coatings

The development of a 'smart' material arises to suit many applications in our lives today. A smart material is a material that has the ability to respond to its environment in a timely manner. It can either receive, transmit or process an external stimulus and in response, produces a useful effect that may include a signal that the material is acting upon it. These stimuli such as strain, stress, temperature, pH, electric field, magnetic field, hydrostatic pressure, light, ionic strength, solvent exposure and different types of radiation may act upon it (Rodríguez-Hernández, 2016).

With the progress experienced by smart materials and the successful introduction of nanotechnology, a new class of smart materials has been developed which is called smart coatings. A coating is defined as a thin layer or covering of a substrate (in the form of paints, wallpapers, etc.). Usually, coatings are used for decorative and protection purposes as well as valorizing materials that are coated with them. Paint is a coating that is widely applied on various substrates such as wood, metal, glass, concrete, road pavement, composite fiber, etc. Paints consist of four main elements, which are binders, dyes or pigments, solvents and additives.

Binders are essentially the main component of any coating. Usually made of polymers, binders bind other ingredients together in a coating and form the coating matrix. Furthermore, binders are responsible for coating adhesion on selected substrates. Dyes and pigments provide color to the coating. In addition, dyes and pigments can also act as additives to improve coating properties. Other additives such as adhesion promoters and

plasticizers are usually added as well. Finally, solvents are used to dissolve all other components together into a homogeneous solution. The solvent should reduce binder viscosity and therefore help with the ease of coating applications on any substrates.

Smart coatings developed today may have anti-fouling and self-cleaning properties, be used as adhesives or repellents and have reversible surface polarity. It is the latter property that we would like to exploit in combating vandalism. It is well established that thermoresponsive and photoresponsive materials are used in fabricating these coatings. Since the work here involves photoresponsive coatings, photoresponsive surfaces will be discussed in great detail.

2.3.1 *Photoresponsive Smart Surfaces*

Photoresponsive smart surfaces such as thin films, self-assembled monolayers (SAMs) and Langmuir-Blodgett (LB) films contained unique molecular architectures of chromophore-containing molecules or polymers. A photoresponsive polymer is a polymer containing photoreceptor chromophores which can transfer light energy into a change in the conformation of the polymer (Kumar & Neckers, 1989). The conformational change will produce a significant change in physical and chemical properties of the polymer solutions and solids. Likewise, these changes would also alter the properties of other types of surfaces mentioned earlier. Azobenzenes are the chromophore of choice as photoswitches although spiropyrans and cinnamic acid derivatives are also widely used (Alexander & Shakesheff, 2006; Xia et al., 2009).

2.3.1.1 *Azo Compounds*

Azo compounds are defined as any molecule containing azo moiety (R-N=N-R_1) where R and R_1 could be either aliphatic or aromatic. These are also known as derivatives of diazene (H-N=N-H). The N=N functional group is known as an azo group. Azo

compounds can be categorized into two main groups, which are aryl/aromatic azo compounds and alkyl/aliphatic azo compounds.

Aromatic azo compounds are of great interest today and not only commonly used as dyes and pigments, but also as photoswitchable agents in smart materials. On the other hand, aliphatic azo compounds are less commonly used than their aromatic counterparts. One such example of an aliphatic azo compound is azobisisobutyronitrile (AIBN) which is commonly used as an initiator in radical reactions.

Aromatic azo compounds are molecules containing an azo group with both R and R_1 being aromatic/aryl groups. They are usually stable, crystalline species and brightly colored. Azobenzene is the most widely known aromatic azo compound. These compounds are highly accessible due to their ease of synthesis in addition to a plethora of synthetic routes and methods in obtaining them (Merino, 2011). Azobenzene and its derivatives exist predominantly as the *trans-* isomer. They can undergo photoisomerization upon UV light irradiation to convert to the *cis-* isomers, which have significantly different physical properties (Kumar & Neckers, 1989). The *cis-* isomer will then revert to the more stable *trans-* isomer upon visible light irradiation or with the presence of thermal energy from the surroundings. In other words, the *trans-cis* photoisomerization process of azobenzene is reversible.

The photoisomerization processes not only bring changes in the azobenzene molecular geometry but also its polarity. *trans-*Azobenzene is planar while its *cis-* isomer is non-planar (Bandara & Burdette, 2012). The planarity of *trans-*azobenzene means that there is no molecular dipole present in the molecule. When it isomerizes to the *cis-*configuration, the non-planarity of the molecule now caused a change in its molecular dipole. As a result, the change in its molecular geometry caused the change in

azobenzene's molecular dipole from zero in the *trans-* isomer to about 3.0 D in the *cis-* isomer (Yager & Barrett, 2006).

Studies have shown that azobenzenes have the ability to isomerize in solid matrices such as in polymer films (Alexander & Shakesheff, 2006; Barrett et al., 1995) or when they are included in a polymer chain (Kumar & Neckers, 1989; Stumpel et al., 2014; Sun et al., 2019). It is these properties that make azobenzenes a popular choice of photoswitches.

2.3.1.2 *Photochemistry of Azobenzene Derivatives*

Azobenzene chromophores are widely used in photoresponsive systems owing to their unique ability to photoreversibly isomerize from their thermally stable *trans-* isomers to the metastable *cis-* isomers cleanly and efficiently. Their absorption spectra consist of two bands; a strong absorption band corresponding to $\pi \rightarrow \pi^*$ transition and another weak absorption band corresponding to $n \rightarrow \pi^*$ transition. The $\pi \rightarrow \pi^*$ transition band is located in the UV-A region (~320 nm) (Bandara & Burdette, 2012). Correspondingly, the $n \rightarrow \pi^*$ transition band is located in the blue light region (~440 nm) (Bandara & Burdette, 2012). Absorption of a photon from the UV-A region excites the $\pi \rightarrow \pi^*$ transition band. Consequently, this induces the movement of the phenyl rings about the $-N=N-$ bond, switching the molecules from *trans-* configuration to the *cis-* configuration. The corresponding $\pi \rightarrow \pi^*$ transition band for the *cis-* configuration is then shifted hypsocromically (indicating higher energy transition). In addition, a slightly stronger absorption at the $n \rightarrow \pi^*$ transition band is also observed. The *cis-* isomers can then revert to the more stable *trans-* isomers either thermally or under the irradiation of blue light (Beharry et al., 2011; Dong et al., 2015).

Substituents on either phenyl rings on the azobenzene skeleton greatly affects the ability of azobenzene molecules to isomerize. Azobenzene derivatives can be classified

into three groups according to the thermal isomerization lifetimes of their *cis-* isomers, which are (i) azobenzenes (ABs), (ii) aminoazobenzenes (aABs) and (iii) pseudo-stilbenes (psABs) as shown in **Figure 2.2** (Rau, 1990).
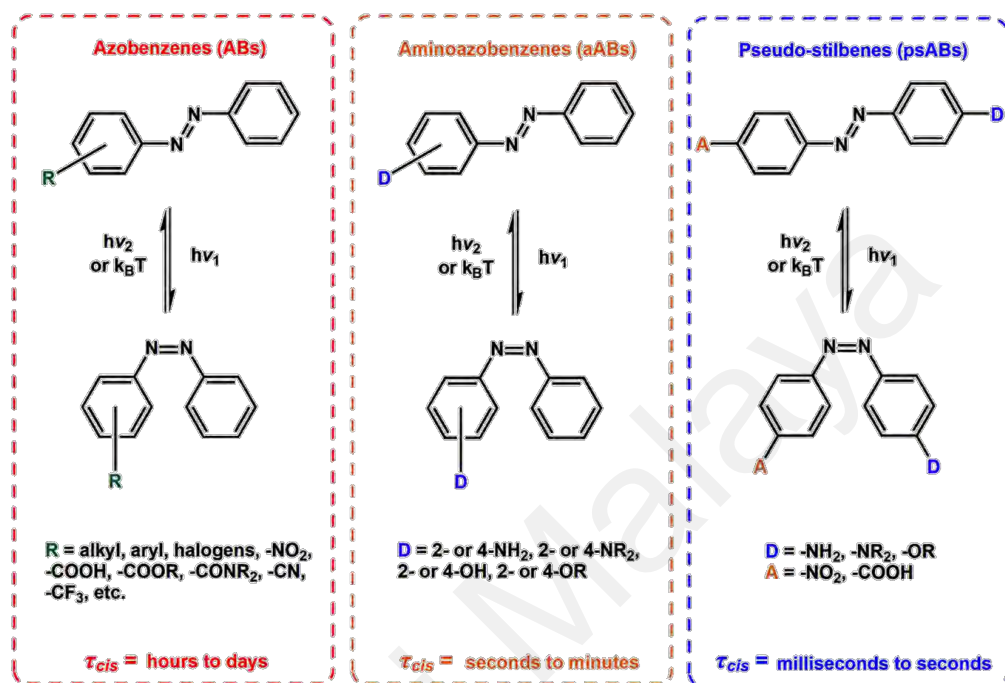
Figure 2.2: Different classes of azobenzene derivatives.

AB class of molecules consists of pure azobenzene and any azobenzene derivatives containing functional groups such as alkyl, halogens, $-NO_2$, $-COOR$, $-CONR_2$, $-CN$, $-CF_3$ and etc (Bandara & Burdette, 2012; Sun et al., 2019). Their *trans-* absorption spectra consist of two distinct bands, a strong absorption band corresponding to $\pi \rightarrow \pi^*$ transition and another weak absorption band corresponding to $n \rightarrow \pi^*$ transition. The $\pi \rightarrow \pi^*$ transition band is located in the UV-A region (about 320 nm). Correspondingly, the $n \rightarrow \pi^*$ transition band is located in the visible light region (about 440 nm). Their *cis-* isomer lifetimes typically ranged from hours to days (Yager & Barrett, 2006).

aABs typically consist of azobenzene derivatives with at least one strong electron-donating group such as $-NH_2$, $-NR_2$, $-OH$ and $-OR$ (Bandara & Burdette, 2012). Their *trans-* $\pi \rightarrow \pi^*$ transition band is shifted bathochromically up to a point where the band

nearly or slightly overlaps with the n→π* transition band (Bandara & Burdette, 2012; Yager & Barrett, 2006). Their *cis*- lifetimes are usually in the order of seconds to minutes (Yager & Barrett, 2006).

A special type of aABs, called hydroxyazobenzenes exhibit markedly different behaviors from other ABs (**Figure 2.3**). In the case of 2-hydroxyazobenzenes (2-hABs), the intramolecular hydrogen bonding between the –OH and azo N=N groups triggers swift thermal isomerization (Bandara & Burdette, 2012). Furthermore, 2-hABs can undergo tautomerization to form the corresponding hydrazone tautomer, which can be initiated by irradiation (Bandara & Burdette, 2012). In the case of 4-hydroxyazobenzenes (4-hABs), they can also undergo tautomerization *via* solvent-assisted proton transfer reactions in polar solvents and in acidic media (Bandara & Burdette, 2012). For compounds exhibiting azo-hydrazone tautomerism, their UV-Visible spectra showed that the π→π* transition band of hydrazone tautomer is typically red-shifted from that of the azo tautomer (Chen et al., 2012; Debnath et al., 2015). Protection of the –OH group by alkylation should make the atypical properties of hydroxyazobenzenes vanish.
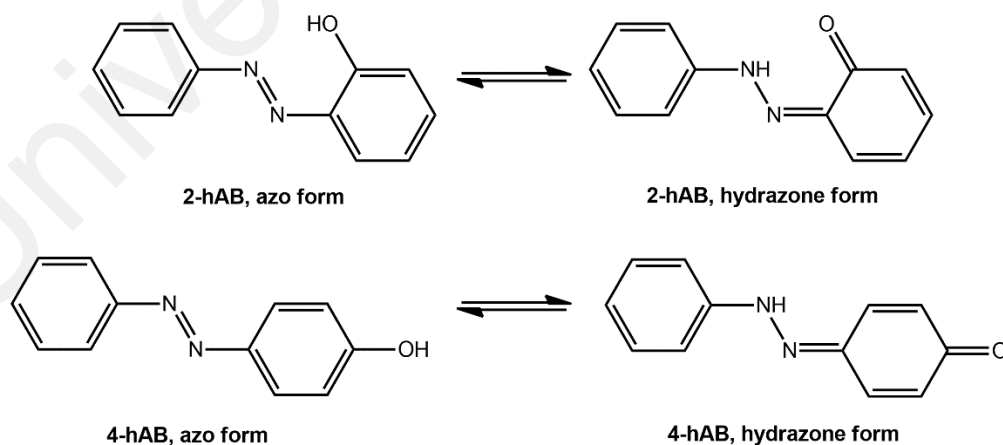
Figure 2.3: Azo-hydrazone tautomerism exhibited by hydroxyazobenzenes.

Push-pull type azobenzenes make up the bulk of psABs. These molecules contain one strong electron-donating group at the 4- position and one strong electron-withdrawing group at the 4'- position of azobenzene (Bandara & Burdette, 2012). These groups cause a substantial increase in the dipole moment of azobenzenes (Bandara & Burdette, 2012). Consequently, their *trans*- $\pi \rightarrow \pi^*$ and $n \rightarrow \pi^*$ transition bands significantly overlap each other, causing the two transitions to become degenerate (Yager & Barrett, 2006). As a result, only one wavelength can be used to trigger both forward and backward photoisomerization processes (Yager & Barrett, 2006). Furthermore, their *cis*- lifetimes are usually very short, ranging from milliseconds to seconds. In other words, they have very fast thermal *cis→trans* isomerization rates (Yager & Barrett, 2006).

2.3.1.3 Azobenzene-Containing Smart Surfaces

There are numerous reports on azobenzene-containing surfaces which showed phototunable properties such as wettability. Usually, azobenzene-containing molecules, macrocycles and polymers are synthesized and formed into thin films or multilayers (Ahmad et al., 2010; Ding & Russell, 2007; Feng et al., 2005; Ge et al., 2006; Huang et al., 2013; Jiang et al., 2005; Lim et al., 2006; Paik et al., 2007; Pan et al., 2015). Some azobenzene derivatives and azo-containing polymers were also formed into Langmuir-Blodgett (LB) films (Feng, Jin, et al., 2001; Feng, Zhang, et al., 2001). However, it was proven that LB films are prone to degradation after a few UV irradiation cycles, thus reducing their efficiency as smart surfaces.

In addition, one of the most commonly used strategies in producing photoresponsive films and surfaces incorporating azobenzene moieties include the fabrication of azobenzene-containing self-assembled monolayers (SAMs). In general, there are two ways to incorporate azobenzene derivatives in SAM fabrication. The first is direct chemisorption/deposition/adsorption of azobenzene-containing adsorbates containing

anchoring groups such as thiols, dithiolates, chlorosilanes, etc. (**Figure 2.4**(a)). Usually, a cleaned or activated substrate is immersed into a solution of the said azobenzene derivative for a period of time until the adsorbates bound onto either Si (Hamelmann et al., 2004; Siewierski et al., 1996), Au (Evans et al., 1998; Han et al., 2011; Han et al., 2010; Tamada et al., 1998) or Pt (Sortino et al., 2004) surfaces. Another way is by *in-situ* reaction of a functionalized SAM containing reactive sites or functional groups such as amino (Pei et al., 2011; Siewierski et al., 1996), iodide (Wen et al., 2005), isocyanate (Delorme et al., 2005), hydride (Min et al., 2010; Zhang et al., 2008), even macrocyclic groups such as calix[4]arene (Oh et al., 2002) and β-cyclodextrin (β-CD) (Nachtigall et al., 2014) with any azobenzene derivative bearing another reactive site. Once the reaction is completed, the azobenzene moiety is covalently attached to the monolayer (**Figure 2.4**(b)).
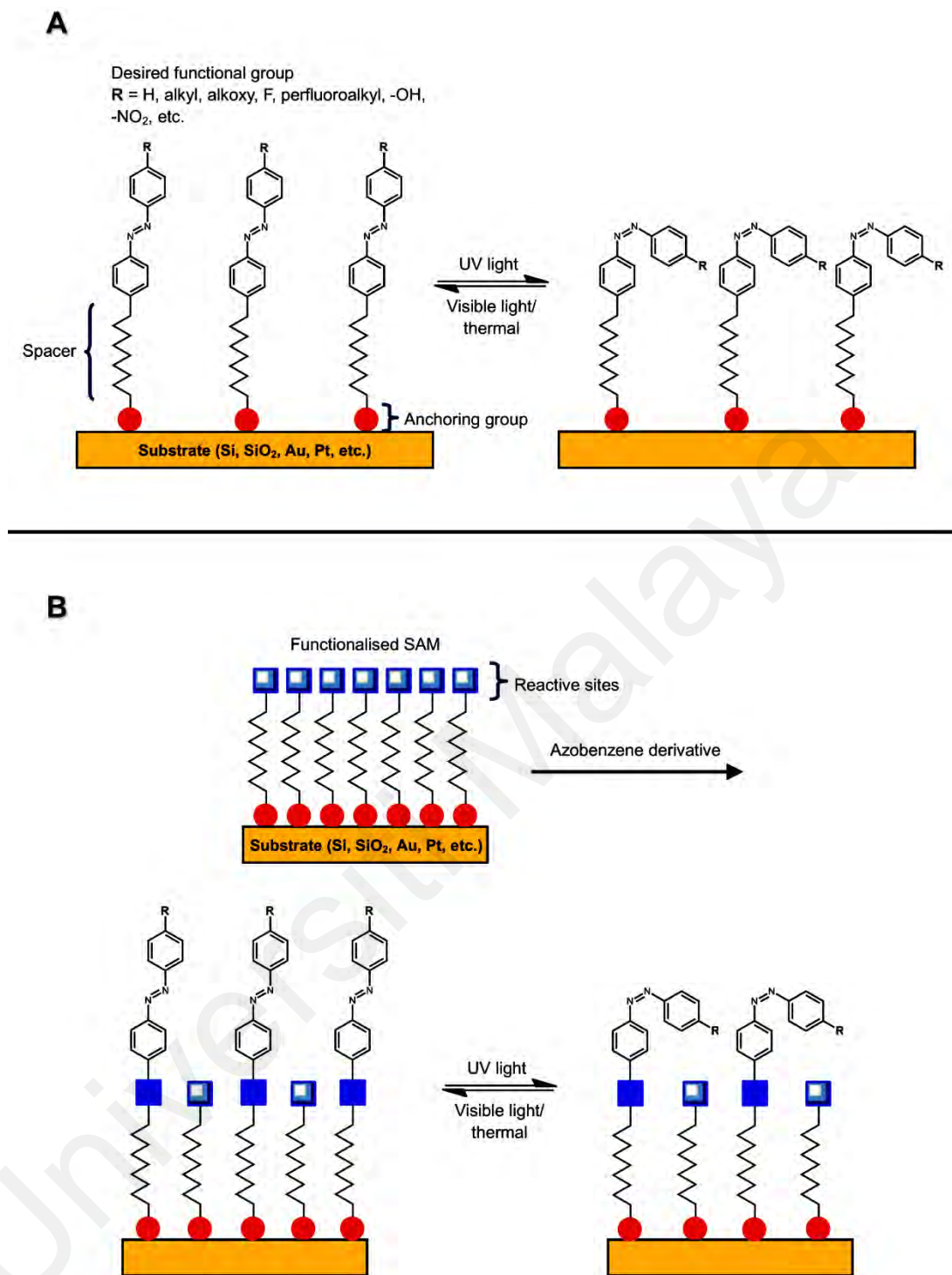
Figure 2.4: Strategies employed to include azobenzene moieties in SAMs (a) direct chemisorption/deposition/adsorption of azobenzene-containing adsorbates and (b) *in-situ* reaction of a functionalized SAM with azobenzene derivatives.

The presence of functional groups in azobenzene-containing surfaces can influence the wettability of surfaces. Azobenzenes bearing non-polar functional groups such as phenyl (Delorme et al., 2005; Evans et al., 1998; Ge et al., 2006; Hamelmann et al., 2004; Huang et al., 2013; Jiang et al., 2005; Min et al., 2010; Oh et al., 2002; Pan et al., 2015; Siewierski

et al., 1996; Sortino et al., 2004), alkyl (Siewierski et al., 1996; Tamada et al., 1998), alkoxy (Evans et al., 1998; Han et al., 2011; Han et al., 2010), tertiary amine (Zhang et al., 2008) or fluorinated (Feng, Jin, et al., 2001; Feng, Zhang, et al., 2001; Lim et al., 2006; Min et al., 2010; Paik et al., 2007) substituents initially showed higher water contact angle values. Subsequently, upon UV light irradiation, the contact angle decreased, indicating the successful conversion to the *cis-* isomer, where the dipole moment is higher than that of the *trans-* isomer. As a result, the surface becomes more polar in *cis-* rich environments. In contrast, polar functional groups such as hydroxyl (Pei et al., 2011), imidazolium (Pei et al., 2011), nitro (Ahmad et al., 2010; Feng et al., 2005; Wen et al., 2005) and polyols (Nachtigall et al., 2014; Pei et al., 2011) showed lower water contact angle values initially. Then, the contact angle increased upon UV light irradiation as a result of the relatively non-polar –N=N− groups getting exposed to the surface.

Surface roughness also showed significant impact on reversible wettability and surface polarity. For example, the changes in water contact angle, $\Delta\theta$ of a poly[2-(4-phenylazophenyl)ethyl acrylate-*co*-acrylic acid], PPAPE polyelectrolyte film on a smooth Si surface was only 1.9° (Jiang et al., 2005). In contrast, it was unraveled that increasing the surface roughness of Si surfaces, the polymer films become superhydrophobic as the contact angle increased drastically in addition to larger $\Delta\theta$ as high as 66° upon UV light irradiation (Jiang et al., 2005). Another example highlighting the importance of surface roughness control is showed using photoresponsive modified poly(allylamines hydrochloride) multilayers containing azobenzene derivatives (Lim et al., 2006). The resulting water contact angle after UV irradiation (364 nm) for a smooth surface decreased by 5° from 76° to 71° and increasing the surface roughness by increasing the deposition cycles caused a significant change in the water contact angle readings where the contact angle changed from 152° to less than 5° (Lim et al., 2006).

Intramolecular hydrogen bonding interactions was shown to be detrimental to the reversibility of *trans-cis* photoisomerization processes of azobenzene-containing polymers (Feng et al., 2005). Thin films of polyaniline derivatives containing photochromic azobenzene moieties, PAPNPAPOA showed irreversible *trans→cis* photoisomerization even after the PAPNPAPOA films were withdrawn from UV light. This is because during UV light irradiation, the azo –N=N− groups are exposed during photoisomerization and thus were able to interact with the amino groups present in PAPNPAPOA through intramolecular N⋯H−N hydrogen bonding interactions (Feng et al., 2005). As a result, the azobenzene moieties are "locked" in place and unable to revert to the *trans-* isomer.

To sum up, many strategies can be used to fabricate azobenzene-containing surfaces, which include preparing polymer thin films, monolayers, multilayers and LB films. The selection of functional groups, surface roughness and the chemical environment of surfaces greatly influenced the performance of azobenzene-containing surfaces. Non-polar groups will cause an increase in water contact angle values whereas polar groups will decrease the water contact angle of surfaces. Subsequently, the rougher the surface, the greater the expected changes in contact angle values upon reversible *trans-cis* isomerization. Finally, the reversible *trans-cis* isomerization of azobenzene derivatives could be drastically impeded by the hydrogen bonding interactions as shown from the work of Feng et al. in 2005. Thus, a careful selection of functional groups, polymers and additives should be kept in mind whenever researchers required to fabricate such coatings and surfaces.

2.4   Polymer Additives in the Modification of Surface Properties

A polymer additive can be defined as any low-molecular weight substance that is added/blended into a bulk polymer matrix in small quantities. Usually, a polymer additive

will improve or enhance the bulk properties of a polymer. Additives can be in the form of dyes and pigments, plasticizers, fire-retardants, stabilizers, fillers, adhesion promoters, fiber reinforcements and etc. Nowadays, the requirement of needing smart polymer surfaces with desired surface properties such as wettability, adhesion, anti-fouling surfaces and many more calls for suitable additives to be added in polymer coatings. A significant advantage of using polymer additives to modify surface properties is cost. It would cost a lot of time and money to synthesize modified polymers compared to those of polymer additives. Polymer additives, due to their relatively lower molecular weights compared to bulk polymers, tend to segregate to the surface, behaving similar to that of micelles in solutions (Hutchings et al., 2011). The principles of polymer segregation are discussed in the next section.

2.4.1   *Principles of Polymer Segregation*

Functional polymers, either block copolymers or end-functionalized polymers, can undergo surface segregation processes. Segregation of functional polymers is favorable if there is a reduction in the surface free energy of the bulk material (Koberstein, 2004). Therefore, if the functional group/moiety has low surface energy, for example, perfluorinated group, then the corresponding functional polymer will segregate to the surface, reducing the overall surface free energy of the bulk material.

Annealing polymer films containing functional polymer additives above their glass transition temperature facilitates the segregation processes (Hardman et al., 2011; Hutchings et al., 2011). Thermal annealing allows the molecules in the film to rearrange. The polymer chains are now mobile and the film is able to reorganize, allowing enhanced surface segregation driven by a reduction in the surface energy (Hardman et al., 2011; Hutchings et al., 2011). Hence, it is preferable to anneal films containing very small

quantities of additive rather than to simply add greater quantities of additive. **Figure 2.5** illustrates the polymer surface segregation process.
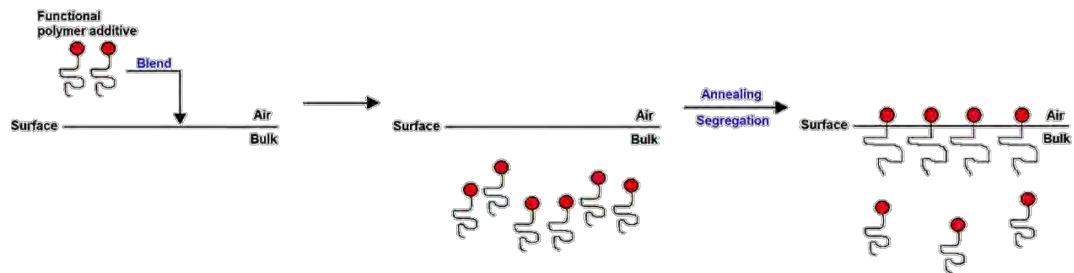
Figure 2.5: Segregation of a functional polymer additive (Hardman et al., 2011; Hutchings et al., 2011).

Fluorinated polymer additives specifically, when present in thin polymer films, behave like micelles in solution and there exists a dynamic equilibrium between free additive chains, molecularly dissolved in bulk phase and aggregates (Hutchings et al., 2011). **Figure 2.6** illustrates this phenomenon:
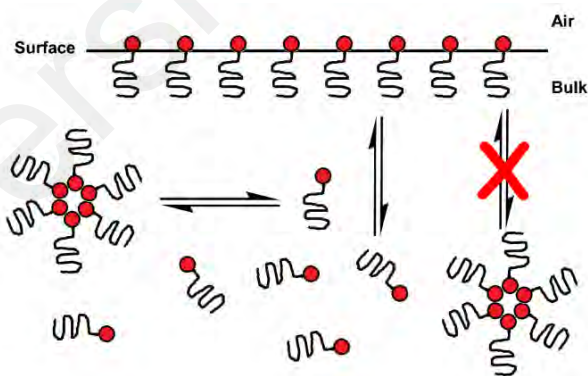
Figure 2.6: Schematic demonstration of dynamic equilibria between free and aggregated additive chains in the bulk and between free additive chains in the bulk and at the surface (Hutchings et al., 2011).

Other factors influencing polymer surface segregation include:

(i)   The surface energy of components (Kurusu & Demarquette, 2017). From

        earlier explanations, segregation is favored if the polymer additive contains a

low surface energy functional group/moiety. The molecular weight of polymer additive (Hardman et al., 2011; Hutchings et al., 2011). Polymer additives with lower molecular weights tend to segregate better compared to additives with higher molecular weights.

(ii)   "Sticking energy" of the functional group to the surface/interface of interest (Ansari et al., 2007), and

(iii)   Mobility of polymer additive (Kurusu & Demarquette, 2017).

2.4.2   *Polymer Additives for Making the Surface More Hydrophobic*

Polymer additives are usually used to make surfaces more hydrophobic. A vast majority of these additives contain perfluorinated groups. In general, the higher the number of perfluorinated groups in an additive, the higher the hydrophobicity of the surface. It can also be said that the higher the additive concentration, the higher the surface hydrophobicity.

Typical tests and characterization of polymer films containing these additives include water contact angle measurement (Hardman et al., 2011; Hutchings et al., 2011), Ion-beam or Rutherford Backscattering (RBS) technique (Hutchings et al., 2011) and X-ray photoelectron spectroscopy (XPS) (Hardman et al., 2011).

As previously explained from the last section, there are two types of functional polymer additives that are used in modifying surface properties, namely, block copolymers and end-functionalized polymers. One example of block copolymer additive exhibiting superhydrophobicity is poly(styrene-*block*-dimethylsiloxane) (PS-*block*-PDMS) (Ma et al., 2005). End-functionalized polymer additives are more robust, with various selections of end capping agents. In addition, various polymerization techniques such as anionic polymerization and ATRP were employed in tailoring these additives.

Desired functional groups were inserted either by a specialized initiator or by termination of the living chain ends with suitable end capping agents. **Table 2.1** shows some of the functional polymer additives used in making the surface more hydrophobic:

Table 2.1: List of some end-functionalized polymer additives for hydrophobic surfaces
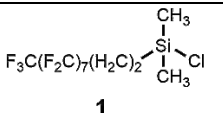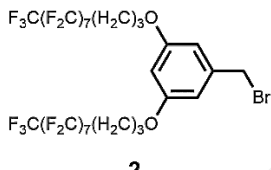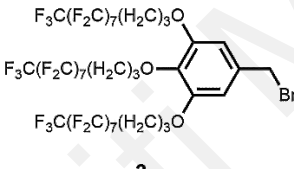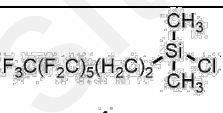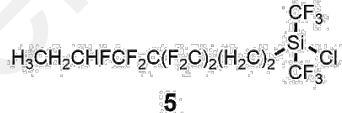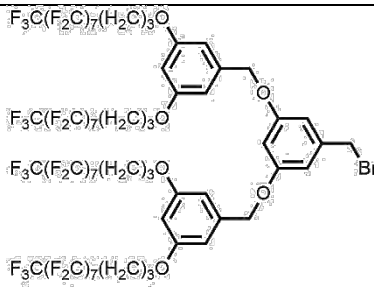
Bulk polymer/Additive	Initiators/End capping agents	Polymerization mechanism	Ref.
Poly(styrene) (PS)/Low-M_w PS	$F_3C(F_2C)_7(H_2C)_2$—Si(CH$_3$)$_2$—Cl **1** $F_3C(F_2C)_7(H_2C)_3O$-, $F_3C(F_2C)_7(H_2C)_3O$-substituted benzyl bromide **2** $F_3C(F_2C)_7(H_2C)_3O$-trisubstituted benzyl bromide **3**	Anionic polymerization	(Hardman et al., 2011; Hutchings et al., 2011)
	$F_3C(F_2C)_5(H_2C)_2$—Si(CH$_3$)$_2$—Cl **4**	Anionic polymerization	(Yuan et al., 1999)
	$H_3CH_2CHFCF_2C(F_2C)_2(H_2C)_2$—Si(CF$_3$)$_2$—Cl **5**	Anionic polymerization	(Schaub et al., 1996)
	$F_3C(F_2C)_7(H_2C)_3O$-substituted dibenzyl ether benzyl bromide **6**	Anionic polymerization	(Ansari et al., 2007)

Table 2.1 (cont.)
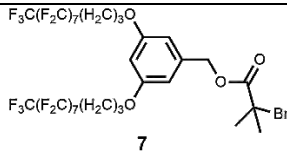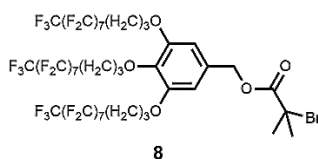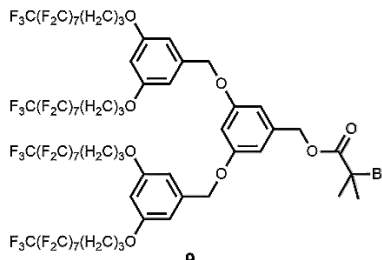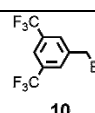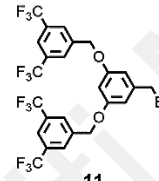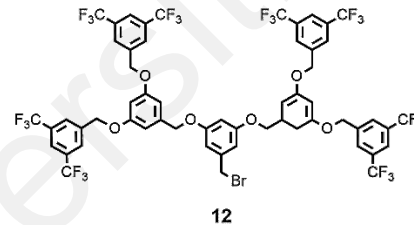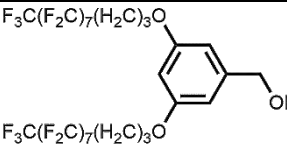
Poly(styrene) (PS)/Low-M_w PS	**7** **8** **9**	Atom transfer radical polymerization (ATRP)	(Narrainen et al., 2007)
	10 **11** **12**	ATRP	(Narrainen, Hutchings, et al., 2006)
Poly(isoprene) (PI)/Low-M_w PI	**1-3**	Anionic polymerization	(Hutchings et al., 2011)
Poly(methyl methacrylate) (PMMA)/Low-M_w PMMA	**2, 3, 6-9**	ATRP	(Narrainen et al., 2007; Thompson et al., 2007)
Polyethylene (PE)/Low M_w PE	**2, 3, 6**	Anionic polymerization	(Hardman et al., 2012)
Polybutadiene (PBd)/Low M_w PBd	**2, 6**	Anionic polymerization	(Kimani et al., 2012)
Poly(lactic acid) (PLA)/Low-M_w PLA	**13**	Ring-opening polymerization (ROP)	(Hutchings et al., 2006)

Table 2.1 (cont.)

Poly(*N*-vinyl pyrrolidone (PVP)/Low-*M*w PVP		Reversible addition-fragmentation transfer (RAFT) polymerization	(Bergius et al., 2013)

*(Chemical structures labeled **14** and **15** with O(CH₂)₃(CF₂)₇CF₃ substituents)*

2.4.3 Polymer Additives for Making the Surface More Hydrophilic

In principle, the component with low surface energy tends to segregate to the solid/air surface while higher surface energy components tend to be immersed in the matrix (Kurusu & Demarquette, 2017). This provides a challenge for researchers to modify and render the surface hydrophilic by using hydrophilic additives. However, there are a few solutions to combat this challenge, either by annealing the thin film containing the additives in high-boiling polar non-solvent (Hutchings et al., 2008) or by annealing in aqueous environments (Rezaei Kolahchi et al., 2014).

In 2017, Kurusu and Demarquette have blended the hydrophobic styrene-ethylene-butylene-styrene (SEBS) polymer with hydrophilic poly(ethylene oxide) (PEO) or with an amphiphilic PEO-PPO-PEO additive (Kurusu & Demarquette, 2017). They have found out that the low surface energy of the PPO blocks drove the segregation of the PEO-PPO-PEO additive and interestingly, segregation continues at room temperature even several weeks after processing (**Figure 2.7**).

Evolution over time
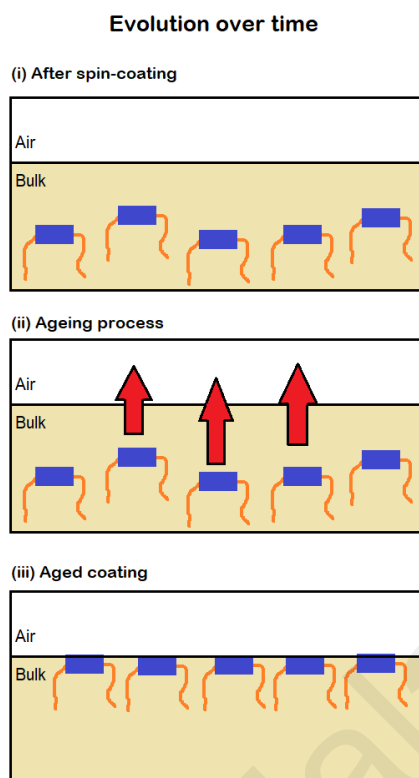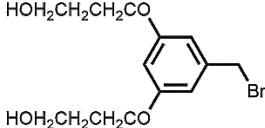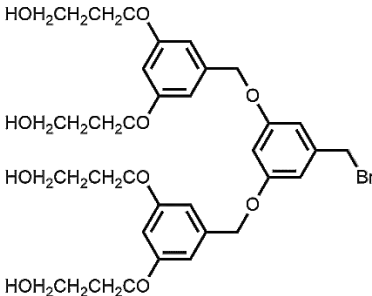
Figure 2.7: Segregation of amphiphilic PPO-PEO-PPO polymer additive. The orange lines represent PEO blocks while the blue rectangles represent PPO block (Kurusu & Demarquette, 2017).

Again, end-functionalized polymer additives provide a robust selection of end capping agents to suit different reaction mechanisms. As mentioned before, specialized initiators or terminators were utilized in order to tune the polymers according to the desired properties. In some cases, a post-polymerization modification is necessary to add desired functionalities into the macromolecule. Examples of hydrophilic end-functionalized polymer additives are shown in **Table 2.2**:

Table 2.2: List of some end-functionalized polymer additives for hydrophilic surfaces

Bulk polymer/Additive	Terminal groups/End capping agents	Polymerization mechanism	Ref.
Polystyrene (PS)/ Low-M_w PS	−COOH −NH$_2$	ATRP (for −COOH functionalized polymer), commercially bought otherwise	(Narrainen, Clarke, et al., 2006; Thompson et al., 2009)

Table 2.2 (cont.)

Polyethylene (PE)/Low-M_w PE	**16**, **17**	Anionic polymerization	(Kimani et al., 2014)
Polybutadiene (PBd)/Low-M_w PBd	**18**	Anionic polymerization, followed by post-polymerization modification and subsequent CuAAC reaction	(Kimani et al., 2012)

2.5 Azobenzene End-Functionalized Polymers

Material scientists are currently paying close attention in preparing smart responsive materials. The ongoing objective in functional polymeric materials research is the preparation of polymers with advanced functionality. Therefore, a great deal of researchers have focused on tailoring such polymers to suit the desired features. Among them, end-functionalization of polymers have shown to be a great strategy in altering the properties of bulk polymeric materials, as discussed in the previous section. Thus, in this section, a brief review on azobenzene end-functionalized polymers will be deliberated.

Azobenzene end-functionalized polymers are widely utilized as smart materials due to the reversible *trans-cis* isomerization of the chromophore as argued earlier. Despite containing only a single unit of azobenzene at the polymer chain ends, the reversible *trans-cis* isomerization of the chromophore is enough to enact substantial changes in the

physical properties of the synthesized polymers (Kim et al., 2020; Schattling et al., 2014; Theato, 2011). A combination of synthetic organic and polymer chemistry has led to the abundance of azobenzene end-functionalized polymers with unique architectures and functionalities, where some of the polymers are shown in **Figure 2.8**:
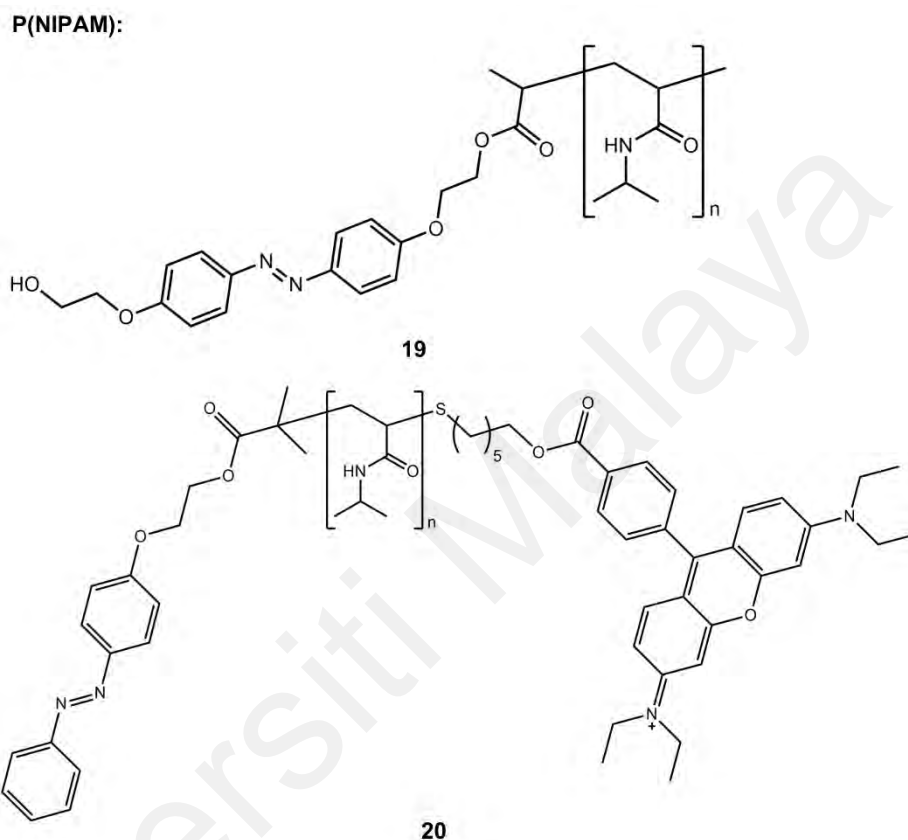
Figure 2.8: Structure of various azobenzene end-functionalized polymers.
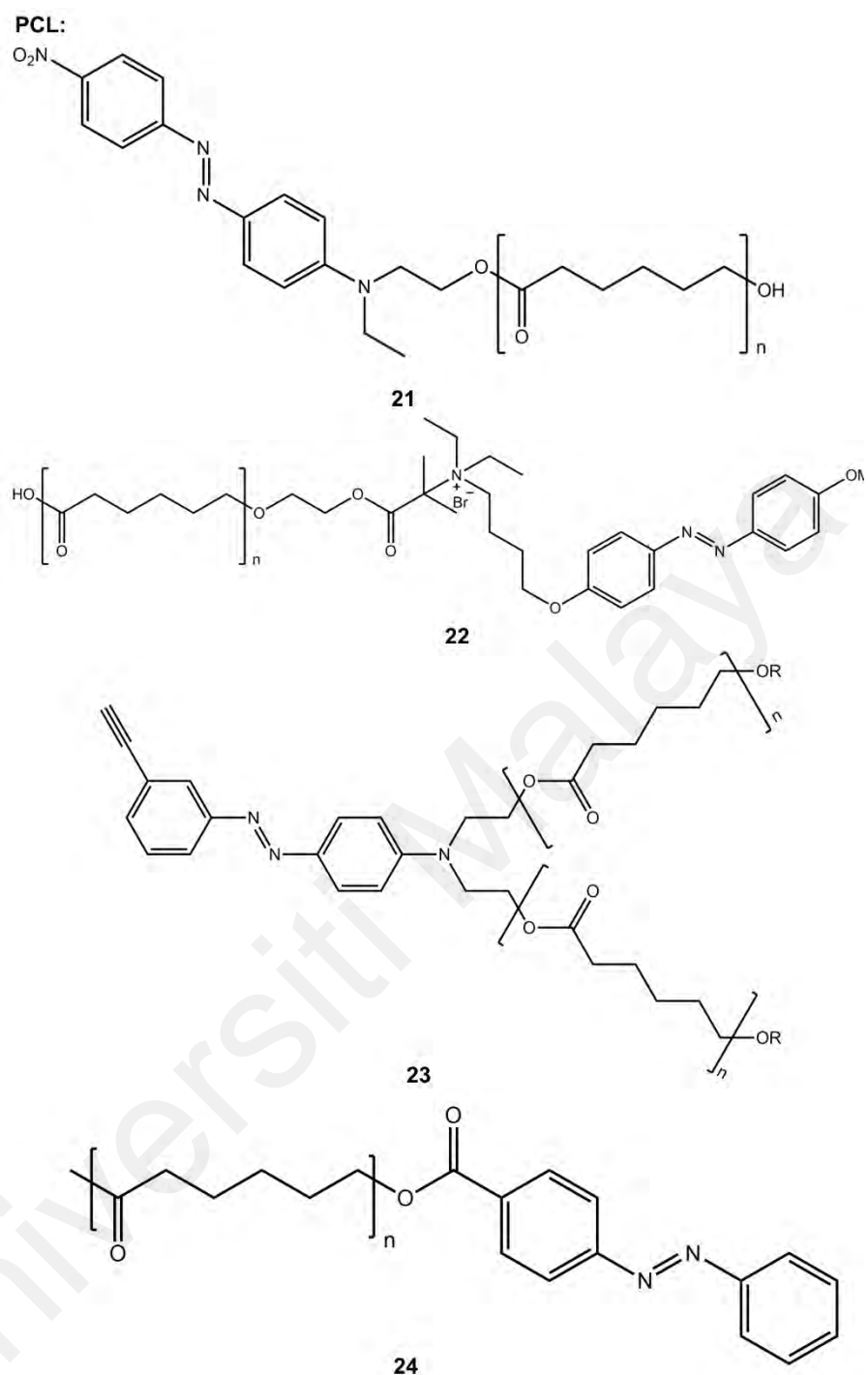
Figure 2.8 (cont.)

HEURs:

25

26

27

PEG:

28

PEO:

29

PS:

30
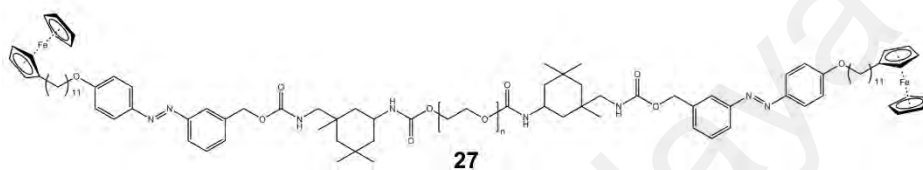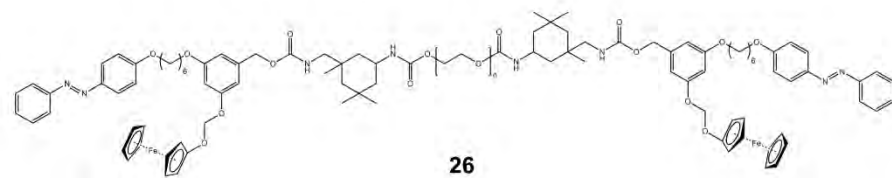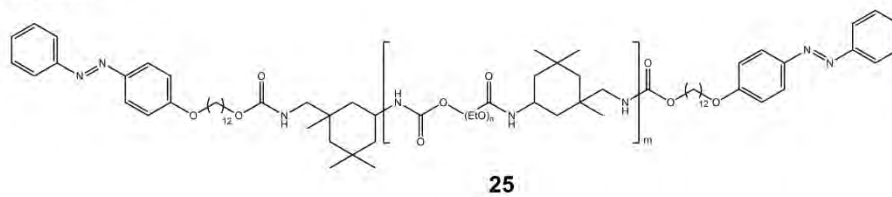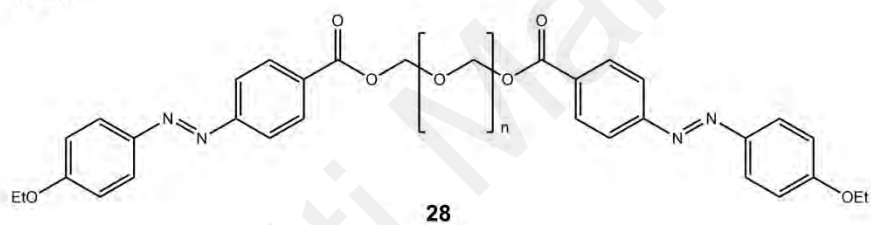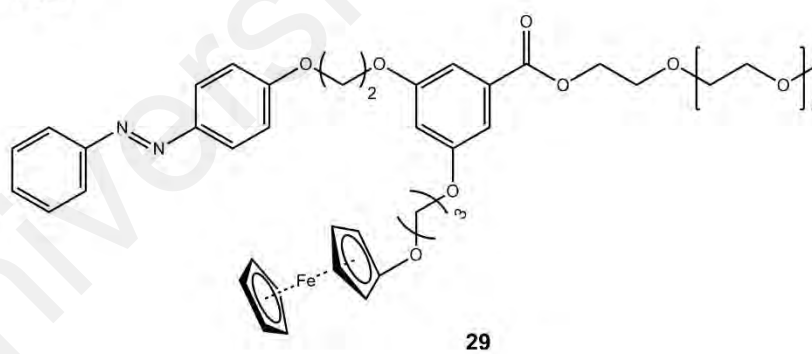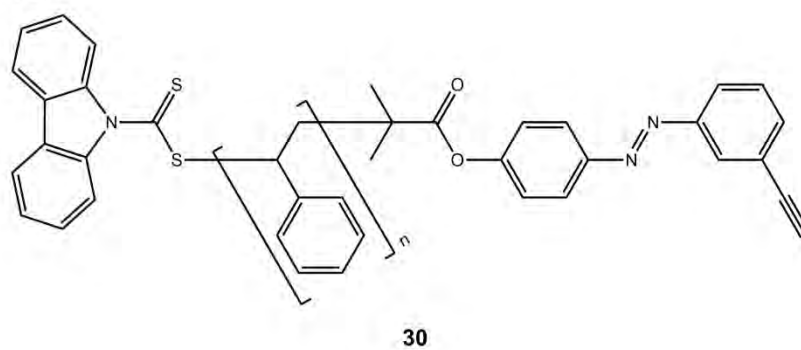
Figure 2.8 (cont.)

Poly(2-isopropyl-2-oxazoline):

31

Poly(2-methoxyvinyl ether):

32

PLA:

33

P(OEGMA):

34
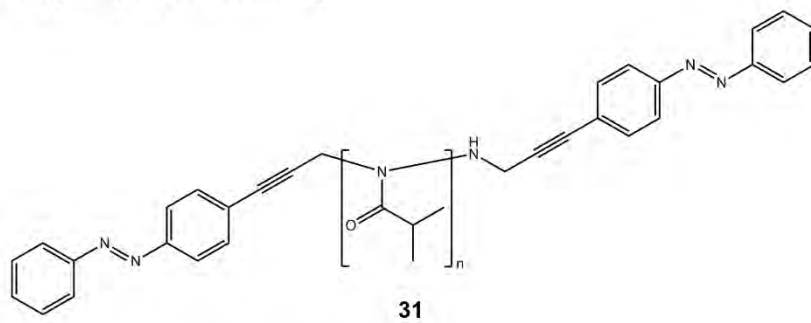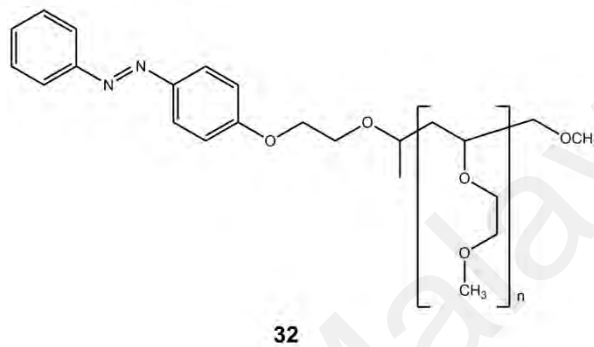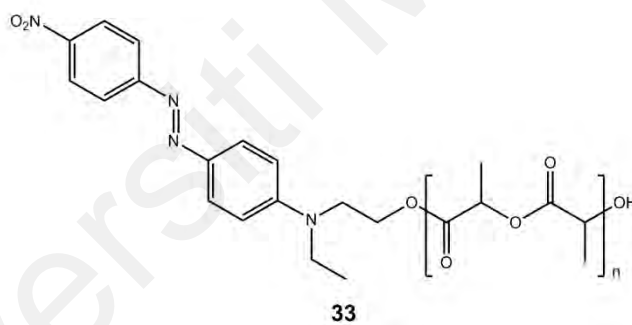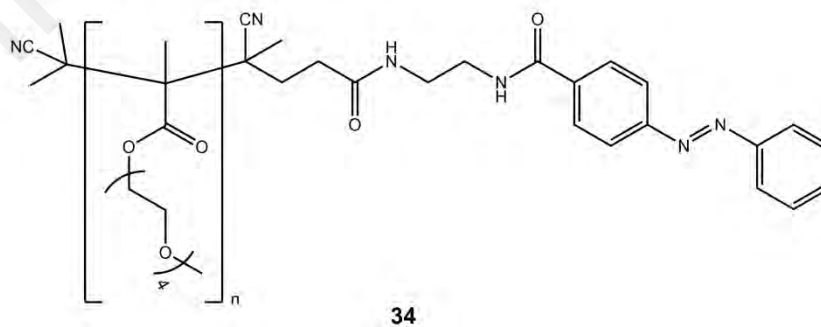
Figure 2.8 (cont.)

P(DMAEMA):

35

Poly(4-phenylazophenyl methacrylate):

36

Poly(propylene imine):

37
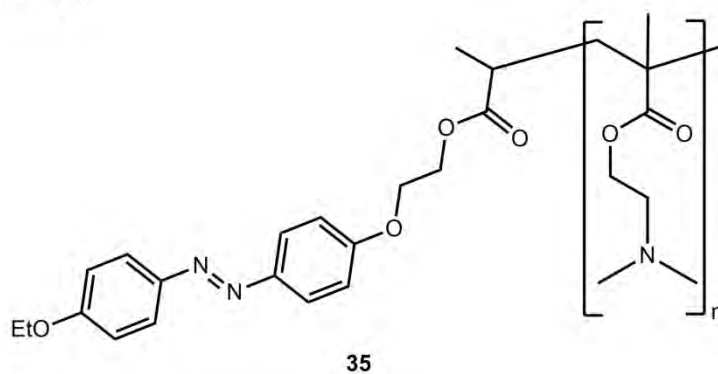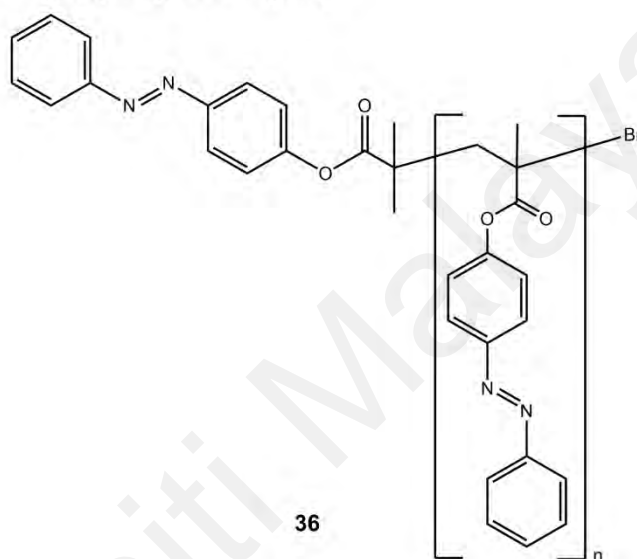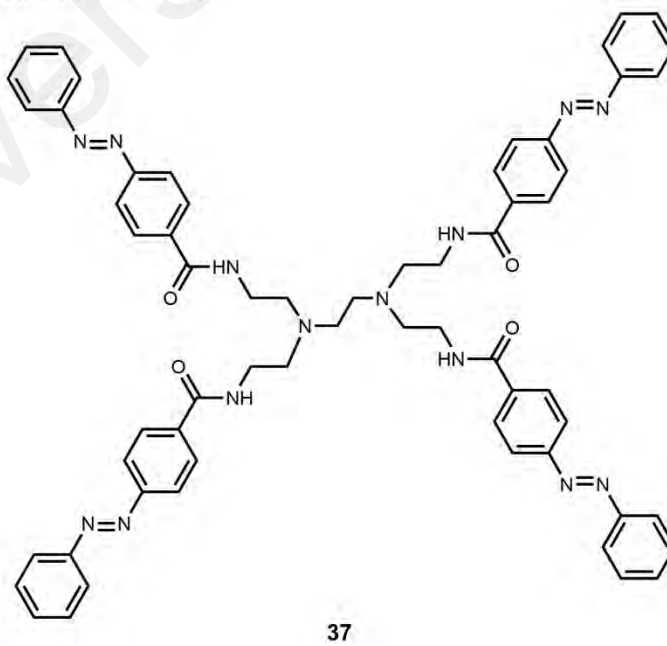
Figure 2.8 (cont.)

Siloxane oligomers:

38

39
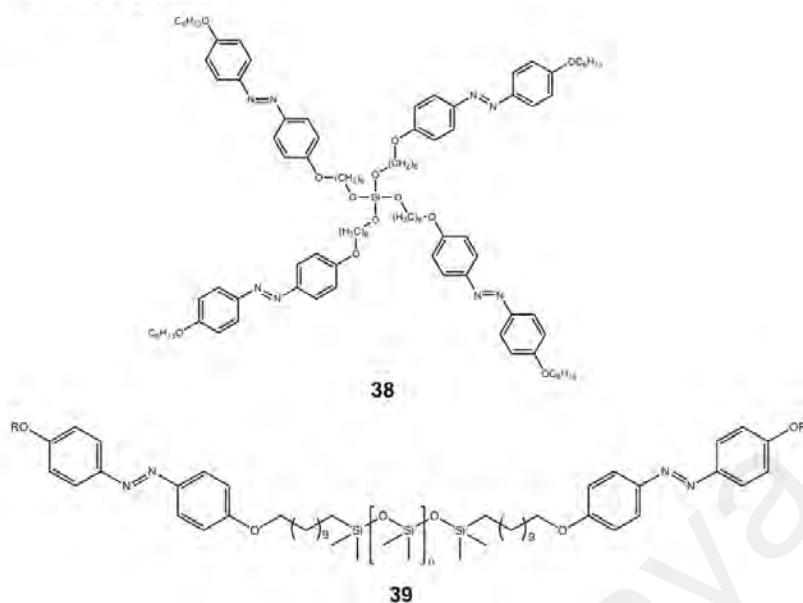
Figure 2.8 (cont.)

The molecular architectures of these polymers were made available due to the significant advancements in synthetic organic and polymer chemistry, which further catalyze the development of smart polymeric materials. Various methods such as ATRP, RAFT, ROP and living cationic polymerization techniques in tandem with the established organic synthesis methods, are employed in tailoring these polymers. **Table 2.3** further summarized the synthesis methods of these polymers:

Table 2.3: List of some azobenzene end-functionalized polymers

Polymer	Structure	Synthesis method	Ref.
Poly(N-isopropylacrylamide), P(NIPAM)	**19**	ATRP	(Akiyama & Tamaoki, 2007)
	20	RAFT	(Shi et al., 2016)
Poly(ε-caprolactone), PCL	**21**	ROP	(Peptu et al., 2009)
	22	ROP, followed by post-polymerization modification	(Tong et al., 2017)

Table 2.3 (cont.)

Polymer	Structure	Synthesis method	Ref.
Poly(ε-caprolactone), PCL	**23**	ROP	(Xue et al., 2015)
	24	ROP, followed by Steglich esterification	(Guo et al., 2021)
Hydrophobically modified ethoxylated urethanes, HEURs	**25-27**	Condensation polymerization, followed by post-polymerization modification	(Du et al., 2018; Du et al., 2016; Du et al., 2017)
Poly(ethylene glycol), PEG	**28**	Post-polymerization modification *via* Steglich esterification	(Zhang et al., 2012)
	Tadpole-shaped poly(ethylene glycol)-polyhedral oligomeric silsesquioxane	Post-polymerization modification *via* thiol-ene reaction	(Wang et al., 2015)
Poly(ethylene oxide), PEO	**29**	Post-polymerization modification *via* Steglich esterification	(Du et al., 2019)
Poly(styrene), PS	**30**	RAFT	(Xue et al., 2010)
	End-functionalized PS beads	Post-polymerization modification	(Dalton et al., 1995)
Poly(2-isopropyl-2-oxazoline)	**31**	ROP, followed by Sonogashira coupling	(Kim et al., 2015)
Poly(2-methoxyvinyl ether)	**32**	Living cationic polymerization	(Shimomoto et al., 2012)
Poly(lactic acid), PLA	**33**	ROP	(Peptu et al., 2009)

Table 2.3 (cont.)

Polymer	Structure	Synthesis method	Ref.
Poly[oligo(ethylene glycol)methyl ether methacrylate], P(OEGMA)	**34**	RAFT, followed by post-polymerization modification	(Jochum et al., 2009)
Poly(*N,N*-dimethylaminoethyl methacrylate), P(DMAEMA)	**35**	ATRP	(Tang et al., 2010)
Poly(4-phenylazophenyl methacrylate)	**36**	ATRP	(Jeong et al., 2017)
Poly(propylene imine)	**37** and higher-genaration dendrimers	Post-polymerization modification	(Archut et al., 1998)
Siloxane oligomers	**38** and higher-generation dendrimers	Post-polymerization modification	(Liu et al., 2007; Liu et al., 2005)
	39	Post-polymerization modification	(Zha et al., 2018)
Poly(aryl ether ketone)	Hyperbranched poly(aryl ether ketone)	Nucleophilic aromatic substitution, S_NAr	(Jiang et al., 2010)

2.6   Living Anionic Polymerization of Alkyl Methacrylates

In this modern era, there is an increasing need and demand for smart materials to fulfil many requirements and applications in today's society. Often, functionalized polymers with well-defined structures are able to accomplish such demands. In essence, living polymerization reactions are a gateway for preparations of such polymers (Hsieh & Quirk, 1996). The revelation of living polymerizations was realized by Szwarc et al. in mid-1950's when he insightfully detailed the "living" nature of anionic polymerizations of styrenes and dienes (Szwarc, 1956; Szwarc et al., 1956). Living polymerization reactions typically proceed bereft of irreversible chain transfer and chain termination steps (Szwarc, 1956; Szwarc et al., 1956).

2.6.1 *Introduction to Living Anionic Polymerization*

Living anionic polymerization has permitted the versatile synthesis of an assortment of well-defined polymers containing desired functionalities since the marvelous discovery made by Szwarc et al. (Szwarc, 1956; Szwarc et al., 1956). Under controlled conditions, they demonstrated that living carbanionic polymers can be produced using sodium naphthalide in an electron-transfer initiation. Furthermore, anionic polymerization progresses by the addition of monomers to active centers bearing a full or partial negative charge. The active (anionic) centers are then regenerated at the chain ends after each monomer addition. Moreover, the negatively charged chain end is typically associated with a metal counterion (usually alkali metals, sometimes alkaline-earth metals). It is well established that in living anionic polymerization systems, the absence of termination reactions has enabled the control of molecular weight, molecular weight distribution, microstructures and copolymer composition during polymer synthesis.

It is worth mentioning that the presence of impurities can severely inhibit the propagation of living polymers since the living chain ends are highly reactive. These chain ends are highly susceptible to reaction with oxygen, carbon dioxide, water and other protic impurities. In other words, these impurities will induce the premature termination of either the initiator or the living chain ends. Thus, care must be taken to exclude any impurities to achieve any successful living anionic polymerizations. To begin with, all solvents, reagents and monomers must be rigorously purified and degassed prior to use. Next, all anionic polymerization reactions are usually carried out either under high-vacuum conditions (Hadjichristidis et al., 2000) or under an inert atmosphere of dry nitrogen or argon (Sarih, 2010). Furthermore, even residual moisture hydrogen bonded to the walls of glassware or reaction vessel could prematurely cause the destruction of initiator or living carbanion species. To overcome such a problem, the reaction vessel is

usually washed with initiator solution prior to polymerization. A detailed experimental procedure will be described in the next chapter.

In this work, methyl methacrylate (MMA) is chosen as the monomer of choice as PMMA is widely used in the coating industry owing to its desirable properties such as having excellent film-forming performance and good cohesiveness (Coan et al., 2013). Furthermore, PMMA also exhibits excellent transparency and hardness (Abidin et al., 2013), gloss (R. Li et al., 2019), thermal- (Ali et al., 2015), photo- (Wang et al., 2007) and environmental stability (Hu & Nair, 1996) in addition to superb weatherability (Ali et al., 2015; Coan et al., 2013; Wang et al., 2007), allowing it to be a highly sought material for outdoor applications. Most importantly, PMMA displays favorable workability and processing conditions (Ali et al., 2015; Demir et al., 2006; Hu & Nair, 1996). Henceforth, all discussions pertaining the living anionic polymerization reactions will only involve alkyl methacrylate monomers, specifically methyl methacrylate due to the great challenges imposed on controlling the polymerization of these types of monomers.

2.6.2 *General Mechanism of Anionic Polymerization of Alkyl Methacrylates*

Ideally, under controlled conditions with the absence of impurities, anionic polymerizations of alkyl methacrylates involve only initiation and propagation steps. Initiation takes place when the initiator, R^-M^+ undergoes a Michael-type addition reaction with the alkyl methacrylate monomer (MMA as an example) to generate the active propagating species (Hsieh & Quirk, 1996). Propagation takes place when the active propagating species react with remaining monomers, elongating the chains in the process. Since this is a living polymerization reaction, neither termination nor chain transfer reactions take place. Therefore, termination is typically done by the addition of a protic

solvent such as methanol to kill the reactive polymer chain ends, forming a final product. The general reaction of initiation, propagation and termination is shown in **Scheme 2.1**.
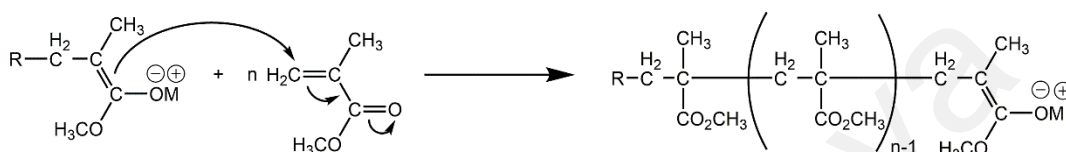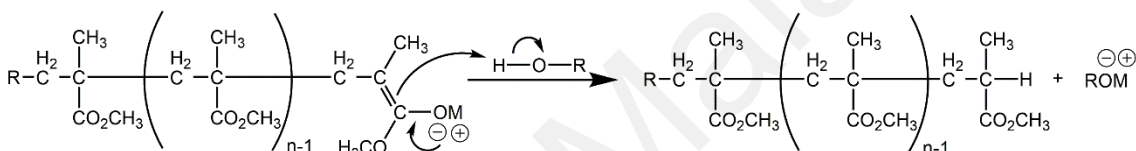
Scheme 2.1: General polymerization mechanism for the anionic polymerization of methyl methacrylate (Hsieh and Quirk, 1996).

However, since alkyl methacrylate anions are essentially enolates, many side reactions can bring about to the premature termination of the living chain ends if one is not careful in the selection of suitable initiating systems and reaction conditions. A detailed insight on the premature termination of the living chain ends of polymeric methacrylate anions will be described in a later part of this section.

2.6.3 Selection of Initiators

The selection of proper initiators for anionic polymerization of alkyl methacrylates is of utmost importance for synthetic polymer chemists to attain polymers with controlled, well-defined structures. The desired Michael-type addition reaction of the initiator, R^-M^+ with a monomer such as methyl methacrylate competes with the nucleophilic acyl

substitution reaction of the initiator with the ester carbonyl group to form the corresponding ketone derivative (**Scheme 2.2**).

Desired Michael-type addition/initiation:
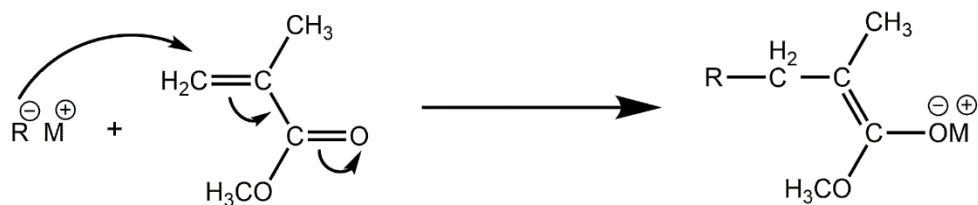
Competing nucleophilic acyl substitution reaction:
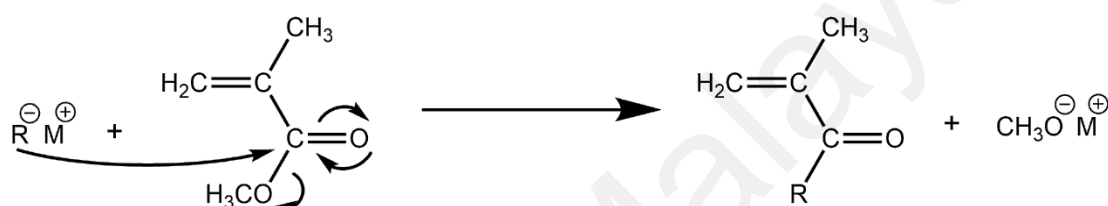
Scheme 2.2: Reactions of initiator, R⁻M⁺ with methyl methacrylate monomer (Hsieh & Quirk, 1996).

The competition between these two modes of addition is dependent on the general reactivity of the initiator and the steric requirements of the initiator (Hsieh & Quirk, 1996). As a general rule of thumb, the reactivity/stability of an initiator of choice must be approximately equal to that of the propagating chain end carbanionic species. One way to approximate the reactivity/stability of a carbanion species (initiator, monomer or propagating chain end) is by referring to the pK_a of its corresponding conjugate acid (Hsieh & Quirk, 1996).

A prime example of a poor choice of initiator for the MMA polymerization is highlighted in the following study (Hatada et al., 1981). In the study, alkyllithium initiators were found to be too reactive with respect to the reactivity of MMA monomers. It was shown that about 51% of lithium methoxide was produced from the reaction of

MMA with *n*-butyllithium in toluene at −78 °C, indicating that more than half of the initiator underwent nucleophilic acyl substitution reaction instead of the Michael-type addition (**Scheme 2.2**). Furthermore, the formation of both a polymer and an oligomer which contain butyl group initiator fragments at their chain ends was detected. It is crystal-clear that the consumption of more than 50% of the initiator by the competing nucleophilic acyl substitution reaction is unacceptable. Hence, a significant number of studies were conducted in order to overcome such bottleneck in the initiation step of alkyl methacrylate polymerization.

Commonly, the most useful initiator for anionic polymerization of methacrylates is 1,1-diphenylhexyllithium (DPHLi), which is formed by the quantitative addition of butyllithium with 1,1-diphenylethene (DPE) (Anderson et al., 1981; Cernohous et al., 1997). Furthermore, the formation of lithium methoxide is markedly reduced to just 17% when DPHLi is used instead of butyllithium (Hatada et al., 1981). This is due to the similarities of the pK_a of the conjugate acid of DPHLi, which is diphenylmethane (pK_a = 32) and that of the propagating ester enolate anion (pK_a = 30-31) (Hsieh & Quirk, 1996). Moreover, the larger and bulkier 1,1-diphenylhexyl anion means that the rate of addition to the ester carbonyl group is diminished.

In essence, the reactivity of initiator and propagating chain ends should be similar in order to minimize the undesired nucleophilic acyl substitution reactions; thus ensuring the complete polymerization processes. Other commonly used initiators include ester enolate anions (Kohsaka et al., 2013; Kohsaka, Yamamoto, et al., 2015; Lochmann et al., 1974), *α*-methylstyryl anions (Warzelhan et al., 1978), 9-fluorenyl anions (Al-Takrity et al., 1990a; Warzelhan et al., 1978), 9-methylfluorenyl anions (Deffieux et al., 1984; Warzelhan et al., 1978), alkoxide salts (Alev et al., 1980; Li et al., 2019a, 2019b; Viguier et al., 1982; Zhang et al., 2019; Zheng et al., 2017; Zou et al., 2018), Grignard reagents

(Allen & Williams, 1985; Hatada et al., 1988; Hatada et al., 1989; Hatada, Ute, et al., 1986; Kitayama et al., 1993) and complexes of *tert*-butyllithium with trialkylaluminum compounds, the so-called "ate" complexes (Ballard et al., 1992; Kitayama et al., 1989), among others. Initiators of specific functionalities for the synthesis of end-functionalized PMMA will be elaborated further in **Section 2.6**.

2.6.4   *Selection of Solvents*

Typical solvents for the polymerization of alkyl methacrylates include toluene and tetrahydrofuran (THF). Some polymerization reactions also used dichloromethane (DCM) as the solvent of choice (Kohsaka et al., 2013; Kohsaka, Yamamoto, et al., 2015). It is worth mentioning that polymerization of MMA in toluene is more complex than in THF, where the polymers obtained showed broad and often multimodal molecular weight distributions (MWDs) – an indication of a multiplicity of active propagating species (Piejko & Höcker, 1982). In addition, it is well known that premature termination reactions can be suppressed by conducting the polymerization at low temperatures (−75 °C or below) in polar solvents, of which at elevated temperatures, the rate of termination increased (Hsieh & Quirk, 1996; Warzelhan et al., 1978). Clearly, solvent polarity dictates the course of anionic polymerization of alkyl methacrylates, including the tacticity of the produced polymers (Baskaran, 2003).

2.6.5   *Premature Termination Reactions*

Due to the polar nature of ester group of alkyl methacrylate monomers and polymers, this functional group is involved in the solvation of counterions and thus, it is highly susceptible to nucleophilic attacks during initiation or propagation steps (Baskaran, 2003). These unwanted side reactions are simply due to either using an initiator with a higher nucleophilicity than the monomer/active chain ends or metal ion solvation

(Baskaran, 2003). **Scheme 2.3** illustrates the possible premature termination reactions using PMMA as an example:

1) Attack of active chain end to monomer:
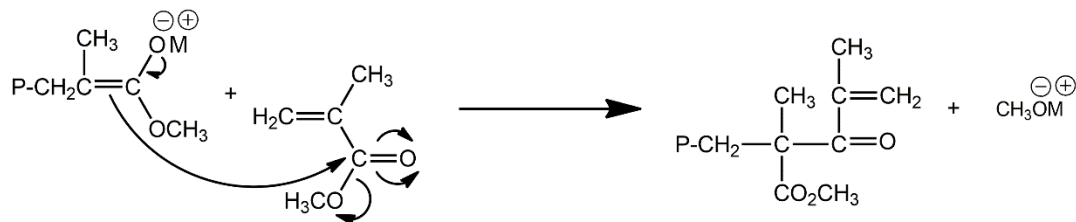
2) Intermolecular polymer termination:
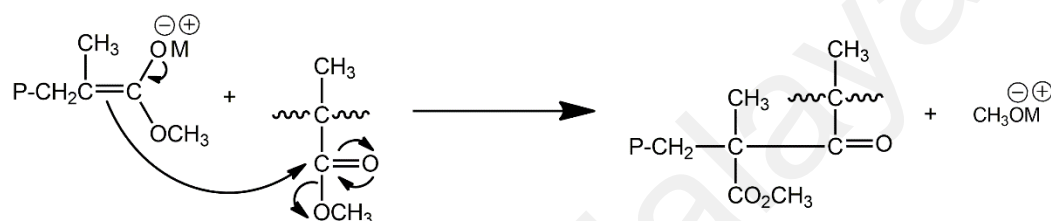
3) Intramolecular back-biting reaction:
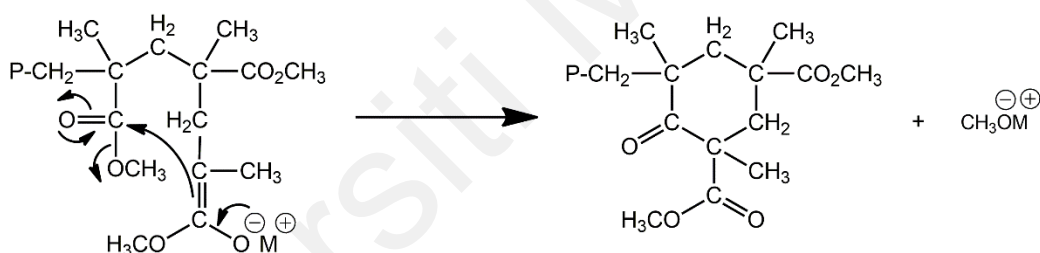
Scheme 2.3: Possible termination reactions in methyl methacrylate polymerization. P denotes PMMA chain (Baskaran, 2003).

Such possible reactions are suggested by a few researchers (Goode et al., 1960; Graham et al., 1960; Schreiber, 1960). It was observed that these termination modes are essentially Claisen-type condensation reactions, forming a *β*-keto ester as the final product. Furthermore, all possible reactions lead to the formation of metal methoxides. The first possible side reaction is the attack of the growing ester enolate to the monomer, of which mechanistically is akin to the nucleophilic acyl substitution reaction as shown in **Scheme 2.2**. It was postulated that this type of reaction is the exclusive mode of

termination (Löhr et al., 1974). However, it was concluded that there is no corroborative evidence supporting such a termination mode (Warzelhan et al., 1978).

Another possible side reaction is postulated where the propagating chain end reacts with a carbonyl ester group of another polymer chain, which leads to chain coupling. This postulation however seems impossible since the intermolecular polymer termination is thermodynamically unfavorable due to the crowded stearic environment surrounding the in-chain ester groups (Baskaran, 2003; Hsieh & Quirk, 1996). Moreover, any such intermolecular reaction would lead to high-molecular weight fraction in the final product, of which a high-molecular weight tailing should appear in size exclusion chromatographic (SEC) curves. In addition, this termination mode is finally disproved since it is determined that this high-molecular weight tailing is absent in SEC curves (Gerner et al., 1984).

The third possible termination mode is an intramolecular back-biting reaction between the propagating enolate anion and the antepenultimate ester carbonyl group, forming a β-ketocyclic ester. It is suggested that such a termination reaction exists since the β-ketocyclic ester functionality in PMMA chains was identified by FTIR as a recognizable band at 1712 cm^{-1} (Goode et al., 1960). Other reports (Glusker, Lysloff, et al., 1961; Warzelhan et al., 1978) also observed such an intramolecular reaction in MMA polymerizations.

2.6.6   *Role of Solvated Contact Ion-Pairs in Propagation Steps*

In view of minimizing the unwanted side reactions as discussed in **Sections 2.5.3** to **2.5.5**, numerous strategies are developed and reported in the literature. It is proposed that the external solvation of metal ions at low temperature by a polar solvent assists in controlling ion-pair aggregation and minimizing the side reactions (Glusker, Lysloff, et al., 1961; Glusker, Stiles, et al., 1961; Kraft et al., 1980). In 1,2-dimethoxyethane (DME),

MMA polymerization initiated by benzyl-oligo-α-methylstyrylsodium showed living characteristics even at 0 °C. Moreover, the produced polymer exhibited narrow MWD when compared to the polymer produced from THF. Kraft and co-workers proposed that the experimental observations are due to the equilibrium existed between different types of contact ion-pairs during propagation steps (**Scheme 2.4**).
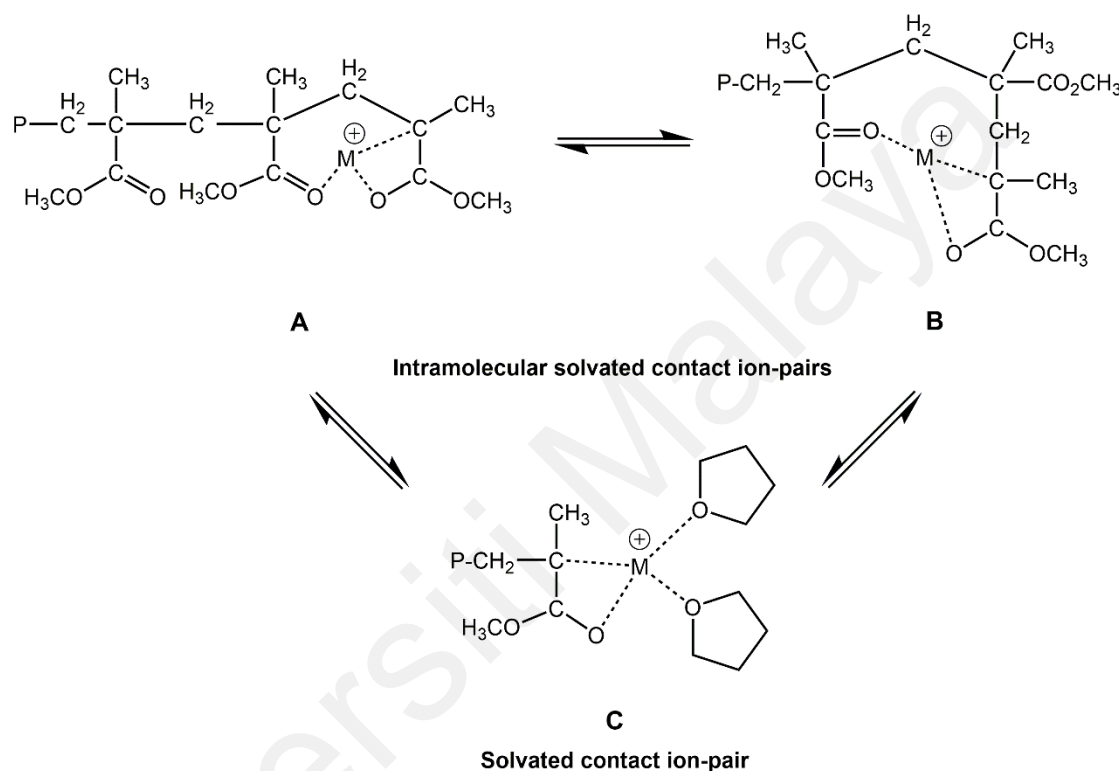
Scheme 2.4: Propagation by contact ion-pairs in anionic polymerization of MMA (Baskaran, 2003).

Intramolecularly solvated contact ion-pairs **A** and **B** promote backbiting termination reactions in low polarity solvents. In contrast, polar solvents such as DME shifts the equilibrium towards solvated ion-pair, **C** and solvent-separated ion-pair. In medium polarity solvents such as THF, the existence of external solvation of the counterion probably competes with the intramolecular solvation species **A** and **B**. Consequently, the lower termination reactions observed in DME compared to in THF were in fact due to the decreased concentration of species **B**, which is highly susceptible to intramolecular termination.

2.6.7 *Controlling the Livingness of Alkyl Methacrylate Polymerization*

In general, controlled anionic polymerization of alkyl methacrylates can be achieved by a careful selection of initiators, counterions, additives and solvents as well as conducting the polymerization at low temperatures (Hirao et al., 2014). Optimally, the use of bulky initiators with bulky counterions in polar solvents at low temperatures should support livingness of methacrylate polymerizations (Baskaran, 2003). However, these strict requirements become a major bottleneck in the application of anionic polymerization of methacrylates in industries. Hence, a significant amount of research focusing on the strategies involved to control the livingness of enolate chain ends are conducted, which include the choice of additives, counterions as well as other strategies to conduct polymerization of alkyl methacrylates at ambient temperatures.

2.6.7.1 *Role of Ligands and Salts as Additives*

Ligands and salts are usually used as additives in improving and controlling the livingness of methacrylate polymerization reactions. Alkyllithium compounds dissociate into smaller aggregates in the presence of chelating agents due to coordination with these ligands (Collum, 1992). The best chelating agents for alkyllithium compounds include crown ethers and cryptands (Varshney et al., 1992; Viguier et al., 1982; Viguier et al., 1987; Wang et al., 1994) and polyamines such as *N,N,N',N'*-tetramethylethylenediamine (TMEDA) (Baskaran et al., 1995; Hatada et al., 1988; Matsuzaki et al., 1973) and pyridine (Anderson et al., 1981; Braun et al., 1962; Long et al., 1986; Subramanian et al., 1985), among others. These are usually used to increase the reactivity of the propagating carbanion species (Baskaran, 2003). Furthermore, salts such as LiCl (Fayt et al., 1987; Varshney et al., 1990; Varshney et al., 1991), LiClO$_4$ (Baskaran & Sivaram, 1997) and metal alkoxides (Lochmann et al., 1977; Lochmann et al., 1966; Lochmann et al., 1965; Schlosser, 1967; Wiles & Bywater, 1962, 1964) are used to solvate and stabilize the living enolate chains. Evidently, specific solvation of lithium enolate has greatly influenced the

enhancement of livingness of polymerization, which in turn is controlled by solvent polarity (see **Section 2.5.6**). Other ligands such as lithium silanolates (Zundel et al., 1998a, 1998b), diethylzinc (Ishizone et al., 1998) and triethylborane (Ishizone et al., 1999) also showed improved controllability of methacrylate polymerizations, indicated by the narrow MWD of the polymers obtained.

2.6.7.2 Controlled Polymerization at Ambient Temperatures

One of the major bottlenecks of living anionic polymerization of alkyl methacrylates is the strict controlled conditions required in conducting such polymerizations. The presence of additives such as LiClO$_4$ (Baskaran & Sivaram, 1997) and *t*-BuOLi (Lochmann et al., 1977) has enabled controlled polymerization of methacrylates at temperatures up to 20 $^{\circ}$C. In this section, other strategies for controlled polymerization of methacrylates at ambient temperatures are discussed.

The use of bulky phosphonium counterions in initiating systems such as tetraphenylphosphonium triphenylmethanide (Ph$_4$P$^+$Ph$_3$C$^-$) in THF at 0 and 25 $^{\circ}$C were first reported (Zagala & Hogen-Esch, 1996). Rapid rate of polymerization was observed, with the produced PMMA showing narrow MWD. They proposed that the bulky Ph$_4$P$^+$ counterion may facilitate the formation of narrow MWD PMMA at ambient temperatures by reducing the rate of back-biting termination reactions. In other words, the large counterion size interacting with the propagating ester enolate essentially prevents such termination reactions from happening due to stearic hindrance. Other phosphonium-based initiators include α-tetraphenylphosphonium methyl isobutyrate (Baskaran & Müller, 1997), 1-naphthyltriphenylphosphonium triphenylmethanide (NTPP$^+$Ph$_3$C$^-$) (Dimov et al., 2000; Ling & Hogen-Esch, 2007; Warner et al., 1999), bis(triphenylphosphoranilydene)ammonium triphenylmethanide (Königsmann et al., 2000), *t*-butyl-P4-phosphazene base (Pietzonka & Seebach, 1993) and 1,1-

diphenylhexyltetrakis[tri(dimethylamino)phosphoranylidenamino]phosphonium (P$_5^+$) (Baskaran & Müller, 2000). Controlled polymerization of MMA was achieved using these initiators even at elevated temperatures (up to 70 ºC). Another advantage of using phosphonium-based initiators is that the polymerization is essentially metal-free. However, the downside of these initiators is that they exhibited poor initiator efficiency ($f < 20\%$).

The "ate" complexes of t-BuLi with trialkylaluminum compounds (usually R$_3$Al ≥ 3.0 equiv. wrt R-Li) were found to be effective in initiating polymerization of alkyl methacrylates in toluene at -78 ºC (Kitayama et al., 1989). These complexes offered polymers with narrow MWD and high monomer conversions in 24 h. To obtained controlled polymerization at ambient temperatures, two bulky "ate" complexes, comprising of the adducts of t-BuLi with either (2,6-di-t-butylphenoxy)diisobutylaluminum (Al(BHT)(iB)$_2$) or (2,6-di-t-butyl-4-methylphenoxy)diisobutylaluminum (Al(BHB)(iB)$_2$) were developed (Ballard et al., 1992). These bulky adducts enabled effective MMA polymerization at ambient temperatures (0 to 40 ºC). Unlike other common "ate" complexes which require [Al]$_o$/[Li]$_o \geq 3.0$ for optimum control of polymerization, these bulky complexes work well with equimolar R$_3$Al and t-BuLi. Furthermore, end-group analysis indicated that only t-butyl groups are inserted at the polymer chain ends. However, the initiator efficiency was only 70% and they attributed this to the existence of a dimeric species, of which only one of its two t-butyl groups can initiate polymerization.

Studies conducted by Guan and co-workers (Chen et al., 2014; Li et al., 2019a, 2019b; Shu et al., 2015; Zhang et al., 2019; Zheng et al., 2017; Zheng et al., 2013; Zou et al., 2018) provided further insights into recent developments of alkyl methacrylate living anionic polymerizations. Firstly, they have introduced the so-called "P-complexes" where

bulky additives such as lithium phenoxide (LiOPh) associate with DPHLi, forming adducts that were subsequently used in initiating methacrylate polymerizations (Chen et al., 2014; Zheng et al., 2013). For example, the DPHLi/LiOPh initiating system provided controlled polymerizations in toluene or THF at 0 to 20 °C. These P-complexes allowed the restriction of polymerization rate and control side reactions due to stearic hindrance. Furthermore, the ligands also showed tight aggregation with the living chain ends, therefore limiting side reactions and lower polymerization rates.

Another study (Shu et al., 2015) utilized DPHLi/*t*-BuOK or *t*-BuONa initiating systems in the synthesis of poly(*t*-butylmethacrylate), P(*t*BMA)-*block*-PMMA at ambient temperatures. It was discovered that the initiator undergoes ion-exchange reaction from Li^+ to K^+ or Na^+. As a result, the larger counterion size helps inhibiting side reactions and lowering polymerization rates due to lowered charge density.

The use of metal alkoxides as initiators for the polymerization of methacrylates in toluene has been discussed in the previous sections, with polymers produced exhibiting broad MWD (Alev et al., 1980; Viguier et al., 1982). Guan and co-workers (Li et al., 2019a, 2019b; Zhang et al., 2019; Zheng et al., 2017; Zou et al., 2018) have recently showed that *t*-BuOK is an efficient initiator for methacrylate polymerization in THF at ambient temperatures (0 to 60 °C). Initially, the produced polymers showed broad MWD but became narrower as polymerization temperature increased, indicating low initiator efficiency (Zheng et al., 2017). They attributed the observations to the high concentrations of initiators used, since *t*-BuOK has a tendency to form tightly-bound aggregates. Hence, lowering the initiator concentration and/or increasing polymerization temperatures are required to break up the *t*-BuOK aggregates, forming ion-pairs. As a result, in subsequent studies (Li et al., 2019a, 2019b; Zhang et al., 2019; Zou et al., 2018), they used low concentrations of *t*-BuOK ([*t*-BuOK] < 0.06 M) and obtained polymers with narrow

MWD. However, upon increasing the concentration of *t*-BuOK to a certain level, they observed that there is no obvious changes in the M_w of produced polymers, due to the tendency of *t*-BuOK forming aggregates at higher concentrations.

Another interesting revelation from *t*-BuOK-initiated polymerization is that terminated PMMA containing *β*-ketocyclic ester formed from intramolecular Claisen reaction can be revived (Li et al., 2019a) by the attack of *t*-BuOK on the *β*-ketocyclic ester as shown in **Scheme 2.5**. Here, *t*-BuOK attacks the *β*-carbonyl carbon, initiating ring-opening reaction. As a result, the antepenultimate MMA unit was converted into a *t*-butyl methacrylate unit. This is evidenced from ^{1}H and ^{13}C NMR spectra of PMMA produced from *t*-BuOK initiator indicating the presence of *t*-butyl groups. Similar observations were noted when *t*-BuONa was used as initiator (Lochmann & Trekoval, 1981). From this revelation, it can be concluded that *t*-BuOK can regenerate dormant PMMA chain ends at the expense of its efficiency as an initiator.
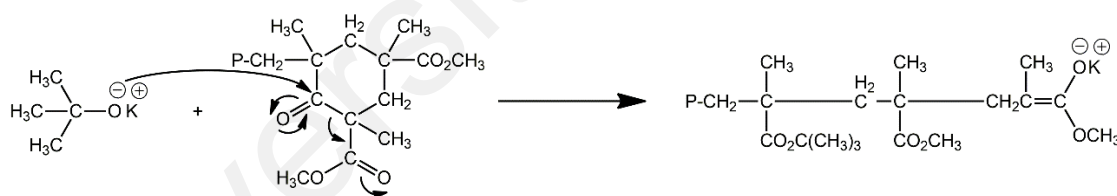
Scheme 2.5: Regeneration of propagating site by attack of *t*-BuOK on the *β*-keto ester (Li et al., 2019a).

2.7   Strategies Involving End-Functionalization of PMMA *via* Living Anionic Polymerization Reactions

There are numerous polymers with well-defined structures and architectures produced since the advent of living anionic polymerization technique. Furthermore, living anionic polymerization reactions provide a gateway to many end-functional polymers with a myriad of applications. This is due to the relative ease of inserting desired functional groups at either ends of the polymer chain. For example, alkyllithium or DPE derivatives

with the desired functionalities can be tailored accordingly and therefore be used as polymerization initiators (initiator method), yielding α-functionalized polymers. On the other hand, the required functionalities can be added by terminating the living polymer end with an electrophile (terminator method), giving rise to ω-functionalized polymers. Many times, a combination of both methods and subsequent post-polymerization modifications are used to produce polymers with specific functionalities at both α- and ω- ends. From these functional polymers, one can make or construct polymers with unique architectures which will be discussed further in this section.

Functionalized initiators (**Figure 2.9**) are used to incorporate desired functional groups at the α-terminus of PMMA. These include 6-(1-ethoxyethoxy)-1,1-diphenylhexyllithium (**40**) (Anderson et al., 1981), 1,1-diphenyl-1-(4-pentenyl)lithium (**41**) (Anderson et al., 1981), 3- (**42**) and 4-vinylbenzylmagnesium chloride (**43**) (Hatada, Nakanishi, et al., 1986), (1-(4-(dimethylamino)phenyl)-3-methyl-1-phenylpentyl)lithium (**44**) (Quirk & Zhu, 1990), 1-(naphthalen-1-yl)-1-phenylhexyllithium (**45**) (Al-Takrity et al., 1990a, 1990c), various lithium *N*-benzylamides (**46-48**) (Kitaura & Kitayama, 2008, 2013; Kohsaka, Kurata, et al., 2015), 1-[4-(*tert*-butyldimethylsilyloxy)phenyl]-1-phenylhexyllithium (**49**) (Dhara et al., 2008; Dhara & Sivaram, 2009; Dhara et al., 2009), 6-(*tert*-butyldimethylsilyloxy)-1,1-diphenylhexyl)lithium (**50**) (Dhara et al., 2008; Dhara & Sivaram, 2009; Dhara et al., 2009) and 2-methyl-1-oxo-1-[3-(trimethylsilyl)prop-2-yn-1-yl]oxypropan-2-yllithium (**51**) (Usuki et al., 2017a, 2017b).

Functionalized initiators:
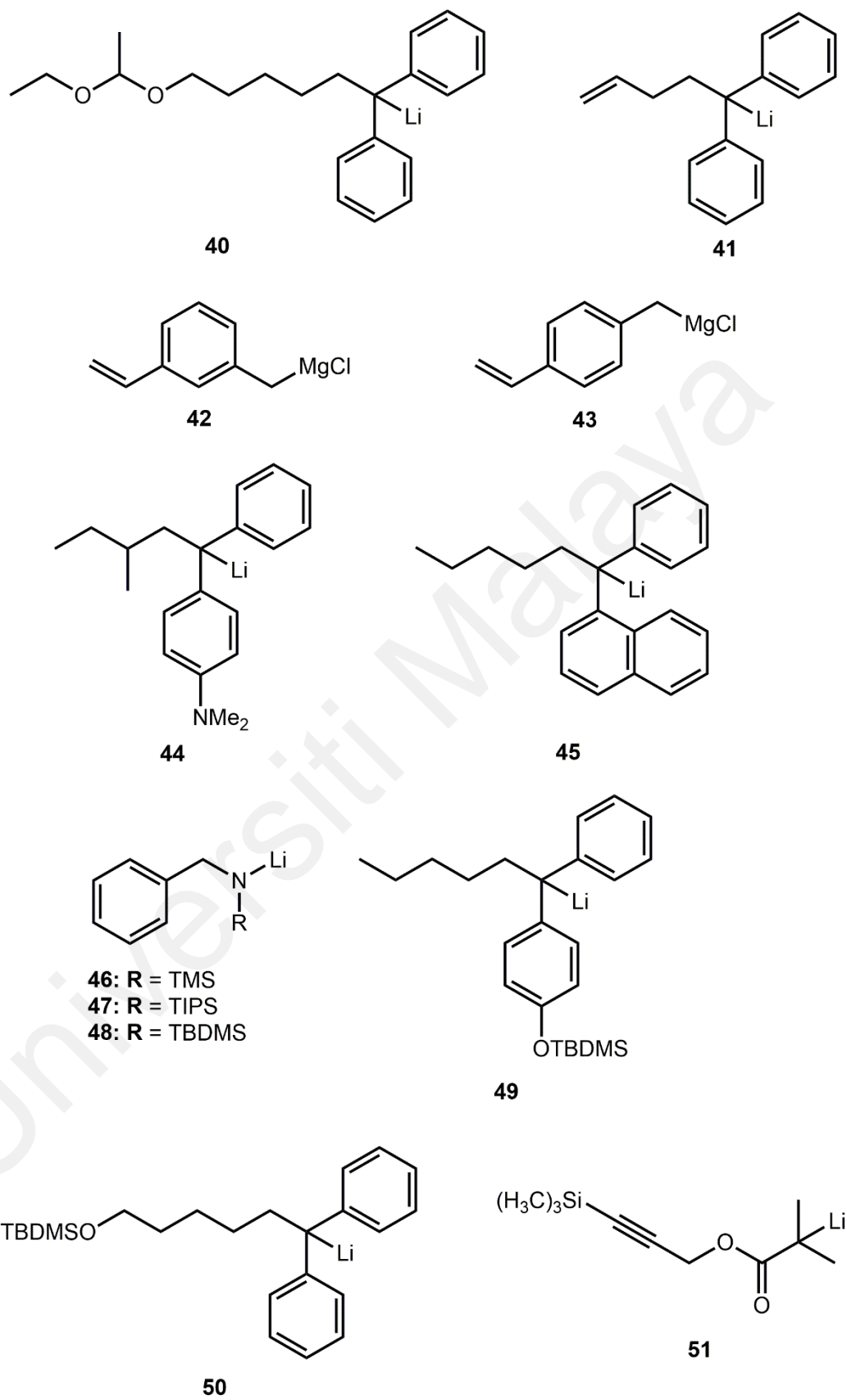
Figure 2.9: Functionalized initiators for living anionic polymerization of MMA.

On the other hand, to obtain functionalized PMMA at the ω-terminus, end capping agents with reactive sites or suitable leaving groups (**Figure 2.10**) are commonly utilized. These various include alkyl and aryl halides (**52-65**) (Al-Takrity et al., 1990b, 1990c; Anderson et al., 1981; Andrews & Melby, 1984; Hatada et al., 1989; Hirao & Matsuo, 2003; Hirao et al., 2005; Hirao et al., 2009; Ho et al., 2009; Ishizu & Fukutomi, 1989; Lazzari et al., 2001; Ling & Hogen-Esch, 2007; Matsuo et al., 2004; Park et al., 2013; Southward et al., 1998; Watanabe et al., 2006; Yoo et al., 2009), various acyl chlorides (**66-69**) (Al-Takrity et al., 1990b, 1990c; Seo et al., 2019) and other compounds with unique functionalities such as di-*tert*-butyl maleate (**70**) (Cernohous et al., 1997), ethylene oxide (**71**) (Dhara et al., 2008), ethylene glycol dimethacrylate, EGDMA (**72**) (Dhara et al., 2009), allyl methacrylate (**73**) (Dhara & Sivaram, 2009), *trans*-β-nitrostyrene (**74**) (Wang et al., 2014) as well as α-(halomethyl)acrylate esters (**75-77**) (Kohsaka et al., 2013; Kohsaka, Yamamoto, et al., 2015). The end-functionalization of living PMMA anions using these end capping agents were highly efficient and nearly quantitative with the exception of 1,4-diiodobutane (**53**) showing only 67% end capping efficiency and 1,2-bis(bromomethyl)benzene (**57**) where low termination efficiency was observed due to steric hindrance (Andrews & Melby, 1984). Other benzyl halide derivatives such as 4-(bromomethyl)benzoyl *tert*-butyl peroxide (BMtB), *tert*-butyl 4-(bromomethyl)benzoate (BMtBB) or bis[3,5-bis(bromomethyl)benzoyl] peroxide (BDBP) were also used in the termination of living PS and PI anions (Hazer et al., 1999). However, living PMMA anions appeared to not react with the terminating agents as evidenced by the same SEC chromatograms and ^{1}H NMR spectra obtained for the control and functionalized PMMA (Hazer et al., 1999).

End capping agents:

Alkyl/aryl halides:
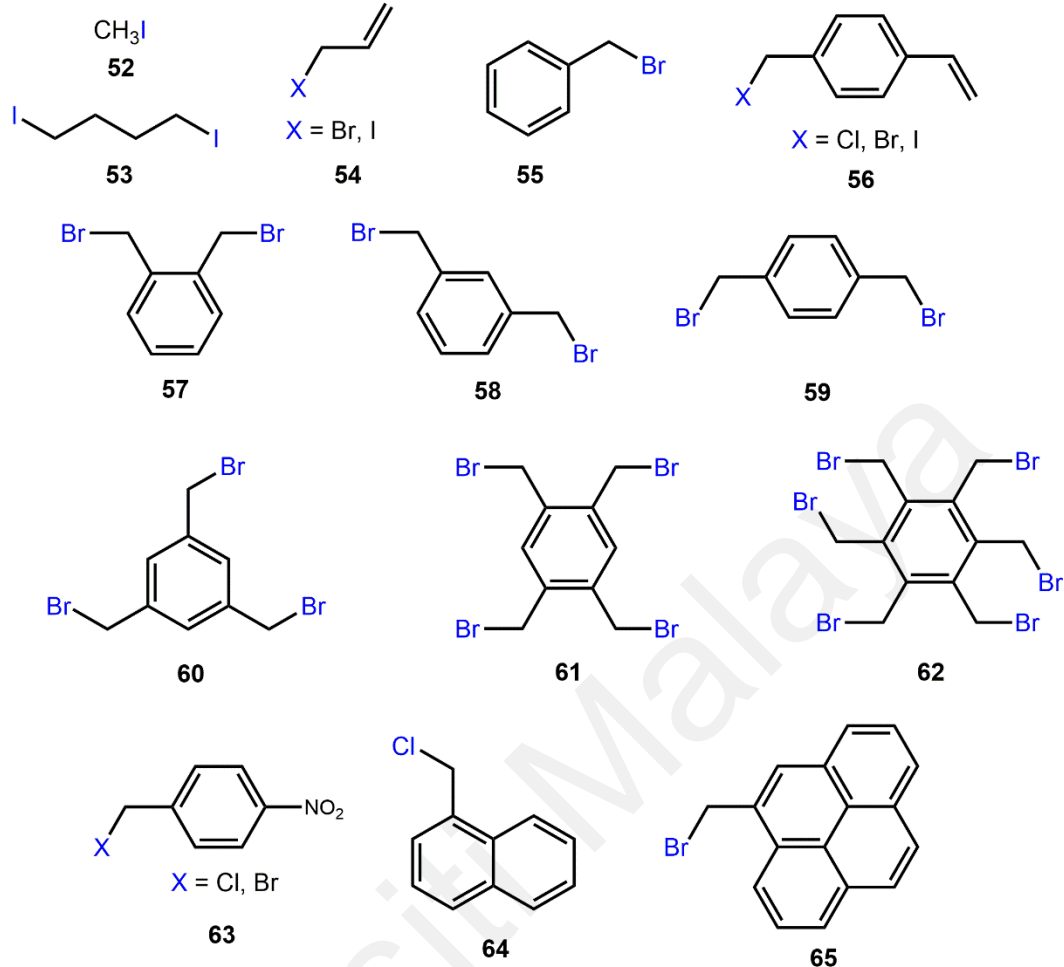
Acid chlorides:

Other end capping agents:

75: R = -CH₂CH₃
76: R = -CH₂CCH
77: R = -CH₂Cl
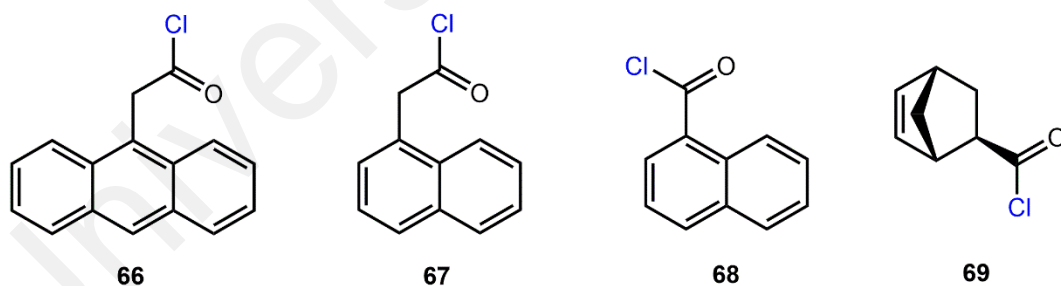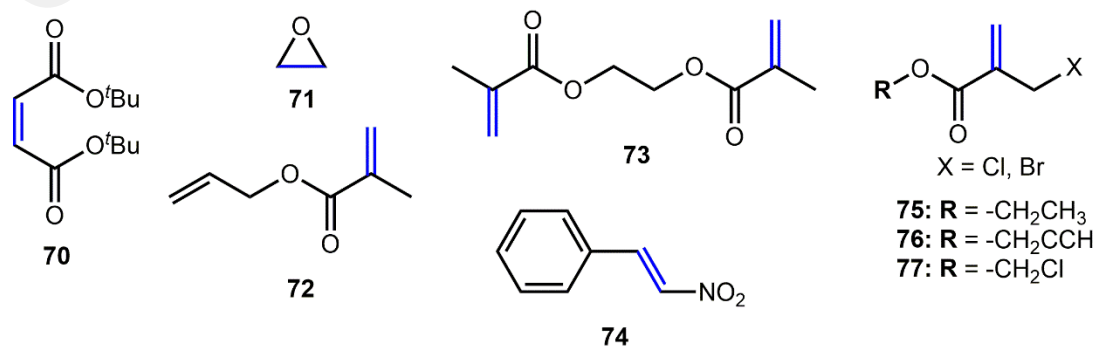
Figure 2.10: Various end capping agents for termination of propagating PMMA anions.

Direct carbanion halogenation reaction as a means of terminating the living PMMA anions is also a feasible means to obtain end-functionalized PMMA using a large excess (40 equiv. wrt initiator) of various halogenated compounds in the presence of strong Lewis bases were used as halogenating agents (**Scheme 2.6**) (Aoshima et al., 2013). SEC and ^{1}H NMR analysis revealed that firstly, the termination reaction was quantative and secondly, the polymers obtained exhibited narrow molecular weight distributions (average PDI ~ 1.1).
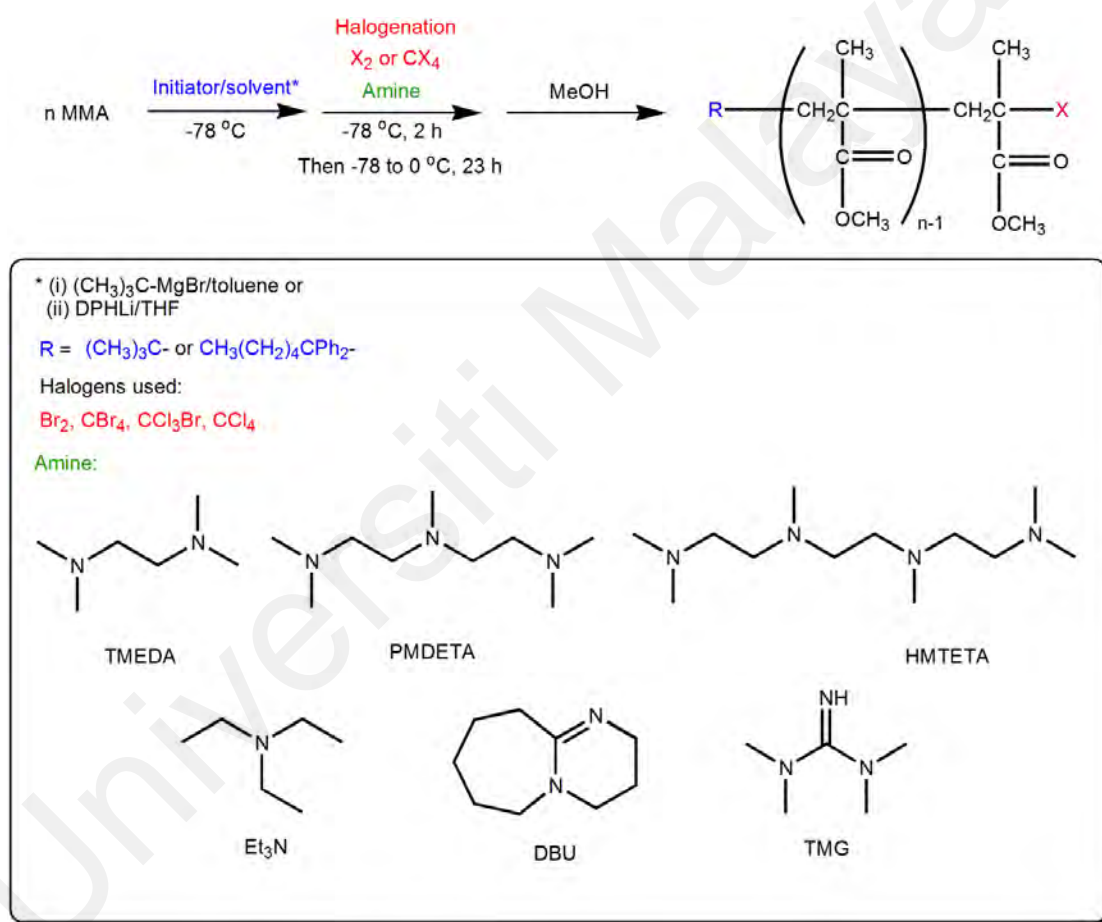
Scheme 2.6: Direct carbanion halogenation of living PMMA ends (Aoshima et al., 2013).

In many occasions, a combination of functional initiators, end capping agents and subsequent post-polymerization modifications were required to tailor PMMA of unique and interesting functionalities and architectures. One of them is synthesizing dendrimer-like star-branched polymers (DSPs) based on an iterative approach (**Figure 2.11**) (Hirao

& Matsuo, 2003; Hirao et al., 2005; Hirao et al., 2009; Matsuo et al., 2004; Watanabe et al., 2006; Yoo et al., 2009). In the synthesis of DSPs, first, living polymer chains were synthesized from a specialized initiator which contained inactive sites (colored blue). Then, the polymer chains were terminated with benzyl bromide derivatives to form a first generation DSP. These two steps are denoted by (a) in **Figure 2.11**. Subsequently, the inactive sites are converted to benzyl bromide moieties (colored red), whereby the step is denoted by (b). Steps (a) and (b) correspond to the "arm introduction" and "regeneration of the reactive site", respectively. These reaction steps were then repeated to produce higher generation DSPs.
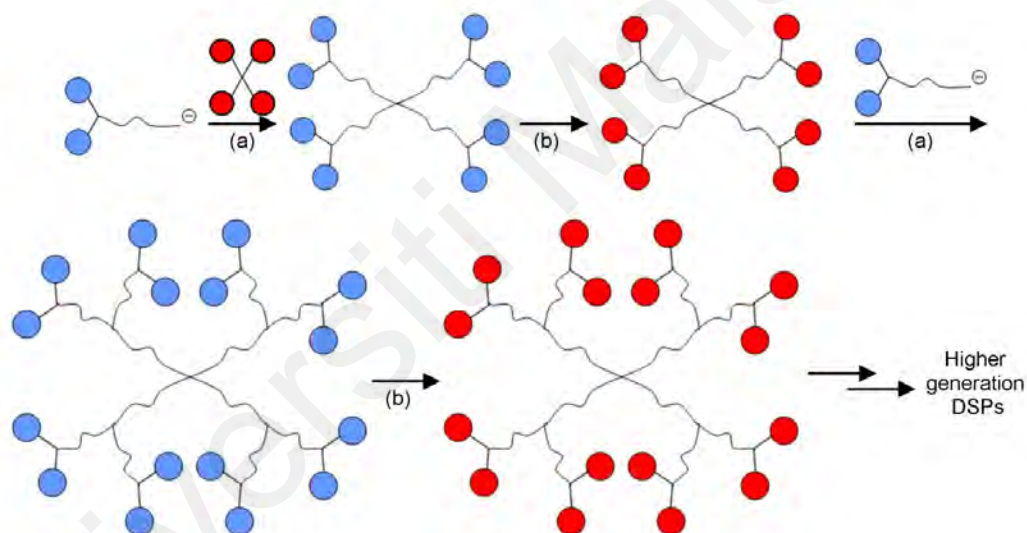
Figure 2.11: Synthetic route of DSPs based on an iterative approach (Hirao & Matsuo, 2003; Hirao et al., 2005; Hirao et al., 2009; Matsuo et al., 2004; Watanabe et al., 2006; Yoo et al., 2009). Step (a) indicates the "arm introduction" whereas step (b) refers to the "regeneration of the reactive sites.

Post-polymerization modification of end-functionalized PMMA incorporating "Click" chemistry also produced PMMA with desired functionalities. For example, the CuAAC reaction was utilized to obtain functionalized PMMA as shown in **Scheme 2.7** (Ho et al., 2009). The living PMMA anions are terminated with an excess of 1,4-bis(bromomethyl)benzene to afford a benzyl bromide end-functionalized PMMA. Then,

the synthesized polymer is converted to an azide and finally, the azide-functionalized PMMA can react with various functional alkynes *via* the copper-catalyzed acetylene-azide cyclisation (CuAAC) "click" reaction, showing quantitative conversions of the terminal ends of PMMA chains (99%).
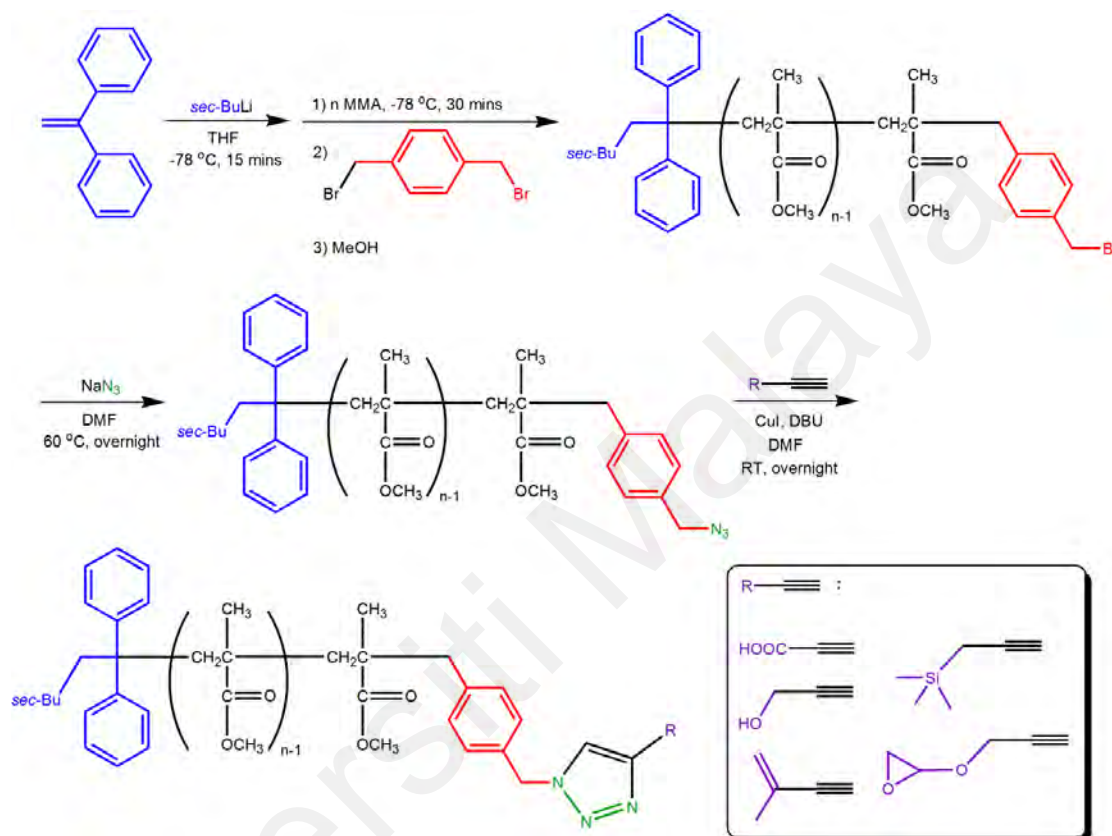
Scheme 2.7: End-functionalization of PMMA and subsequent CuAAC reactions to introduce desired functional groups (Ho et al., 2009).

Another example of combining living anionic polymerization technique and "Click" chemistry in the construction of well-defined PMMA of unique architecture is shown in **Scheme 2.8** (Park et al., 2013). Here, a well-defined A_2B miktoarm star copolymer consisting of poly(3-hexylthiophene) and PMMA are synthesized where the living PMMA chains are first terminated with 1,3,5-tris(bromomethyl)benzene to obtain a PMMA precursor. Subsequently, treatment with NaN_3 formed the active azide PMMA before finally "clicking" with an alkyne-terminated poly(3-hexylthiophene) to produce the miktoarm star copolymer with a narrow MWD (1.18).
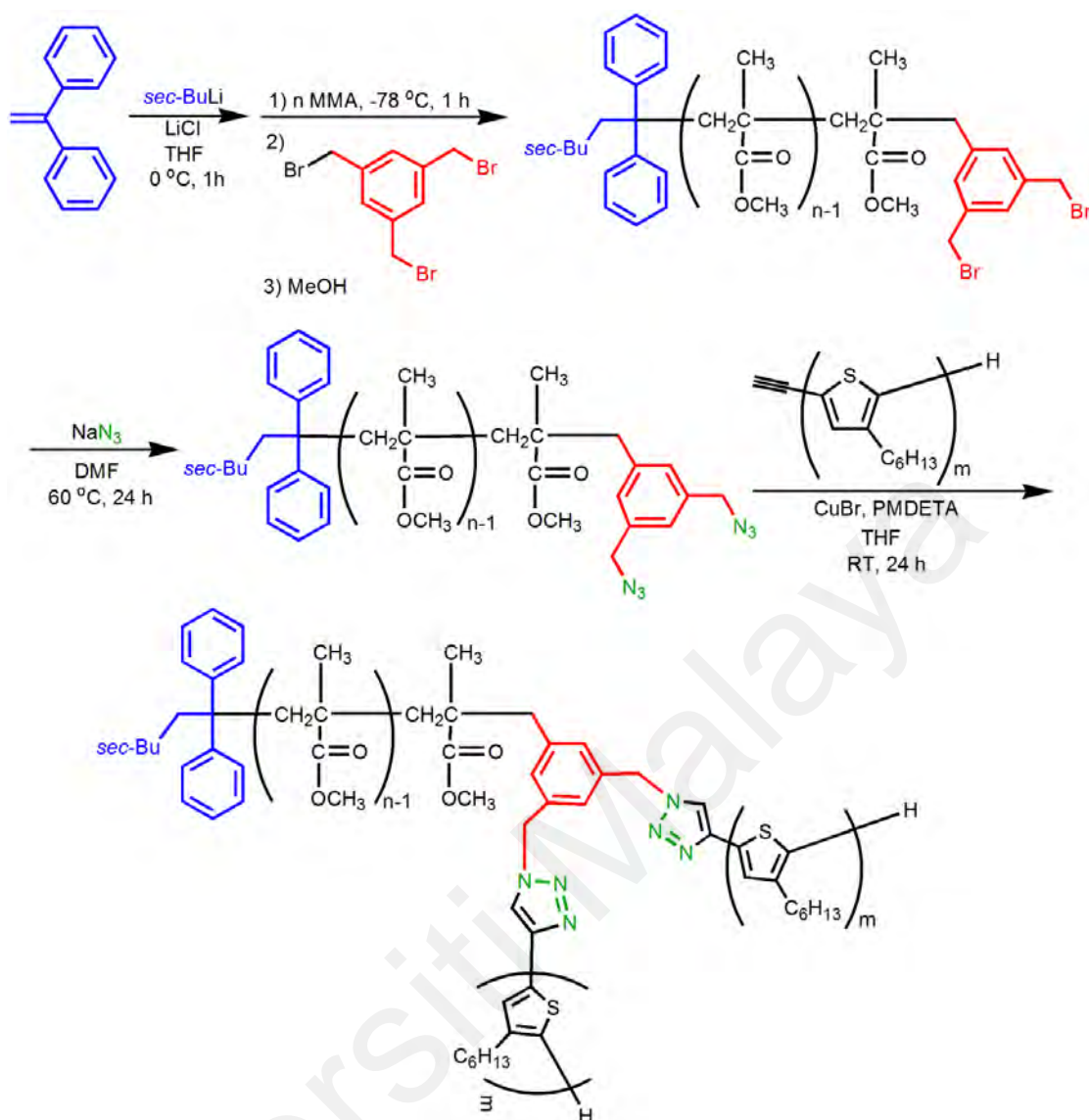
Scheme 2.8: Synthesis of A$_2$B miktoarm star copolymer (Park et al., 2013).

Successful exploitation of CuAAC "click" chemistry to produce an isotactic-*block*-syndiotactic PMMA (Usuki et al., 2017a) and a macrocyclic PMMA (Usuki et al., 2017b) again showcased the versatility of living anionic polymerization of PMMA in tailoring polymers with unique architectures. In the case of isotactic-*block*-syndiotactic PMMA (**Scheme 2.9**) (Usuki et al., 2017a), each azide- and alkyne-functionalized PMMA are synthesized separately before subsequent coupling, forming the desired block copolymer.
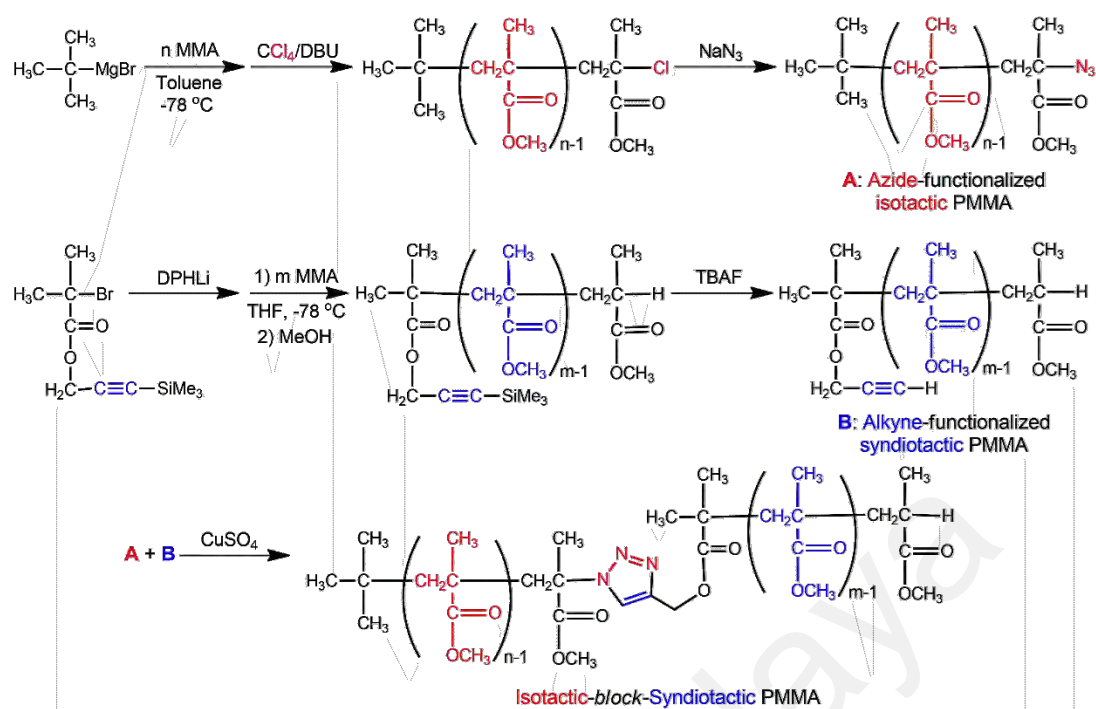
Scheme 2.9: Synthesis of isotactic-*block*-syndiotactic PMMA incorporating living anionic polymerization and CuAAC reactions (Usuki et al., 2017a).

Then, in the case of macrocyclic PMMA synthesis (**Scheme 2.10**) (Usuki et al., 2017b), initiation of polymerization with 3-(trimethylsilyl)propargyl α-lithioisobutyrate (which itself is produced from metal-halogen exchange of 3-(trimethylsilyl)propargyl α-bromoisobutyrate and DPHLi) is done to incorporate the alkyne functionality at the α-terminus of the PMMA chains before subsequent termination *via* halogenation reaction to afford halogen-terminated PMMA chains. Then, the halogen functionality is converted to the corresponding azide. Finally, the two reactive ends are then coupled to form the macrocyclic polymer.

Scheme 2.10: Synthesis of macrocyclic syndiotactic PMMA incorporating anionic polymerization and CuAAC reactions (Usuki et al., 2017b).

A clickable alkene functionality can be incorporated at the ω- end of PMMA by terminating the living PMMA chains with ethyl α-(halomethyl)acrylates (Kohsaka et al., 2013). Subsequently, the terminal alkene is reacted with various thiols to form PMMA with diverse functionalities which can be useful for many applications (**Scheme 2.11**).

Scheme 2.11: PMMA end-functionalization strategy using Click chemistry (Kohsaka et al., 2013).

A heterotelechelic α,ω-PMMA with clickable ends can be made by using either a functionalized lithium amide or a lithium enolate of ethyl 2-methylpent-4-enoate as initiators to incorporate one clickable moiety at the α- end of the polymer (Kohsaka, Kurata, et al., 2015). Then, the living polymer chains were terminated with ethyl α-(chloromethyl)acrylate as discussed previously to introduce another clickable functionality at the ω- end of the polymer. Utilizing the synthesized heterotelechelic α,ω-PMMA, they added various functionalities at both ends (**Scheme 2.12**) and even attempted to synthesized a macrocyclic PMMA by reacting two ends of the same chain together, although the latter attempt was only met with limited success.
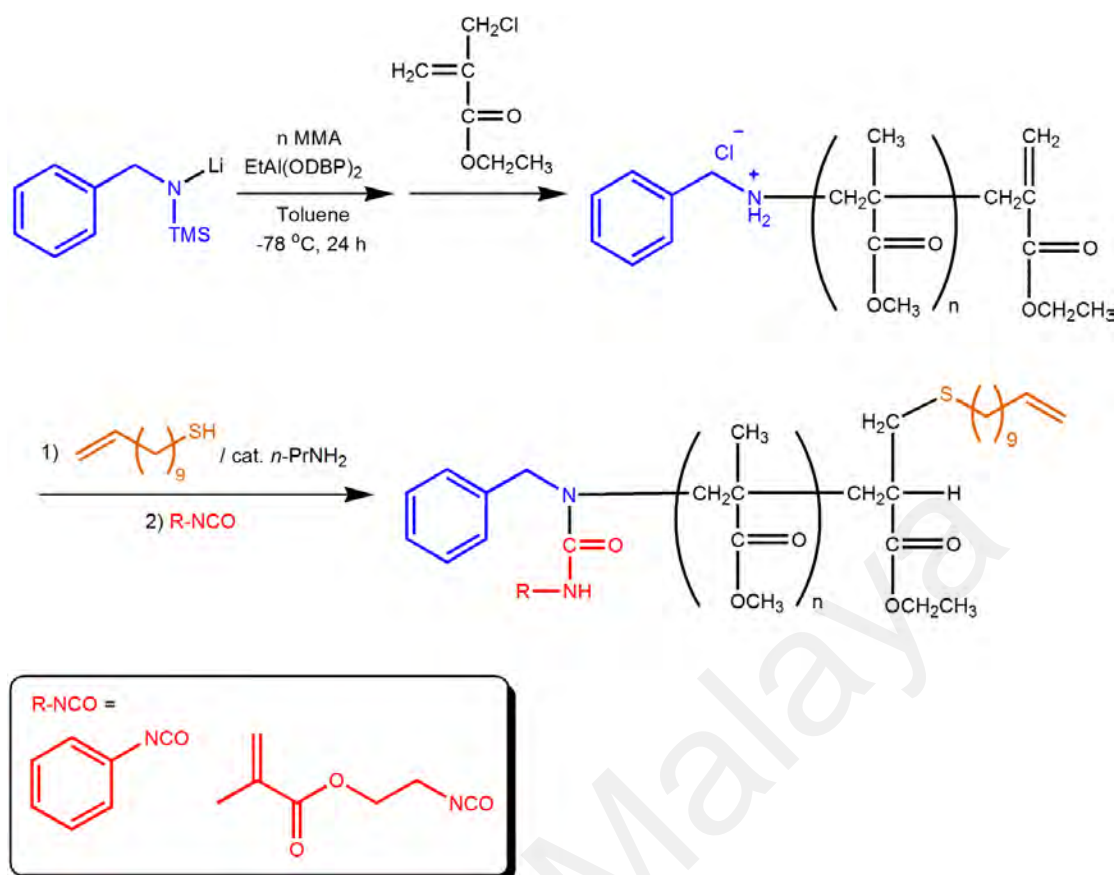
Scheme 2.12: Synthesis of various heterotelechelic α,ω-PMMA (Kohsaka, Kurata, et al., 2015).

Another example of utilization of both living anionic polymerization and click reactions to produce multi-end-functionalized PMMA at the ω- end is shown in **Scheme 2.13** (Kohsaka, Yamamoto, et al., 2015). This time, termination of PMMA anions was conducted using functionalized α-(chloromethyl)acrylates. Then, CuAAC and thiol-ene reactions were carried out to produce a number of multi-end-functionalized PMMA.
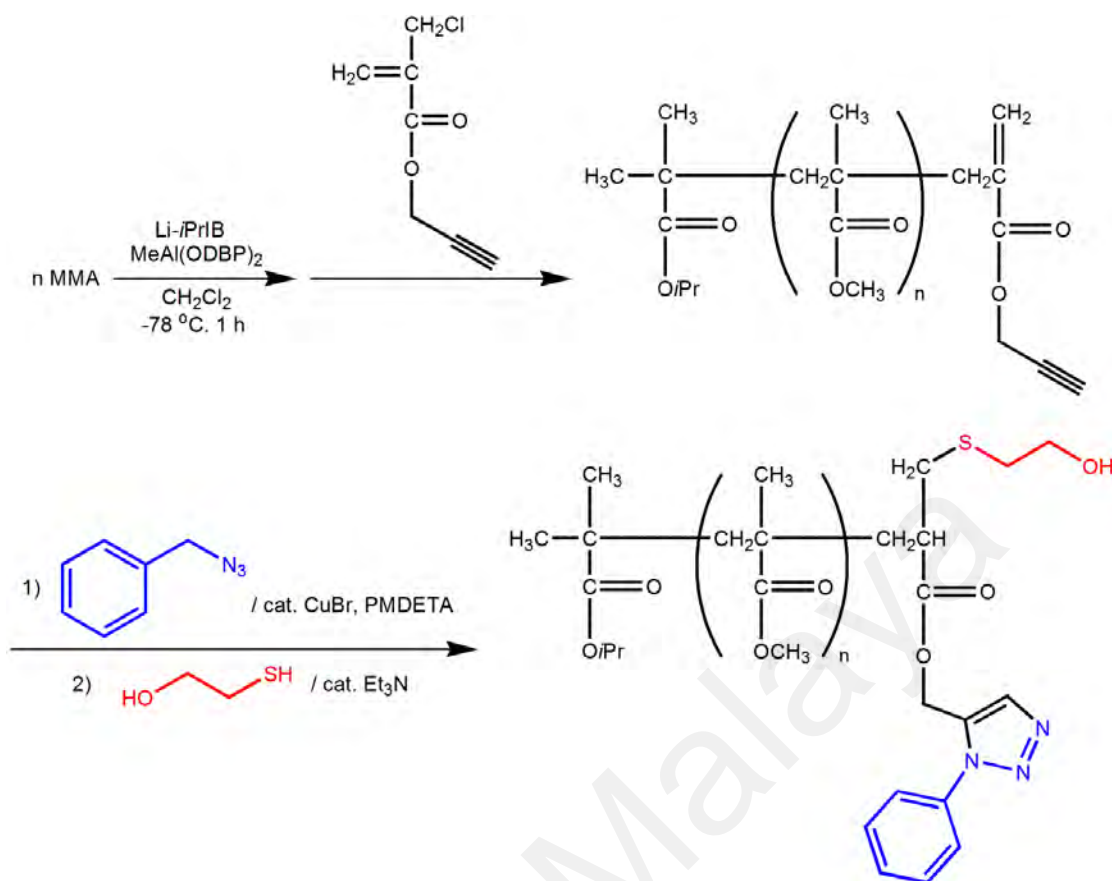
Scheme 2.13: Synthesis of multi-ω-end-functionalized PMMA (Kohsaka, Yamamoto, et al., 2015).

2.8 Concluding Remarks and Future Prospects

There are many photoresponsive surfaces which have the ability of reversible wettability/surface polarity. For photoresponsive surfaces, azobenzene derivatives are the chromophore of choice due to their clean and efficient *trans-cis* photoisomerization processes. Numerous reports showed that azobenzene-containing SAMs, LB and thin films indeed allow UV-light irradiation to dictate the polarity of surfaces *via* reversible *trans-cis* photoisomerization processes. However, to date, there are no reports on the application of these surfaces or films in overcoming the problems associated with illegal sticker advertisements.

Apart from SAMs, a careful selection of low-M_w polymer additives can also improve the surface properties to become either more hydrophilic or hydrophobic. In principle,

segregation of these additives to the surface allows researchers to change the surface properties of a particular bulk material. The most commonly used method in synthesizing end-functionalized polymer additives is by living anionic polymerization, due to the ease of inserting end groups either at the initiating end (α-end) or at the terminating end (ω-end).

The bulk of the work carried out in this thesis involves PMMA coatings. Hence, there are challenges and bottlenecks imposed in living anionic polymerization of methacrylates due to their polar nature as well as their reactive ester functional groups. Numerous reports have found unique and elegant ways of controlling the polymerization of methacrylates even at ambient temperatures. The use of commercially available t-BuOK as the initiator has given a new hope for synthetic polymer chemists to synthesize polymethacrylates of different functionalities and architectures from living anionic polymerization.

Despite many reports on the synthesis of azobenzene end-functionalized polymers, to the best of our knowledge, there are still no reports of azobenzene end-functionalized PMMA synthesized via living anionic polymerization as of now. Hence, from this review, we can propose a fabrication of a smart polymer coating by simply blending either various azobenzene derivatives or a low-M_w azobenzene end-functionalized PMMA additive to obtain the desired reversible switching in surface polarities. Furthermore, the changes in dipole moments of azobenzene derivatives by repeated isomerization process should allow changes in the chemical interactions between the surface and adhesive. As a result of these changes, the initial surface-sticker interactions should be broken apart and thus, inflicting the peeling off process of the stickers. We can then reduce the cost of fabricating functionalized polymer backbones by simply doping polymer films with azobenzene derivatives or synthesizing polymer additives instead.

CHAPTER 3: EXPERIMENTAL

3.1 Materials

All chemicals, reagents and solvents were purchased from suppliers without further purification unless otherwise stated. For the synthesis of compounds, 1,2-dibromoethane ($\geq$ 99%), 1,4-dibromobutane ($\geq$ 98%), 4-aminobenzoic acid ($\geq$ 99%), 4-chloroaniline ($\geq$ 99%), 4-ethylaniline ($\geq$ 98%), 4-hydroxycoumarin ($\geq$ 98%), aniline ($\geq$ 99%), benzophenone ($\geq$ 99%), hydrochloric acid (HCl) solution 37%, iodomethane (MeI) (stabilized with silver, $\geq$ 99%), methyl methacrylate (MMA) (stabilized, $\geq$ 99%), *p*-anisidine ($\geq$ 98%), phenol ($\geq$ 99%), potassium hydroxide (KOH) pellets, pyridine ($\geq$ 99.5%), sodium chloride (NaCl), sodium hydroxide (NaOH) pellets and styrene (stabilized, $\geq$ 99%) were purchased from Merck. 4-bromoaniline (97%), 4-iodoaniline (98%), 4-(trifluoromethyl)aniline (99%), *n*-butyllithium (*n*-BuLi) solution (1.6 M in hexanes), *p*-nitrophenol (98%), *p*-toluidine (99%) and potassium *tert*-butoxide (*t*-BuOK) solution (1.0 M in THF) were obtained from Sigma-Aldrich. 1,1-diphenylethene (1,1-DPE) (98%), 2-fluoroaniline (99%), 3-fluoroaniline (98%), 4-fluoroaniline (98%), copper(I) bromide (CuBr) (98%) and magnesium turnings (99.9%) were obtained from Acros Organics. Potassium carbonate (K_2CO_3) and sodium nitrite ($NaNO_2$) were purchased from Friendemann-Schmidt. Sulfuric acid 98% was obtained from Fisher Scientific. 7-amino-4-methylcoumarin was obtained from Exciton Inc. All chemicals are of synthesis and analytical grades unless otherwise stated. CuBr was purified by stirring in AcOH overnight under nitrogen atmosphere, then filtered, washed with EtOH and dried. 2-fluoroaniline, 3-fluoroaniline and 4-fluoroaniline were purified by distillation prior to use. Purification of *p*-anisidine was done by recrystallization from distilled water.

Drying agents sodium sulfate (Na_2SO_4) anhydrous, calcium chloride ($CaCl_2$) anhydrous were acquired from Merck. Molecular sieves 4Å beads was purchased from

Sigma-Aldrich. Sodium (Na) metal (99.8%) and calcium hydride (CaH$_2$) (93%) were acquired from Acros Organics. For compound purification, silica gel 60 F$_{254}$ coated aluminum thin layer chromatography (TLC) plates and silica gel 60 for column chromatography were procured from Merck.

Solvents used in the synthesis and purification of compounds that were obtained from Merck include benzene, chloroform (CH$_3$Cl), dichloromethane (DCM), ethyl acetate (EtOAc), *n*-hexane, methanol (MeOH), *N,N*-dimethylformamide (DMF) and tetrahydrofuran (THF). Denatured absolute ethanol (EtOH) was obtained from J. Kollin Chemicals. Glacial acetic acid (AcOH) was purchased from R&M Chemicals. Toluene was purchased from Friendemann-Schmidt. All solvents were of analytical grade. For NMR analyses, deuterochloroform (CDCl$_3$) (stabilized with silver, $\geq$ 99.8 atom % D) and deuterated dimethyl sulfoxide (DMSO-d_6) ($\geq$ 99.8 atom % D) were purchased from Merck.

For the preparation of coating binders, poly(methyl methacrylate) (PMMA) (average $M_w \sim$ 120,000 g mol^{-1} by GPC), poly(methyl vinyl ether-*alt*-maleic acid monoethyl ester) (PMVEMA-ES) solution (average $M_w \sim$ 130,000 g mol^{-1}, 50 wt. % in ethanol) were obtained from Sigma-Aldrich. Xylene (mixture of isomers, $\geq$ 98.5 %) was also obtained from Sigma-Aldrich and used as a solvent to prepare coating formulations. Glass substrates (clear glass) for the fabrication of coatings were purchased from Sail Brand, China.

3.2 Compound Characterization Methods

3.2.1 *Melting Point Analysis*

The melting points of the synthesized dyes were measured in a melting point glass capillary tube using a Laboratory Devices Inc. Mel-Temp II melting point apparatus. For known compounds, the melting points were compared with the literature values.

3.2.2 Fourier Transform Infrared (FTIR) Spectroscopy

The FTIR spectra of synthesized compounds were measured on a Perkin-Elmer ATR-400 series FTIR spectrometer using the attenuated total reflectance (ATR) mode. The spectra were recorded from 400 to 4000 cm^{-1}. All analyses and interpretations were conducted using the Perkin-Elmer Spectrum 10 software.

3.2.3 Nuclear Magnetic Resonance (NMR) Spectroscopy

The ^{1}H, ^{13}C and ^{19}F NMR spectra of the synthesized compounds were obtained using Bruker Avance III (400MHz) NMR spectrometer using CDCl$_3$ or DMSO-d_6 as solvent with tetramethylsilane as the internal standard. The coupling constant, J was reported in Hertz (Hz). All chemical shifts are reported in ppm. Multiplicity is given as follows: s = singlet, d = doublet, t = triplet, q = quartet, quint = quintet, m = multiplet, b = broad peak. All analyses and interpretations were conducted using the Bruker TopSpin (version 3.62) software.

3.3 Synthesis of Hydroxycoumarin Derivatives CAD1-9

In this section, the synthesis and characterization of hydroxycoumarin derivatives **CAD1-9** are described. In turn, **CAD1-9** were used as dyes in PMMA coating formulations.

3.3.1 3-(phenylhydrazono)-2,4-chromandione (CAD1)

CAD1 was synthesized using the azo coupling reaction between aryldiazonium salts generated from aniline and phenoxide of 4-hydroxycoumarin (4-HC). Aniline (10 mmol), HCl 37% (5 mL) and distilled water (20 mL) were mixed and cooled to 0 ºC. A solution of NaNO$_2$ (12 mmol) in distilled water (5 mL) was prepared separately and cooled to 0 ºC. The NaNO$_2$ solution was added dropwise to the acidic amine solution over 5 minutes at 0 ºC. After stirring for 30 minutes at 0 ºC, the resulting aryldiazonium salt solution was added dropwise to a solution of 4-hydroxycoumarin (10 mmol), NaOH (100 mmol) and

distilled water (20 mL) prepared earlier at 0 °C. The resulting colored mixture was stirred for 2 h at 0 °C, followed by precipitation of the product by the addition of HCl solution (5%). Then, the precipitate was collected, washed with H_2O and dried in an oven at 60 °C for 24 h. Purification of crude product was done by recrystallization from EtOH:CHCl₃ 1:1 solution to obtain **CAD1** as an orange solid (37.8%), mp. 174-180 °C [Lit: 183-184 °C (Yazdanbakhsh et al., 2007)]; FTIR (v_{max}, cm^{-1}): 3046 (Ar-**H**), 1730 (lactone **C=O**), 1593 (aromatic **C=C**); ^{1}H NMR (400 MHz, DMSO-d_6) δ = 7.35-7.41 (m, 3H, Ar-**H**), 7.53 (t, J = 7.72 Hz, 2H, Ar-**H**), 7.74-7.79 (m, 3H, Ar-**H**), 8.00 (d, J = 7.68 Hz, 2H, Ar-**H**), 13.88 (s, N-**H**, Z-isomer), 15.68 (s, N-**H**, E-isomer); ^{13}C NMR (100 MHz, DMSO-d_6) δ = 117.77, 118.30, 120.69, 123.05, 125.07, 126.83, 128.26, 130.35 (aromatic **C**), 136.82 (coumarin **C**=N-NH-C), 141.39 (phenyl **C**-NH-N=C), 154.50 (aromatic **C**-O-C=O), 158.67 (lactone **C**=O), 178.05 (**C**=O).

3.3.2 3-((p'-tolyl)hydrazono)-2,4-chromandione (CAD2)

CAD2 was successfully synthesized from *p*-toluidine and 4-hydroxycoumarin according to the method described in **Section 3.3.1** to afford a yellow solid (50.4%), mp. 184-188 °C [Lit: 192-194 °C (Yazdanbakhsh et al., 2007)]; FTIR (v_{max}, cm^{-1}): 2989 (Ar-**H**), 1738 (lactone **C=O**) 1579, (aromatic **C=C**); ^{1}H NMR (400 MHz, DMSO-d_6) δ = 2.33 (s, 3H, -C**H₃**), 7.31-7.39 (m, 4H, Ar-**H**), 7.63 (d, J = 8.28 Hz, 2H, Ar-**H**), 7.75 (td, J = 7.06, 1.00 Hz, 1H, Ar-**H**), 7.97 (dd, J = 7.78, 1.20 Hz, 1H, Ar-**H**), 13.92 (s, N-**H**, Z-isomer), 15.79 (s, N-**H**, E-isomer); ^{13}C NMR (100 MHz, DMSO-d_6) δ = 21.17 (-**C**H₃), 117.72, 118.30, 120.65, 122.51, 125.02, 126.74 (aromatic **C**), 136.66 (phenyl **C**-CH₃), 138.31 (coumarin **C**=N-NH-C), 139.07 (phenyl **C**-NH-N=C), 154.42 (aromatic **C**-O-C=O), 158.70 (lactone **C**=O), 177.83 (**C**=O).

3.3.3   3-((4'-ethylphenyl)hydrazono)-2,4-chromandione (CAD3)

CAD3 was successfully synthesized from 4-ethylaniline and 4-hydroxycoumarin according to the method described in **Section 3.3.1** to afford a brown solid (47.0%), mp. 144-148 °C; FTIR (ν_{max}, cm^{-1}): 2960 (Ar-**H**), 1730 (lactone **C=O**), 1606 (aromatic **C=C**); ^{1}H NMR (400 MHz, DMSO-d_6) δ = 1.19 (t, J = 7.52 Hz, 3H, -C**H$_3$**), 2.64 (q, J = 7.52 Hz, 2H, -C**H$_2$**-), 7.35-7.39 (m, 4H, Ar-**H**), 7.65 (d, J =8.00 Hz, 2H, Ar-**H**), 7.75 (t, J = 7.52 Hz, 1H, Ar-**H**), 7.97 (d, J = 7.68 Hz, 1H, Ar-**H**), 13.94 (s, N-**H**, Z-isomer), 15.81 (s, N-**H**, E-isomer); ^{13}C NMR (100 MHz, DMSO-d_6) δ = 15.80 (-**C**H$_3$), 28.24 (-**C**H$_2$-), 117.72, 118.40, 120.65, 122.54, 125.02, 126.74, 129.64 (aromatic **C**), 136.67 (phenyl **C**-CH$_2$CH$_3$), 139.25 (coumarin **C**=N-NH-C), 144.54 (phenyl **C**-NH-N=C), 154.42 (aromatic **C**-O-C=O), 158.71 (lactone **C**=O), 177.84 (**C**=O).

3.3.4   3-((4'-fluorophenyl)hydrazono)-2,4-chromandione (CAD4)

CAD4 was successfully synthesized from 4-fluoroaniline and 4-hydroxycoumarin according to the method described in **Section 3.3.1** to afford an orange solid (49.0%), mp. 226-230 °C; FTIR (ν_{max}, cm^{-1}): 3072 (Ar-**H**), 1737 (lactone **C=O**), 1604 (aromatic **C=C**); ^{1}H NMR (400 MHz, DMSO-d_6) δ = 7.34-7.40 (m, 4H, Ar-**H**), 7.74-7.82 (m, 3H, Ar-**H**), 7.98 (d, J = 7.24 Hz, 1H, Ar-**H**), 13.86 (s, N-**H**, Z-isomer), 15.64 (s, N-**H**, E-isomer); ^{13}C NMR (100 MHz, DMSO-d_6) δ = 117.30 (d, J = 22.9 Hz, phenyl **C**=C-F), 117.83 (aromatic **C**), 120.48 (d, J = 8.5 Hz, phenyl **C**=CH-CH=C-F), 120.70, 123.01, 125.15, 126.87 (aromatic **C**), 136.89 (coumarin **C**=N-NH-C), 138.14 (phenyl **C**-NH-N=C), 154.53 (aromatic **C**-O-C=O), 158.76 (lactone **C**=O), 161.57 (d, J = 251.7 Hz, phenyl **C**-F), 177.96 (**C**=O); ^{19}F NMR (376 MHz, DMSO-d_6) δ = −113.67 (C-**F**).

3.3.5   3-((4'-chlorophenyl)hydrazono)-2,4-chromandione (CAD5)

CAD5 was successfully synthesized from 4-chloroaniline and 4-hydroxycoumarin according to the method described in **Section 3.3.1** to afford an orange solid (56.0%), mp.

234-238 °C [Lit: 232 °C (Shawali et al., 1985)]; FTIR (ν_{max}, cm^{-1}): 3054 (Ar-**H**), 1726 (lactone **C=O**), 1624 (aromatic **C=C**); ^{1}H NMR (400 MHz, DMSO-d_6) δ = 7.35-7.41 (m, 2H, Ar-**H**), 7.57 (d, J = 8.64 Hz, 2H, Ar-**H**), 7.75-7.79 (m, 3H, Ar-**H**), 7.99 (d, J = 7.60 Hz, 1H, Ar-**H**), 13.77 (s, N-**H**, *Z*-isomer), 15.49 (s, N-**H**, *E*-isomer); ^{13}C NMR (100 MHz, DMSO-d_6) δ = 117.80, 119.96, 120.72, 123.42, 125.13, 126.90, 130.24, 132.01 (aromatic **C**), 136.92 (coumarin **C**=N-NH-C), 140.60 (phenyl **C**-NH-N=C), 154.52 (aromatic **C**-O-C=O), 158.61 (lactone **C**=O), 178.04 (**C**=O).

3.3.6   3-((4'-bromophenyl)hydrazono)-2,4-chromandione (CAD6)

CAD6 was successfully synthesized from 4-bromoaniline and 4-hydroxycoumarin according to the method described in **Section 3.3.1** to afford a yellow solid (62.0%), mp. 244-246 °C [Lit: 223-225 °C (Shawali et al., 1985)]; FTIR (ν_{max}, cm^{-1}): 3053 (Ar-**H**), 1727 (lactone **C=O**), 1624 (aromatic **C=C**); ^{1}H NMR (400 MHz, DMSO-d_6) δ = 7.35-7.41 (m, 2H, Ar-**H**), 7.71 (bs, 4H, Ar-**H**), 7.75-7.80 (m, 1H, Ar-**H**), 8.00 (d, J = 7.52 Hz, 1H, Ar-**H**), 13.76 (s, N-**H**, *Z*-isomer), 15.48 (s, N-**H**, *E*-isomer); ^{13}C NMR (100 MHz, DMSO-d_6) δ = 117.81 (phenyl **C**-Br), 120.22, 120.71, 123.52, 125.13, 126.89, 129.47, 133.47 (aromatic **C**), 136.95 (coumarin **C**=N-NH-C), 140.92 (phenyl **C**-NH-N=C), 154.53 (aromatic **C**-O-C=O), 158.61 (lactone **C**=O), 178.13 (**C**=O).

3.3.7   3-((4'-iodophenyl)hydrazono)-2,4-chromandione (CAD7)

CAD7 was successfully synthesized from 4-iodoaniline and 4-hydroxycoumarin according to the method described in **Section 3.3.1** to afford a brown solid (62.5%), mp. 155-158 °C; FTIR (ν_{max}, cm^{-1}): 2973 (Ar-**H**), 1727 (lactone **C=O**), 1574 (aromatic **C=C**); ^{1}H NMR (400 MHz, DMSO-d_6) δ = 7.35-7.41 (m, 2H, Ar-**H**), 7.56 (d, J = 8.16 Hz, 2H, Ar-**H**), 7.77 (t, J = 7.36, 1H, Ar-**H**), 7.87 (d, J = 8.32 Hz, 2H, Ar-**H**), 7.99 (d, J = 7.64 Hz, 1H, Ar-**H**), 13.75 (s, N-**H**, *Z*-isomer), 15.50 (s, N-**H**, *E*-isomer); ^{13}C NMR (100 MHz, DMSO-d_6) δ = 93.37 (phenyl **C**-I), 117.81, 120.25, 120.73, 123.48, 125.12, 126.88,

136.95 (aromatic **C**), 138.96 (coumarin **C**=N-NH-C), 141.38 (phenyl **C**-NH-N=C),

154.53 (aromatic **C**-O-C=O), 158.61 (lactone **C**=O), 178.14 (**C**=O).
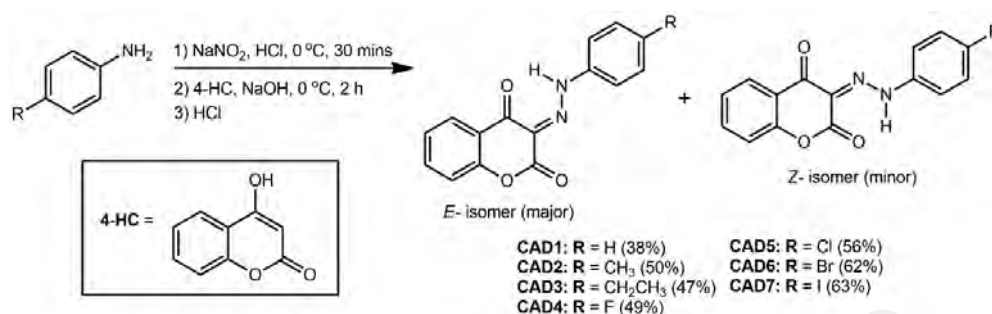
Scheme 3.1: Synthesis of **CAD1-7**.

3.3.8   7-((4'-hydroxyphenyl)azo)-4-methyl-2H-chromen-2-one (CAD8)

CAD8 was successfully synthesized from 7-amino-4-methylcoumarin and phenol

according to the method described in **Section 3.3.1** to afford a brown solid (62.5%), mp.

284-288 ºC; FTIR (v_{max}, cm^{-1}): 3219 (**O-H**), 2973 (Ar-**H**), 1675 (lactone **C=O**), 1603

(aromatic **C=C**), 1272, 1067 (**C-O-C**); ^{1}H NMR (400 MHz, DMSO-d_6) δ = 2.44 (s, 3H,

-C**H₃**), 6.43 (s, 1H, Ar-**H**), 6.95 (d, J = 8.80 Hz, 2H, Ar-**H**), 7.66 (d, J = 1.76 Hz, 1H, Ar-

H), 7.77 (dd, J = 8.44, 1.76 Hz, 1H, Ar-**H**), 7.83 (d, J = 8.80 Hz, 2H, Ar-**H**), 7.90 (d, J =

8.44 Hz, 1H, Ar-**H**); ^{13}C NMR (100 MHz, DMSO-d_6) δ = 18.61 (-**CH₃**), 109.76, 115.41,

116.60, 118.68, 121.39, 125.98, 126.84 (aromatic **C**), 145.66 (phenyl **C**-N=N-), 153.34

(coumarin **C**-N=N-), 154.03 (aromatic **C**-O-C=O), 154.23 (aromatic **C**-CH₃), 160.28

(aromatic **C**-OH), 162.30 (lactone **C**=O).
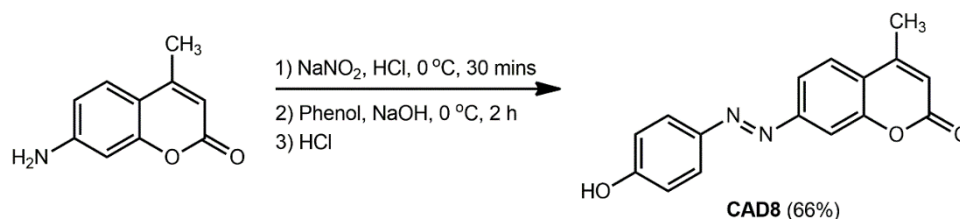
Scheme 3.2: Synthesis of **CAD8**.

3.3.9   7-((4'-methoxyphenyl)azo)-4-methyl-2H-chromen-2-one (CAD9)

CAD9 was synthesized using the Williamson ether coupling method. **CAD8** (1.0 mmol) was treated with K_2CO_3 (3.0 mmol) in 50 mL dried DMF (pre-dried over molecular sieves 4Å for 24 h, then degassed with nitrogen). After 10 minutes, 2.2 equivalents of MeI was injected into the reaction mixture with vigorous stirring at room temperature. After 24 h, the mixture was filtered and washed with a sufficient amount of EtOAc. The filtrate was then washed with distilled water (3×50 mL), followed by saturated NaCl solution (1×50 mL) and dried over anhydrous Na_2SO_4. Removal of EtOAc by vacuum distillation afforded **CAD9** as a yellow solid without any further purification (99%), mp. 140-142 ℃; FTIR (v_{max}, cm^{-1}): 2989 (Ar-**H**), 1724 (lactone **C=O**), 1597 (aromatic **C=C**), 1249, 1060 (**C-O-C**); ^{1}H NMR (400 MHz, DMSO-d_6) δ = 2.44 (s, 3H, -**CH₃**), 3.86 (s, 3H, -**OCH₃**), 6.43 (s, 1H, Ar-**H**), 7.13 (d, J = 8.97 Hz, 2H, Ar-**H**), 7.67 (d, J = 1.52 Hz, 1H, Ar-**H**), 7.78 (dd, J = 8.40, 1.52 Hz, 1H, Ar-**H**), 7.89-7.92 (m, 3H, Ar-**H**); ^{13}C NMR (100 MHz, DMSO-d_6) δ = 18.60 (-**CH₃**), 56.20 (-**OCH₃**), 109.92, 115.21, 115.54, 118.79, 121.64, 125.65, 126.93 (aromatic **C**), 146.53 (phenyl **C**-N=N-), 153.34 (coumarin **C**-N=N-), 153.98 (aromatic **C**-O-C=O), 154.06 (aromatic **C**-CH₃), 160.28 (lactone **C**=O), 163.20 (aromatic **C**-OCH₃).
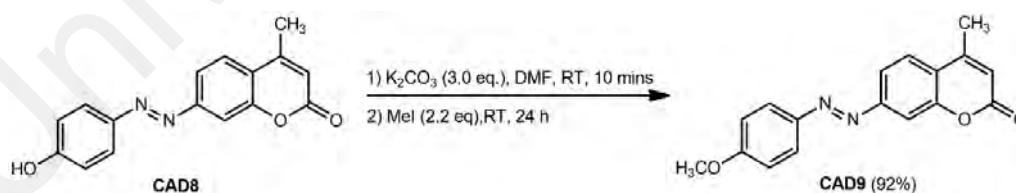
Scheme 3.3: Synthesis of **CAD9**.

3.4   Synthesis of Azobenzene Derivatives AZO1-9

In this section, the synthesis and characterization of azobenzene derivatives **AZO1-9** were described. In turn, **AZO1-9** were used as dyes in PMMA coating formulations.

3.4.1   4-hydroxy-4'-methylazobenzene (AZO1)

AZO1 was synthesized from *p*-toluidine and phenol according to the method described in **Section 3.3.1** to afford an orange solid (74%), mp. 155-158°C [Lit: 143-144°C (Haghbeen & Tan, 1998)]; FTIR (ν_{max}, cm^{-1}): 3025 (br, **O-H**), 1581 (aromatic **C=C**), 1504 (**N=N**), 1274 (**C-O**); ^{1}H NMR (400 MHz, CDCl$_3$) δ = 2.35 (s, 3H, -**CH$_3$**), 5.76 (bs, 1H, -**OH**), 6.85 (d, *J* = 7.56 Hz, 2H, Ar-**H**), 7.22 (d, *J* = 7.72 Hz, 2H, Ar-**H**), 7.71 (d, *J* = 7.44 Hz, 2H, Ar-**H**), 7.77 (d, *J* = 7.56 Hz, 2H, Ar-**H**); ^{13}C NMR (100MHz, CDCl$_3$) δ = 20.44 (-**CH$_3$**), 114.76, 121.50, 123.77, 128.70 (aromatic **C**), 139.93 (aromatic **C**-CH$_3$), 146.03, 149.67 (aromatic **C**-N=N-), 157.14 (aromatic **C**-OH).
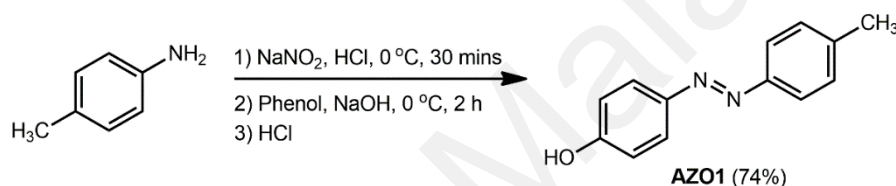
Scheme 3.4: Synthesis of **AZO1**.

3.4.2   4,4'-dimethylazobenzene (AZO2)

AZO2 was synthesized *via* oxidative aniline coupling according to a previously reported method (Zhang & Jiao, 2010). Into a suspension of CuBr (0.6 mmol) and pyridine (1.8 mmol) in toluene, *p*-toluidine (10 mmol) was added. The reaction mixture was stirred vigorously at 60°C for 24 h. The reaction was then quenched with 5% HCl solution, the organic layer separated and washed with distilled water (3×50 mL), followed by saturated NaCl solution (1×50 mL) and dried over anhydrous Na$_2$SO$_4$. Removal of solvent by vacuum distillation followed by flash chromatography over silica gel with 100% hexane as eluent afforded **AZO2** as an orange solid (48%), mp. 134-138 °C [Lit: 144-146 °C (Srinivasa et al., 2003)]; FTIR (ν_{max}, cm^{-1}): 2987 (aromatic **C-H**), 2921 (methyl **C-H**), 1598 (aromatic **C=C**); ^{1}H NMR (400 MHz, CDCl$_3$) δ = 2.35 (s, 6H, -**CH$_3$**), 7.22 (d, *J* = 7.60 Hz, 4H, Ar-**H**), 7.73 (d, *J* = 7.80 Hz, 4H, Ar-**H**); ^{13}C NMR (100MHz,

CDCl$_3$) δ = 21.49 (-**CH**$_3$), 122.74, 129.72 (aromatic **C**), 141.21 (aromatic **C**-CH$_3$), 150.85 (aromatic **C**-N=N-).

3.4.3   4,4'-di(trifluoromethyl)azobenzene (AZO3)

AZO3 was synthesized from 4-(trifluoromethyl)aniline according to the method described in **Section 3.4.2** to afford a red solid (20%), mp. 96-98 ºC [Lit: 101 ºC (Patel & Smalley, 1984)]; FTIR (ν_{max}, cm^{-1}): 2923 (aromatic **C-H**), 1611 (aromatic **C=C**), 1317 (**C-F**); ^{1}H NMR (400 MHz, CDCl$_3$) δ =, 7.81 (d, J = 8.40 Hz, 4H, Ar-**H**), 8.04 (d, J = 8.20 Hz, 4H, Ar-**H**); ^{13}C NMR (100 MHz, CDCl$_3$) δ = 122.30 (aromatic **C**), 122.78 (q, J = 270.66 Hz, -**CF**$_3$), 125.38 (q, J = 3.69 Hz, aromatic **C**=C-C-CF$_3$), 131.96 (q, J = 32.53 Hz, aromatic **C**-CF$_3$), 153.05 (aromatic **C**-N=N-); ^{19}F NMR (376 MHz, CDCl$_3$), δ = -62.66 (-C**F**$_3$).

3.4.4   2,2'-difluoroazobenzene (AZO4)

AZO4 was synthesized from 2-fluoroaniline according to the method described in **Section 3.4.2** to afford an orange solid (23%), mp. 105-106 ºC [Lit: 94-96 ºC (Leyva et al., 2004)]; FTIR (ν_{max}, cm^{-1}): 2901 (aromatic **C-H**), 1588 (aromatic **C=C**), 1215 (**C-F**); ^{1}H NMR (400 MHz, CDCl$_3$) δ = 7.21-7.30 (m, 4H, Ar-**H**), 7.45-7.50 (m, 2H, Ar-**H**), 7.80 (td, J = 7.80, 1.70 Hz, 2H, Ar-**H**); ^{13}C NMR (100 MHz, CDCl$_3$) δ = 117.08 (d, J = 19.69 Hz, aromatic **C**=C-F), 117.89 (aromatic **C**), 124.37 (d, J = 3.70 Hz, aromatic **C**=C-C-F), 133.02 (d, J = 8.49 Hz, aromatic **C**=C-C-F), 140.85 (d, J = 6.69 Hz, aromatic **C**-N=N-), 160.38 (d, J = 256.91, aromatic **C**-F); ^{19}F NMR (376 MHz, CDCl$_3$), δ = -124.17 (Ar-**F**).

3.4.5   3,3'-difluoroazobenzene (AZO5)

AZO5 was synthesized from 3-fluoroaniline according to the method described in **Section 3.4.2** to afford an orange solid (64%). mp. 70-72 ºC [Lit: 70-72 ºC (Leyva et al., 2004)]; FTIR (ν_{max}, cm^{-1}): 2974 (aromatic **C-H**), 1580 (aromatic **C=C**), 1239 (**C-F**); ^{1}H NMR (400 MHz, CDCl$_3$) δ = 7.19-7.23 (m, 2H, Ar-**H**), 7.48-7.54 (m, 2H, Ar-**H**), 7.61

(dt, J = 9.40, 2.20 Hz, 2H, Ar-**H**), 7.77 (dq, J = 7.90, 0.60 Hz, 2H, Ar-**H**); ^{13}C NMR (100 MHz, CDCl$_3$) δ = 108.13 (d, J = 22.69 Hz, aromatic **C**=C-F), 118.19 (d, J = 21.88 Hz, aromatic **C**=C-F), 120.81 (d, J = 2.92 Hz, aromatic **C**=C-C=C-F), 130.32 (d, J = 8.43 Hz, aromatic **C**=C-C-F), 153.76 (d, J = 6.91 Hz, aromatic **C**-N=N-), 163.27 (d, J = 246.43 Hz, aromatic **C**-F); ^{19}F NMR (376 MHz, CDCl$_3$), δ = -111.83 (Ar-**F**).

3.4.6   *4,4'-difluoroazobenzene (AZO6)*

AZO6 was synthesized from 2-fluoroaniline according to the method described in **Section 3.4.2** to afford a yellow solid (84%). mp. 104-106 °C [Lit: 99-100 °C (Leyva et al., 2004)]; FTIR (ν_{max}, cm^{-1}): 2910 (aromatic **C-H**), 1590 (aromatic **C=C**), 1227 (**C-F**); ^{1}H NMR (400 MHz, CDCl$_3$) δ = 7.17-7.23 (m, 4H, Ar-H), 7.90-7.95 (m, 4H, Ar-**H**); ^{13}C NMR (100 MHz, CDCl$_3$) δ = 115.01 (d, J = 22.97 Hz, aromatic **C**=C-F), 123.78 (d, J = 9.02 Hz, aromatic **C**=C-C-F), 147.94 (d, J = 2.30 Hz, aromatic **C**-N=N-), 163.34 (d, J = 250.48 Hz, aromatic **C**-F); ^{19}F NMR (376 MHz, CDCl$_3$), δ = -109.24 (Ar-**F**).
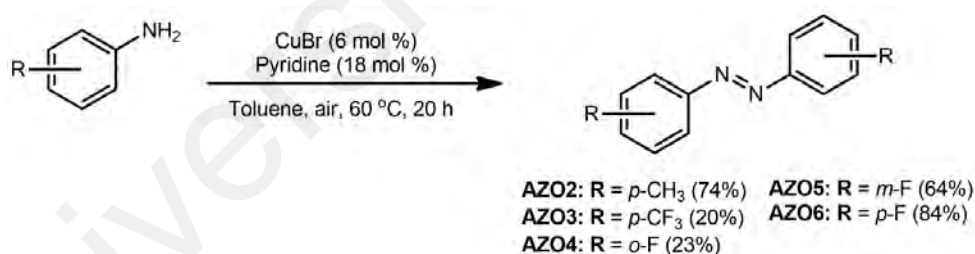
Scheme 3.5: Synthesis of **AZO2-6**.

3.4.7   *4-hydroxy-4'-(trifluoromethyl)azobenzene (AZO7)*

AZO7 was synthesized from 4-(trifluoromethyl)aniline and phenol according to the method described in **Section 3.3.1** and purified by recrystallization from toluene to afford an orange solid (52%), mp. 155-158°C [Lit: 130-132 °C (Zhang et al., 2009)]; FTIR (ν_{max}, cm^{-1}): 3186 (**O-H**), 1586 (aromatic **C=C**), 1315 (**C-F**), 1289 (**C-O**); ^{1}H NMR (400MHz, CDCl$_3$) δ = 6.90 (d, J = 8.80 Hz, 2H, Ar-**H**), 7.68 (d, J = 8.40 Hz, 2H, Ar-**H**), 7.84-7.89

(m, 4H, Ar-**H**); ^{13}C NMR (100 MHz, CDCl$_3$) δ = 114.95, 121.70 (aromatic **C**), 122.96 (q, J = 270.50 Hz, -**C**F$_3$), 124.45 (aromatic **C**), 125.23 (q, J = 3.72 Hz, aromatic **C**=C-CF$_3$), 130.65 (q, J = 32.21 Hz, aromatic **C**-CF$_3$), 145.94, 153.48 (aromatic **C**-N=N-), 157.99 (aromatic **C**-OH); ^{19}F NMR (376 MHz, CDCl$_3$) δ = −62.5 (-C**F$_3$**).
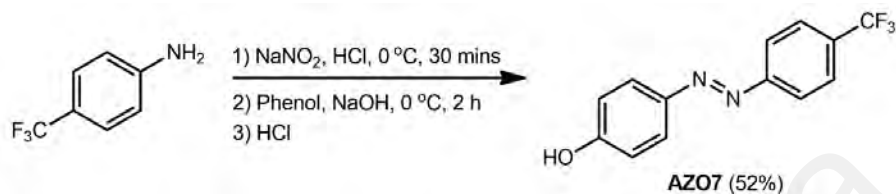
Scheme 3.6: Synthesis of **AZO7**.

3.4.8   *4,4'-dimethoxyazobenzene (AZO8)*

The diazonium salt of *p*-anisidine was coupled with phenol using the method described in **Section 3.3.1**, affording 4-hydroxy-4'-methoxyazobenzene (23%). Subsequently, **AZO8** was synthesized from 4-hydroxy-4'-methoxyazobenzene and MeI using the method described in **Section 3.3.9** to obtain a yellow solid (99%), mp. 158-160 °C [Lit: 158-160 °C (Rezaeifard et al., 2009)]; FTIR (v_{max}, cm^{-1}): 2964 (aromatic **C-H**), 1595 (aromatic **C=C**), 1242, 1021 (**C-O-C**); ^{1}H NMR (400 MHz, CDCl$_3$) δ = 3.88 (s, 6H, -OC**H$_3$**), 7.00 (d, J = 8.90 Hz, 4H, Ar-**H**), 7.88 (d, J = 8.90 Hz, 4H, Ar-**H**); ^{13}C NMR (100 MHz, CDCl$_3$) δ = 54.51 (-OCH$_3$), 113.14, 123.31 (aromatic **C**), 146.06 (aromatic **C**-N=N-), 160.54 (aromatic **C**-OCH$_3$).
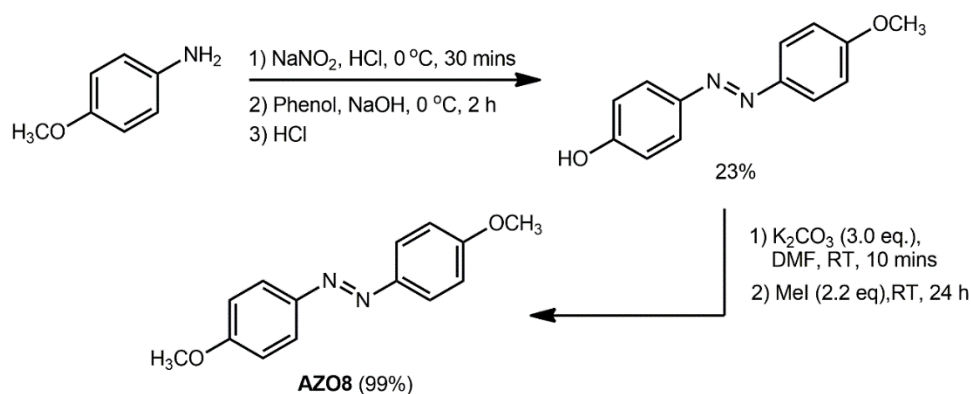
Scheme 3.7: Synthesis of **AZO8**.

3.4.9   4,4'-dihydroxyazobenzene (AZO9)

The synthesis of **AZO9** from reductive nitro coupling reaction was done according to the method described by Abbaszad Rafi et al. (2018). Into a round-bottomed flask, 4-nitrophenol (5 g), KOH (25 g) and water (6 mL) were heated together at 120 °C for 1 h. Then, the reaction temperature was slowly raised to 195-200 °C and a vigorous reaction occurred. The temperature was maintained at 195-200 °C until all bubbling have subsided and the reaction mixture turned dark brown. The reaction was cooled to room temperature and dissolved with water (50 mL) to form a dark red solution. Diluted HCl was added until the pH of the solution was about 3. Subsequrntly, the product was extracted with EtOAc (3×50 mL), followed by washing the organic layer with distilled water (3×50 mL) and then with saturated NaCl solution (1×50 mL). The washed organic layer was dried over anhydrous Na_2SO_4. Removal of EtOAc by vacuum distillation afforded **AZO9** (48%) as a yellow-brown solid without any purification, mp. 212-220 °C [Lit: 215-216 °C (Mossety-Leszczak et al., 2008)]; FTIR (ν_{max}, cm^{-1}): 2928 (broad, **O-H**), 1589 (aromatic **C=C**), 1250 (**C-O**); ^{1}H NMR (400 MHz, CDCl$_3$) δ = 6.92 (d, J = 9.00 Hz, 4H, Ar-**H**), 8.16 (d, J = 9.00 Hz, 4H, Ar-**H**); ^{13}C NMR (100 MHz, CDCl$_3$) δ = 114.84, 123.25 (aromatic **C**), 145.11 (aromatic **C**-N=N-), 158.85 (aromatic **C**-OH).
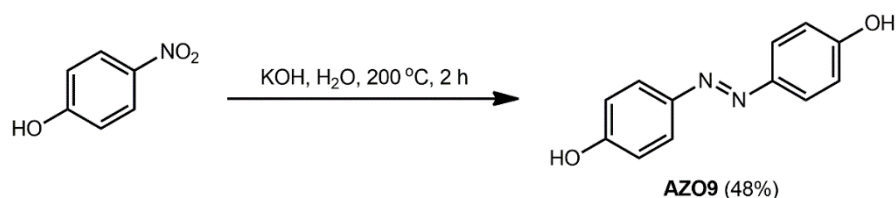
Scheme 3.8: Synthesis **of AZO9**.

3.5 Synthesis Attempts of End-Functionalized PMMA using Termination Strategies

In this section, synthesis attempts of end-functionalized PMMA using termination strategies are reported. Firstly, the synthesis and characterization of azobenzene derivatives **AZO10** and **AZO11** are described. Subsequently, **AZO10** was used as a nucleophile in an attempt to modify end-functionalized PMMA bearing bromoalkyl groups. Meanwhile, **AZO11** was used as an end capping agent in an attempt to directly terminate living PMMA enolate chains. The synthesis route for **AZO10** and **AZO11** is shown in **Scheme 3.9**.
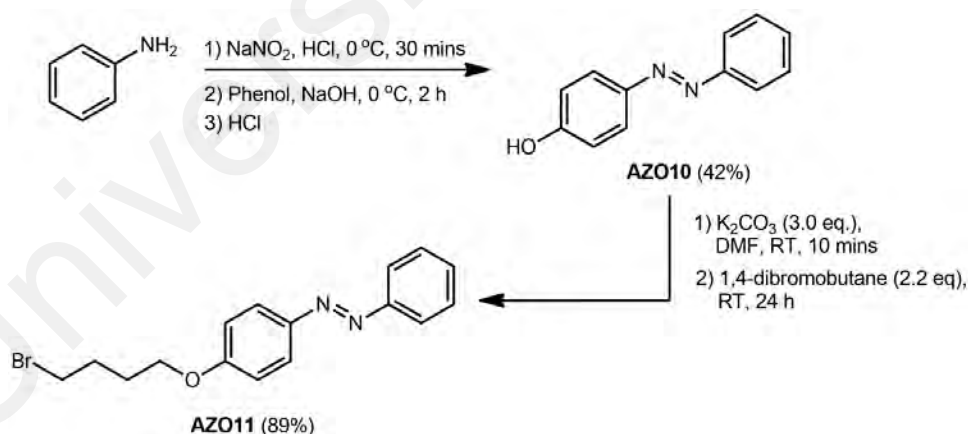
Scheme 3.9: Synthesis of **AZO10** and **AZO11**

3.5.1 Synthesis of 4-hydroxyazobenzene (AZO10)

AZO10 was synthesized from aniline and phenol according to the method described in **Section 3.3.1** to yield an orange solid (42%), mp. 158-160 °C [Lit: 152 °C (Furin et al., 1985)]; FTIR (ν_{max}, cm^{-1}): 2990 (broad, **O-H**), 1584 (aromatic **C=C**), 1274 (**C-O**); ^{1}H

NMR (400MHz, CDCl$_3$) δ = 6.96 (d, J = 8.64 Hz, 2H, Ar-**H**), 7.41 (t, J = 6.92 Hz, 1H, Ar-**H**), 7.48 (t, J = 7.36 Hz, 2H, Ar-**H**), 7.83-7.86 (m, 3H, Ar-**H**), 8.80 (s, 1H, O-**H**); ^{13}C NMR (100 MHz, CDCl$_3$) δ = 114.95, 121.42, 123.92, 127.98, 129.11 (aromatic **C**), 145.36, 151.78 (aromatic **C**-N=N-), 159.08 (aromatic **C**-OH).

3.5.2 *Synthesis of 4-(4'-bromobutoxy)azobenzene (AZO11)*

AZO11 was synthesized from **AZO10** and 1,4-dibromobutane using the method described in **Section 3.3.9** to obtain an orange solid (89%), mp. 78-80 ºC [Lit: 73-74 ºC (Jog & Gin, 2008)]; FTIR (ν_{max}, cm^{-1}): 2957 (aromatic **C-H**), 1603 (aromatic **C=C**), 1252, 1034 (**C-O-C**), 654 (**C-Br**); ^{1}H NMR (400 MHz, CDCl$_3$) δ = 1.99 (quint, J = 5.84 Hz, 2H, -C**H$_2$**-), 2.11 (quint, J = 6.56 Hz, 2H, -C**H$_2$**-), 3.51 (t, J = 6.56 Hz, 2H, -C**H$_2$**Br), 4.08 (t, J = 5.84 Hz, 2H, -OC**H$_2$**-), 7.00 (d, J = 8.88 Hz, 2H, Ar-**H**), 7.44 (t, J = 7.08 Hz, 1H, Ar-**H**), 7.50 (t, J = 7.24 Hz, 2H, Ar-**H**), 7.88 (d, J = 7.72 Hz, 2H, Ar-**H**), 7.92 (d, J = 8.84 Hz, 2H, Ar-**H**); ^{13}C NMR (100 MHz, CDCl$_3$) δ = 26.80 (-**C**H$_3$), 28.37 (-**C**H$_2$CH$_3$), 32.32 (-**C**H$_2$CH$_2$O-), 66.16 (-O**C**H$_2$-), 113.65, 121.53, 123.75, 128.01, 129.35 (aromatic **C**), 145.99, 151.72 (aromatic **C**-N=N-), 160.33 (aromatic **C**-O(CH$_2$)$_3$CH$_3$).

3.5.3 *Polymerization of Methyl Methacrylate via Living Anionic Polymerization*

Here, the synthesis attempts to obtain the desired end-functionalized PMMA bearing azobenzene moieties are described. Before any polymerization reaction was carried out, all monomers, solvents, initiators and end capping agents were purified thoroughly to remove as much moisture and impurities as possible. Styrene, methyl methacrylate, 1,2-dibromoethane, 1,4-dibromobutane and benzene were pre-dried over anhydrous CaH$_2$ overnight. Meanwhile, THF was pre-dried over Na metal with benzophenone overnight. Subsequently, all monomers, solvents and end capping agent (either 1,2-dibromoethane or 1,4-dibromobutane) were purified and dried using the freeze-pump-thaw technique at least three times using a high-vacuum line. For the case of THF, at least three freeze-

pump-thaw cycles were conducted until the Na-benzophenone ketyl indicator turned dark purple, indicating moisture and air-free solvent. After purification, all monomers and solvents were distilled freshly before use. End capping agent **AZO11** was purified using azeotropic distillation with THF to remove residual moisture. This process was repeated two more times to ensure moisture-free dye.

A special reaction vessel, known as a 'Christmas tree' (**Figure 3.1**) was used to conduct anionic polymerization reactions. The Christmas tree apparatus must be thoroughly cleaned and dried to avoid unwanted side reactions as discussed in **Section 2.5**. The reaction vessel was first rinsed thoroughly with acetone and then flame-dried. The apparatus was flushed with N_2 to remove as much air and moisture as possible before evacuation using a high-vacuum line overnight. The apparatus (still under vacuum) was sealed with a Young's tap and removed from the high-vacuum line. Then, living poly(styryl)lithium for the purpose of rinsing the inner surface of the apparatus was prepared directly inside the Christmas tree main reaction flask by distilling sufficient amounts of benzene and styrene. Subsequently, sufficient amount of *n*-BuLi initiator was injected into the reaction mixture with stirring using a gas syringe until a bright orange color persists, indicating that living poly(styryl)lithium was successfully synthesized. Next, the whole interior of the apparatus was rinsed with the living poly(styryl)lithium to remove any remaining air/moisture present. The living polymer solution was then transferred to bulb A and any remaining poly(styryl)lithium was returned to bulb A as well by distilling benzene from the polymer solution in bulb A to the main reaction vessel. The process was repeated four to five times until no traces of orange color was seen in the solvent. Finally, the polymer solution in bulb A was frozen in liquid N_2 and any remaining solvent was returned by distillation to bulb A. The apparatus was reattached to the vacuum line and evacuated until further use.
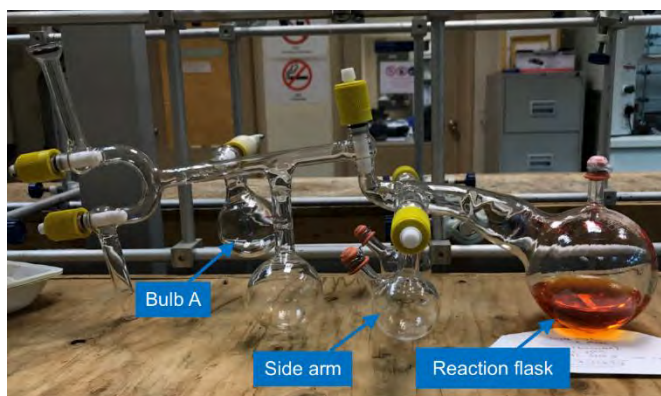
Figure 3.1: Christmas tree apparatus containing living poly(styryl)lithium solution (orange color) in the main reaction flask.

Equation 3.1 was then utilized to calculate the amount of initiator needed to produce polymers with a number-average molecular weight, M_n:

$$M_n = m/n_i \qquad (3.1)$$

where M_n = number-average molecular weight

m = mass of monomer

n_i = number of moles of initiator

The initiating solution of 1,1-diphenylhexyllithium (DPHLi) was first prepared by transferring adequate amounts of n-BuLi and equimolar DPE into the Christmas tree main reaction vessel (contains freshly distilled THF). Upon the addition of n-BuLi into 1,1-DPE solution, the solution turned dark red indicating the presence of active DPHLi species. Subsequently, the reaction vessel was cooled to −78 °C and sufficient amount of MMA was distilled slowly into the main reaction. The reaction mixture was allowed to stir for 30 minutes before termination of living polymer by injecting sufficient amounts of either 1,2-dibromoethane, 1,4-dibromobutane or **AZO11** (dissolved in THF). After the respective end capping agent was added, the reaction was continued at −78 °C for 24 h. Then, N_2-purged MeOH was injected into the reaction vessel to quench any living anionic

species. Finally, purification of PMMA was done by reprecipitation of the polymer solution in hexane, filtered using a sintered glass and dried in an oven at 60 °C for 24 h.

Synthesized PMMA end capped with either 1,2-dibromoethane or 1,4-dibromobutane (1.0 eq) was then subsequently used in the coupling of **AZO10** (2.0 eq) using the method described in **Section 3.3.9**. The synthesis attempts and predicted products are highlighted in **Scheme 3.10**.
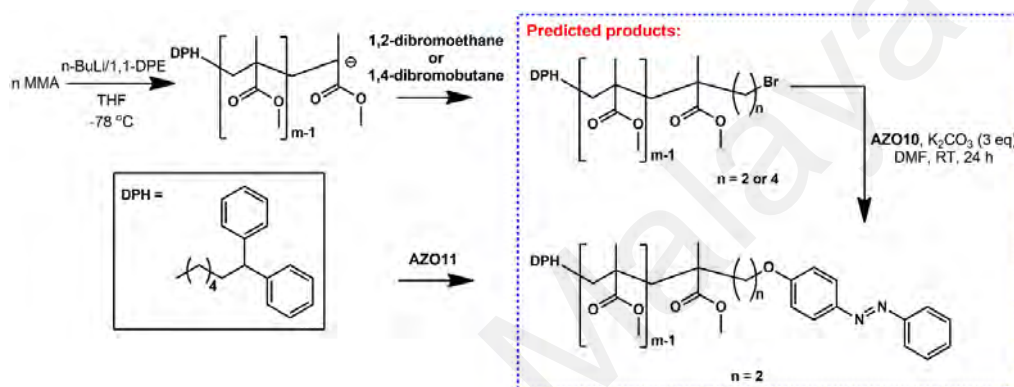
Scheme 3.10: Synthesis attempts of end-functionalized PMMA and the predicted product. Unfortunately, evidence from ^{1}H and ^{13}C NMR spectroscopy showed that these reactions failed.

3.6 Synthesis of End-Functionalized PMMA using Initiation Strategy

In this section, the synthesis of end-functionalized PMMA initiated by **I1** is described. In addition, the synthesis of **I1** and the generation of active initiator alkoxide are also reported. The synthetic route of **P1** is illustrated in **Scheme 3.11**.
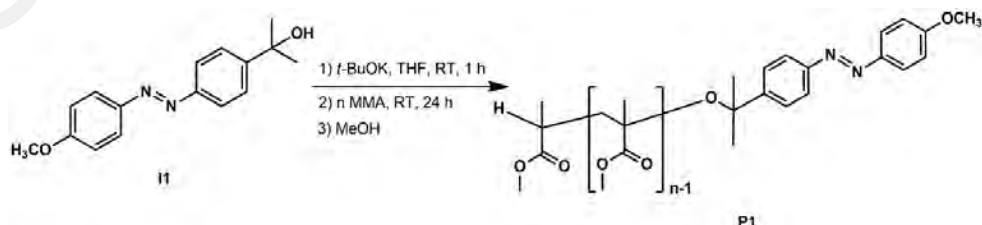
Scheme 3.11: Living anionic polymerization of MMA initiated by **I1**.

3.6.1 Synthesis of Initiator 4-(((4'-methoxyphenyl)diazenyl)phenyl)propan-2-ol, I1

Into a 500-mL round-bottomed flask, 4-aminobenzoic acid (20 g, 0.146 mol), MeOH (250 mL) and concentrated H_2SO_4 (20 mL) were refluxed for 24 h. After 24 h, excess MeOH was removed by vacuum distillation. Then, the crude product was washed with a saturated solution of K_2CO_3 until the pH of the mixture reached about 4. Then, the product was extracted with EtOAc (3×50 mL), washed with distilled water (3×100 mL) and followed by saturated NaCl solution (1×50 mL). The washed organic layer was then dried over anhydrous Na_2SO_4 before removing the solvent by vacuum distillation to obtain methyl 4-aminobenzoate (83%) without any further purification.
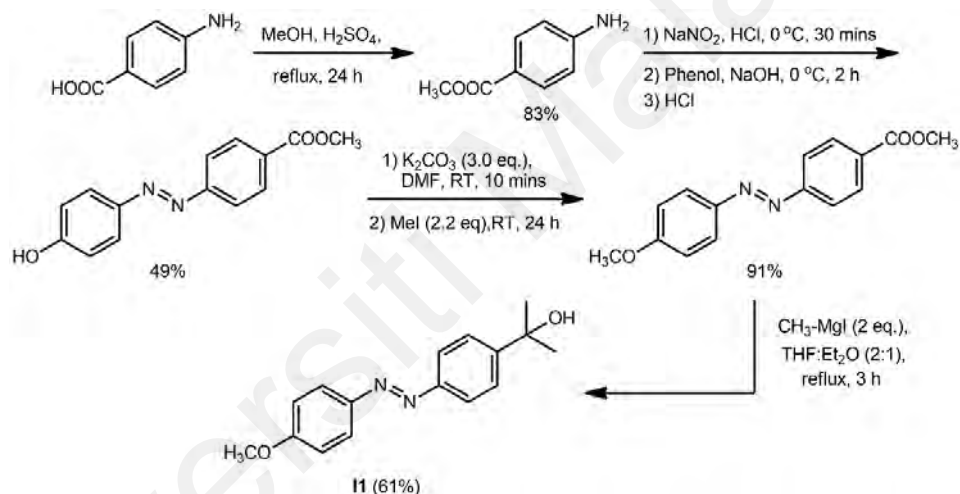
Scheme 3.12: Synthesis of **I1**.

Next, methyl 4-aminobenzoate was converted to its diazonium salt and coupled with phenol as described in **Section 3.3.1** and the crude product of this reaction was recrystallized from EtOH to give methyl 4-(4'-hydroxyphenylazo)benzoate as an orange solid (49%). Then, methyl 4-(4'-hydroxyphenylazo)benzoate was reacted with MeI using the method described in **Section 3.3.9** to give methyl 4-(4'-methoxyphenylazo)benzoate (91%) and subsequently used without further purification.

Methyl 4-(4'-methoxyphenylazo)benzoate was then converted to **I1** *via* a Grignard reaction. All glassware were flame-dried prior to reaction. Firstly, the Grignard reagent was prepared by reacting magnesium turnings (0.01875 mol) and MeI (0.02 mol, 1.25 mL) in sodium-dried diethyl ether (25 mL). The mixture was allowed to reflux gently with a CaCl₂ drying tube equipped on top of the condenser until the magnesium was completely consumed. Then methyl 4-(4'-methoxyphenylazo)benzoate (0.0075 mol), dissolved in sodium-dried THF (50 mL) was injected into the reaction vessel containing the Grignard reagent. After the addition of methyl 4-(4'-methoxyphenylazo)benzoate, the reaction mixture was allowed to reflux for 3 h. After cooling down, all of the contents were poured into crushed ice and dilute H_2SO_4 was added. The slurry was stirred for about 10 minutes to hydrolyze the magnesium adduct. Then, the crude product was extracted with EtOAc (3×50 mL). Subsequently, the organic layer was washed with distilled water (3×50 mL) and followed by saturated NaCl solution (1×50 mL). The washed organic layer was then dried over anhydrous Na_2SO_4 before concentrating the solution under vacuum. The crude product was purified using flash chromatography over silica gel using 25% EtOAc in hexane to give **I1** as an orange solid (61%), mp. 99-101 °C [Lit: 104-105 °C (Byrne et al., 1987)]. FTIR (ν_{max}, cm^{-1}): 3302 (broad, **O-H**), 2963 (aromatic **C-H**), 1599 (aromatic **C=C**), 1244, 1025 (**C-O-C**); ¹H NMR (400 MHz, CDCl₃) δ = 1.62 (s, 6H, -C**H₃**), 2.01 (bs, 1H, -O**H**), 3.88 (s, 3H, -OC**H₃**), 7.01 (d, J = 8.9 Hz, 2H, Ar-**H**), 7.61 (d, J = 8.5 Hz, 2H, Ar-**H**), 7.85 (d, J = 8.5 Hz, 2H, Ar-**H**), 7.92 (d, J = 9.0 Hz, 2H, Ar-**H**); ¹³C NMR (100 MHz, CDCl₃) δ = 30.72 (-**C**H₃), 54.56 (-O**C**H₃), 71.58 (-**C**H₂OH), 113.18, 121.39, 123.67, 124.13 (aromatic **C**), 146.04, 150.40 (aromatic **C**-N=N-), 150.53 (aromatic **C**-C(CH₃)₂CH₂OH), 160.96 (aromatic **C**-OCH₃).

3.6.2   *Preparation of Active Initiator Solution*

I1 was first purified by azeotropic distillation with THF to remove residual moisture. Subsequently, the purified dyes were left to dry under a high vacuum. Then, dried THF

(100 mL) was added into the reaction vessel to dissolve the dyes and 1.0 eq *t*-BuOK solution (1.0 M in THF) was injected into the reaction vessel. The reaction mixture was stirred under high vacuum for 1 h at room temperature to ensure complete deprotonation of alcohol group, generating the active initiator species. After the deprotonation reaction, the active initiator species was purified by distilling the solvent and residual *t*-BuOH generated under high vacuum until complete dryness. Next, fresh dried THF (100 mL) was distilled into the reaction vessel to redissolve the initiator.

3.6.3   *Polymerization of MMA via Living Anionic Polymerization*

Required amounts (calculated using equation 3.1) of purified methyl methacrylate was distilled into the reaction vessel containing the prepared initiator solution earlier and the reaction mixture was stirred for 24 h under high vacuum at room temperature. After 24 h, degassed MeOH was injected into the reaction vessel to terminate the living chain ends. Afterwards, the crude PMMA solution was concentrated by vacuum distillation and purified by reprecipitation in MeOH. The purified PMMA was then allowed to dry at 60 °C until a constant mass was achieved. The ^{1}H NMR spectrum of **P1** will be shown in **Section 4.3**.

3.7   **Preparation of Coatings**

For coating films without PMVEMA-ES additive, PMMA and either **CAD2**, **CAD9**, **AZO1-9** or **P1** were dissolved in xylene by stirring in a water bath at 60 °C until a homogeneous solution is formed (i.e. until all components dissolved completely, about 30-60 minutes). The composition of the coatings is shown in **Table 3.1**. It was noted that **CAD8** has poor solubility in xylene and hence, no coating contained **CAD8**. The prepared solutions were capped and left to cool to room temperature overnight before applying to clear glass substrates. The substrates were cleaned with detergent, followed by rinsing with distilled water. Then, they were sonicated in distilled water for 15 minutes, and then

in EtOH. Prior to the application of coating solutions, the substrates were dried by purging under the flow of N_2 gas to remove residual EtOH. The coating solutions were applied using either doctor blade or brushing method. Afterwards, the coating films were dried overnight in the open air to evaporate the solvents. The dry film thickness for all coating films were measured using a micrometer screw gauge and were found to be in the range of 30 to 40 μm. For coating films containing **P1**, thermal annealing above the T_g of the bulk polymer (105 °C) was carried out prior to water contact angle measurements and sticker peel-off test. This was done by placing the coating films in an oven at 120 °C for 1 to 10 hours. As a result, it is expected that **P1** would segregate spontaneously to the surface (Hardman et al., 2011; Hutchings et al., 2011; Sarih, 2010).

Table 3.1: Composition of PMMA coating formulations*

Coating	Dye	Binder
PMMA	-	
PMMA/**CAD2**(5)	**CAD2**	
PMMA/**CAD9**(5)	**CAD9**	
PMMA/**AZO1**(0.04)		
PMMA/**AZO1**(5)		
PMMA/**AZO1**(13)	**AZO1**	
PMMA/**AZO1**(33)		
PMMA/**AZO1**(50)		
PMMA/**AZO2**(5)	**AZO2**	
PMMA/**AZO2**(13)		
PMMA/**AZO3**(5)	**AZO3**	PMMA
PMMA/**AZO4**(5)	**AZO4**	(20 wt. % solution
PMMA/**AZO5**(5)	**AZO5**	in xylene)
PMMA/**AZO6**(5)		
PMMA/**AZO6**(13)	**AZO6**	
PMMA/**AZO6**(20)		
PMMA/**AZO7**(5)	**AZO7**	
PMMA/**AZO8**(5)	**AZO8**	
PMMA/**AZO9**(5)	**AZO9**	
PMMA/**P1**(5)	**P1**	

* The nomenclature of coating films is as follows: PMMA stands for the bulk polymer or binder, followed by the type of dyes and finally, the number in parenthesis represents the weight percent (wt. %) of dyes in dry film.

To prepare binder containing PMVEMA-ES additive, the binder was prepared by first dissolving PMMA with xylene until the solution contains 25 wt. % of PMMA. To ensure homogeneity, the solution was stirred using magnetic stirrer in the water bath at 65 ºC until PMMA was completely dissolved. Then, the PMMA solution (25 wt. % in xylene) was mixed together with PMVEMA-ES solution at a ratio of 19:1. To ensure complete mixing, the mixture was stirred at about 120 ºC until it became a clear and homogeneous solution. After that, the mixture was left to cool at room temperature under continuous stirring. This resulting solution is named as PMMA/PMVEMA-ES (19:1 solution in xylene). When this coating solution was applied onto a glass substrate, the dry film contained about 10 wt. % PMVEMA-ES. Dyes were then mixed together with the binder at appropriate ratios where the composition of the prepared coating films is shown in **Table 3.2**. The coating solutions were applied by brushing onto the glass substrates. Afterwards, the coating films were dried overnight in the open air to let the solvents evaporate. The dry film thickness for all coating films were measured using a micrometer screw gauge and were found to be in the range of 70 to 90 μm.

Table 3.2: Composition of PMMA/PMVEMA-ES coating formulations*

Coating	Dye	Binder
PMMA/PMVEMA-ES	-	
PMMA/PMVEMA-ES/**CAD1**(0.03)	**CAD1**	
PMMA/PMVEMA-ES/**CAD2**(0.03)	**CAD2**	
PMMA/PMVEMA-ES/**CAD3**(0.03)	**CAD3**	
PMMA/PMVEMA-ES/**CAD4**(0.03)	**CAD4**	PMMA/PMVEMA-ES (19:1 solution in xylene)
PMMA/PMVEMA-ES/**CAD5**(0.03)	**CAD5**	
PMMA/PMVEMA-ES/**CAD6**(0.03)	**CAD6**	
PMMA/PMVEMA-ES/**CAD7**(0.03)	**CAD7**	
PMMA/PMVEMA-ES/**AZO1**(0.04) PMMA/PMVEMA-ES/**AZO1**(13)	**AZO1**	

* The nomenclature of coating films is as follows: PMMA stands for the bulk polymer or binder, followed by the type of dyes and finally, the number in parenthesis represents the weight percent (wt. %) of dyes in dry film.

3.8 Instrumentation and Coating Characterization Methods

3.8.1 UV-Vis E-/Z- Kinetic Studies

The UV-Vis absorption spectra of selected compounds (**CAD2**, **CAD8** and **CAD9**) were measured from 300 to 600 nm using a Cary 60 UV-Vis spectrometer at a scan rate of 600 points per second. The spectra were recorded in a 1.0 cm quartz cuvette at 25 °C unless stated otherwise. The results are presented in terms of absorbance (A) against wavelength.

The *E-/Z-* isomerization kinetics of **CAD2**, **CAD8** and **CAD9** in different solvents were also studied. In addition, the *E-/Z-* isomerization kinetics of PMMA/**AZO1**(0.04) and PMMA/PMVEMA-ES/**AZO1**(0.04) coating films at different temperatures were also investigated. Since the samples have absorption peaks at the UV-A region, they were irradiated with UV light (λ_{max} = 365 nm) using a 5V USB cable equipped with an EOLD 365-525 365 nm UV-A LED for *E-/Z-* photoisomerization. Meanwhile, the samples were either kept in the dark or irradiated with white light using a 5V USB cable equipped with a white LED for *Z-/E-* isomerization. The experimental data were then fitted with equation 3.2:

$$A(t) = (A_0 - A_{PSS})\exp(-kt) + A_{PSS} \qquad (3.2)$$

where A_0 and A_{PSS} are the initial absorbance and absorbance at the photostationary state (PSS), respectively, k is the rate constant and t corresponds to time. Additionally, the fraction of *Z-* isomers during PSS, α_Z at 25 °C was calculated using equation 3.3:

$$\alpha_Z = (A_0 - A_{PSS})/A_0 \qquad (3.3)$$

For PMMA/**AZO1**(0.04) and PMMA/PMVEMA-ES/**AZO1**(0.04) systems, the activation energy of isomerization, E_a was determined using the Arrhenius equation (equation 3.4):

$$\ln k = -Ea/RT + \ln A \qquad (3.4)$$

where R is the universal gas constant (8.314 J mol^{-1} K^{-1}), T is the temperature and A is the pre-exponential factor. Additionally, other thermodynamic parameters such as enthalpy of activation, $\Delta H^{\ddagger}$, and entropy of activation, $\Delta S^{\ddagger}$ were determined from the Eyring equation (equation 3.5):

$$-\ln (k/T) = - \Delta H^{\ddagger}/RT + \Delta S^{\ddagger}/R + \ln(k_B/h) \qquad (3.5)$$

where k_B is the Boltzmann constant and h is the Planck's constant.

3.8.2 Cross-Hatch Adhesion Test

To investigate the capability of PMVEMA-ES as an adhesion promoter, the adhesive strength of PMMA, PMMA/PMVEMA-ES and PMMA/PMVEMA-ES/**CAD1-7**(0.03) coating films on glass surfaces was assessed from ASTM D3359 procedure. The coating surfaces were scratched in a lattice pattern using a six-bladed knife with 1 mm width between the blades. Subsequently, a Scotch masking tape was applied on top of the scratch marks and then it was peeled off. The scratch marks were later compared with ASTM D3359 standard classification.

3.8.3 Thermogravimetric Analysis (TGA)

TGA was carried out using a Perkin-Elmer TGA4000 thermogravimetric analyzer to investigate the effect of intermolecular hydrogen bonding interactions on the thermal properties of the prepared coating films. About 10 mg of selected samples (PMMA, PMMA/PMVEMA-ES, **CAD2**, PMMA/**CAD2**(5) and PMMA/PMVEMA-ES/**CAD2**(0.03)) were heated from 30 to 1000 $^{\circ}$C at a heating rate of 10 $^{\circ}$C min^{-1} under nitrogen atmosphere. The onset degradation temperature (T_o) was defined as the 1% weight loss drawn from the TGA thermograms at which the samples begin to degrade. At this point, a deflection was observed from the established baseline before the thermal

event. The maximum thermal degradation temperature (T_{max}) was also obtained from the derivative thermogravimetry (DTG) peaks minima.

3.8.4 Differential Scanning Calorimetry (DSC)

DSC measurements were performed using a TA Instruments DSC Q20 differential scanning calorimeter to unravel the effect of intermolecular hydrogen bonding interactions on the thermal properties of the prepared coatings at a nitrogen flow rate of 20 mL min^{-1}. About 5-10 mg of selected samples (PMMA, PMMA/PMVEMA-ES, **CAD2**, PMMA/**CAD2**(5), PMMA/PMVEMA-ES/**CAD2**(0.03), PMMA/**AZO1**(5) and PMMA/**AZO2**(5)) were first heated to 150 °C to remove any remaining solvent and moisture as well as to erase the thermal history (1st scan). Then, they were cooled to −50 °C and then reheated to 200 °C at a rate of 10 °C min^{-1} (2nd scan). Glass transition and melting temperatures, indicated as T_g and T_m, respectively, were determined from the second heating scans. T_g was defined as the inflection point of the heat flow curve whereas T_m was defined as the temperature at the peak apex.

3.8.5 Gloss Measurements

Gloss is defined as the amount of the light reflected on the surface of a coating. The glossiness of selected coating films was measured using a Novo Dual Glossmeter at angles of 20° and 60°, respectively. The coating films glossiness were analyzed to investigate the effects brought upon by the added dyes and additives to the surface of the prepared coatings. In addition, changes in gloss measuremens during the *E-/Z-* and *Z-/E-* isomerization processes of **AZO1** in PMMA and PMMA/PMVEMA-ES coating films were also recorded.

3.8.6 Contact Angle Measurements

Static contact angle measurements were conducted using Krüss G23 goniometer with deionised water as the contacting liquid at room temperature. At least three separate

measurements were made for each data point. E-/Z- (*trans→cis*) photoisomerization kinetics of PMMA/chromophore coating films were conducted by irradiating them with UV-A light (300-400 nm, λ_{max} = 365 nm, 20W) using a Toki T8/20W UV lamp in a dark photo box at room temperature. The distance between the UV lamp and the samples were kept constant at 10 cm. The contact angles of samples were then measured with respect to the irradiation time until a plateau of contact angles was observed, signifying that the samples have reached a photostationary state (PSS). Upon reaching the PSS, the coating films were then kept in dark conditions for the thermal Z-/E- (*cis→trans*) isomerization kinetic studies where the contact angles were recorded with respect to the relaxation time until a plateau of contact angles was noticed. For the isomerization kinetic studies, the contact angles were measured at 10-60 minutes intervals. In addition, all measurements were carried out within 60 seconds to minimise the exposure of chromophores to ambient light. The experimental setup is shown in **Figure 3.2**. Then, the relationship between contact angle values against time is correlated using equation 3.6:

$$\theta(t) = (\theta_0 - \theta_{PSS})\exp(-kt) + \theta_{PSS} \qquad (3.6)$$

where θ_0 and θ_{PSS} are the initial contact angle and contact angle at the photostationary state (PSS), respectively.
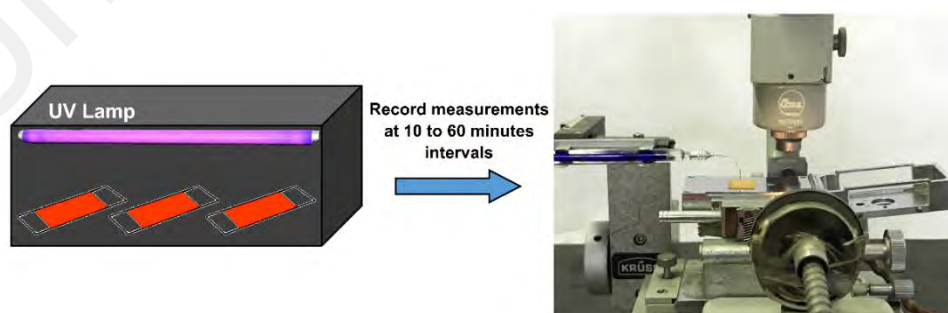
Figure 3.2: Schematic diagram of isomerization kinetic studies using contact angle measurements. Note that the distance between the lamp and the samples was 10 cm.

3.8.7   *Sticker Peel-Off Test*

Commercial acrylic-based pressure-sensitive stickers (about 1 cm × 1 cm squares) were applied to the selected coating films. Then, the backside of the prepared coating films (i.e. the side which was not in contact with the adhesive) was irradiated first with UV-A light (365 nm) for 12 hours using a Toki T8/20W UV lamp, with the same setup as shown in **Figure 3.2**. After 12 hours of irradiation, the UV lamp was switched off as the samples were allowed to undergo thermal isomerization in dark conditions for another 12 hours. These processes were repeated for 14 days. The extent of sticker peeling off was calculated by recording the area of sticker that has peeled off from the surface. The part where the sticker remained unpeeled on the surface appeared to be darker than other parts of the surface.

CHAPTER 4: RESULTS AND DISCUSSION

In this chapter, we will discuss firstly, the application of hydroxycoumarin dyes (**CAD1-9**) as photoswitchable additives in PMMA-based coating films for reversible surface polarities (**Section 4.1**). Since **CAD1-7** exhibited azo-hydrazone tautomerism and predominantly exist as the hydrazone tautomer, it is of great interest to determine their suitability as photoswitchable additives. The results were then compared to **CAD8-9**, which predominantly exist as the azo tautomer, showing reversible *trans-cis* isomerization processes. Next, in **Section 4.1.2**, PMVEMA-ES was used as an adhesion enhancer to overcome the low adhesion ability of PMMA onto polar substrates such as glass. Various studies were conducted to study the effect of PMVEMA-ES and **CAD1-9** on the adhesion strength of PMMA coating film onto glass substrates.

In **Section 4.2**, the azobenzene derivatives **AZO1-9** were used as photoswitchable additives. The effect of strong electron-donating substituents on the *trans-cis* isomerization processes of azobenzene derivatives is explained in detail (**AZO1** vs **AZO2**). Subsequently, other PMMA/azobenzene blends as coating films were fabricated to further elucidate the trends in the water contact angle measurements shown by **AZO1** and **AZO2**. Furthermore, PMVEMA-ES was again utilized as an adhesion enhancer. The *E-/Z-* and *Z-/E-* isomerization kinetics of **AZO1** in PMMA and PMMA/PMVEMA-ES matrices were compared, in addition to sticker peel-off tests using commercial acrylic-based pressure-sensitive stickers.

Finally, the synthesis and application of azobenzene end-functionalized PMMA, **P1** are discussed in **Section 4.3**. The importance of thermal annealing of coating films is highlighted here, with contact angle measurements and sticker peel-off tests compared with the unannealed coating films.

4.1 Hydroxycoumarin Dyes as Photoswitchable Additives in PMMA Coating Films for Reversible Surface Polarity

4.1.1 Synthesis and Structure of Hydroxycoumarin Dyes

CAD1-7 were successfully synthesized using the well-known azo coupling reaction. The diazonium derivatives of anilines were coupled with 4-hydroxycoumarin to yield **CAD1-7** with moderate yields (38-63% after purification).

An indication to the successful conversion of 4-hydroxycoumarin into the corresponding azo dyes is the disappearance of a singlet peak at $\delta = 5.60$ ppm (**Appendix A.1**). This peak indicates the presence of a proton attached to the C3 position of the coumarin moiety. Their ^{1}H NMR spectra have indicated the disappearance of this peak for all synthesized compounds (**Appendices A.2, 4, 6, 8, 11, 13** and **15**), ergo showing the successful conversion of 4-hydroxycoumarin into **CAD1-7**.

Upon a closer look at the downfield-most region, it is found that there are two singlets: one within the range of $\delta = 13.75\text{-}13.94$ ppm and another within the range of $\delta = 15.48\text{-}15.81$ ppm with a significantly higher intensity than the peak mentioned before (**Appendices A.2, 4, 6, 8, 11, 13** and **15**). It is also discovered that the sum of integration of these two peaks is unity. These two peaks have indicated that **CAD1-7** underwent azo-hydrazone tautomerization reactions in solution (Metwally et al., 2012; Shawali et al., 1985). If **CAD1-7** are predominantly the azo tautomer, it is expected that a singlet representing the O-H proton is present at around $\delta = 12.53$ ppm (from 4-hydroxycoumarin ^{1}H NMR spectrum, **Appendix A.1**). The presence of two singlets of the lower field have indicated that the proton is attached to the N atom instead of O. Thus, it is suggested that **CAD1-7** are predominantly the hydrazone tautomer.

An additional assessment should be carried out to confirm the singlets representing the hydrazone tautomer extrapolated from the NMR spectra. Therefore, a closer examination

of the molecular structure of **CAD1-7** have indicated that their hydrazone tautomers could possibly exist as two geometrical isomers, which are the *E-* and *Z-* isomers, as illustrated in **Figure 4.1**.
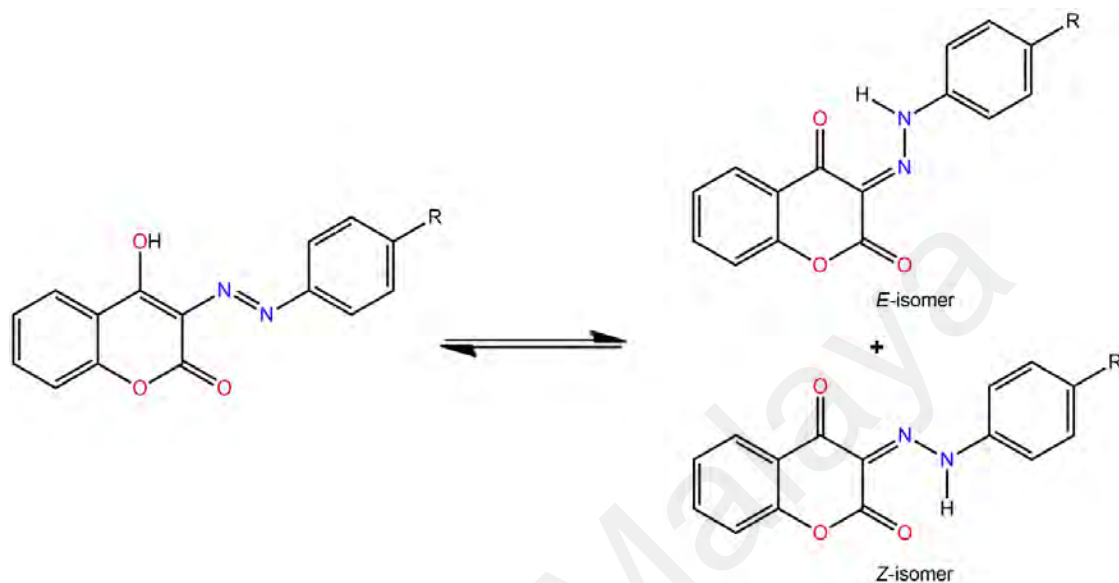
Figure 4.1: Azo-hydrazone tautomerism exhibited in **CAD1-7**.

The electron density of the two carbonyl oxygens present in the coumarin moiety could be considered to determine the corresponding singlets in the proposed tautomerization. The ketone carbonyl should have a higher electron density compared to that of the lactone carbonyl. The imbalanced electron density is due to the neighboring oxygen pulling the lactone carbonyl electrons towards itself. Consequently, the lactone carbonyl suffered from a lower electron density. It is then presumed that the hydrazone N-H favors interacting with the ketone carbonyl oxygen *via* hydrogen bonding interactions. Thus, it is plausible that **CAD1-7** are predominantly *E*-isomers with the N-H···O interactions favoring the ketone carbonyl oxygen rather than the lactone carbonyl oxygen (Metwally et al., 2012). Besides, the ratio of the two singlets from ^{1}H NMR spectra of **CAD1-7** could be used to determine the proportion of *E-*/*Z-* isomers. For all compounds investigated in solution, the *E-*/*Z-* ratio is about 85:15.

The tautomerization of the dyes could potentially be used as photoswitchable additives to achieve our research objectives. The X-ray crystallographic study of a 2-hydroxyazobenzene derivative, 6-[(2-hydroxy-1-naphthyl)diazenyl]benzothiazole exhibiting azo-hydrazone tautomerism was referred (Pavlović et al., 2009). From the study, it was shown that the compound exists predominantly as a hydrazone tautomer even in solid form. Thus, the results from X-ray crystallography supported by FTIR results from other studies (Metwally et al., 2012; Shawali et al., 1985; Yordanov et al., 2020) have confirmed that **CAD1-7** exist predominantly as hydrazone tautomers in solid as well.

Hence, to determine the effectiveness of **CAD1-7** as photoswitchable additives in PMMA coating films, the UV-Vis spectroscopy was utilized to study their photochemistry which will be discussed further in the next section. Besides that, their photochemistry is then compared to **CAD8** and **CAD9**, which exist predominantly as azo tautomers.

CAD8 was also synthesized according to the azo coupling reaction procedure. 7-amino-4-methylcoumarin was diazotized and subsequent coupling with phenol yielded **CAD8** with a yield of 66% after recrystallization from ethanol. Then, the –OH moiety in **CAD8** was then methylated with CH$_3$I according to the Williamson coupling reaction protocol to obtain **CAD9** with high yield (92%). The presence of two doublets at 6.95 and 7.83 ppm have confirmed the presence of a phenolic group, which indicated the successful coupling of 7-amino-4-methylcoumarin with phenol, yielding **CAD8** (**Appendix A.17**). Subsequent protection of the –OH group yielded **CAD9**, where a singlet representing the methoxy group at 3.86 ppm (**Appendix A.19**).

4.1.2 *Photochemistry of Selected Hydroxycoumarin Dyes*

Photochemical properties of the dyes were investigated prior to their application as additives in the coating. In this section, the UV-Vis spectra of compounds **CAD2**, **CAD8** and **CAD9** (10 μM solutions in toluene, DCM, EtOAc and AcOH) will be explained in detail. Different types of solvents were used to investigate the effect of solvents on the photochemistry of the dyes. Their differences in photochemistry are highlighted in this section. **Table 4.1** summarized the UV-Vis absorption data for **CAD2**, **CAD8** and **CAD9**:

Table 4.1: UV-Vis absorption data for **CAD2**, **CAD8** and **CAD9**

Compound	Solvent	Absorption, λ_{max} (nm)/ε ($\times 10^5$ M^{-1} cm^{-1})
CAD2	Toluene	435 (0.31)
	DCM	433 (0.27)
	EtOAc	429 (0.29)
	AcOH	430 (0.32)
CAD8	Toluene	376 (0.08)
	DCM	371 (0.29)
	EtOAc	375 (0.47)
	AcOH	285 (0.11), 375 (0.46)
CAD9	Toluene	378 (0.29)
	DCM	376 (0.36)
	EtOAc	375 (0.24)
	AcOH	286 (0.11), 371 (0.32)

For **CAD2** (**Table 4.1**), it was observed that the absorption bands maxima were located in the Soret region at 435, 433, 429 and 430 nm in toluene, DCM, EtOAc and AcOH, respectively. These bands correspond to the absorption of the hydrazone species (Moradi Rufchahi & Ghanadzadeh Gilani, 2019; Yordanov et al., 2020). Whereas for **CAD8**, the absorption bands maxima were located in the UV-A region at 376, 371, 375 and 375 nm in toluene, DCM, EtOAc and AcOH, respectively. These bands indicated that the absorbing species is the azo tautomer (Yordanov et al., 2020). The similar mechanism applies for the absorption bands of **CAD9**.

It was noted that the absorption maxima of **CAD2** regardless of solvents showed bathochromic shifting compared to that of **CAD8** and **CAD9**. It was also reported elsewhere (Moradi Rufchahi & Ghanadzadeh Gilani, 2019; Yordanov et al., 2020) that the hydrazone tautomer has absorption bands that showed bathochromic shifting compared to that of the azo tautomer. In our case, a simple comparison of the absorption spectra between **CAD2** (hydrazone tautomer) and **CAD8-9** (azo tautomer) showed a similar trend.

It is clear from **Table 4.1** that there is minimal negative solvatochromism observed for all compounds tested. An increase in solute-solvent interactions, especially intermolecular hydrogen bonding interactions in the excited state could result in solvatochromism (Zhao & Han, 2012). If positive solvatochromism (bathochromic shifting) is observed due to the intermolecular hydrogen bonding, the hydrogen bond in the excited state will be strengthened or stabilized and *vice versa* if negative solvatochromism (hypsochromic shifting) is observed (Zhao & Han, 2012). In our case, as the solvent polarity increased, the absorption maxima shifted hypsochromically. This indicated that the chromophores' excited states is destabilized by the intermolecular hydrazono N-H⋯O hydrogen bonding interactions in **CAD2** and phenolic O-H⋯O hydrogen bonding interactions in **CAD8-9** compared to their ground states. Consequently, a slight increase in the electronic transition energy from the ground state to the excited state led to the observed minimal blue-shift in both the hydrazono –C=N– N– $\pi \rightarrow \pi^*$ transition band in **CAD2** as well as the azo –N=N– $\pi \rightarrow \pi^*$ transition bands in **CAD8** and **CAD9**. Hence, it is sufficient to deduce that **CAD2**, **CAD8** and **CAD9** exhibited minimal negative solvatochromism.

The investigation was also furthered with kinetic studies of the (i) *E-/Z-* and (ii) *Z-/E-* photoisomerization reactions of **CAD2**, **CAD8** and **CAD9**. This study was conducted

with the sole objective of determining whether **CAD1-7** can be used as photoswitchable additives to induce tunable wettability and surface polarity. The photoisomerization kinetics of **CAD8-9** will be explained first. Then, the results can be used to explain any discrepancies between **CAD2** and **CAD8-9**. The photoisomerization kinetic parameters for **CAD8-9** are tabulated in **Table 4.2**:

Table 4.2: *E-/Z-* and *Z-/E-* photoisomerization kinetic parameters for **CAD8-9** at 25 °C

Compound	Solvent	Rate of photoisomerization, k (min^{-1})	
		E-/Z- photoisomerization	*Z-/E-* photoisomerization
CAD8	Toluene	0.29 ± 0.02	0.21 ± 0.01
	DCM	0.25 ± 0.03	0.152 ± 0.006
	EtOAc	0.208 ± 0.007	0.095 ± 0.003
	AcOH	–	–
CAD9	Toluene	0.264 ± 0.003	0.173 ± 0.003
	DCM	0.261 ± 0.004	0.1167 ± 0.0004
	EtOAc	0.258 ± 0.003	0.051 ± 0.001
	AcOH	0.25 ± 0.01	0.101 ± 0.002

The *E-/Z-* and *Z-/E-* photoisomerization reactions of **CAD8-9** followed first-order kinetics with $R^2 > 0.95$. For *E-/Z-* photoisomerization processes, it can be seen that as solvent polarity increased, the photoisomerization rate decreased as well. Similarly, the *Z-/E-* photoisomerization rates for **CAD8-9** also showed a reduction as solvent polarity increases.
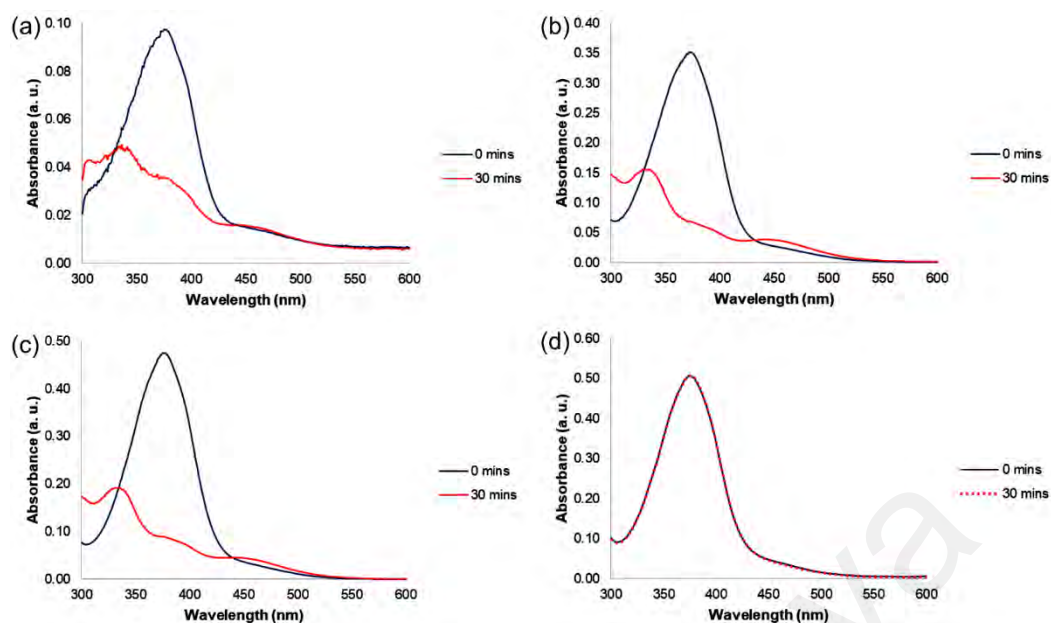
Figure 4.2: Absorption spectra of **CAD8** (10 μM) at 0 mins (blue line) and after 30 minutes of UV light irradiation (red line) in (a) toluene, (b) DCM, (c) EtOAc and (d) AcOH.

A noticeable difference between **CAD8** and **CAD9** lies in their photoisomerization kinetics in polar protic solvent AcOH (**Figures 4.2**(d) and **4.3**(d)). It is shown that **CAD8** did not undergo any photoisomerization processes. This observation can be seen with similar 4-hydroxyazobenzene compounds where they can undergo tautomerization by solvent-assisted proton transfer in polar solvents (Bandara & Burdette, 2012). Consequently, these compounds did not readily undergo photoisomerization processes in polar protic solvents. This peculiarity was eliminated upon methylation of the –OH group as evidenced by the photoisomerization behavior of **CAD9** in AcOH.
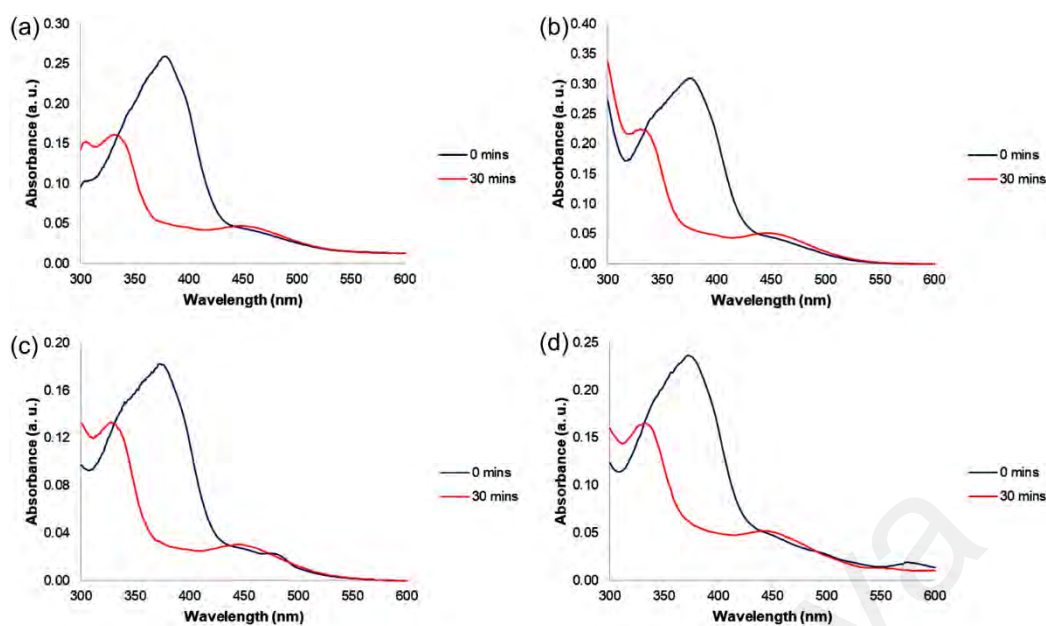
Figure 4.3: Absorption spectra of **CAD9** (10 μM) at 0 mins (blue line) and after 30 minutes of UV light irradiation (red line) in (a) toluene, (b) DCM, (c) EtOAc and (d) AcOH.

Numerous reports showed that hydrazone derivatives can also undergo *E*-/*Z*- and *Z*-/*E*- photoisomerization reactions (Landge et al., 2011; Su & Aprahamian, 2014; Zheng et al., 2019). Hence, taking into account of the ability of hydrazone derivatives to undergo reversible photoisomerization processes, we have decided to probe whether **CAD1-7**, and specifically **CAD2** can undergo photoisomerization processes as well.

From the UV-Vis spectra (**Figure 4.4**), it can be seen that there is little to no differences in the absorption band of **CAD2** before and after UV light irradiation. This alone suggested that **CAD2** may be incapable of *E*-/*Z*- photoisomerization. The difference of about 5 nm between the λ_{max} of *E*- and *Z*- isomers in toluene and DCM is also not a strong indication of *E*-/*Z*- photoisomerization processes. Moreover, a recent study has also indicated that the absorption spectra of *E*- and *Z*- isomers of **CAD1** and other 4-hydroxycoumarin hydrazone dyes have strong overlapping, thus making the selective excitation impossible, as evidenced from the absorption spectra that did not change upon UV light irradiation (Yordanov et al., 2020). Hence, on the basis of UV-Vis studies alone, there was insufficient evidence of reversible *E*-/*Z*- photoisomerization of **CAD2**.
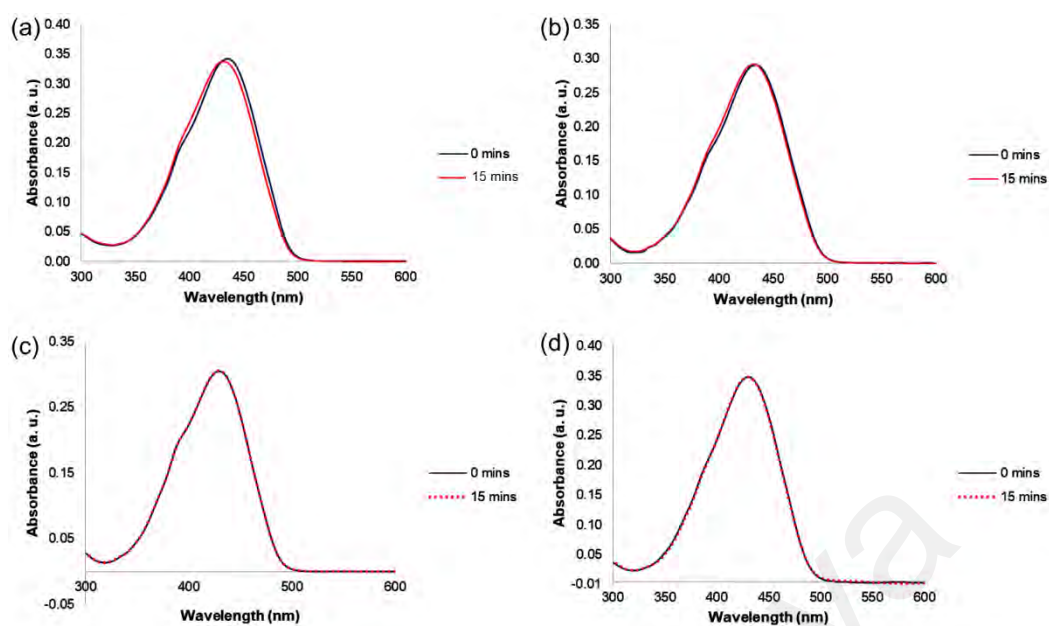
Figure 4.4: Absorption spectra of **CAD2** (10 μM) at 0 mins (blue line) and after 15 minutes of UV light irradiation (red line) in (a) toluene, (b) DCM, (c) EtOAc and (d) AcOH.

4.1.3 Water Contact Angle Measurements for PMMA/CAD2(5) and PMMA/CAD9(5) Coating Films

An important method to determine the suitability of **CAD1-7** as photoswitchable additives in PMMA coating films is by conducting contact angle measurements before and after UV-A irradiation. **CAD2** was chosen as a representative for the dyes and the results will be compared with **CAD9**, which clearly exhibited reversible *trans-cis* photoisomerization processes. Therefore, PMMA/**CAD2**(5) and PMMA/**CAD9**(5) coating films were prepared and applied onto glass substrates. The water contact angle values should change upon UV light irradiation due to the changes in the dipole moment of chromophores, reflecting photoisomerization processes. A higher water contact angle value should indicate lower surface free energy, hence lower surface polarity.

Figure 4.5 illustrates the changes in contact angle values of PMMA/**CAD9**(5) coating film upon UV light irradiation cycles. Initially, the contact angle value is $64.1 \pm 0.8°$. Then, after 1 h exposure to UV light, the contact angle increased to $69.3 \pm 1.2°$. An increase in contact angle indicated that **CAD9** underwent *trans*→*cis* isomerization, with

the *cis*- isomer possibly showing lower dipole moment than that of the *trans*- isomer. Then, when the coating was kept in the dark for 24 h, the contact angle decreased to 63.5 ± 0.8°, signifying complete thermal *cis→trans* isomerization. The reversible *trans-cis* isomerization of **CAD9** in PMMA matrices is confirmed as the contact angle values changed upon irradiation cycles.
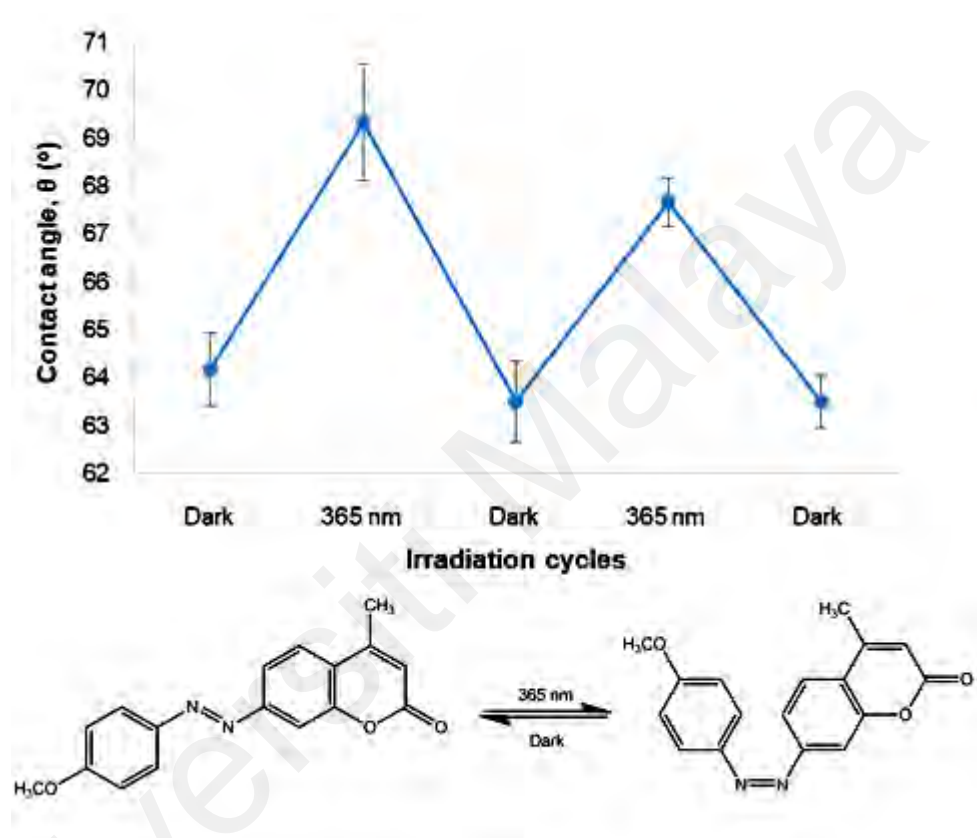
Figure 4.5: Changes in contact angle values for PMMA/**CAD9**(5) coating film upon UV light irradiation cycles.

Then, the contact angle for PMMA/**CAD2**(5) coating film was measured. Initially, the contact angle was $60.0 \pm 0.9°$. Then, after 1 h of UV light illumination, the contact angle increased to $66.7 \pm 0.5°$. This indicated the possibility of **CAD2** undergoing *E*-/*Z*- photoisomerization, with the *Z*- isomer possibly having a lower dipole moment. The contact angle decreased to $62.5 \pm 1.1°$ after keeping the coating in the dark for 24 h, signaling thermal *Z*-/*E*- isomerization of **CAD2** chromophores. Again, the reversibility of *E*-/*Z*- isomerization processes is confirmed as the contact angle values changed accordingly upon UV irradiation cycles as shown in **Figure 4.6**.
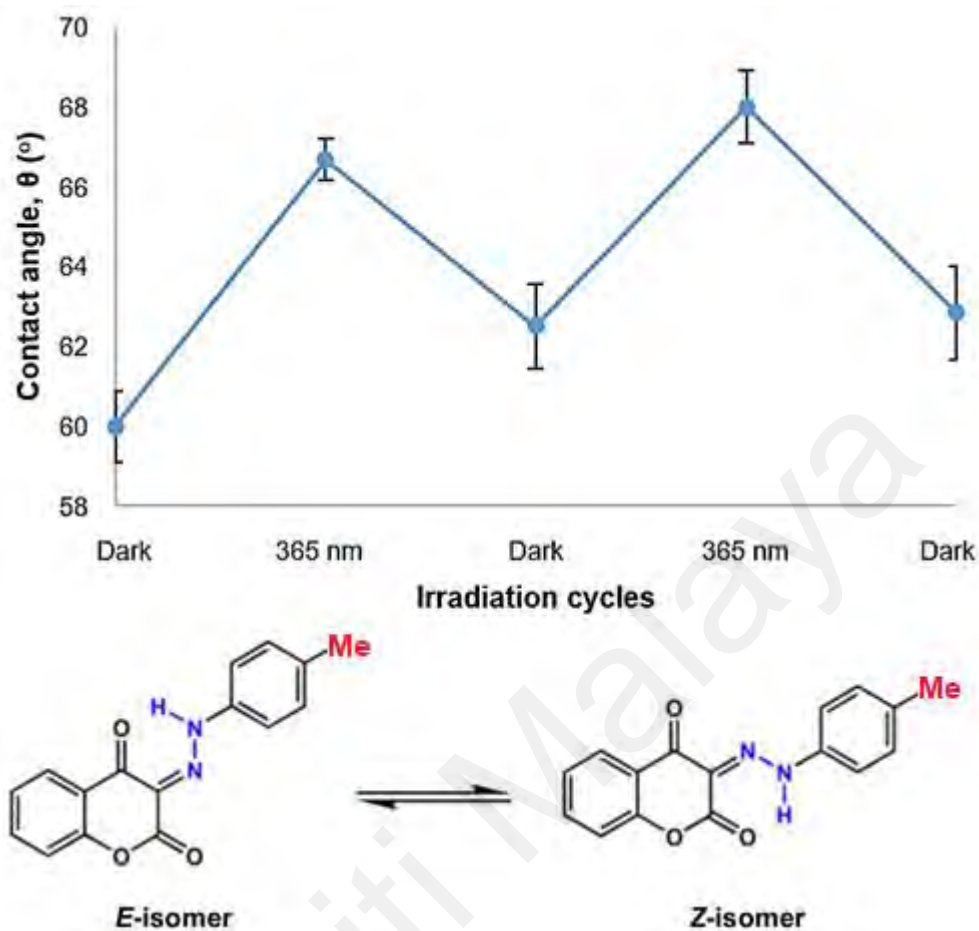
Figure 4.6: Changes in contact angle values for PMMA/**CAD2**(5) coating film upon UV light irradiation cycles.

Thus, it is highly possible that *E-/Z-* isomerization of **CAD1-7** has occurred due to the changes in contact angle values after responding to either UV light or dark conditions. The isomerization of **CAD1-7** could not be monitored using UV-Vis spectroscopy possibly due to the significant overlapping of the absorption bands of *E-* and *Z-* isomers (Yordanov et al., 2020).

4.1.4 Effect of PMVEMA-ES and CAD1-7 on the Physicooptical Properties of PMMA Coating Films

As shown in the previous section, **CAD1-7** could have possibly underwent reversible *E-/Z-* isomerization, in which changes in water contact angle values are observed upon UV light irradiation. However, UV-Vis studied have shown otherwise. Hence, **CAD1-7** dyes may not be suitable as photoswitching additives desired for this work due to the

contrasting evidences from the previous experiments. Nevertheless, they were blended into PMMA and formed into coating films to study their effects on the properties of PMMA coating films.

Owing to its relatively low surface energy, PMMA has low adhesion property on high surface energy substrates (Abidin et al., 2013). Thus, difficulties arise when PMMA-based resins are applied onto high surface energy substrates such as mild steel and glass. As a result, pure PMMA usually forms a free-standing film and is deemed unsuitable to be applied on glass and mild steel as a coating (Abidin et al., 2013). On top of that, PMMA-based coatings may also flake or peel off, consequently diminishing their aesthetic values. To compensate the lack of adhesion of PMMA on these substrates, polar additives such as 2-hydroxyethylmethacrylate (Wang et al., 2006), glycidylmethacrylate (Wang et al., 2006), tetramethylammonium formate (Alemdar et al., 2007), acrylic polyol (Abidin et al., 2013; Manah et al., 2019) and dammar gum from *Dipterocarpus grandiflorus* tree (Nasir et al., 2013) are added to enhance the adhesion property of PMMA-based coatings on high surface energy substrates.

One of the potential polar additives to be used as adhesion promoters for PMMA-based coatings are the commercially available PMVEMA-ES where it contains polar carboxylic acid (−COOH) groups. In addition, PMVEMA-ES is also biodegradable with low toxicity, high biocompability and useful bioadhesive properties (Gałka et al., 2014; Martínez-Ortega et al., 2019; Mira et al., 2017). Up until now, no reports of PMVEMA-ES as adhesion promoters for PMMA coating formulations are available and therefore, its effectiveness as an adhesion promoter are not known. Since −COOH groups are excellent hydrogen bond donors, it is hypothesized that PMVEMA-ES would enhance the adhesion properties of PMMA onto glass substrates by acting as a binding agent. Therefore, it is proposed that PMVEMA-ES binds PMMA and glass together *via*

hydrogen bonding interactions with (i) carbonyl ester groups in PMMA molecules and (ii) naturally occurring silanol groups on glass surfaces. As a result, it is expected that PMMA would adhere better on glass surfaces.

The structure of **CAD1-7** also contains a hydrogen bond donor, which is the hydrazone N-H. Therefore, it is expected that the hydrazone N-H may also help in improving the adhesion of PMMA coating film onto glass substrate by means of intermolecular hydrogen bonding interactions. Thus, in this section, the efficiency of PMVEMA-ES and **CAD1-7** as adhesion promoters for PMMA-based coatings were investigated. Cross-hatch, TGA and DSC analyses were carried out on selected coating films to unravel the role of intermolecular hydrogen bonding between PMMA/PMVEMA-ES and PMMA/**CAD** dyes in influencing the physical properties and adhesion ability of the prepared coating films on glass substrates. In addition, the effect of PMVEMA-ES and **CAD1-7** on the glossiness of coating films is explored as well.

4.1.4.1 Cross-Hatch Adhesion Test

To unravel the role of PMVEMA-ES as adhesion promoters, a cross-hatch adhesion test was carried out. **Figure 4.7** shows the cross-hatch adhesion test results.
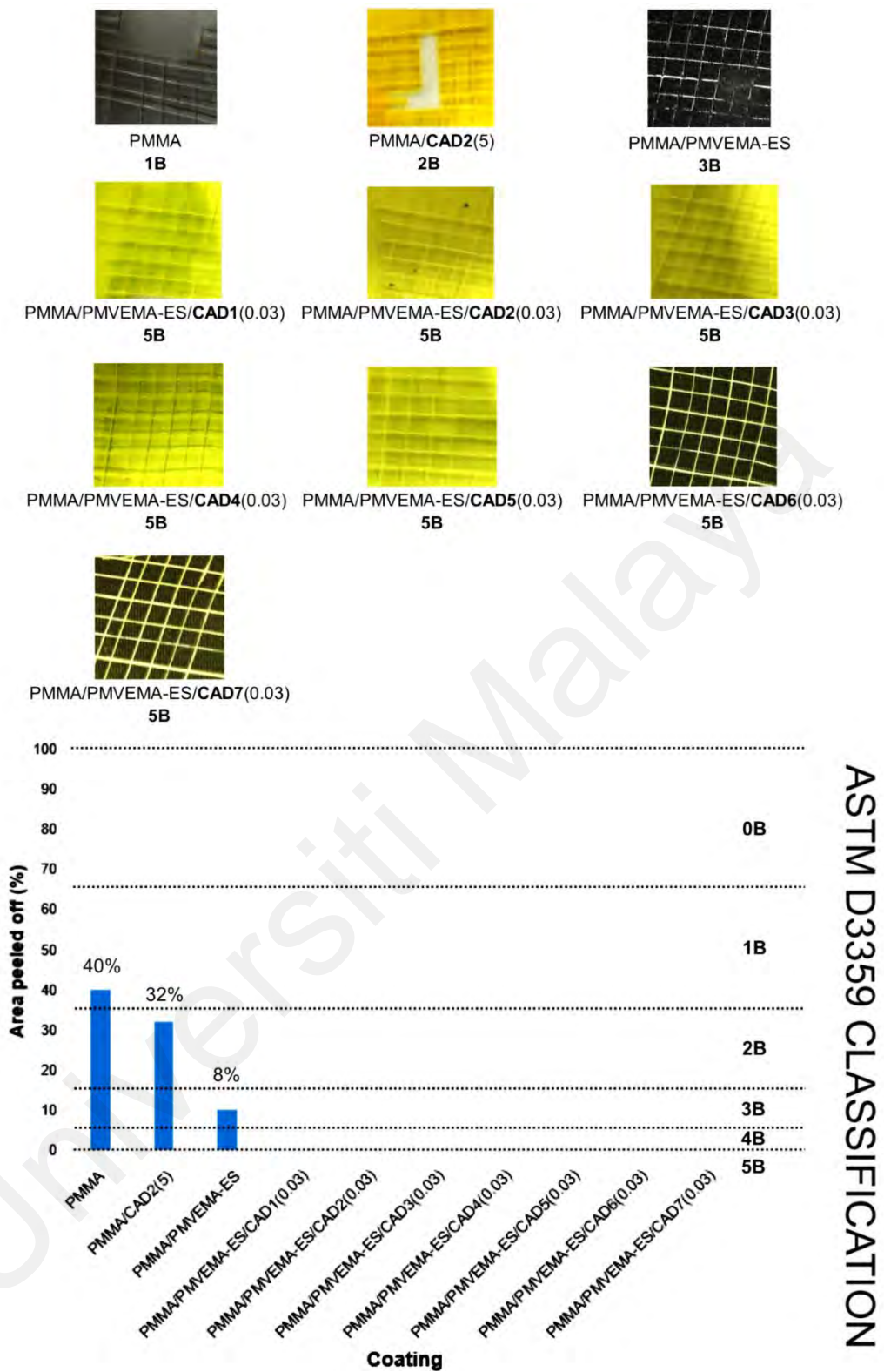
Figure 4.7: Cross-hatch adhesion test results for all coating films.

From **Figure 4.7**, it is indicated that pure PMMA did not adhere well to glass surfaces since about 40% of the coating surface were peeled off together with the masking tape. It

is possible that the intermolecular hydrogen bonding interactions between PMMA and glass surface (**Figure 4.8**(a)) is not strong enough to adhere PMMA onto glass.
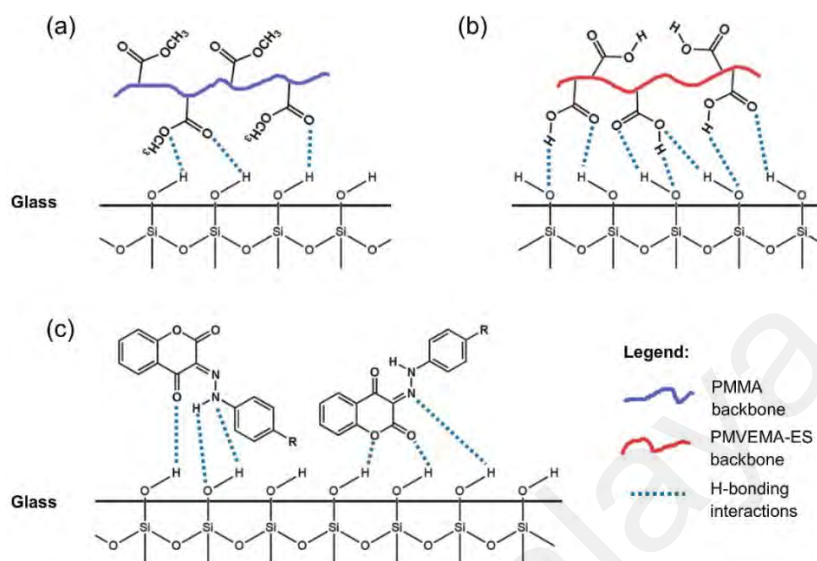
Figure 4.8: Intermolecular hydrogen bonding interactions between (a) PMMA/glass, (b) PMVEMA-ES/glass and (c) **CAD** dyes/glass surfaces.

The addition of **CAD2** dyes into the coating system increased the coating adhesion slightly, with 32% of the coating surface peeled off. The dye molecules contained (i) lactone groups, which are hydrogen bond acceptors and (ii) hydrazono -C=N-N-H groups, which are both hydrogen-bond donors and acceptors. As a result, the dye molecules are believed to have contributed to the enhanced adhesion of PMMA onto glass surfaces, also from intermolecular hydrogen bonding interactions, as illustrated in **Figure 4.8**(c).

Moreover, the coating containing PMVEMA-ES additive showed better adhesion quality where only 8% of the coating surface peeled off. The testing results indicated that PMVEMA-ES can behave as an adhesion promoter on glass surfaces. This is due to PMVEMA-ES chains containing free –COOH groups. Consequently, the –COOH groups allowed better adhesion of PMMA on glass surfaces possibly due to more intermolecular hydrogen bonding between PMVEMA-ES and glass. This is illustrated in **Figure 4.8**(b).

The addition of PMVEMA-ES and **CAD** dyes into the coating formulations further enhanced the adhesion of PMMA onto glass surfaces. Based on these results, it is likely shown that PMVEMA-ES has higher intermolecular hydrogen bonding contribution to adhesion of PMMA onto glass surface compared to that of **CAD** dyes.

It was also revealed that substituents on the phenyl ring seemingly do not have any contribution to the overall adhesiveness of PMMA onto glass surfaces since all PMMA/PMVEMA-ES/**CAD1-7** coating films showed no difference in the cross-hatch results.

4.1.4.2 Thermal Properties of Selected Coating Films

TGA and DSC studies were carried out to investigate the contribution of intermolecular hydrogen bonding interactions between PMMA, PMVEMA-ES and **CAD** dyes on the properties of the prepared coating films (**Figure 4.9**). **CAD2** dye was chosen as a representative for all dyes. Furthermore, pure PMVEMA-ES coating film was prepared for the purpose of this study. This coating solution was prepared by diluting PMVEMA-ES in EtOH to form a final concentration of 25 wt. %. **Table 4.3** summarizes the thermal properties of analyzed coatings and dyes.
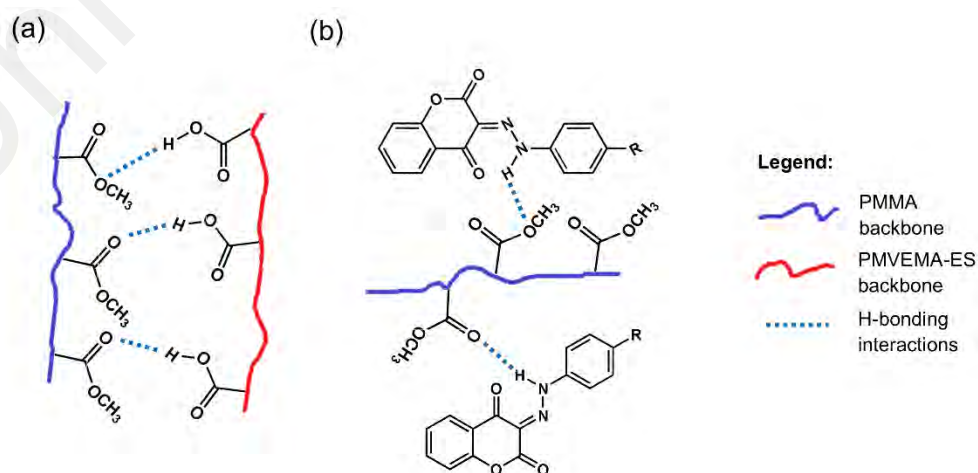
Figure 4.9: Intermolecular hydrogen bonding interactions between (a) PMMA/PMVEMA-ES and (b) PMMA/**CAD** dyes.

Table 4.3: Thermal properties of selected coating films

Sample	T_g (°C)	T_m (°C)	T_o (°C)	T_{max} (°C)				
				Stage 1	Stage 2	Stage 3	Stage 4	Stage 5
PMMA	68.3	193.0	238.1	332.7	426.5	n. d.	n. d.	n. d.
PMVEMA-ES	41.3	182.7	90.5	97.1	185.6	292.6	424.5	697.5
CAD2	n. d.	192.0	257.2	286.3	584.4	n. d.	n. d.	n. d.
PMMA/PMVEMA-ES	64.2	n. d.	226.8	262.4	340.4	444.6	615.1	n. d.
PMMA/**CAD2**(5)	70.6	n. d.	273.2	332.5	430.1	n. d.	n. d.	n. d.
PMMA/PMVEMA-ES/**CAD2**(0.03)	67.9	n. d.	235.5	253.9	339.9	437.6	593.4	n. d.

* n.d. = not detected

4.1.4.2.1   Thermogravimetric Analysis (TGA)

TGA thermograms relates the percentage mass of samples with temperature. **Figure 4.10** shows the TGA and DTG curves for the samples analyzed. For PMMA (**Figure 4.10**(a)), it is observed that there are two decomposition stages: the first stage at T_{max} = 332.7 °C which indicated breakage of head-to-head linkages and the second stage at T_{max} = 426.5 °C which is attributed to the scission of methoxycarbonyl side groups (Gałka et al., 2014; Manring, 1989, 1991; Manring et al., 1989).

Figure 4.10(b) indicates that the decomposition of PMVEMA-ES consisted of five stages. The first stage at T_{max} = 97.1 °C is probably due to the evaporation of volatiles and moisture. This also explained the apparent low T_o of 90.5 °C observed for PMVEMA-ES coating. The second decomposition stage at T_{max} = 185.6 °C is possibly its melting temperature. The appearance of this small DTG peak implied a temporary mass loss presumably owing to a buoyancy correction as a result of air or vapours escaping from the crystal lattice as the solid melts (O'connell & Dollimore, 1999). The melting endotherm of PMVEMA-ES at 182.7 °C as observed from its DSC thermogram (**Figure 4.11**(a)) further supported the possibility of its melting point indication from the TGA/DTG curves. The third and fourth decomposition stages at T_{max} = 292.6 and 424.5

ºC is probably attributed to a combination of deesterification and decarboxylation of –COOEt and –COOH groups in the PMVEMA-ES chains. The combined percentage weight losses from these two stages is about 64.3%, which is close to the calculated weight percentages of –COOH and –COOEt groups in PMVEMA-ES chains (58.4%). Furthermore, the TGA thermogram of its diacid counterpart, poly(methyl vinyl ether-*alt*-maleic acid), PMVEMA showed that the decarboxylation of –COOH groups occurred at T_{max} = 325 ºC. (Chung et al., 1990) Therefore, from this previous study, it is suggested that PMVEMA-ES may also undergo decarboxylation at this temperature. Finally, the final decomposition stage at T_{max} = 697.5 ºC is possibly due to random chain scissions.
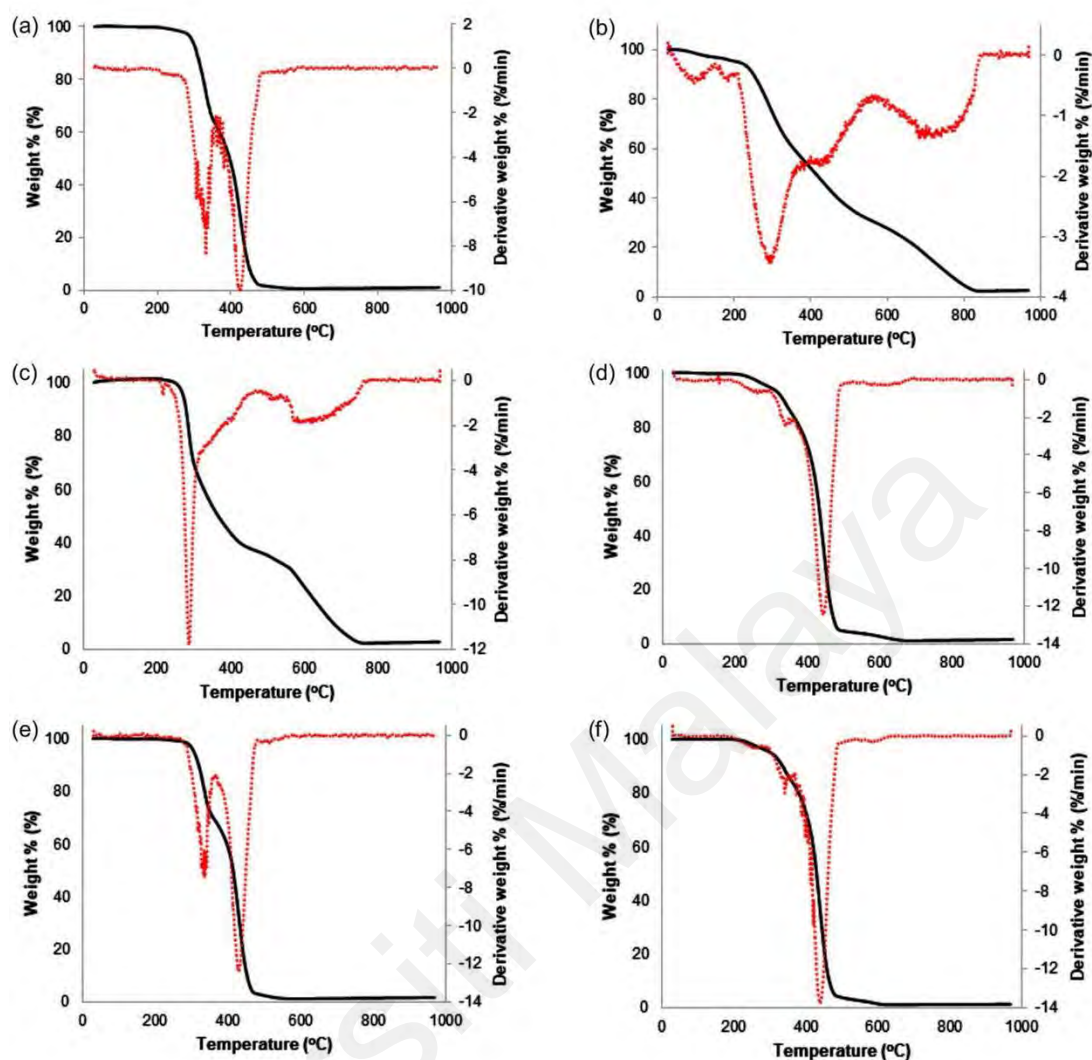
Figure 4.10: TGA (black solid lines) and DTG (red dotted lines) plots for (a) PMMA, (b) PMVEMA-ES, (c) **CAD2**, (d) PMMA/PMVEMA-ES, (e) PMMA/**CAD2**(5), and (f) PMMA/PMVEMA-ES/**CAD2**(0.03).

When PMVEMA-ES was blended together with PMMA, its TGA/DTG curves (**Figure 4.10**(d)) indicate four decomposition stages. The first stage at T_{max} = 262.4 °C indicated the decomposition of PMVEMA-ES component. The second and third stages at T_{max} = 340.4 and 444.6 °C, respectively, are attributed to scission of head-to-head linkages and scission of methoxycarbonyl side groups of PMMA, respectively. By comparing the TGA/DTG curves of pure PMMA, it was observed that the T_{max} of decomposition stage involving the scission of methoxycarbonyl side groups in PMMA/PMVEMA-ES blend

shifted to a higher temperature. This indicated the possibility of intermolecular hydrogen bonding interactions between the two components (Hu et al., 2012; Kuo et al., 2009).

The TGA/DTG curves of PMMA/**CAD2**(5) blends (**Figure 4.10**(e)) indicate two decomposition stages at T_{max} = 332.5 and 430.1 °C, which corresponded to the decomposition stages of PMMA. Again, an increase in T_{max} corresponding to the scission of PMMA methoxycarbonyl side groups was observed, albeit less pronounced compared to that of PMMA/PMVEMA-ES blend. The increase in T_{max} is caused by the intermolecular hydrogen-bonding interactions between PMMA and **CAD2** components. Furthermore, the increase in T_{max} corresponding to PMMA methoxycarbonyl side group cleavage from 426.5 °C to 437.6 °C is also observed for PMMA/PMVEMA-ES/**CAD2** blend. Hence, from the TGA/DTG thermograms, it can be inferred that the strength of intermolecular hydrogen bonding interactions between PMMA/PMVEMA-ES is stronger than that of between PMMA/**CAD2**.

4.1.4.2.2   Differential Scanning Calorimetry (DSC)

The DSC analysis provided sufficient information about the compatibility of polymer blends. Generally, if two components are compatible with each other, the DSC curve will indicate only a single T_g transition. From **Figure 4.11**, the T_g of pure PMMA and PMVEMA-ES coating films are 68.3 and 41.3 °C, respectively. The T_g of PMMA coating film is lower than that of the pure PMMA granules supplied by Sigma-Aldrich (T_g = 105 °C). It has been reported that the selection of solvents can influence the T_g of a polymer by altering the packing density and morphology of the polymer (Jeong et al., 2017). Moreover, it has been observed that the T_g of a polymer film can change with film thickness and the type of substrate that the film is casted on (Singh et al., 2003). Therefore, it is possible that the lower value of T_g observed for PMMA coating is probably due to a combination of these reasons.
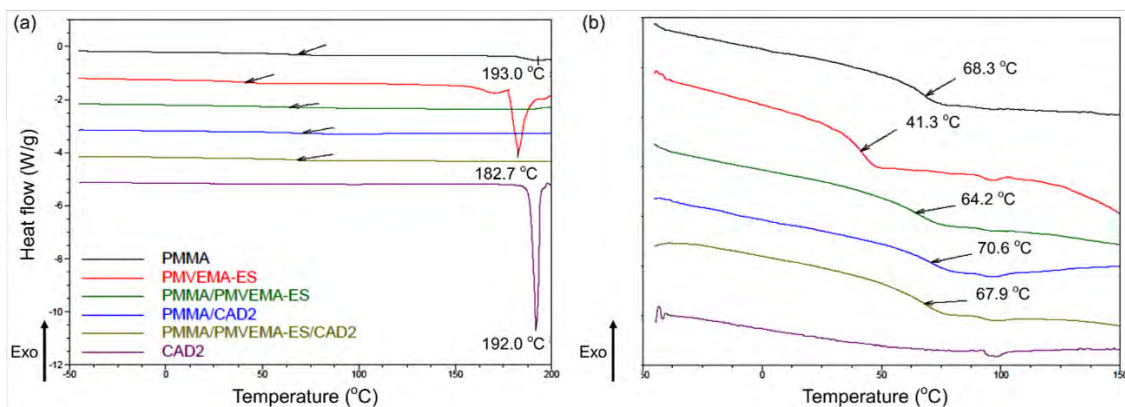
Figure 4.11: (a) DSC curves of analyzed samples and (b) close-up of DSC curves to indicate T_g transitions.

From the DSC thermograms, it is suggested that the prepared PMMA/PMVEMA-ES blend is compatible due to the presence of only a single T_g in its DSC thermogram. In addition, the same could be said for both PMMA/**CAD2** and PMMA/PMVEMA-ES/**CAD2** blends as both of their DSC thermograms showed a single T_g. Thus, PMMA, PMVEMA-ES and **CAD2** are compatible with each other.

A careful observation indicated that the addition of PMVEMA-ES into PMMA has decreased the T_g of PMMA from 68.3 °C to 64.2 °C, which showed a possible indication of intermolecular hydrogen-bonding interactions between the two components. Meanwhile, it was expected that the addition of **CAD2** dyes into PMMA will decrease the T_g of PMMA due to its low molecular weight where **CAD2** dye can be acted as a plasticizer. But, the result obtained has shown that the addition of **CAD2** into PMMA has increased the T_g to 70.6 °C. This may also indicate a possibility of intermolecular hydrogen-bonding interactions between PMMA and **CAD2** components.

The Kwei equation (Kwei, 1984) can be used to estimate the dependence of T_g on the intermolecular interactions between two components:

$$T_g = \frac{(1-x)T_{g1} + kxT_{g2}}{(1-x) + kx} + qx(1-x) \qquad (4.1)$$

112

where $(1-x)$ and x are weight fractions of components 1 and 2, T_{g1} and T_{g2} are the glass transition temperatures of components 1 and 2, k and q are fitting constants. The constant q indicates the strength of the specific interactions between the components. In this case, hydrogen-bonding interactions.

The q values obtained from nonlinear least squares fitting for PMMA/PMVEMA and PMMA/**CAD2**(5) blends are −17.8 and −79.1, respectively (**Figure 4.12**). A negative q value indicated favorable intermolecular hydrogen bonding interactions between the two components (Yang et al., 2017). From the obtained q values, the relative hydrogen bonding strength is in the order of PMMA/PMVEMA-ES > PMMA/**CAD2**, which is in agreement with cross-hatch adhesion test and TGA results.
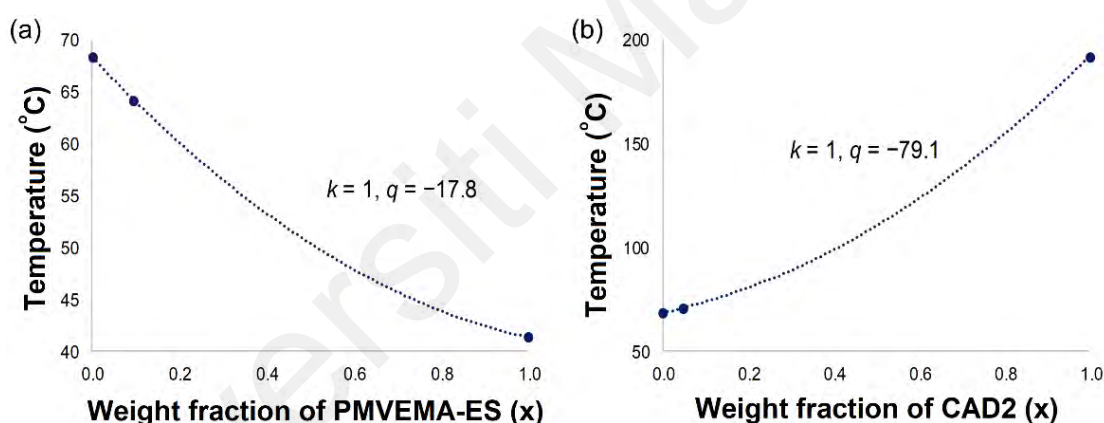
Figure 4.12: T_g against composition curves for (a) PMMA/PMVEMA-ES and (b) PMMA/**CAD2**(5) blends.

4.1.4.3 Glossiness

The amount of light reflected on the surface of the coating films was measured by using a gloss meter at 60° and 20°. The data collection for glossiness started with a measurement angle of 60° as a standard angle of glossiness. If the glossiness value at 60° exceeds 70 gloss units, GU (i.e. high gloss surfaces), the measurement angle should be changed to 20° for measurement accuracy optimization. In this work, all coating samples showed gloss values at 60° greater than 100 GU, indicating that all prepared coating

samples have high glossiness. Consequently, gloss measurements at 20° are used for further analysis. **Table 4.4** shows the glossiness of the prepared coatings measured at 20° and 60°.

Table 4.4: Glossiness of coating films at 20° and 60°

Coating	Gloss (GU)	
	20°	60°
PMMA	84.3 ± 1.3	138.6 ± 1.9
PMMA/PMVEMA-ES	64.1 ± 0.9	110.6 ± 0.5
PMMA/PMVEMA-ES/**CAD1**(0.03)	94.2 ± 11.1	123.0 ± 2.7
PMMA/PMVEMA-ES/**CAD2**(0.03)	118.2 ± 5.1	132.3 ± 2.3
PMMA/PMVEMA-ES/**CAD3**(0.03)	127.7 ± 4.2	135.0 ± 1.0
PMMA/PMVEMA-ES/**CAD4**(0.03)	84.1 ± 4.7	113.0 ± 0.8
PMMA/PMVEMA-ES/**CAD5**(0.03)	88.0 ± 0.0	115.1 ± 2.2
PMMA/PMVEMA-ES/**CAD6**(0.03)	103.9 ± 2.9	126.7 ± 0.6
PMMA/PMVEMA-ES/**CAD7**(0.03)	73.0 ± 0.7	106.2 ± 1.1

Surfaces with high refractive indices (Xie et al., 2020), low surface roughness (Bierwagen & Tallman, 2001; Dashtizadeh et al., 2011; Järnström et al., 2008; Xie et al., 2020; Yang et al., 2018) and narrow particle size distribution (Trezza & Krochta, 2001) have optical homogeneity. As a consequence, these surfaces will have high glossiness. Therefore, it is implied from the glossiness values that all the prepared coatings have smooth surfaces and optical uniformity.

Although not considered to be a high-refractive index polymer ($\eta > 1.50$), PMMA itself has a refractive index of 1.49 (Lee & Chen, 2001). The presence of unsaturated bonds in PMMA, namely the carbonyl C=O bonds allow PMMA to have a relatively high refractive index value (Xie et al., 2020). As indicated in **Table 4.4**, pure PMMA coating has gloss value of 84.3 and 138.6 GU at 20° and 60°, respectively. Thus, PMMA itself contributed to the overall high glossiness of the prepared coating films. It is also implied that the addition of PMVEMA-ES into the coating formulation decreased the glossiness

of the prepared coating films due to the lower glossiness values compared to that of pure PMMA. This is perhaps due to the lower amount of conjugation present in the PMVEMA-ES backbone.

Table 4.4 has also illustrated that the addition of dyes into the coating formulations have increased the gloss values at 20°. The intermolecular hydrogen bonding interactions between PMMA, PMVEMA-ES and dyes may have contributed to better mixing of the coating resin and consequently, higher coating homogeneity. As a result, an increase in glossiness readings are observed.

Figure 4.13 further illustrates the effect of substituents on the glossiness of the coating films. It can be observed that the alkylated dyes (R = Me, Et) gave rise to coating films with higher glossiness relative to the coating film containing **CAD1** (R = H) dye. It can also implied that the coating film containing dye with a longer alkyl substituent (R = Et) has higher gloss compared to the coating film containing methyl-substituted dye. These observations indicated that the alkylated dyes have higher homogeneity in the coating formulation. As xylene is a relatively non-polar solvent, increasing the length of alkyl chains in the dye caused the dye to be better solubilized in the coating formulation. Thus, a better homogeneity is obtained, and hence increased the coating film glossiness.

With the exception of Br, the coating films containing halogen-containing dyes (R = F, Cl, I) has shown a decrease in glossiness relative to the coating film containing **CAD1** dye. This may indicate that the halogenated dyes have lower solubility in the coating formulation. Consequently, a lower optical homogeneity is obtained and for this reason, decreased the coating film glossiness.
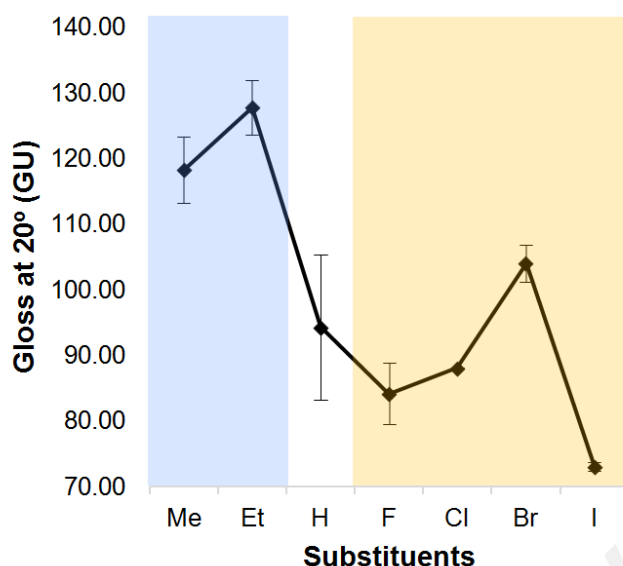
Figure 4.13: Influence of substituents on coating glossiness measured at 20°. The blue region represents alkyl substituents while the orange region represents halogen substituents.

4.1.5   *Remarks on Hydroxycoumarin Dyes as Photoswitchable Additives*

The synthesis of **CAD1-9** dyes were successful as indicated by spectroscopic techniques. Initially, it is thought that **CAD1-7** were predominantly azo tautomers. However, spectroscopic studies and previous reports showed that **CAD1-7** were predominantly hydrazone tautomers. Nevertheless, hydrazones also exhibited reversible *E-/Z-* isomerization. UV-Vis spectroscopy provided insufficient evidence of reversible *E-/Z-* isomerization of **CAD2** dyes probably due to the significant overlapping of the absorption bands for *E-* and *Z-* isomers. In contrast, water contact angle measurements indicated that **CAD2** indeed underwent reversible *E-/Z-* isomerization processes as the contact angle values change upon UV light irradiation. Due to the contrasting findings from UV-Vis and contact angle studies, only azobenzene derivatives are considered for further testing (**Section 4.2** onwards) to achieve the main objective of study.

Besides the disappointing hydrazone performance as photoswitchable additives, the native PMMA also can be further improved. Due to the inherently poor adhesion of PMMA onto polar surfaces, PMVEMA-ES was selected as an additive to improve the

coating film adhesion onto glass substrates. Cross-hatch, TGA and DSC studies indicated that PMVEMA-ES indeed improved the overall adhesion of all prepared coating films onto glass substrates at the expense of the overall glossiness of coating films. The effect of PMVEMA-ES on the photochemistry of azobenzene derivatives in PMMA coating films are also studied and will be discussed in **Section 4.2.4**.

4.2 Azobenzene Dyes as Photoswitchable Additives in PMMA Coating Films for Reversible Surface Polarity

The results obtained in **Section 4.1** gave directions to continue the study using azobenzene derivatives as they clearly showed reversible *trans-cis* isomerization processes. In this section, the application of azobenzene derivatives as photoswitchable additives in PMMA coating films is explained in detail.

4.2.1 Synthesis of AZO1 and AZO2

Azobenzene derivatives **AZO1** and **AZO2** were chosen as dopants to study the effects of functional group on the properties of PMMA coating films. They were synthesized using established methods, producing moderate to good yields. **AZO1** contains one methyl group and one –OH group whereas **AZO2** consists of only methyl groups. The ¹H NMR spectrum of **AZO1** (**Appendix A. 21**) has exhibited the presence of a singlet at 2.35 ppm, which corresponded to the methyl group. Furthermore, a broad singlet at 5.76 ppm has indicated the presence of –OH functionality. In addition, two doublets at 6.85, 7.22, 7.71 and 7.77 ppm have shown the presence of two phenyl rings, with both rings indicated *para-* substitution. The ¹H NMR spectrum of **AZO2** (**Appendix A. 23**) is simpler: a singlet at 2.35 ppm showing the presence of methyl groups and two singlets at 7.81 and 8.04 ppm indicating two phenyl rings, also showing *para-* substitution pattern.

The –OH groups in **AZO1** molecules may improve its solubility in PMMA matrix possibly due to the formation of intermolecular C=O···H hydrogen bonds. Therefore, it is

expected that **AZO1** showed better homogeneity in PMMA matrix compared to that of **AZO2**. In addition, results from **Section 4.1.4** revealed that intermolecular hydrogen bonding interactions could enhance the adhesion of coating films onto glass substrates.

It is well-known that the presence of strong electron donors such as –OH groups could also influence the speed of *trans→cis* isomerization of azobenzene derivatives (Bandara & Burdette, 2012). Hence, the performance of **AZO1** and **AZO2** dyes in *trans→cis* and *cis→trans* isomerization reactions in PMMA can be compared.

4.2.2   *Physical Characterization of PMMA/AZO1 and PMMA/AZO2 Coating Films*

Figure 4.14 shows the prepared coating films. It was discovered that increasing the weight percentage of **AZO1** chromophores beyond 33% resulted in inhomogeneity of mixture, as evidenced by the significantly rough surface of PMMA/**AZO1**(50) coating film (**Figure 4.14**(e)), in comparison to the other coating films. Consequently, this led to the composition being inapplicable for coating systems. Hence, only coating films with 5, 13 and 33 wt. % of **AZO1** dyes were further characterized.
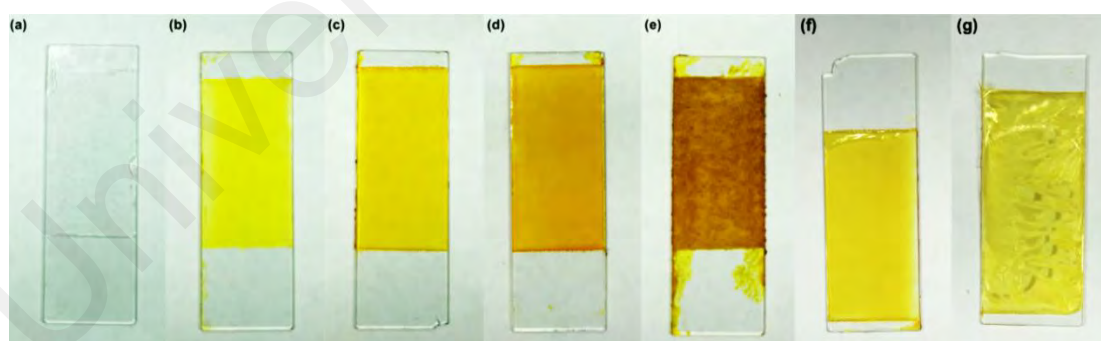
Figure 4.14: (a) PMMA, (b) PMMA/**AZO1**(5), (c) PMMA/**AZO1**(13), (d) PMMA/**AZO1**(33), (e) PMMA/**AZO1**(50), (f) PMMA/**AZO2**(5) and (g) PMMA/**AZO2**(13) coating films.

It is also noted that increasing the content of **AZO2** chromophores beyond 5 wt. % triggered the crystallization of **AZO2** in PMMA films, as shown in **Figure 4.14**(g). This is possibly due to the poor solubility of **AZO2** dyes in PMMA matrices (Pakula et al.,

2011). By changing one of the methyl groups in **AZO2** to –OH, the solubility of azobenzene dyes in PMMA matrices is enhanced, evidenced by the higher content of **AZO1** dyes able to be blended homogeneously in PMMA coating films. This is possibly due to the intermolecular C=O···H hydrogen bonding between PMMA and **AZO1**. Another way to circumvent the crystallization of dyes in polymer matrix is by synthesizing azobenzene derivatives containing long alkyl chains or branches in order to increase the solubility in polymer matrix (Pakula et al., 2011). It can also be seen that PMMA/**AZO2** coating films have poor adhesion onto glass substrates as some parts of the film peeled off (**Figures 4.14**(f) and (g)). In contrast, the presence of −OH groups in **AZO1** have enabled better adhesion of films onto glass substrates possibly by intermolecular hydrogen bonding interactions between the glass and coating film.

In order to investigate the role of –OH groups in increasing the homogeneity of **AZO1** in PMMA, DSC studies were carried out for PMMA/**AZO1**(5) and PMMA/**AZO2**(5) coating films for comparison study. DSC studies can provide sufficient information about the compatibility of polymer blends. Typically, the DSC curve will indicate only a single T_g transition if two components are compatible with each other. From **Figure 4.15**, the T_g of pure PMMA is 68.30 $^\circ$C. The probable reasons of lower T_g value of PMMA coating film compared with that of PMMA granules supplied from Sigma-Aldrich are explained in **Section 4.1.4.2.2**.
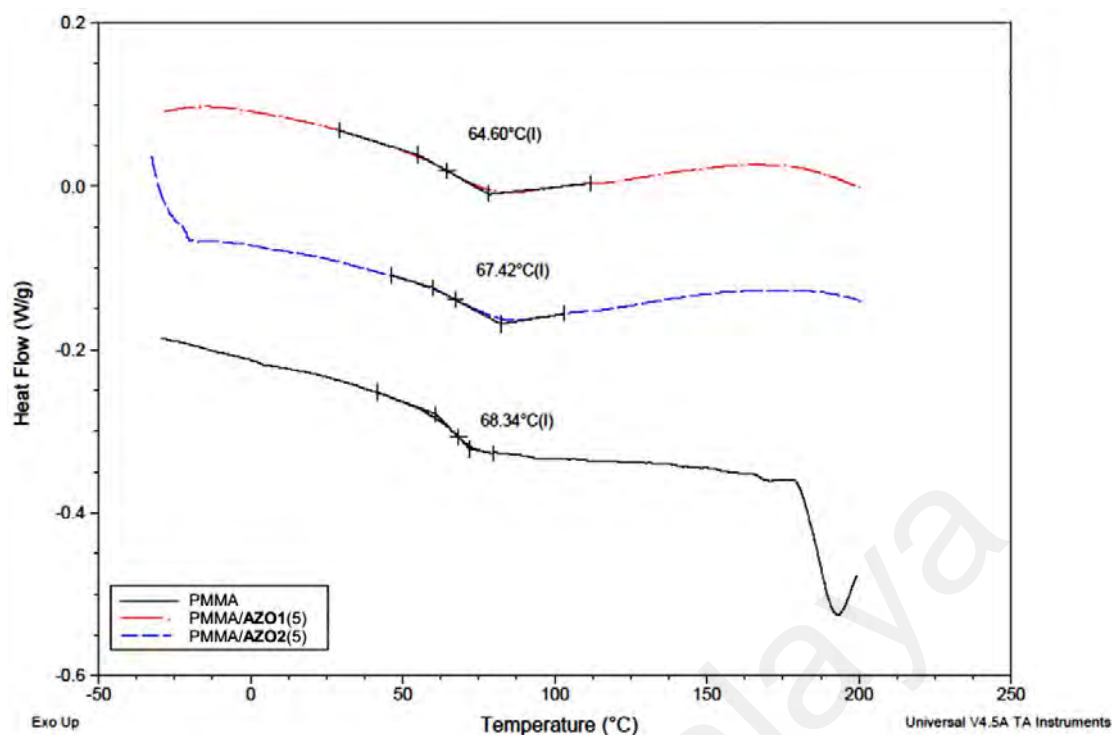
Figure 4.15: DSC thermograms of PMMA (black solid line), PMMA/**AZO1**(5) (red dash dot line) and PMMA/**AZO2**(5) (blue dash line) coating films.

From the DSC thermograms, it is suggested that the **AZO1** and **AZO2** dyes (5 wt. % dry film content) are compatible in PMMA matrices since only a single T_g is present in both PMMA/**AZO1**(5) and PMMA/**AZO2**(5) DSC thermograms. It is expected that the addition of a low-molecular weight component would decrease the T_g of bulk polymer, where the small amount of small-molecule additives could change the molecular arrangement and crystallinity of the bulk polymer. Therefore, a careful observation indicated that the addition of **AZO1** and **AZO2** dyes into PMMA decreased the T_g of PMMA from 68.30 °C to 64.55 and 67.05 °C, respectively. The addition of **AZO1** dyes decreased the T_g further than that of **AZO2** dyes. These observations are a possible indication of intermolecular C=O···H hydrogen bonding interactions between PMMA and **AZO1**. The addition of **AZO1** dyes decreased the T_g further than that of **AZO2** dyes. The larger T_g deviation of the PMMA/**AZO1**(5) film in comparison to that of PMMA/**AZO2**(5) film is a possible sign of intermolecular C=O···H hydrogen bonding interactions between PMMA and **AZO1**.Previous studies have also indicated that

intermolecular hydrogen bonding interactions between two components in polymer blends caused a decrease in T_g of the bulk material (Kuo et al., 2001; Poutanen et al., 2016). Thus, it is possible that the presence of –OH groups in **AZO1** enhanced its solubility in PMMA matrix due to intermolecular hydrogen bonding interactions.

4.2.3   *Water Contact Angle Measurements*

Due to the extremely low M_w of azobenzene derivatives compared to that of bulk PMMA, they tend to segregate to the surface. Segregation is thermodynamically favorable if there is a total reduction in the surface free energy of the bulk material (Hardman et al., 2011; Hutchings et al., 2011; Koberstein, 2004; Sarih, 2010). Segregation of azobenzene molecules was probably driven by the relatively hydrophobic phenyl moieties.

4.2.3.1   *Contact Angles of PMMA/AZO1 and PMMA/AZO2 Coating Films*

Upon a closer look at the structure of **AZO1**, dye itself is asymmetric, i.e. there are two different substituents at the 4- and 4'- positions, which are −OH and −CH$_3$. Therefore, **AZO1** molecules can have a few possible arrangements on the coating surface, as illustrated in **Figure 4.16**:
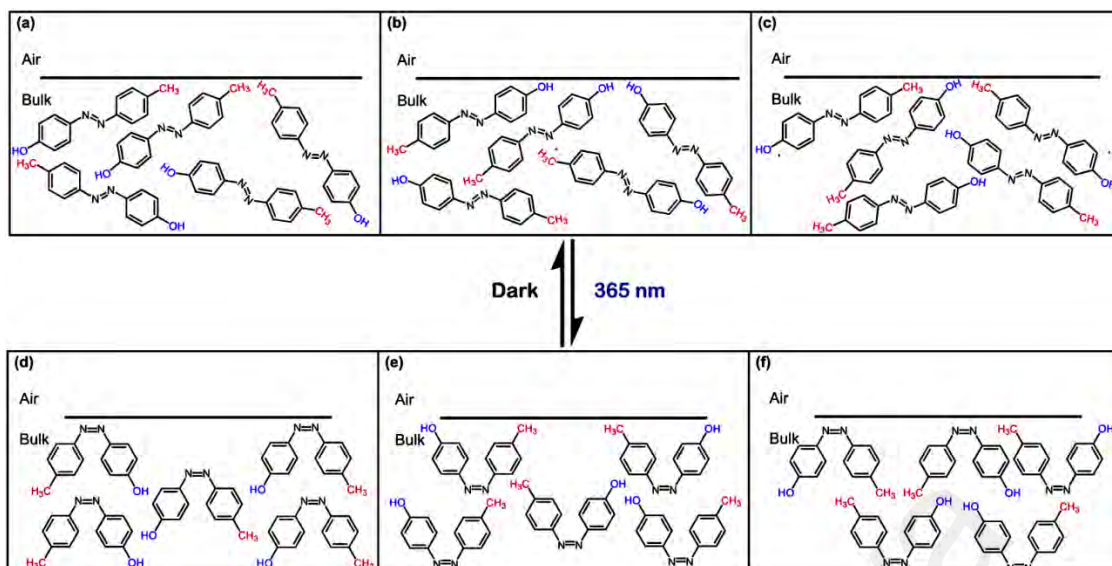
Figure 4.16: Possibilities of arrangement of **AZO1** molecules on coating surface as *trans*-**AZO1** with (a) −CH₃ (colored red) saturated surface, (b) −OH (colored blue) saturated surface or (c) random arrangements of −CH₃ and –OH. Upon UV irradiation, *cis*-**AZO1** can have orientations with either (d) functional groups facing down, (e) functional groups facing up or (f) random arrangements of −CH₃ and –OH.

From **Figure 4.16**(a), *trans*-**AZO1** molecules arrange in a way that −CH₃ groups are saturated on the coating surface while in **Figure 4.13**(b), the −OH groups are saturated on the coating surface. *trans*-**AZO1** molecules can also arrange in a random manner, shown in **Figure 4.16**(c). Then, when irradiated with UV-A, *cis*-**AZO1** can also have different possibilities of arrangements in the coating surface, depicted in **Figure 4.16**(d-f).

Surfaces containing alkyl groups can give water contact angle values from 74-142° depending on surface composition, alkyl chain length and surface roughness (Arima & Iwata, 2007; Henry et al., 2000; Schmohl et al., 2004; Shanmugharaj et al., 2013; Song et al., 2006; Taborelli et al., 1995). However, water contact angle values of surfaces containing hydroxyl (−OH) groups could be from 22-44° (Arima & Iwata, 2007; Jayasekara et al., 2004; Lee et al., 1994). Furthermore, surfaces containing −COOH groups can provide water contact angle values from 30° to as low as 15° depending on

surface compositions (An et al., 2007; Arima & Iwata, 2007; Lee et al., 1994; Sasai et al., 2008; Toworfe et al., 2006).

If *trans*-**AZO1** can have well-ordered arrangements in a way that −CH$_3$ groups saturate the coating surface (**Figure 4.16**(a)), then, it is anticipated that static water contact angle value increases to more than 70º (hydrophobic surface). Conversely, if −OH groups saturate the coating surface (**Figure 4.16**(b)), then, it is predicted that static water contact angle value should decrease to below 40º (hydrophilic surface). To unravel which scenario is the best to describe the arrangement of **AZO1** in the coating surface, water contact angle measurements were taken for the blank PMMA coating as well as the dyed coatings and suitable comparisons can be made.

Figure 4.17 represents the water contact angle values of the PMMA/**AZO1** coating films after a few UV-A irradiation cycles. It is clear that the water contact angle measurements for blank PMMA coating are relatively constant before and after UV-A exposure. The average contact angle of about 63º has indicated that the coating film is relatively hydrophilic (< 90º). However, when **AZO1** chromophores were added, the water contact angles of the coating films have remained the same regardless of dye concentration – proposing that the coating surface was neither saturated with hydrophobic −CH$_3$ groups nor hydrophilic −OH groups from the dye molecules. This can only mean that *trans*-**AZO1** molecules are suggested to have random arrangements on the coating surface (**Figure 4.16**(c)).
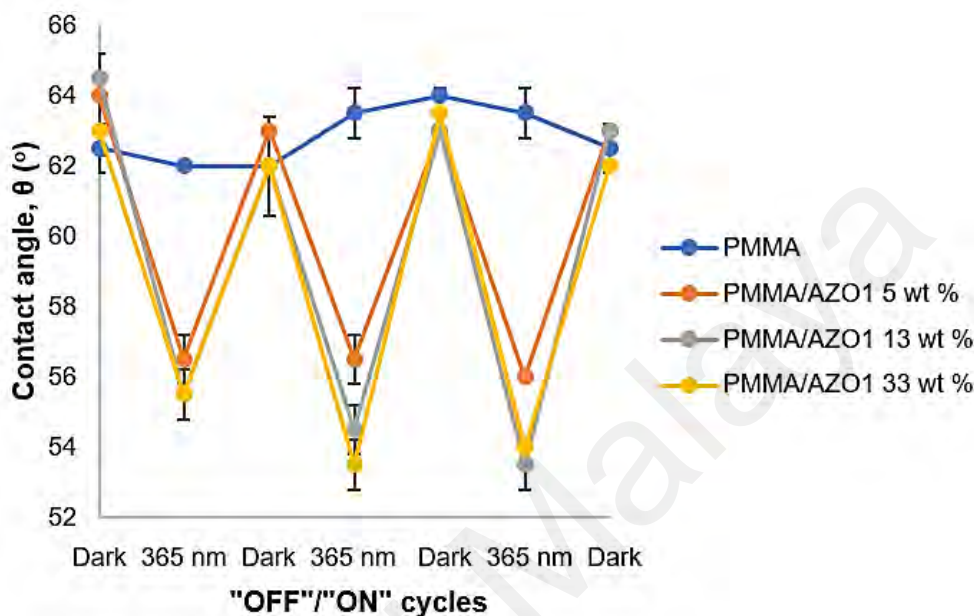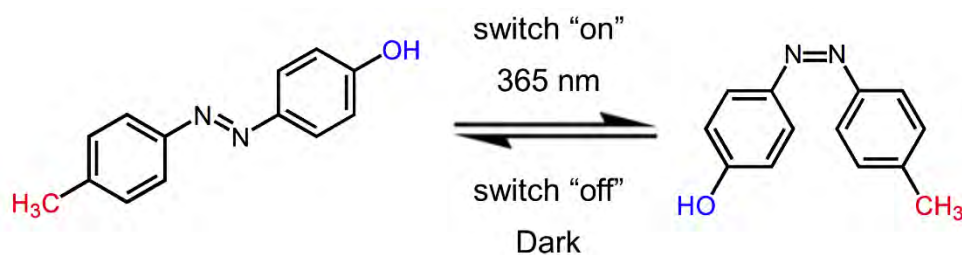
Figure 4.17: Changes in contact angle values for PMMA/**AZO1** coating films upon UV light irradiation cycles.

After the exposure of UV-A irradiation, the water contact angles have dropped to 55.5º-56.5º, which have clearly shown that *trans→cis* photoisomerization of **AZO1** occurred in the coating films. Moreover, this indicated that the *cis-* isomer is more polar, and the changes in the dipole moment of the azo molecules contributed to an overall reduction in the contact angle values (Lim et al., 2006). It can also be shown that increasing the content of **AZO1** chromophores in coating films from 13 wt. % to 33 wt. % did not give any significant decrease in the water contact angle values. This possibly showed that saturation of the surface with chromophores has occurred, most likely due to the segregation of chromophores to the coating film surface (Hutchings et al., 2011). Moreover, crystallisation of chromophores due to phase separation of chromophores from

the coating film may also happen at higher concentrations as indicated in **Figure 4.14**, further signifying the segregation processes of chromophores.

It is suggested that *cis*-**AZO1** molecules could have random arrangements on the coating surfaces as well (**Figure 4.16**(f)). A combination of dipole moments of *cis*-**AZO1** and −OH groups on the surfaces led to the reduction in static water contact angles. As a result, the coating films become more hydrophilic after UV-A exposure. Subsequently, when the coating films containing **AZO1** chromophores were kept in the dark, the contact angles reverted, signifying that the thermal *cis→trans* isomerization process has occurred and this has confirmed the reversibility of **AZO1** isomerization. The reversibility of *trans-cis* isomerization processes is confirmed as the contact angle values changed accordingly upon UV irradiation cycles.

Since the **AZO1** chromophores were found to have random arrangements in the PMMA matrices, it is proposed that the *trans-cis* isomerization processes could change the interaction sites on the coating film surface. This is illustrated in **Figure 4.18**. Initially, the interaction sites of PMMA/**AZO1** coating films mainly consist of hydrophilic –OH groups. Then, when *trans→cis* photoisomerization has occurred, there are new interaction sites available, in the form of dipole moments from the lone pair electrons in the azo N atoms. When *cis*-**AZO1** thermally relaxed, these additional interactions disappeared.
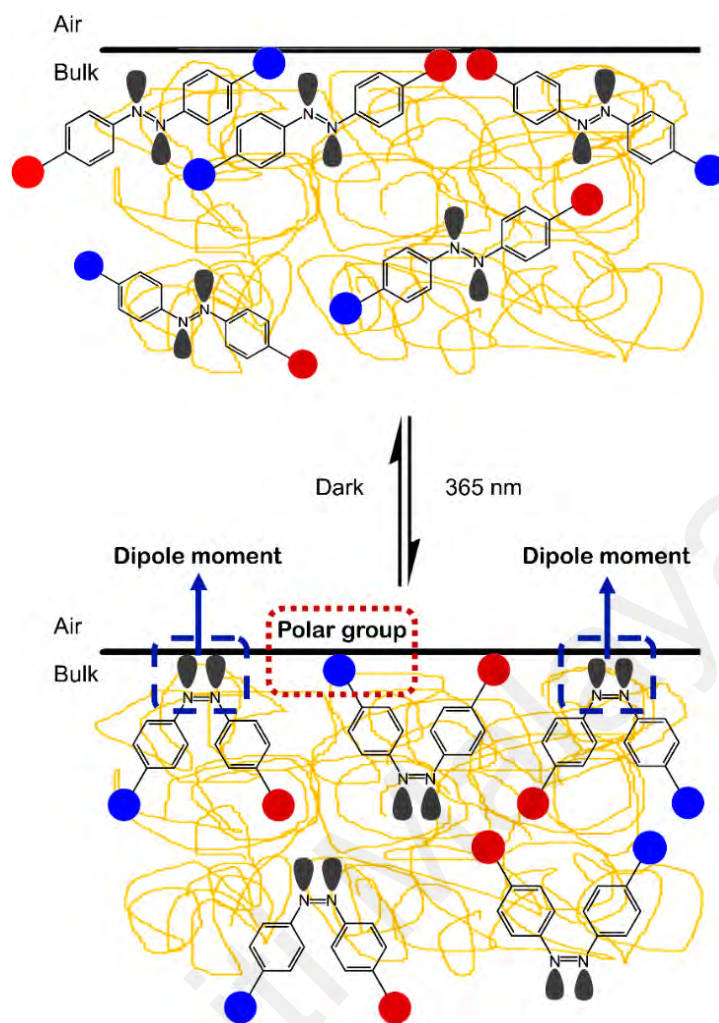
Figure 4.18: The possible interaction sites of PMMA/**AZO1** blends as coating films before and after UV-A irradiation. Red circles represent $-CH_3$ groups and blue circles represent $-OH$ groups. Nonbonding lone pair electrons are shown in grey.

To prove our proposed theory, the contact angle measurements on PMMA/**AZO2**(5) coating film were conducted as well. From **Figure 4.19**, it can be observed that initially, the contact angle is 71.5°, which indicates that the PMMA surface is less polar. In this case, only $-CH_3$ groups are present in **AZO2** molecules, therefore eliminating the various probable arrangements of molecules as discussed previously. Thus, the presence of $-CH_3$ groups on the surface has caused the surface to be more hydrophobic. By comparing the contact angle values of PMMA/**AZO1** coating films (63.0-64.5°), it is clear that **AZO1** molecules do have random arrangements in PMMA coating films, contributing to the lower contact angles than that of PMMA/**AZO2**(5) coating film.

Upon UV light irradiation, the PMMA/**AZO2**(5) surface became more hydrophilic as a result of the formation of *cis*-**AZO2**, in which its higher dipole moment increased the polarity of the surface. Moreover, it was shown that the changes in contact angle values, $\Delta\theta$ for PMMA/**AZO2**(5) coating was higher ($\Delta\theta = 10.5°$) than that of PMMA/**AZO1**(5) ($\Delta\theta = 7.5°$). Again, the reversibility of *trans-cis* isomerization processes is confirmed as the contact angle values changed accordingly upon UV irradiation cycles.
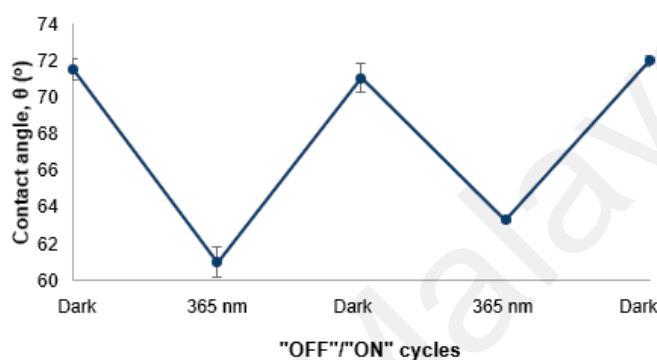
Figure 4.19: Changes in contact angle values for PMMA/**AZO2**(5) coating film upon UV light irradiation cycles.

4.2.3.2 Contact Angles of Other PMMA/Azobenzene Coating Films

To further probe our suggestion of azobenzene dyes to have random arrangements on the coating surface, **AZO3-10** are blended into PMMA and applied as coating films. The results of static water contact angle measurements are shown in **Table 4.5**:

Table 4.5: Static water contact angle values of various PMMA/azobenzene coating films

Coating	Water contact angle, θ (°)		Δθ (°)
	Before UV exposure	After UV exposure	
PMMA/**AZO3**(5)	62.0 ± 0.8	56.3 ± 1.0	5.8
PMMA/**AZO4**(5)	62.3 ± 1.0	58.8 ± 1.0	3.5
PMMA/**AZO5**(5)	62.5 ± 0.6	62.5 ± 0.6	0.0
PMMA/**AZO6**(5)	62.8 ± 0.5	62.5 ± 0.6	0.3
PMMA/**AZO6**(13)	65.3 ± 1.3	60.8 ± 1.0	4.5
PMMA/**AZO6**(20)	65.3 ± 1.0	60.7 ± 1.0	4.6
PMMA/**AZO7**(5)*	73.7 ± 0.8	64.8 ± 1.0	8.9
PMMA/**AZO8**(5)	71.3 ± 0.5	61.5 ± 0.6	9.8
PMMA/**AZO9**(5)	65.4 ± 0.9	71.0 ± 1.0	5.6

* forward and reverse isomerization occurred very fast

As expected, the PMMA/**AZO8** coating film (−OCH$_3$ groups) displays an average water contact angle value of 71.3°. This signify that −OCH$_3$ groups are present on the coating surfaces. Furthermore, when compared to the PMMA/**AZO1** coating films, which has an average water contact angle of 63.2°, it is suggested that there may be a mixture of −CH$_3$, −OH and phenyl groups on the surface as discussed in **Section 4.2.2.1**.

The coating containing **AZO9** however, has a water contact angle of 65.4°, which probably indicated that the phenyl groups are on the surfaces instead of −OH groups. This is expected as the −OH groups prefer to have hydrogen-bonding interactions with the carbonyl esters in the PMMA matrix. In addition, the segregation of molecules or polymers is favorable only if there is a reduction in surface energy. In order to increase the polarity of the surface, it is suggested that the PMMA/**AZO9** coating film should be thermally annealed in a high-boiling point polar non-solvent as described in **Section 2.4.3**.

Surprisingly, when dyes containing only fluorinated substituents (**AZO3-6**) are blended into PMMA, there are no significant changes in water contact angle values before and after the addition of dyes, even when the composition of dyes is increased. This is surprising since fluorinated groups should reduce the surface energy of surfaces significantly. This peculiar phenomenon is probably due to the tendency of fluorine atoms forming hydrophobic interactions with the electron-deficient carbon atoms found in carbonyl esters in the PMMA matrix (Mani & Arunan, 2013). It is also possible, though highly unlikely that the fluorine atoms form halogen bonds with the carbonyl esters in the PMMA matrix (Leonard, Halary, & Monnerie, 1985) since oxygen and fluorine are too electronegative to form non-covalent interactions (Kharandiuk et al., 2019). However, when a hydroxyl group is present in a fluorinated dye (**AZO7**), the water contact angle increased to 73.7°. It is possible that the dyes prefer to have hydrogen bonding interactions

with the carbonyl esters in the PMMA matrix since halogen bonds are weaker than hydrogen bonds (Cavallo et al., 2016).

AZO9 shows the best changes in water contact angle values (about 10º) when subjected to UV-A irradiation. Other dyes show good changes (about 5-6º) whereas the fluorinated chromophores **AZO3-6** show poor to no changes, which is peculiar due to the reasons explained earlier. In addition, it was shown that azobenzene moieties can be confined in hydrophobic regions, resulting in the restricted photoisomerization of azobenzene moieties (Morishima et al., 1992). Unfortunately, for **AZO7**, its fast forward and backward isomerization processes meant that accurate water contact angle readings could not be taken.

4.2.3.3 E-/Z- (trans→cis) Photoisomerization Kinetics of PMMA/**AZO1** and PMMA/**AZO2** Coating Films

It is expected that the *trans→cis* isomerization kinetics would deviate from the monoexponential decay curve since the isomerization of azobenzene derivatives in glassy polymers showed such behavior, thereby requiring stretched exponential or multiexponential functions for accurate data fitting (Poutanen et al., 2016). However, our results have indicated that the isomerization kinetics for PMMA/**AZO1** and PMMA/**AZO2** coating films showed monoexponential decay since the data fitted well with equation (3.5) with a high R^2 value (> 0.98). Similar observations where the azobenzene chromophores showed monoexponential decay behavior in PMMA matrices even at high chromophore concentrations were reported (Pakula et al., 2011). From **Figure 4.20** and **Table 4.6**, the rate of *trans→cis* photoisomerization of PMMA/**AZO1**(5) and PMMA/**AZO1**(13) coating films are similar. A slight reduction in the *trans→cis* photoisomerization rate for PMMA/**AZO1**(33) coating was possibly attributed to the matrix effect: at a certain concentration, **AZO1** dyes have limited free volume required to undergo photoisomerization (Pakula et al., 2011; Poutanen et al.,

2016). Further increase in the amount of **AZO1** dyes would further decrease the free volume of photoisomerization. As a result, a reduction in the photoisomerization rate was observed.
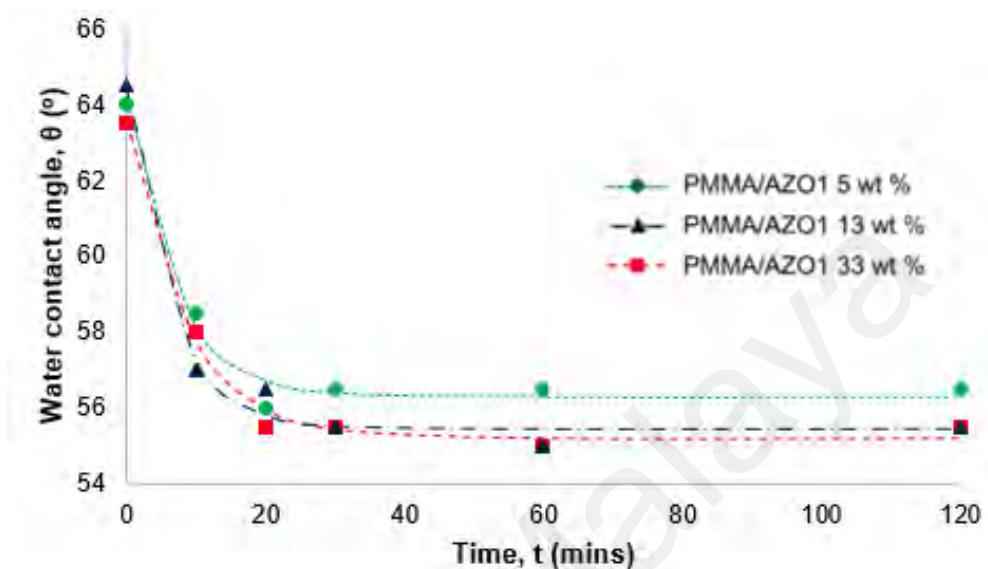
Figure 4.20: *E-/Z-* (*trans→cis*) photoisomerization of PMMA/**AZO1** coating films.

It can also be seen that the photostationary state (PSS) is reached for all coatings at about the 30th minute mark. In other words, 30 minutes of UV light irradiation should provide sufficient time for the dyes to convert into the *cis-* isomers. It is also worth mentioning that the formation of a plateau or maximum contact angle when the amount of **AZO1** dyes increased beyond 13 wt. % possibly implied that the chromophores are saturated on the surfaces, as discussed earlier.

Table 4.6: *E-/Z-* (*trans→cis*) photoisomerization kinetic parameters of PMMA/**AZO1** and PMMA/**AZO2** coating films

Coating	$k_{E→Z}$ (min⁻¹)	$t_{1/2}$ (min)	R^2
PMMA/**AZO1**(5)	0.1434	4.8337	0.9838
PMMA/**AZO1**(13)	0.1603	4.3241	0.9884
PMMA/**AZO1**(33)	0.1181	5.8692	0.9921
PMMA/**AZO2**(5)	0.0444	15.6114	0.9995

The rate of isomerization of **AZO2** in PMMA is markedly slower than that of **AZO1**, with **AZO2** reaching PSS only after 2 hours (**Figure 4.21**). In addition, its half-life of 15.6 mins is also significantly slower than **AZO1** (4.3 to 5.9 minutes). This has clearly indicated that the presence of a strong electron donor on one side of azobenzene molecule increases the photoisomerization rate.
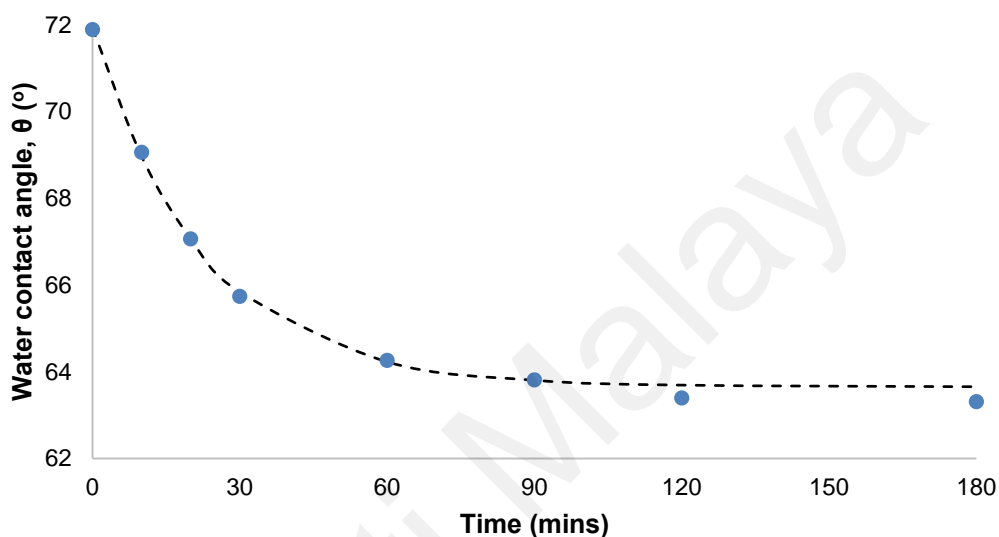
Figure 4.21: *E-/Z-* (*trans→cis*) photoisomerization of PMMA/**AZO2**(5) coating film.

4.2.3.4 Thermal Z-/E- (cis→trans) Isomerization Kinetics of PMMA/*AZO1* and PMMA/*AZO2* Coating Films

The thermal *cis→trans* isomerization of **AZO1** and **AZO2** dyes in PMMA coating films have also exhibited a monoexponential increase where the data fitted well with equation (3.5) with a high R^2 value (> 0.98). From **Figure 4.22** and **Table 4.7**, they have shown that the rate of thermal *cis→trans* isomerization of PMMA/**AZO1**(5) and PMMA/**AZO1**(13) coating films were similar. Like the *trans→cis* photoisomerization, a slight reduction in the thermal *cis→trans* isomerization rate is observed for the PMMA/**AZO1**(33) coating film. The **AZO1** dyes fully reverted to their *trans*-configuration after about 180 minutes in the dark.

Table 4.7: Thermal *Z*-/*E*- (*cis→trans*) isomerization kinetic parameters of PMMA/**AZO1** and PMMA/**AZO2** coating films

Coating	$k_{Z \to E}$ (min⁻¹)	$t_{1/2}$ (min)	R^2
PMMA/**AZO1**(5)	0.0280	24.7553	0.9818
PMMA/**AZO1**(13)	0.0299	23.1822	0.9939
PMMA/**AZO1**(33)	0.0211	32.8506	0.9929
PMMA/**AZO2**(5)	0.0044	157.2832	0.9968
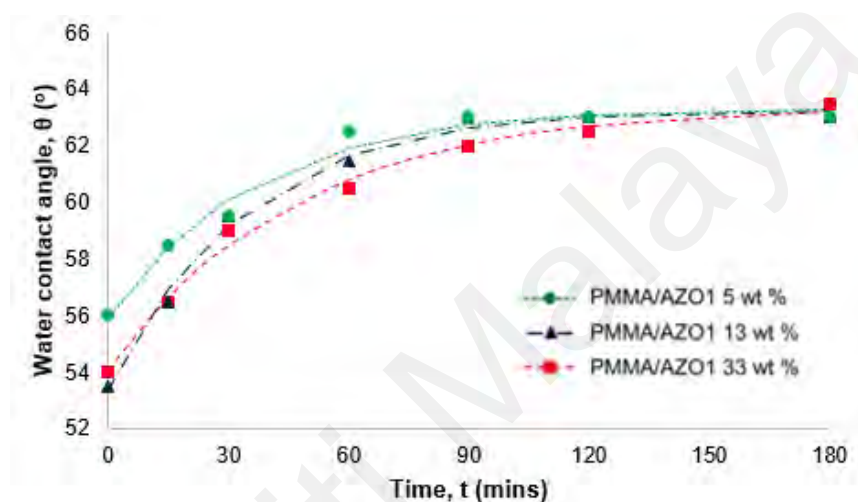
Figure 4.22: Thermal *Z*-/*E*- (*cis→trans*) isomerization of PMMA/**AZO1** coating films.

In contrast, **AZO2** chromophores have shown a significantly lower thermal isomerization rate, where the molecules fully revert after 10 hours, with a half-life of 157.3 minutes (**Figure 4.23**). Meanwhile, the half-life of *cis*-**AZO1** in PMMA coating films ranged from 23.2 to 32.9 minutes. These indicate that the thermal *cis→trans* isomerization process is fast, albeit considerably slower than pseudostilbene-type molecules (lifetimes of their *cis*-isomers are usually in the order of milliseconds/seconds (Barrett et al., 2007; Yager & Barrett, 2006). In contrast, for the case of azobenzene-type molecules (in this respect, **AZO2**), the lifetimes of their *cis*- isomers could be in the order of hours or even days (Barrett et al., 2007; Yager & Barrett, 2006). As a consequence, this specific property of azobenzene-type molecules may prove to be disadvantageous for the current work as it will take a significantly longer time for the *cis*- isomer to thermally

revert to the more thermodynamically stable *trans*- isomer. However, rapid regeneration of the *trans*- isomer can be done easily and efficiently by irradiation of the *cis*- isomer with blue or white light (Beharry et al., 2011; Dong et al., 2015; Pakula et al., 2011).
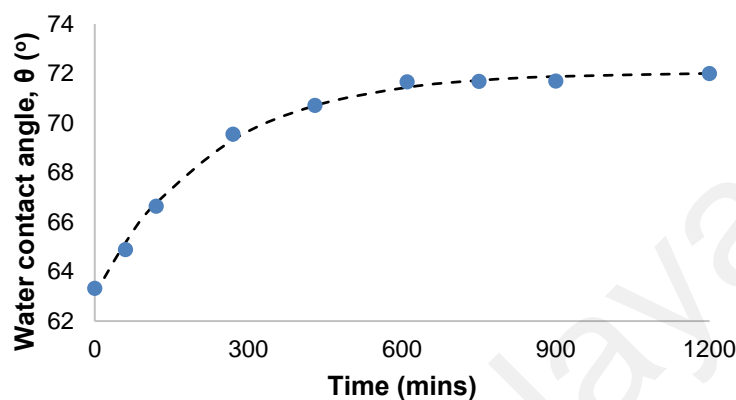
Figure 4.23: Thermal *Z-/E-* (*cis→trans*) isomerization of PMMA/**AZO2**(5) coating film.

4.2.4 Sticker Peel-Off Test

From the results of static contact angle measurements, the polarity of surfaces can indeed be tuned. The random orientations of **AZO1** chromophores in the coating films may bring about different interaction sites on the surface. Therefore, it is interesting to study whether interfacial interactions between coating film surface and any adhesive can be altered when subjected to UV light irradiation. Thus, as a proof of concept, commercial acrylic-based pressure-sensitive stickers were applied on top of PMMA and PMMA/**AZO1**(13) coating films. Subsequently, both coating films were subjected to a cycle of UV light irradiation for 12 hours and then in dark for another 12 hours for 14 consecutive days. PMMA/**AZO1**(13) coating film was chosen for the sticker peel-off test since it showed the best photoswitching performance whereas PMMA/**AZO2**(5) coating film was not chosen due to the slower isomerisation rate of **AZO2** in comparison to that of **AZO1**. **Figure 4.24** shows the conditions of the stickers on the coating films after 14 irradiation cycles:
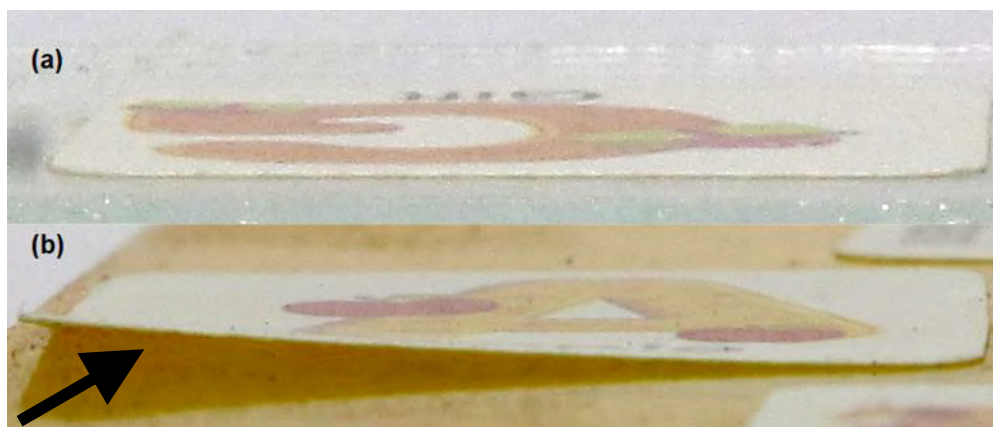
Figure 4.24: Condition of paper stickers on (a) blank PMMA and (b) PMMA/**AZO1**(13) coating films after 14 UV-A irradiation cycles (for 14 days).

The extent of sticker peeling off from coating surfaces was determined by recording the area that the sticker has peeled off. **Figure 4.25** shows the extent of sticker peeling off from coating surfaces. The darker regions represent the area of sticker still sticking onto the surface whereas the lighter regions represent the area of sticker already peeled off. It was discovered that the sticker remained unpeeled on the pure PMMA coating film after 14 days. In contrast, the sticker has peeled nearly half of itself off from the PMMA/**AZO1**(13) coating surface within 14 days as shown in **Figure 4.25**.
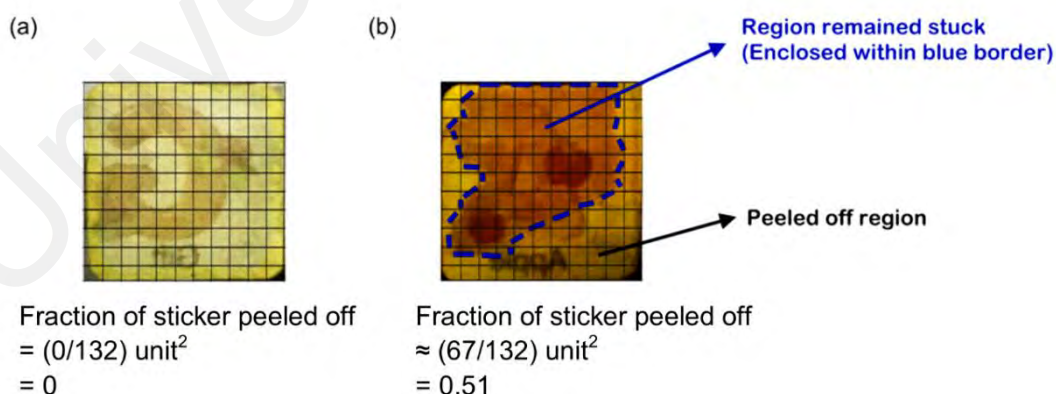
Figure 4.25: Estimated area of sticker peeled off after 14 UV-A irradiation cycles (for 14 days) for (a) PMMA and (b) PMMA/**AZO1**(13) coating films.

Despite the limitations of the study, it is proposed that the repeated excitation of dye molecules in the coating caused substantial changes in the sticker/coating interfacial

interactions (**Figure 4.26**). Initially, the coating-sticker interfacial interactions consisted of weak van der Waals forces and hydrogen bonding interactions (sticker and −OH moieties in **AZO1**). Subsequently, when the dye molecules are excited upon UV-A irradiation to form *cis*- isomers, there are additional dipole-dipole interactions between the coating and sticker surfaces. However, these additional interactions are lost once the dye molecules reverted to the *trans*- isomer. The repetition of *trans-cis* isomerization processes caused random reorientation and arrangements of the chromophores (Kaneta et al., 2017). As a result, there is a considerable amount of alterations to sticker/coating interactions and consequently, the sticker peeled itself off slowly from the coating film surface. Furthermore, the proposed peeling-off mechanism is in agreement with the results of static contact angle measurements.
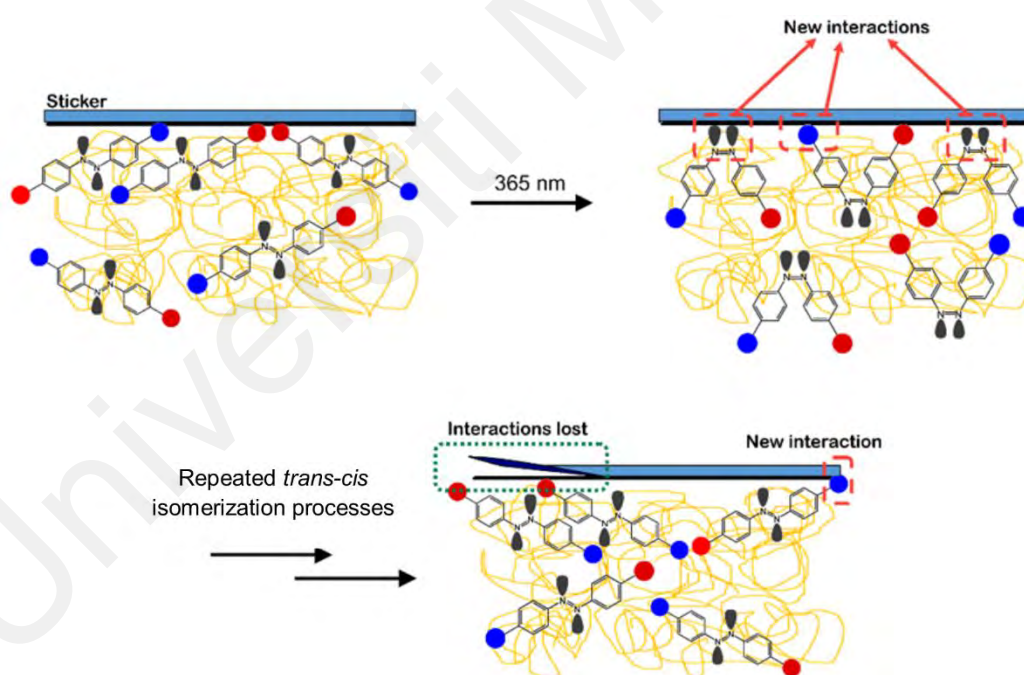
Figure 4.26: Proposed sticker peeling-off mechanism.

4.2.5 *Effect of PMVEMA-ES on the Physicooptical Properties of PMMA/AZO1 Coating Films*

As discussed in **Section 4.1.4**, PMMA has a tendency to form free standing films after application on polar substrates. Therefore, to overcome this problem, PMVEMA-ES was

added as an additive to enhance the coating adhesion onto glass substrates. Moreover, the results of using PMVEMA-ES as an adhesion promoter were indeed promising, reflected by the cross-hatch adhesion test. Ergo, it is of great interest to study the photochemical behavior of **AZO1** molecules in PMMA matrix with the presence of PMVEMA-ES.

4.2.5.1 Water Contact Angle Measurements

The *trans→cis* isomerization of azobenzene derivatives should bring about changes in polarity, with the *cis-* isomer typically having a higher dipole moment than that of the *trans-* isomer. As a result, the effect of dipole moment changes can be reflected from contact angle measurements. As deionized water is used as the contacting fluid, it is expected that as *trans→cis* photoisomerization progresses, the contact angle would decrease as the overall dipole moment of the surface increases with increasing *cis-* isomer content. Meanwhile, the contact angle values should revert when the coating films are placed either in dark conditions or illuminated under visible light, where the *cis-* isomer reverts to its original configuration. **Figure 4.27** shows the effect of contact angle values on the *trans-cis* isomerization processes of **AZO1** in PMMA and PMMA/PMVEMA-ES matrices.
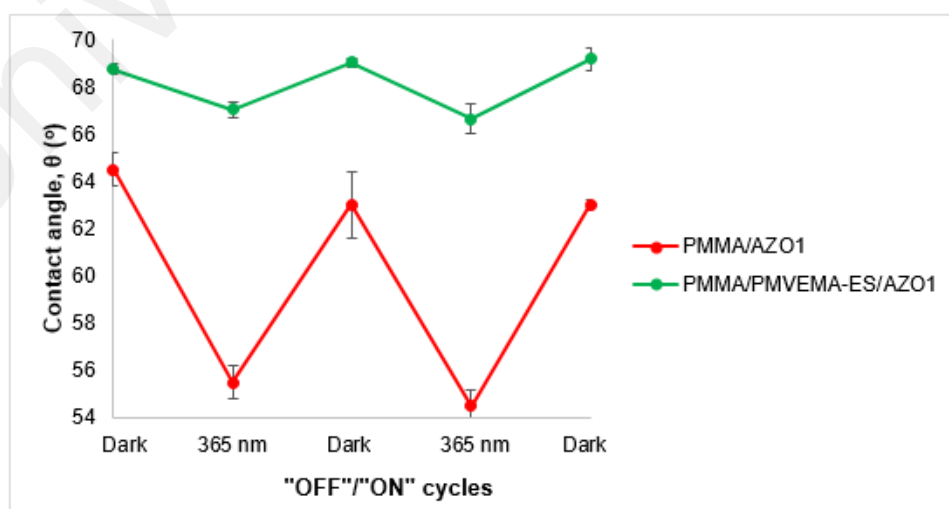
Figure 4.27: Changes in contact angle values for PMMA/**AZO1**(13) and PMMA/PMVEMA-ES/**AZO1**(13) coating films upon UV light irradiation cycles.

136

It can be seen that **AZO1** showed reversible *trans-cis* isomerization processes in both PMMA and PMVEMA-ES matrices, as reflected in **Figure 4.27**. The initial contact angle of PMMA/**AZO1**(13) coating film is 64.5º whereas for PMMA/PMVEMA-ES/**AZO1**(13) is 68.8º. We expect that the contact angle value of PMMA/PMVEMA-ES/**AZO1**(13) is lower due to the polar nature of PMVEMA-ES. However, the value is higher possibly due to the rougher surface of PMMA/PMVEMA-ES/**AZO1**(13) coating film. Upon UV light illumination, both coating films showed a decrease in contact angle values, indicating that the coating films contain *cis*- rich chromophores. The contact angle values reverted when the coating films are kept in the dark, indicating reversible isomerization processes.

It was found that the changes in contact angle values, $\Delta\theta$ for PMMA/**AZO1**(13) coating film ($\Delta\theta = 9.0$º) is greater than that of PMMA/PMVEMA-ES/**AZO1**(13) coating film ($\Delta\theta = 2.4$º). The low $\Delta\theta$ value of PMMA/PMVEMA-ES/**AZO1**(13) system possibly reflected the incomplete isomerization of **AZO1**. The effect of incomplete isomerization can be seen where labeling stickers did not peel off even after a few days, as opposed to the observation made for PMMA/**AZO1**(13) system.

It was discovered that hydrogen bonding interactions, especially if the azo –N=N− groups were involved, proved to be detrimental to reversible *trans-cis* isomerization processes of azobenzene moieties (Feng et al., 2005). Additionally, intermolecular hydrogen bonds lowered the proportion of *cis*-azobenzenes at PSS (Ya et al., 2008). In PMMA matrices, the azo –N=N− of **AZO1** molecules are not involved in any intermolecular hydrogen bonding interactions since PMMA is not a hydrogen bond donor (**Figure 4.28**(a)). As a result, the azo –N=N− is free to rotate or undergo inversion processes suitable for reversible *trans-cis* isomerization processes. The performance of **AZO1** in PMMA/PMVEMA-ES matrix is in stark contrast to that of in PMMA matrix.

This is possibly due to the intermolecular COOH···O−H, O−H···O=C and azo N···HOOC hydrogen bonding interactions between the carboxylic acid groups in PMVEMA-ES chains and the hydrogen bond sites (−OH and –N=N−) in **AZO1** (**Figure 4.28**(b)). These interactions caused **AZO1** to be confined inside the coating matrix. Therefore, the azobenzene dyes are locked and could not undergo reversible photoisomerization processes freely.
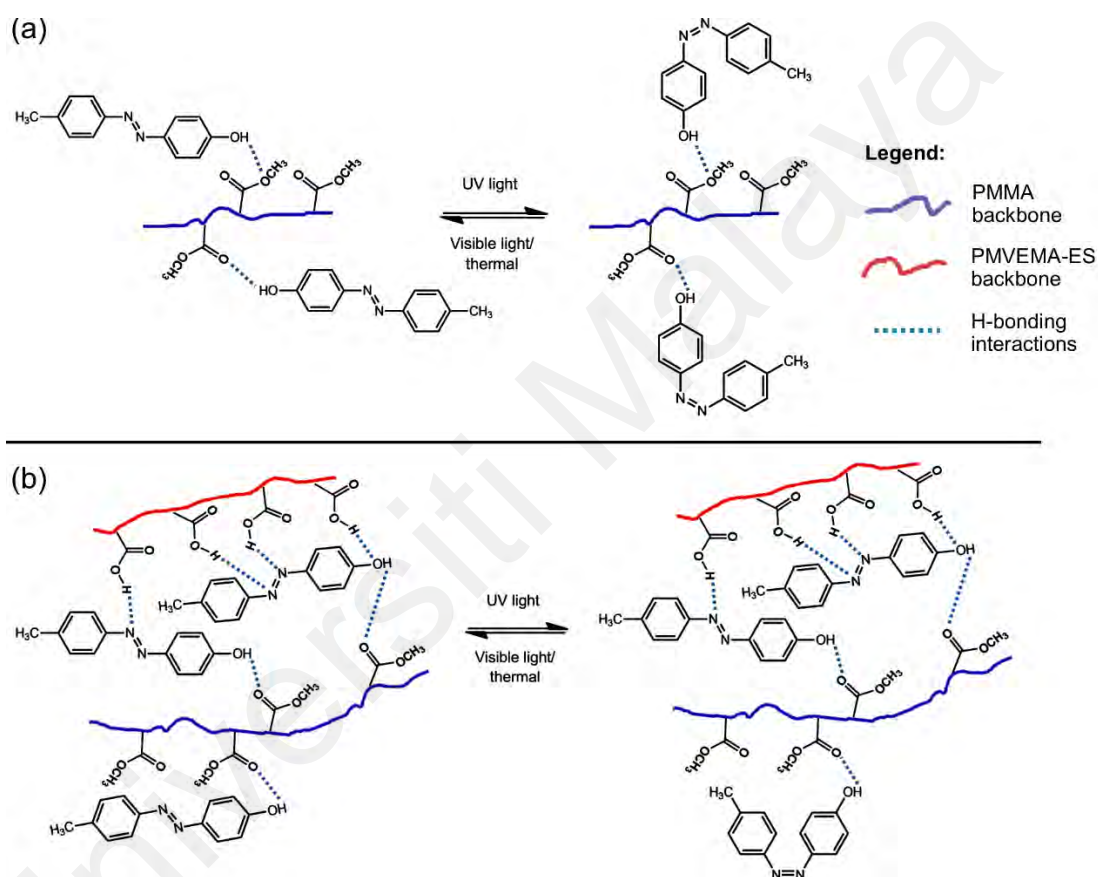
Figure 4.28: Reversible *E*-/*Z*- and *Z*-/*E*- isomerization processes of **AZO1** in (a) PMMA and (b) PMMA/PMVEMA-ES matrices. Note that in (b), only a fraction of **AZO1** is able to undergo isomerization processes due to intermolecular hydrogen bonding interactions.

4.2.5.2 *Photoisomerization Kinetic Studies*

To gain a deeper understanding on the observed results from the contact angle measurements, photoisomerization kinetics of **AZO1** blended into PMMA and PMMA/PMVEMA-ES coating films were investigated. Kinetic parameters such as activation energy, E_a and pre-exponential factor, A are discussed here.

It is expected that the photoisomerization kinetics of **AZO1** will deviate from the exponential model due to matrix effect. As shown in **Section 4.1.4**, the T_g of PMMA and PMMA/PMVEMA-ES blends were higher than room temperature. Hence, it can be assumed that the prepared coating films have glassy characteristic at room temperature. Having said that, the *trans→cis* isomerization of **AZO1** in PMMA and PMMA/PMVEMA-ES matrices decayed/increased exponentially, as reflected by the high R^2 values (> 0.99) when the data were fitted using equation (3.1) (**Figures 4.29** and **4.30**).
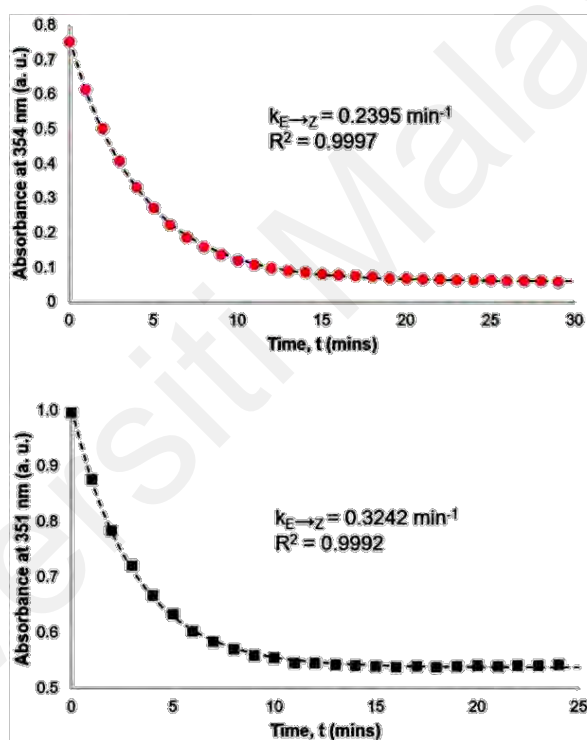
Figure 4.29: *E-/Z-* (*trans→cis*) photoisomerization of PMMA/**AZO1**(0.04) (top) and (b) PMMA/PMVEMA-ES/**AZO1**(0.04) (bottom) coating films.
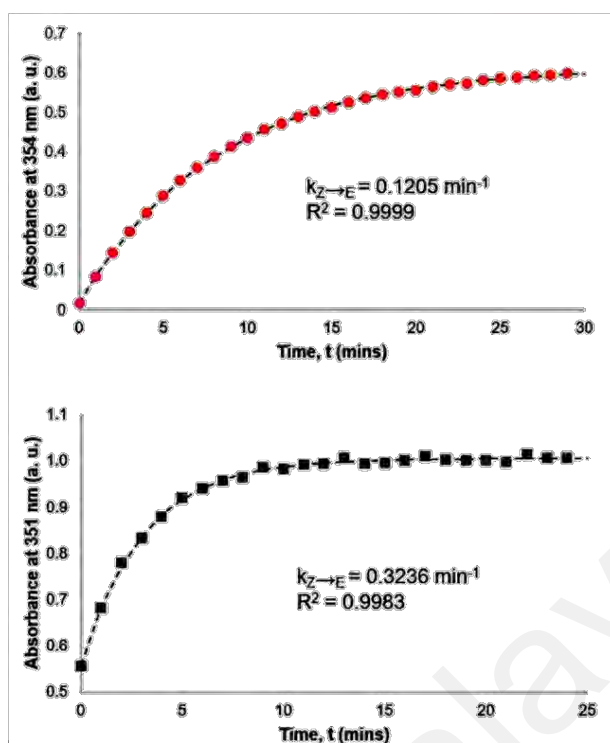
Figure 4.30: *Z-/E-* (*cis→trans*) photoisomerization of PMMA/**AZO1**(0.04) (top) and PMMA/PMVEMA-ES/**AZO1**(0.04) (bottom) coating films.

AZO1 can be classified as a hydroxyazobenzene derivative. This fact will play an important role in its *E-/Z-* and *Z-/E-* photoisomerization kinetics. From **Table 4.8**, it is observed that **AZO1** in PMMA/PMVEMA-ES matrix showed higher rates of photoisomerization. This is probably due to intermolecular hydrogen bond-assisted tautomerization of **AZO1** (**Figure 4.31**), which contributed to the observed increase in isomerization rates (Poutanen et al., 2016). This effect is not observed in PMMA system because the PMMA is not a hydrogen bond donor. Hence, in order for tautomerization to occur, chromophore-chromophore interactions should be considered (Poutanen et al., 2016). Note that in this experiment, the concentration of dyes was relatively low (only 0.04 wt. % dry film content). Thus, there is a lower probability of hydrogen bond-assisted tautomerization of **AZO1** occurring in PMMA matrix. The significantly lower values of α_Z of **AZO1** in PMMA/PMVEMA-ES matrix compared to that of in PMMA matrix indicated that a significant proportion of **AZO1** does not switch from *E*-configuration to the *Z*-configuration. This further highlights the possibility of intermolecular

140

COOH⋯O−H, O−H⋯O=C and azo N⋯H−OOC hydrogen bonding interactions between **AZO1** and PMVEMA-ES, making the chromophores more rigid, thus lowering their free volume for isomerization to take place.
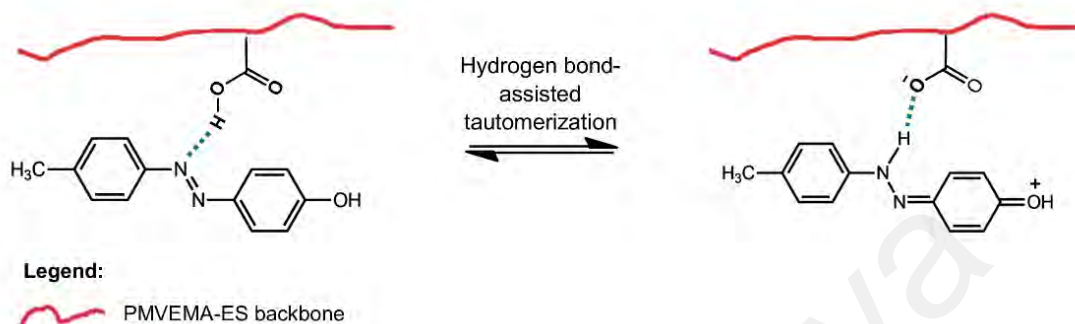
Figure 4.31: Hydrogen bond-assisted tautomerization reaction between **AZO1** and PMVEMA-ES.

Table 4.8: *E*-/*Z*- and *Z*-/*E*- photoisomerization rate constants of **AZO1** in different matrices at 25 °C

Matrix	$k_{E-/Z-}$ (s⁻¹)	α_Z (%)	$k_{Z-/E-}$ (s⁻¹)
PMMA	0.2395	92.09	0.1205
PMMA/PMVEMA-ES	0.3242	46.32	0.3236

The thermodynamic parameters of *E*-/*Z*- and *Z*-/*E*- photoisomerization processes of **AZO1** in PMMA and PMMA/PMVEMA-ES matrices such as activation energy, E_a, pre-exponential factor, A, activation enthalpy, $\Delta H^{\ddagger}$ and activation entropy, $\Delta S^{\ddagger}$ were studied as well (**Table 4.9**). It is observed that A, E_a, $\Delta H^{\ddagger}$ and $\Delta S^{\ddagger}$ increased from PMMA to PMMA/PMVEMA-ES matrices for both *E*-/*Z*- and *Z*-/*E*- photoisomerizations of **AZO1**. Moreover, all $\Delta H^{\ddagger}$ values are positive, indicating non-spontaneous changes. Meanwhile, all $\Delta S^{\ddagger}$ values are negative, indicating non-spontaneous changes.

Table 4.9: *E-/Z-* and *Z-/E-* photoisomerization thermodynamic parameters for **AZO1** in different matrices

Matrix		PMMA	PMMA/PMVEMA-ES
A (sec^{-1})	*E-/Z-*	1.526×10^1	1.131×10^5
	Z-/E-	3.510×10^4	1.344×10^6
E_a (kJ mol^{-1})	*E-/Z-*	10.438	28.923
	Z-/E-	34.283	37.734
$\Delta H^{\ddagger}$ (kJ mol^{-1})	*E-/Z-*	7.919	26.422
	Z-/E-	31.764	35.233
$\Delta S^{\ddagger}$ (J mol^{-1} K^{-1})	*E-/Z-*	−230.712	−166.298
	Z-/E-	−156.626	−135.993

A higher E_a indicates a higher transition state energy, leading to slower chemical reaction. Higher E_a values gave higher A values, a possible indication of the pre-exponential factor tending to compensate the change of activation energy (Katada et al., 2015). The values of $\Delta H^{\ddagger}$ and $\Delta S^{\ddagger}$ also seemed to complement the values of E_a and A. Higher E_a gave higher A, $\Delta H^{\ddagger}$ and $\Delta S^{\ddagger}$. The positive values of $\Delta H^{\ddagger}$ indicated that the enthalpy of transition state is higher than the reactant. The negative values of $\Delta S^{\ddagger}$ indicated that the entropy of transition state is lower. In terms of E_a and $\Delta H^{\ddagger}$, the values are highest in PMMA/PMVEMA-ES, indicating higher energy required to convert **AZO1** from *E-* to *Z-* and from *Z-* to *E-*. The higher $\Delta S^{\ddagger}$ value for PMMA/PMVEMA-ES matrix indicated the possibility of **AZO1** undergoing hydrogen bond-assisted tautomerization, which further increased the disorder of the system.

4.2.5.3 Glossiness

In addition to water contact angle measurements and UV-Vis studies, gloss measurements may also indicate changes in coating properties upon UV light irradiation. To the best of our knowledge, there is no report on monitoring the *trans-cis* isomerization processes of azobenzene derivatives in coating blends using gloss measurements. Thus, this section highlights our findings on gloss measurements as one of the tools in monitoring the *trans-cis* isomerization processes.

Gloss measurements were taken at 20° because the surface of coating films showed high glossiness at 60°. From **Figure 4.32**, both coating films display high gloss values (> 70 GU), with PMMA/**AZO1**(13) coating film showing higher glossiness than that of PMMA/PMVEMA-ES/**AZO1**(13) coating film. The observed lower glossiness for the PMMA/PMVEMA-ES/**AZO1**(13) coating film was due to the PMVEMA-ES molecular structure, which was similar to the findings described in **Section 4.1.4**. *E-/Z-* (*trans→cis*) isomerization of **AZO1** in both coating films have occurred due to the changes in gloss values before and after UV exposure. It is expected that PMMA/**AZO1**(13) will show higher difference since a higher proportion of **AZO1** can isomerize compared to that of PMMA/PMVEMA-ES/**AZO1**(13). However, a higher gloss difference was observed for PMMA/PMVEMA-ES/**AZO1**(13) (3.06 GU) compared to that of PMMA/**AZO1**(13) (2.25 GU). Besides, when both coating films were exposed to UV light, the gloss values were higher, since *cis*-**AZO1** $\pi→\pi^*$ transition band was shifted hypsochromically to lower wavelength, thus having lower absorption at the near UV-Vis region, resulting in more light that was reflected and detected by the gloss meter. The gloss values of coating films reverted when both coating films were kept in the dark for 24 h, indicating that *cis*-**AZO1** reverted to *trans*-**AZO1**. This showed that gloss measurements can be used as one of the methods to study the changes in optical properties of films and coatings due to *trans-cis* isomerization processes.
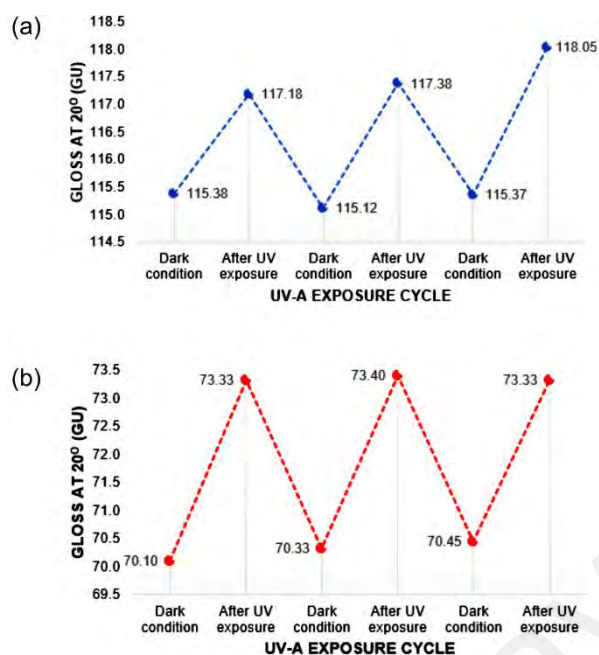
Figure 4.32: Gloss measurements for (a) PMMA/**AZO1**(13) and (b) PMMA/PMVEMA-ES/**AZO1**(13) coating films upon UV light irradiation cycles.

4.2.5.4 Sticker Peel-Off Test

We compared the performance of (a) PMMA/**AZO1**(13) and (b) PMMA/PMVEMA-ES/**AZO1**(13) coating films on their abilities to peel the labeling stickers off upon UV-A irradiation cycles. **Figure 4.33** illustrates the results of the test. It is shown that without PMVEMA-ES additive, the labeling stickers peeled off from the coating surface (**Figure 4.33**(a) and (b)) after a few days. In contrast, there is no evidence of stickers peeling off from PMMA/PMVEMA-ES/**AZO1**(13) coating film even after a few UV-A irradiation cycles (**Figure 4.33**(c) and (d)). This is possibly due to the intermolecular COOH⋯O−H, O−H⋯O=C and azo N⋯HOOC hydrogen bonding interactions between the carboxylic acid groups in PMVEMA-ES chains and the hydrogen bond sites (−OH and –N=N−) in **AZO1**. These interactions inevitably caused the **AZO1** chromophores to be confined inside the coating matrix. Therefore, the azobenzene dyes were less flexible in the matrix and could not undergo reversible photoisomerization processes freely.
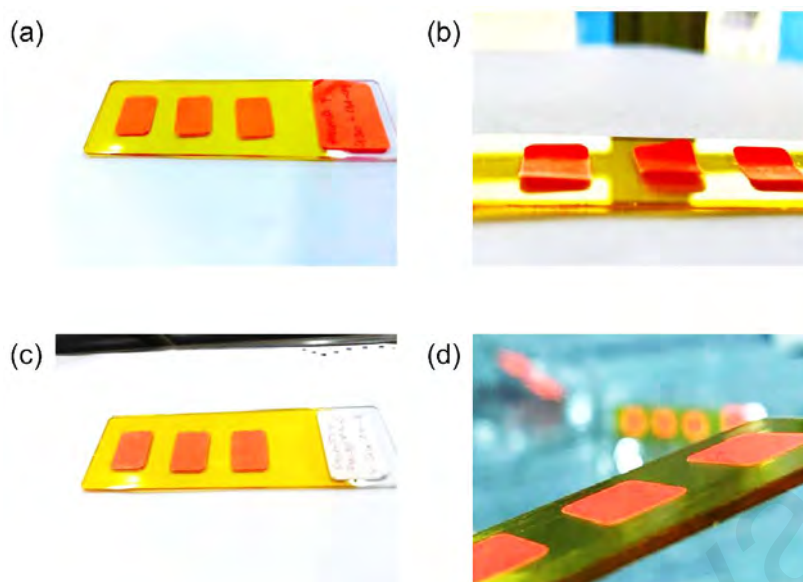
Figure 4.33: Condition of labeling stickers on PMMA/**AZO1**(13) coating film (top half) (a) before UV-A irradiation cycles and (b) after a few UV-A irradiation cycles. Bottom half shows the condition of labeling stickers on PMMA/PMVEMA-ES/**AZO1**(13) coating film (c) before UV-A irradiation cycles and (d) after a few UV-A irradiation cycles.

4.2.6   *Remarks on Azobenzene Derivatives as Photoswitchable Additives*

Since PMMA/**CAD2**(5) coating film exhibited contrasting evidence of reversible *E-/Z-* isomerization, the focus was shifted towards azobenzene derivatives which clearly displayed reversible *E-/Z-* isomerization processes. It was shown that the preparation of PMMA/azobenzene coating films showing desirable phototunable surface polarities have been successful. The isomerization rate was higher for azobenzene derivatives containing strong electron-donating groups, as showcased by **AZO1**. The choice of substituents on the azobenzene moiety also influenced their photochemical behavior in PMMA matrices, as fluorinated dyes showed peculiar behavior possibly due to the hydrophobic interactions between the fluorine atoms and the electron-deficient carbonyl carbon atoms found in PMMA. These interactions in turn may have possibly locked the azobenzene derivatives in place from undergoing complete isomerization, as evidenced by the low $\Delta\theta$ values. Upon multiple isomerization cycles, PMMA/**AZO1**(13) coating film showed the ability to peel stickers off as a result of ever-changing sticker/coating interfacial interactions.

As indicated in **Figure 4.14**, a further increase in the concentration of **AZO2** molecules caused the crystallization of the chromophores in PMMA matrices. Thus, the dyes in general needed to be modified so that their solubility in PMMA matrices will be enhanced. Additionally, the use of small molecules as an additive would also alter the bulk properties of a polymer where the T_g of the bulk polymer is usually reduced (Ansari et al., 2007). In our case, the addition of **AZO1** and **AZO2** reduced the T_g of PMMA as highlighted in the DSC results. Therefore, an azobenzene end-functionalized PMMA, **P1** is synthesized in order to overcome such problems mentioned earlier. Further details of the synthesis and application of **P1** as a photoswitchable additive are highlighted in **Section 4.3** later.

Upon the addition of PMVEMA-ES into the coating formulation, it was shown that the intermolecular COOH···O−H, O−H···O=C and azo N···H−OOC hydrogen bonding interactions between **AZO1** and PMVEMA-ES possibly contributed to the lower proportions of *cis*-**AZO1** at PSS as a result of restricted isomerization of **AZO1** chromophores. As a consequence, there is lower changes in surface polarity which contributed to the poorer sticker peel-off performance.

In addition to conventional methods such as UV-Vis spectroscopy and contact angle measurements, we have successfully utilized gloss measurements to observe and study the reversible *trans-cis* isomerizations of **AZO1**.

4.3   Low-M_w Azobenzene End-Functionalized PMMA as a Photoswitchable Additive in PMMA Coating Films for Reversible Surface Polarity

As discussed in **Section 4.2.3**, azobenzene derivatives with short alkyl chains such as **AZO2** tend to crystallize in the PMMA matrix. Hence, the azobenzene derivatives needed to be modified so that their solubility in PMMA matrices will be enhanced. Increasing the length of alkyl chains or degree of branching in azobenzene derivatives allowed their

solubility in PMMA matrices to be enhanced (Pakula et al., 2011). In addition, small-molecule additives are hardly ideal for surface modification since they usually reduce the T_g of the bulk polymer (Ansari et al., 2007). Thus, a low-M_w, azobenzene end-functionalized PMMA additive, **P1** was synthesized, in which it consisted of an azobenzene "head" and a PMMA "tail". The structure of **P1** is similar to a surfactant, in which the PMMA tail should enhance the solubility in bulk PMMA matrix. Due to the relatively low molecular weight compared to the bulk polymer, the modified PMMA should be able to segregate to the surface, with a behavior similar to micelles in solution (Hardman et al., 2011; Hutchings et al., 2011; Sarih, 2010). Additionally, surface modification of bulk polymers with polymer additives are advantageous since they do not alter the properties of the bulk polymers (Ansari et al., 2007). Only one such example is available due to time constraints.

4.3.1 *Synthesis Attempts of Azobenzene End-Functionalized PMMA Additives via Living Anionic Polymerization Reaction – Termination Method*

As discussed in **Section 2.6**, end-functionalized polymers synthesized *via* living anionic polymerization techniques are widely applied, regardless of monomer types as well as the nature of the living polymer. For methacrylate polymers especially, controlled temperature is necessary for the success of polymerization and subsequently, end capping reactions. Polymerization reactions of methacrylates carried out in polar solvents such as THF are advantageous since end groups can be easily inserted (Kohsaka & Kitayama, 2015). Termination of living PMMA anions with an electrophile such as allyl halide (Al-Takrity et al., 1990c), aryl halides (Al-Takrity et al., 1990b; Matsuo et al., 2004), acid chlorides (Al-Takrity et al., 1990b) as well as olefins such as di-*tert*-butyl maleate (Cernohous et al., 1997) and *trans-β*-nitrostyrene (Wang et al. 2014) were reported with great success.

Scheme 4.1 highlights our synthesis attempts using termination method. However, our attempts to synthezise PMMA additives by end capping with various alkyl and aryl halides proved to be futile as there is no evidence of end capping from ^{1}H NMR data.
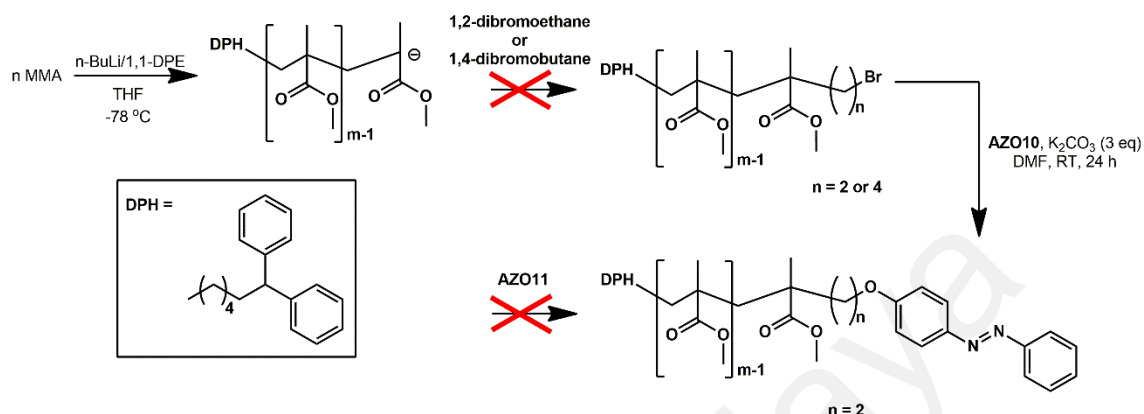
Scheme 4.1: Synthesis attempts of end-functionalized PMMA additives *via* termination method. All polymerization and end capping reactions were carried out using high vacuum techniques.

4.3.2 *Synthesis of Azobenzene End-Functionalized PMMA Additive, P1 via Living Anionic Polymerization Reaction – Initiation Method*

After a series of failures, we have finally synthesized an azobenzene end-functionalized PMMA, **P1**. Regrettably, the conventional termination of living PMMA species with 4-(bromoalkyl)azobenzene derivatives or dibromoalkanes did not yield the expected product. Hence, an alternative way was to synthesize an azobenzene-containing initiator.

Recently, researchers from Zheng and Guan's group discovered that *t*-BuOK can be used as an initiator for living anionic polymerization of methacrylate monomers using THF as a solvent in ambient conditions (Li et al., 2019a, 2019b; Zhang et al., 2019; Zheng et al., 2017). Their works proved to be one of the most industrially significant breakthroughs in living anionic polymerization of methacrylate monomers as there is no requirement to use very low temperatures (usually −78 °C or below) for polymerization

reactions. Inspired from their works, our synthetic plan was to synthesize an azobenzene-based initiator containing a tertiary alkoxide group, hoping that the synthesized alkoxide could initiate the polymerization of methyl methacrylate.

The strategy was to incorporate a tertiary alcohol into the azobenzene derivative. This was accomplished by the Grignard reaction of azobenzene derivative containing an ester group with methyl magnesium iodide to yield the tertiary alcohol. After purification, the tertiary alcohol azobenzene derivative was deprotonated with equimolar t-BuOK to generate the active initiator species. Residual t-BuOH generated from the deprotonation reaction was vacuum distilled using high vacuum techniques. Then, the required amount of dried THF was added, followed by the required amount of monomer. After that, the polymerization mixture was stirred for 24 hours at room temperature before the addition of degassed MeOH to terminate the living polymer. Reprecipitation of the polymer solution in excess hexane or methanol resulted in a yellow-colored solid polymer, **P1**, with the structure of **P1** confirmed by ^{1}H NMR (**Figure 4.34**).

It is shown that the doublet at 7.61 ppm initially from **I1** has shifted to 7.50 ppm, indicating that there is a change in the chemical environment of the said protons. Thus, proving that polymerization has indeed taken place. Moreover, the presence of a small singlet at 3.90 ppm also indicated the presence of $-OCH_3$ groups in **P1**.
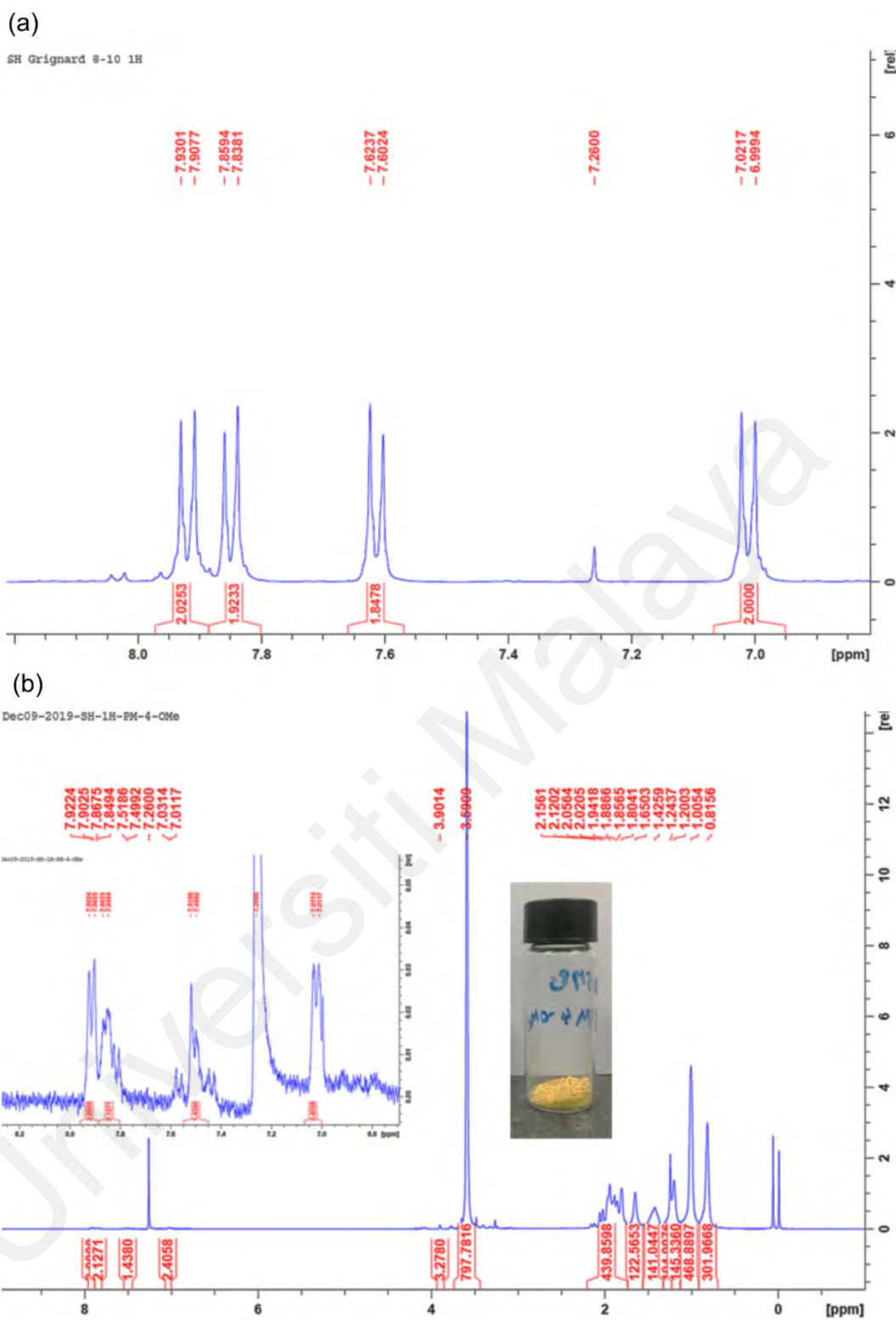
Figure 4.34: [^1]H NMR of (a) **I1** (only the aromatic regions) and (b) **P1**. Inset of **Figure 4.34**(b) shows the presence of four doublets, indicating phenyl moieties of azobenzene moiety near the aromatic region.

This method of obtaining azobenzene end-functionalized PMMA has its own problems and challenges, mainly the efficiency of initiator. For this particular reaction, the targeted

number-average molecular weight (M_n) is 5,000 g mol^{-1}. However, integration values from ^{1}H NMR showed that the observed M_n is about 26,500 g mol^{-1}. Then, by taking the ratio of targeted M_n to observed M_n, the initiator efficiency was found to be only 18.9%. Previous works (Li et al., 2019a, 2019b; Zhang et al., 2019; Zheng et al., 2017) have also highlighted the same issue with *t*-BuOK. After a certain concentration, further addition of *t*-BuOK resulted in no change in the molecular weight distribution of synthesized polymers owing to the agglomeration of *t*-BuOK molecules. From this revelation, it was inferred that our synthesized initiator may also formed agglomerates, which has reduced its efficiency. From our observations, to obtain very low-M_w PMMA additives, the initiator concentration should be very dilute to prevent agglomeration.

4.3.3 Characterization of Coating Films Containing Azobenzene End-Functionalized PMMA Additive, P1

4.3.3.1 Water Contact Angle Measurements

As discussed previously in **Section 2.4.1**, annealing polymer films above their T_g can speed up the segregation of polymer additives to the surface (Hardman et al., 2011; Hutchings et al., 2011; Sarih, 2010). The T_g of bulk PMMA granules (average molecular weight = 120,000 g mol^{-1}) is 105 ^{o}C (from Sigma-Aldrich). Hence, PMMA/**P1**(5) coating films were annealed at 120 ^{o}C at different times. **Figure 4.35** illustrates the effect of polymer segregation when **P1** was used as the polymer additive.
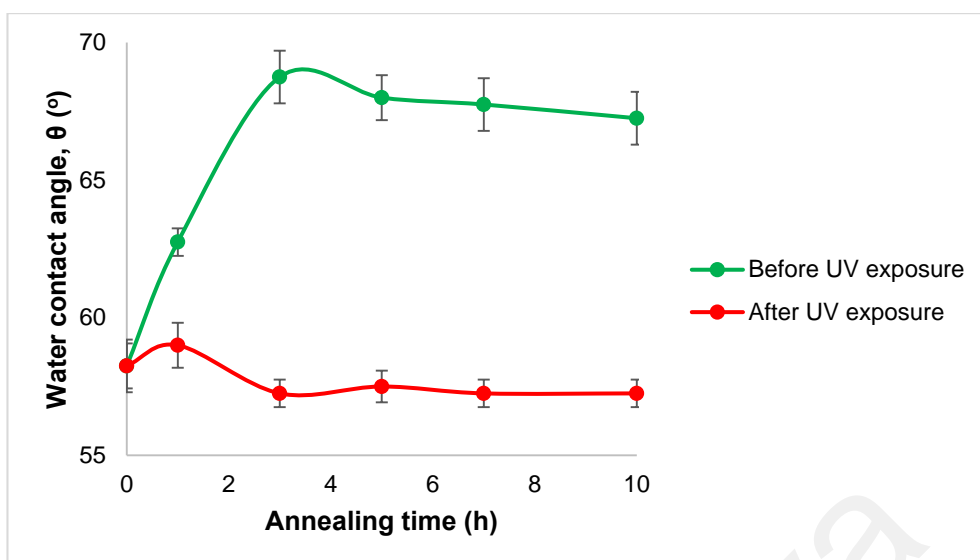
Figure 4.35: Effect of annealing time on contact angle values of PMMA/**P1**(5) coating films.

As the annealing time increased, the water contact angle also increased. This indicated that the surface became more concentrated with −OCH₃ groups that were covalently bonded to the azobenzene moiety of **P1** molecules. The water contact angle changed drastically during the first hour and subsequently slowing down up to 3 h. After 3 h, the water contact angle remained nearly constant.

The effects of thermal annealing can also be seen when the same coating films were treated with UV-A light. Under the irradiation of UV-A light, *trans→cis* photoisomerization of the azobenzene moieties in **P1** has taken place. With the absence of thermal annealing, the water contact angle of PMMA coating film did not change and remained constant at about 58º. This indicated that the surface contained low amounts of azobenzene moieties. However, as annealing time increased, the difference in water contact angle values before and after UV-A irradiation became more prominent. Thus, indicated that more azobenzene moieties have segregated to the coating surface. It was also observed that the contact angle value reverted after the coating films were kept in the dark for 24 h. The reversibility of *trans-cis* photoisomerization is observed as the contact angle values change after each irradiation cycles (**Figure 4.36**).
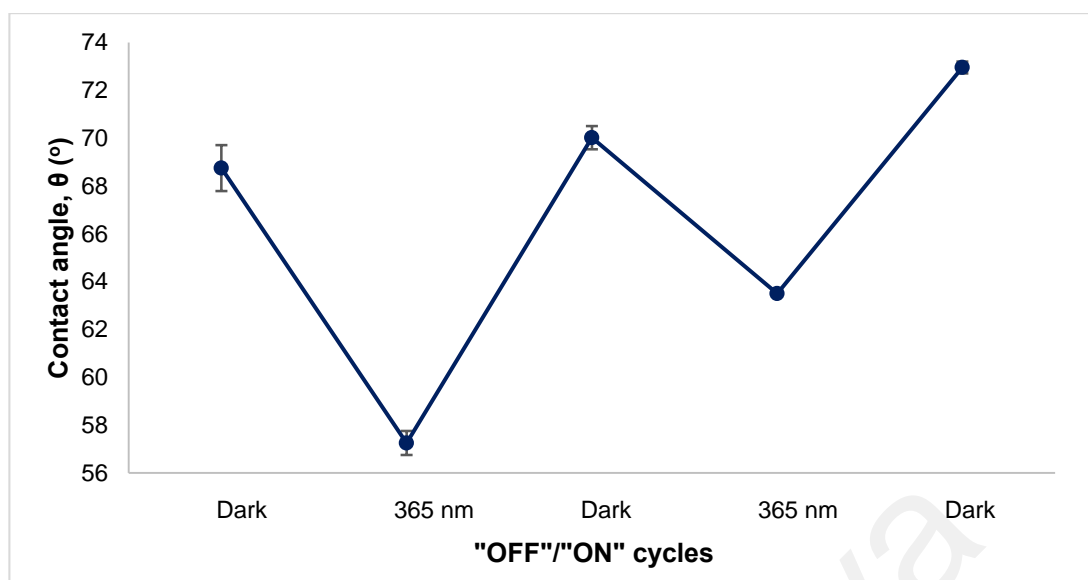
Figure 4.36: Changes in contact angle values for annealed PMMA/**P1**(5) coating film upon UV light irradiation cycles.

4.3.3.2 E-/Z- (trans→cis) Photoisomerization Kinetics of Annealed PMMA/*P1* Coating Film

The results indicated that the *trans→cis* isomerization of PMMA/**P1**(5) coating film showed monoexponential decay since the data fitted well with equation (3.5) with a high R^2 value (> 0.99), which was quite similar to the observations made in the earlier sections. From **Figure 4.37**, it is shown that the rate of *trans→cis* photoisomerization of PMMA/**P1**(5) coating is 0.0462 min^{-1}. Then, it is revealed that the PSS is reached about the 120th minute mark. In other words, 120 minutes of UV light irradiation should provide sufficient time for the azobenzene end-functionalized PMMA molecules to convert into the *cis*- isomers. The observed photoisomerization rate was slower than expected, since **P1** contains a strong electron donor (−OCH₃). Having said that, the azobenzene moiety was covalently bonded at the terminal ends of PMMA, therefore increasing the overall free volume required for photoisomerization to take place. Thus, the photoisomerization rate was lower than that of the free azobenzene dyes as shown in the earlier sections.
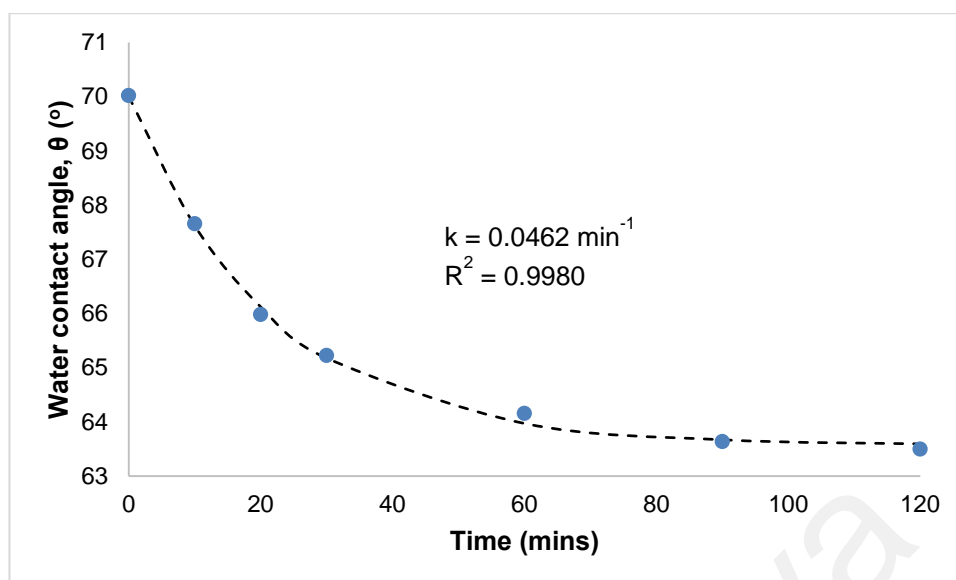
Figure 4.37: *E-*/Z- (*trans→cis*) photoisomerization of annealed PMMA/**P1**(5) coating film.

4.3.3.3 Thermal Z-/E- (cis→trans) Isomerization Kinetics of Annealed PMMA/*P1* Coating Film

The thermal *cis→trans* isomerization of PMMA/**P1**(5) coating film also showed monoexponential increase where the data fitted well with equation (3.5) with a high R^2 value (> 0.99). From **Figure 4.38**, it is shown that the rate of *cis→trans* thermal isomerization of PMMA/**P1**(5) coating film is 0.0092 min^{-1}. The **P1** additives fully reverted to their *trans-* configuration after about 670 minutes in the dark. The presence of a strong electron donor group seemed to have enhanced the rate of thermal isomerization of **P1**, where the rate was faster than that of **AZO2**, albeit still slower than **AZO1**. It was due to the significantly larger size of the **P1** molecules than that of the free dye molecules. As a result, an increase in the free volume of isomerization has lowered the isomerization rate.
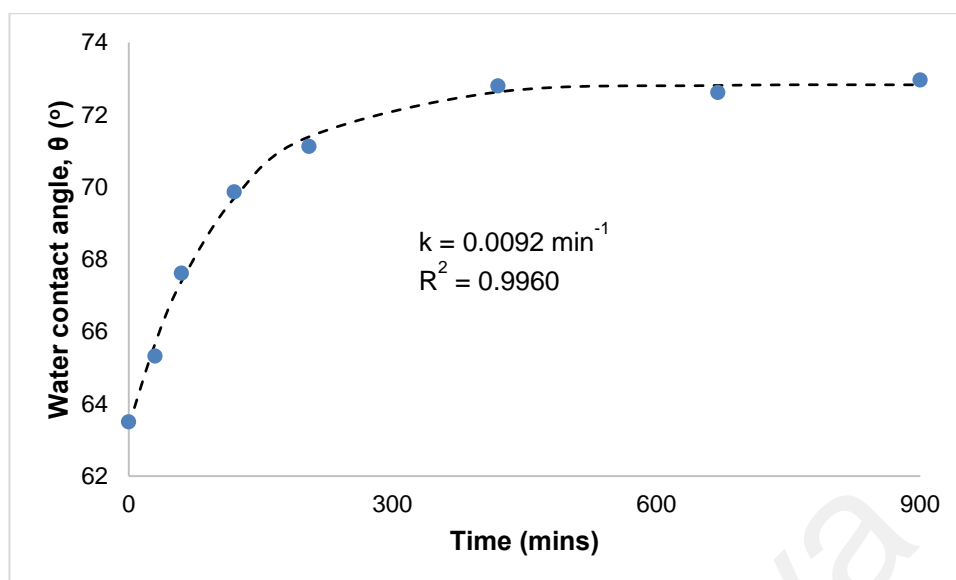
Figure 4.38: Thermal *Z-/E-* (*cis→trans*) isomerization of annealed PMMA/**P1**(5) coating film.

4.3.3.4 Sticker Peel-Off Test

The performance of (a) unannealed PMMA/**P1**(5) and (b) thermally annealed PMMA/**P1**(5) coating films on their abilities to peel the labeling stickers off upon UV-A irradiation cycle was investigated. **Figure 4.39** displays the results of the test. It is shown that without thermal annealing, the labeling sticker remained unpeeled from the coating surface (**Figure 4.39**(a)) even after a few days. In contrast, when the coating was thermally annealed, the sticker is peeled off from the surface after a few UV-A irradiation cycles (**Figure 4.39**(b)) due to the changes in sticker/coating interface upon UV light irradiation, as discussed in **Section 4.2.3**. This further supported the findings from the water contact angle measurements indicating that the segregation of end-functionalized PMMA molecules have occurred and that the photoactive azobenzene moiety was present at the coating surface. Therefore, it is crystal clear that the thermal annealing of polymer coating above its T_g allowed the enhanced surface segregation of PMMA additives driven by a reduction in surface free energies (Hardman et al., 2011; Hutchings et al., 2011; Sarih, 2010). Consequently, the performance of the annealed coating was better than that of its unannealed counterpart.
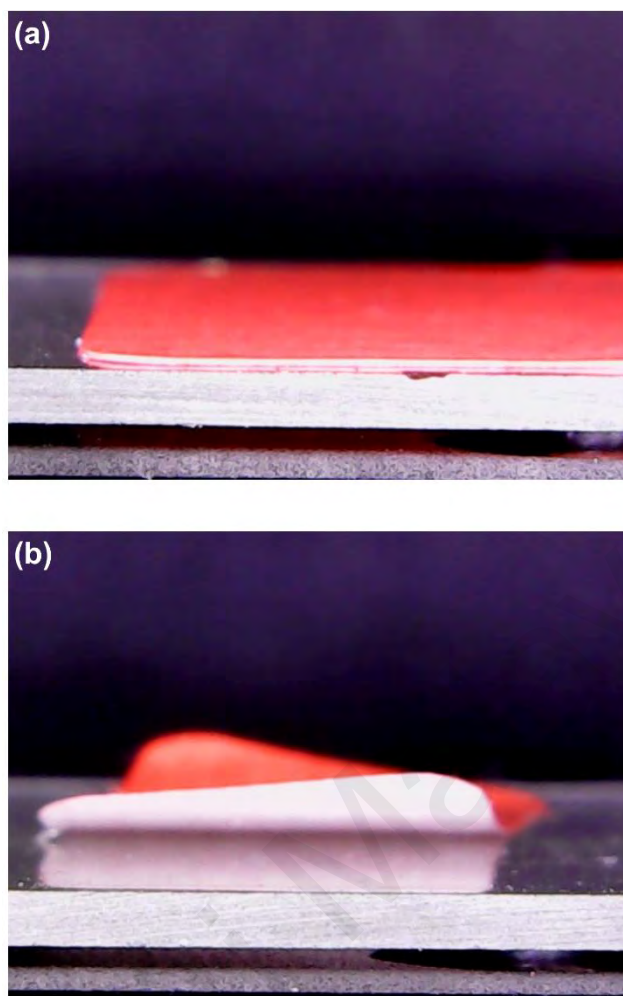
Figure 4.39: Condition of labeling stickers after a few days of UV irradiation cycles for (a) unannealed and (b) thermally annealed PMMA/**P1**(5) coating films.

4.3.4 Remarks on Azobenzene End-Functionalized PMMA as a Photoswitchable Additive

The widely used end-functionalization strategy *via* termination reactions proved to be a failure in producing the targeted end-functionalized PMMA containing azobenzene moieties. Therefore, a new strategy involving synthesizing a tertiary alcohol initiator containing the desired azobenzene moiety, **I1** was devised. **I1** has successfully initiated the polymerization of MMA *via* living anionic polymerization mechanism to yield **P1**. Despite the success of synthesizing **P1**, the polymerization reaction itself had a drawback, especially the efficiency of initiator. Lowered initiator efficiency has directly affected the

experimental M_n of **P1**, where it deviated from the calculated M_n. This is possibly due to the agglomeration of **I1** in solution, especially at high initiator concentration.

Nevertheless, **P1** was subsequently used as an additive in PMMA coating films. Thermal annealing has greatly enhanced the performance of PMMA/**P1**(5) coating films largely due to the segregation of **P1** molecules to the coating surface. In addition, the reversibility *trans-cis* isomerization processes of the azobenzene units in **P1** was observed as evidenced from the changes of contact angle measurements upon UV light irradiation. The thermally annealed PMMA/**P1**(5) coating film also showed that labeling sticker was peeled off in a few days of UV light irradiation cycles due to the changing of sticker/coating interfacial interactions.

CHAPTER 5: CONCLUSIONS

Firstly, PMMA/**CAD1-9** blends have been used successfully as coating films on glass substrates using only brushing method. It was initially thought that **CAD1-7** were predominantly azo tautomers. However, spectroscopic studies and previous reports have shown that **CAD1-7** were predominantly hydrazone tautomers while exhibited reversible *E-*/*Z-* isomerization as shown in the changes in contact angles of the coating films. On the other hand, they displayed contrasting evidence of reversible *E-*/*Z-* isomerization in solution form due to the significant overlapping of *E-* and *Z-* absorption bands as indicated from UV-Vis spectroscopy. Instead, the azobenzene derivatives **AZO1-9** were employed as additives. The isomerization rate was higher for azobenzene derivatives containing strong electron-donating groups, as showed by **AZO1**. The fluorinated dyes **AZO3-6** showed unexpected behavior, revealed by the low $\Delta\theta$ values possibly owing to the hydrophobic interactions between the fluorine atoms and the electron-deficient carbonyl carbon atoms found in PMMA. These interactions in turn may have possibly restricted the reversible isomerization processes. By comparing the contact angles of PMMA/**AZO1** and PMMA/**AZO2** coating films, it was revealed that the chromophores have random orientation in the coating matrices due to the repeated *trans-cis* isomerization processes. A proof of concept sticker peel-off test showed that upon multiple isomerization cycles, PMMA/**AZO1**(13) coating displayed the ability to peel the stickers off as a result of ever-changing sticker/coating interfacial interactions.

It is then found that PMVEMA-ES could enhance the adhesion of coating films onto glass substrates at the expense of significantly lowered proportion of *cis-***AZO1** molecules during *trans→cis* photoisomerization owing to intermolecular N=N⋯H-OOC hydrogen bonding interactions between PMVEMA-ES and azobenzene chromophores. Another problem was exhibited by **AZO2** where the crystallization inside the PMMA

matrix occurred when the concentration of chromophores is increased beyond 5 wt. %. Thus, the dyes needed to be modified so that their solubility in PMMA matrices will be enhanced. Additionally, the use of small molecules as an additive would also alter the bulk properties of a polymer, where the T_g of the bulk polymer was reduced. Therefore, the azobenzene end-functionalized PMMA, **P1** was synthesized in order to overcome such problems.

We have succeeded in synthesizing the end-functionalized PMMA, **P1** *via* living anionic polymerization reaction. An azobenzene-based initiator, **I1** was tailored such that there is a bulky tertiary alkoxide moiety present, mimicking the functions of *t*-BuOK. However, our in-house azobenzene-based initiator suffered from low initiator efficiency (only 18.9%). The synthesized **P1** was then blended into bulk PMMA coating film as an additive. Water contact angle measurements were conducted to study the effect of annealing time on contact angle values before and after UV-A irradiation. In this attempt, annealing the coating above its T_g drives the segregation of **P1** macromolecules to the surface forward, indicated by the increase in water contact angle values as annealing time increased. As anticipated, a greater change in water contact angle values was observed as the annealing time increased. The effect of thermal annealing has clearly been seen when the sticker remained unpeeled on the unannealed coating even after several UV irradiation cycles. These proof of concept experiments will lead to more development of photoresponsive coatings capable of reversible surface polarity to potentially reduce the problems associated with stickers and adhesives.

REFERENCES

Abbaszad Rafi, A., Hamidi, N., Bashir-Hashemi, A., & Mahkam, M. (2018). Photo-switchable nanomechanical systems comprising a nanocontainer (montmorillonite) and light-driven molecular jack (azobenzene-imidazolium ionic liquids) as drug delivery systems; synthesis, characterization, and in vitro release studies. *ACS Biomaterials Science & Engineering*, *4*(1), 184-192.

Abidin, Z., Nasir, K., Jamari, S., Saidon, N., Lee, S., Halim, N., & Yahya, R. (2013). The characteristics of a coating system containing lawsone dye colorant and PMMA-acrylic polyol blended resin. *Pigment & Resin Technology*, *42*(2), 128-136.

Ahmad, N. M., Lu, X., & Barrett, C. J. (2010). Stable photo-reversible surface energy switching with azobenzene polyelectrolyte multilayers. *Journal of Materials Chemistry*, *20*(2), 244-247.

Akiyama, H., & Tamaoki, N. (2007). Synthesis and photoinduced phase transitions of poly (N-isopropylacrylamide) derivative functionalized with terminal azobenzene units. *Macromolecules*, *40*(14), 5129-5132.

Alemdar, N., Karagoz, B., Erciyes, A. T., & Bicak, N. (2007). A method for polymethymetacrylate coating via self-curable unsaturated polyester primer on metal and glass surfaces. *Progress in Organic Coatings*, *60*(1), 69-74.

Alev, S., Collet, A., Viguier, M., & Schué, F. (1980). Utilisation du dicyclohéxyl-18 couronne-6 en polymérisation anionique. II. Polymérisation du methacrylate de methyle amorcee par les metaux alcalins. *Journal of Polymer Science: Polymer Chemistry Edition*, *18*(4), 1155-1161.

Alexander, C., & Shakesheff, K. M. (2006). Responsive polymers at the biology/materials science interface. *Advanced Materials*, *18*(24), 3321-3328.

Ali, U., Karim, K. J. B. A., & Buang, N. A. (2015). A review of the properties and applications of poly(methyl methacrylate) (PMMA). *Polymer Reviews*, *55*(4), 678-705.

Allen, P. E., & Williams, D. R. (1985). Stereoregulation of methyl methacrylate polymerization. *Industrial & Engineering Chemistry Product Research and Development*, *24*(2), 334-340.

Al-Takrity, E. T. B., Jenkins, A. D., & Walton, D. R. (1990a). The synthesis of polymers bearing terminal fluorescent and fluorescence-quenching groups, 1. The incorporation of fluorescent groups at one end of the macromoleculer by means of the initiation process. *Die Makromolekulare Chemie: Macromolecular Chemistry and Physics*, *191*(12), 3059-3067.

Al-Takrity, E. T. B., Jenkins, A. D., & Walton, D. R. (1990b). The synthesis of polymers bearing terminal fluorescent and fluorescence-quenching groups, 2. The incorporation of fluorescent and fluorescence-quenching groups by means of a direct termination process. *Die Makromolekulare Chemie: Macromolecular Chemistry and Physics*, *191*(12), 3069-3072.

Al-Takrity, E. T. B., Jenkins, A. D., & Walton, D. R. (1990c). The synthesis of polymers bearing terminal fluorescent and fluorescence-quenching groups, 3. The incorporation of fluorescent and fluorescence-quenching groups by means of an indirect termination process. *Die Makromolekulare Chemie: Macromolecular Chemistry and Physics*, *191*(12), 3073-3076.

An, Y., Chen, M., Xue, Q., & Liu, W. (2007). Preparation and self-assembly of carboxylic acid-functionalized silica. *Journal of Colloid and Interface Science*, *311*(2), 507-513.

Anderson, B., Andrews, G., Arthur Jr, P., Jacobson, H., Melby, L., Playtis, A., & Sharkey, W. (1981). Anionic polymerization of methacrylates. Novel functional polymers and copolymers. *Macromolecules*, *14*(5), 1599-1601.

Andrews, G., & Melby, L. (1984). New functional methacrylate polymers by anionic polymerization. In *New Monomers and Polymers* (pp. 357-380). Springer.

Ansari, I. A., Clarke, N., Hutchings, L. R., Pillay-Narrainen, A., Terry, A. E., Thompson, R. L., & Webster, J. R. (2007). Aggregation, adsorption, and surface properties of multiply end-functionalized polystyrenes. *Langmuir*, *23*(8), 4405-4413.

Aoshima, H., Satoh, K., & Kamigaito, M. (2013). Direct mechanistic transformations from isotactic or syndiotactic living anionic polymerizations of methyl methacrylate into metal-catalyzed living radical polymerizations. *ACS Macro Letters*, *2*(1), 72-76.

Archut, A., Vögtle, F., De Cola, L., Azzellini, G. C., Balzani, V., Ramanujam, P., & Berg, R. H. (1998). Azobenzene-functionalized cascade molecules: photoswitchable supramolecular systems. *Chemistry–A European Journal*, *4*(4), 699-706.

Arima, Y., & Iwata, H. (2007). Effect of wettability and surface functional groups on protein adsorption and cell adhesion using well-defined mixed self-assembled monolayers. *Biomaterials*, *28*(20), 3074-3082.

Azni, E. S. (2021). DBKL turunkan 518,644 iklan haram sekitar Kuala Lumpur. *Sinar Harian*.
https://www.sinarharian.com.my/article/118997/BERITA/Semasa/DBKL-turunkan-518644-iklan-haram-sekitar-Kuala-Lumpur

Ballard, D., Bowles, R., Haddleton, D., Richards, S., Sellens, R., & Twose, D. (1992). Controlled polymerization of methyl methacrylate using lithium aluminum alkyls. *Macromolecules*, *25*(22), 5907-5913.

Bandara, H. D., & Burdette, S. C. (2012). Photoisomerization in different classes of azobenzene. *Chemical Society Reviews*, *41*(5), 1809-1825.

Barrett, C. J., Mamiya, J.-i., Yager, K. G., & Ikeda, T. (2007). Photo-mechanical effects in azobenzene-containing soft materials. *Soft Matter*, *3*(10), 1249-1261.

Barrett, C., Natansohn, A., & Rochon, P. (1995). Cis-trans thermal isomerization rates of bound and doped azobenzenes in a series of polymers. *Chemistry of Materials*, *7*(5), 899-903.

Baskaran, D. (2003). Strategic developments in living anionic polymerization of alkyl (meth)acrylates. *Progress in Polymer Science*, *28*(4), 521-581.

Baskaran, D., & Müller, A. H. (1997). Kinetic investigation on metal free anionic polymerization of methyl methacrylate using tetraphenylphosphonium as the counterion in tetrahydrofuran. *Macromolecules*, *30*(7), 1869-1874.

Baskaran, D., & Müller, A. H. (2000). Anionic polymerization of methyl methacrylate using tetrakis[tris(dimethylamino)phosphoranylidenamino]phosphonium (P_5^+) as counterion in tetrahydrofuran. *Macromolecular Rapid Communications*, *21*(7), 390-395.

Baskaran, D., & Sivaram, S. (1997). Specific salt effect of lithium perchlorate in living anionic polymerization of methyl methacrylate and *tert*-butyl acrylate. *Macromolecules*, *30*(6), 1550-1555.

Baskaran, D., Chakrapani, S., & Sivaram, S. (1995). Effect of chelation of the lithium cation on the anionic polymerization of methyl methacrylate using organolithium initiators. *Macromolecules*, *28*(22), 7315-7317.

Beharry, A. A., Sadovski, O., & Woolley, G. A. (2011). Azobenzene photoswitching without ultraviolet light. *Journal of the American Chemical Society*, *133*(49), 19684-19687.

Bergius, W. N., Hutchings, L. R., Sarih, N. M., Thompson, R. L., Jeschke, M., & Fisher, R. (2013). Synthesis and characterisation of end-functionalised poly(*N*-vinylpyrrolidone) additives by reversible addition–fragmentation transfer polymerisation. *Polymer Chemistry*, *4*(9), 2815-2827.

Bierwagen, G. P., & Tallman, D. E. (2001). Choice and measurement of crucial aircraft coatings system properties. *Progress in Organic Coatings*, *41*(4), 201-216.

Braun, D., Herner, M., Johnsen, U., & Kern, W. (1962). Uber die stereospezifische polymerisation mit alkaliorganischen verbindungen V. Polymerisation von methyl-Methacrylat mit alkaliorganischen verbindungen. *Makromol Chem*, *51*, 15.

Byrne, C. J., Happer, D. A., Hartshorn, M. P., & Powell, H. K. J. (1987). The electronic effect of the phenylazo and *t*-butylazo groups. *Journal of the Chemical Society*, *Perkin Transactions*, *2*(11), 1649-1653.

Cavallo, G., Metrangolo, P., Milani, R., Pilati, T., Priimagi, A., Resnati, G., & Terraneo, G. (2016). The halogen bond. *Chemical Reviews*, *116*(4), 2478-2601.

Cernohous, J., Macosko, C., & Hoye, T. R. (1997). Anionic synthesis of polymers functionalized with a terminal anhydride group. *Macromolecules*, *30*(18), 5213-5219.

Chen, B., Wang, J., Shu, M., Zou, B., Guan, Y., & Zheng, A. (2014). A Novel Efficient Ligand in Anionic Polymerization at Elevated Temperature. *Chinese Journal of Chemistry*, *32*(11), 1128-1134.

Chen, X.-C., Tao, T., Wang, Y.-G., Peng, Y.-X., Huang, W., & Qian, H.-F. (2012). Azo-hydrazone tautomerism observed from UV-vis spectra by pH control and metal-ion complexation for two heterocyclic disperse yellow dyes. *Dalton Transactions*, *41*(36), 11107-11115.

Chung, K., Wu, C., & Malawer, E. (1990). Glass transition temperatures of poly(methyl vinyl ether-co-maleic anhydride) (PMVEMA) and poly(methyl vinyl ether-co-maleic acid) (PMVEMAC) and the kinetics of dehydration of PMVEMAC by thermal analysis. *Journal of Applied Polymer Science*, *41*(3-4), 793-803.

Coan, T., Barroso, G. S., Motz, G., Bolzán, A., & Machado, R. A. F. (2013). Preparation of PMMA/hBN composite coatings for metal surface protection. *Materials Research*, *16*(6), 1366-1372.

Collum, D. B. (1992). Is *N,N,N′,N′*-tetramethylethylenediamine a good ligand for lithium? *Accounts of Chemical Research*, *25*(10), 448-454.

Creton, C., & Papon, E. (2003). Materials science of adhesives: how to bond things together. *MRS Bulletin*, *28*(6), 419-423.

Dalton, L. R., Harper, A. W., Zhu, J., Steier, W. H., Salovey, R., Wu, J., & Efron, U. (1995, September). Ultrastructure synthesis of special architectures for photonic applications: high-frequency electro-optic modulators and high-density optical memories. In *Optical and Photonic Applications of Electroactive and Conducting Polymers* (Vol. 2528, pp. 106-115). International Society for Optics and Photonics.

Dashtizadeh, A., Abdouss, M., Mahdavi, H., & Khorassani, M. (2011). Acrylic coatings exhibiting improved hardness, solvent resistance and glossiness by using silica nano-composites. *Applied Surface Science*, *257*(6), 2118-2125.

Debnath, D., Roy, S., Li, B.-H., Lin, C.-H., & Misra, T. K. (2015). Synthesis, structure and study of azo-hydrazone tautomeric equilibrium of 1,3-dimethyl-5-(arylazo)-6-amino-uracil derivatives. *Spectrochimica Acta Part A: Molecular and Biomolecular Spectroscopy*, *140*, 185-197.

Deffieux, A., Sigwalt, P., & Boileau, S. (1984). Reactivities of fluorenyl species as ethylene oxide polymerization initiators—IV. Kinetic studies with cryptated 9-methylfluorenylsodium. *European Polymer Journal*, *20*(1), 77-80.

Delorme, N., Bardeau, J.-F., Bulou, A., & Poncin-Epaillard, F. (2005). Azobenzene-containing monolayer with photoswitchable wettability. *Langmuir*, *21*(26), 12278-12282.

Demir, M. M., Memesa, M., Castignolles, P., & Wegner, G. (2006). PMMA/zinc oxide nanocomposites prepared by in-situ bulk polymerization. *Macromolecular Rapid Communications*, *27*(10), 763-770.

Dhara, M. G., & Sivaram, S. (2009). Synthesis of Hydroxy-Functional PMMA Macromonomers by Anionic Polymerization. *Journal of Macromolecular Science®, Part A: Pure and Applied Chemistry*, *46*(10), 983-988.

Dhara, M. G., Baskaran, D., & Sivaram, S. (2008). Synthesis of amphiphilic poly(methyl methacrylate-b-ethylene oxide) copolymers from monohydroxy telechelic poly(methyl methacrylate) as macroinitiator. *Journal of Polymer Science Part A: Polymer Chemistry*, *46*(6), 2132-2144.

Dhara, M. G., Sivaram, S., & Baskaran, D. (2009). Synthesis of hydroxy-functionalized star-branched PMMA by anionic polymerization. *Polymer Bulletin*, *63*(2), 185-196.

Dimov, D. K., Warner, W. N., Hogen-Esch, T. E., Juengling, S., & Warzelhan, V. (2000). Synthesis of PMMA and PMMA block copolymers at elevated temperatures by phosphor ylide-mediated polymerizations. In *Macromolecular Symposia* (Vol. 157, No. 1, pp. 171-182). Weinheim: WILEY-VCH Verlag.

Ding, L., & Russell, T. P. (2007). A photoactive polymer with azobenzene chromophore in the side chains. *Macromolecules*, *40*(6), 2267-2270.

Dong, M., Babalhavaeji, A., Samanta, S., Beharry, A. A., & Woolley, G. A. (2015). Red-shifting azobenzene photoswitches for in vivo use. *Accounts of Chemical Research*, *48*(10), 2662-2670.

Du, Z., Dong, R., Ke, K., & Ren, B. (2018). Multiple stimuli-responsive rheological behavior of a functionalized telechelic associative model polymer in aqueous solution. *Journal of Rheology*, *62*(5), 1233-1243.

Du, Z., Ren, B., Chang, X., Dong, R., Peng, J., & Tong, Z. (2016). Aggregation and rheology of an azobenzene-functionalized hydrophobically modified ethoxylated urethane in aqueous solution. *Macromolecules*, *49*(13), 4978-4988.

Du, Z., Ren, B., Chang, X., Dong, R., & Tong, Z. (2017). An end-bifunctionalized hydrophobically modified ethoxylated urethane model polymer: multiple stimuli-responsive aggregation and rheology in aqueous solution. *Macromolecules*, *50*(4), 1688-1699.

Du, Z., Yan, X., Sun, N., & Ren, B. (2019). Dual stimuli-responsive nano-structure transition of three-arm branched amphiphilic polymers containing ferrocene (Fc) and azobenzene (Azo) moieties in aqueous solution. *Soft Matter*, *15*(43), 8855-8864.

Evans, S., Johnson, S., Ringsdorf, H., Williams, L., & Wolf, H. (1998). Photoswitching of azobenzene derivatives formed on planar and colloidal gold surfaces. *Langmuir*, *14*(22), 6436-6440.

Fayt, R., Forte, R., Jacobs, C., Jérôme, R., Ouhadi, T., Teyssié, P., & Varshney, S. K. (1987). New initiator system for the living anionic polymerization of *tert*-alkyl acrylates. *Macromolecules*, *20*(6), 1442-1444.

Feng, C. L., Jin, J., Zhang, Y. J., Song, Y. L., Xie, L. Y., Qu, G. R., Xu, Y., & Jiang, L. (2001). Reversible light-induced wettability of fluorine-containing azobenzene-derived Langmuir–Blodgett films. *Surface and Interface Analysis: An International Journal devoted to the development and application of techniques for the analysis of surfaces, interfaces and thin film*s, *32*(1), 121-124.

Feng, C. L., Zhang, Y. J., Jin, J., Song, Y. L., Xie, L. Y., Qu, G. R., Jiang, L., & Zhu, D. B. (2001). Reversible wettability of photoresponsive fluorine-containing azobenzene polymer in langmuir−blodgett films. *Langmuir*, *17*(15), 4593-4597.

Feng, W., Kun, H., Kun, & Wan, M.-X. (2005). Photophysical characteristics of polyaniline with photochromic azobenzene side groups. *Chinese Physics*, *14*(2), 306.

Furin, G., Andreevskaya, O., Rezvukhin, A., & Yakobson, G. (1985). Fluoroaromatic derivatives. CI. Transformations of polyfluoroazoxybenzenes in strong acids. Wallach rearrangement of polyfluoroazoxybenzenes. *Journal of Fluorine Chemistry*, *28*(1), 1-22.

Gałka, P., Kowalonek, J., & Kaczmarek, H. (2014). Thermogravimetric analysis of thermal stability of poly(methyl methacrylate) films modified with photoinitiators. *Journal of Thermal Analysis and Calorimetry*, *115*(2), 1387-1394.

Ge, H., Wang, G., He, Y., Wang, X., Song, Y., Jiang, L., & Zhu, D. (2006). Photoswitched wettability on inverse opal modified by a self-assembled azobenzene monolayer. *ChemPhysChem*, *7*(3), 575-578.

Gerner, F., Höcker, H., Müller, A., & Schulz, G. (1984). On the termination reaction in the anionic polymerization of methyl methacrylate in polar solvents—I. Kinetic studies. *European Polymer Journal*, *20*(4), 349-355.

Gledhill, R., Kinloch, A., & Shaw, S. (1977). Effect of relative humidity on the wettability of steel surfaces. *The Journal of Adhesion*, *9*(1), 81-85.

Glusker, D. L., Lysloff, I., & Stiles, E. (1961). The mechanism of the anionic polymerization of methyl methacrylate. II. The use of molecular weight distributions to establish a mechanism. *Journal of Polymer Science*, *49*(152), 315-334.

Glusker, D. L., Stiles, E., & Yoncoskie, B. (1961). The mechanism of the anionic polymerization of methyl methacrylate. I. Quantitative determination of active chains using radioactive terminators. *Journal of Polymer Science*, *49*(152), 297-313.

Goode, W., Owens, F., & Myers, W. (1960). Crystalline acrylic polymers. II. Mechanism studies. *Journal of Polymer Science*, *47*(149), 75-89.

Graham, R. K., Dunkelberger, D. L., & Goode, W. E. (1960). Anionic copolymerization: the inability of the poly-(methyl methacrylate) anion to initiate the polymerization of styrene[1]. *Journal of the American Chemical Society*, *82*(2), 400-403.

Guo, Y., Xiao, J., Sun, Y., Song, B., Zhang, H., & Dong, B. (2021). Photoswitching of the melting point of a semicrystalline polymer by the azobenzene terminal group for a reversible solid-to-liquid transition. *Journal of Materials Chemistry A*, *9*(14), 9364-9370.

Hadjichristidis, N., Iatrou, H., Pispas, S., & Pitsikalis, M. (2000). Anionic polymerization: high vacuum techniques. *Journal of Polymer Science Part A: Polymer Chemistry*, *38*(18), 3211-3234.

Haghbeen, K., & Tan, E. W. (1998). Facile synthesis of catechol azo dyes. *The Journal of Organic Chemistry*, *63*(13), 4503-4505.

Hamelmann, F., Heinzmann, U., Siemeling, U., Bretthauer, F., & der Brüggen, J. V. (2004). Light-stimulated switching of azobenzene-containing self-assembled monolayers. *Applied Surface Science*, *222*(1-4), 1-5.

Han, M., Honda, T., Ishikawa, D., Ito, E., Hara, M., & Norikane, Y. (2011). Realization of highly photoresponsive azobenzene-functionalized monolayers. *Journal of Materials Chemistry*, *21*(12), 4696-4702.

Han, M., Ishikawa, D., Honda, T., Ito, E., & Hara, M. (2010). Light-driven molecular switches in azobenzene self-assembled monolayers: effect of molecular structure on reversible photoisomerization and stable *cis* state. *Chemical Communications*, *46*(20), 3598-3600.

Hardman, S. J., Hutchings, L. R., Clarke, N., Kimani, S. M., Mears, L. L., Smith, E. F., Webster, J. R., & Thompson, R. L. (2012). Surface modification of polyethylene with multi-end-functional polyethylene additives. *Langmuir*, *28*(11), 5125-5137.

Hardman, S. J., Muhamad-Sarih, N., Riggs, H. J., Thompson, R. L., Rigby, J., Bergius, W. N., & Hutchings, L. R. (2011). Electrospinning superhydrophobic fibers using surface segregating end-functionalized polymer additives. *Macromolecules*, *44*(16), 6461-6470.

Hatada, K., Kitayama, T., & Ute, K. (1988). Stereoregular polymerization of α-substituted acrylates. *Progress in Polymer Science*, *13*(3), 189-276.

Hatada, K., Kitayama, T., Fujikawa, K., Ohta, K., & Yuki, H. (1981). Anionic Polymerization: Kinetics, Mechanisms, and Synthesis. In *ed. JE McGrath, ACS Symposium Series* (No. 166, p. 327).

Hatada, K., Kitayama, T., Ute, K., Masuda, E., Shinozaki, T., & Yamamoto, M. (1989). Preparation of highly isotactic and syndiotactic poly(methyl methacrylate) macromonomers having the same chemical structure and their polymerization. *Polymer Bulletin*, *21*(2), 165-172.

Hatada, K., Nakanishi, H., Ute, K., & Kitayama, T. (1986). Studies on *p*-and *m*-vinylbenzylmagnesium chlorides as initiators and monomers—preparations of macromers and poly(grignard reagent). *Polymer Journal*, *18*(8), 581-591.

Hatada, K., Ute, K., Tanaka, K., Okamoto, Y., & Kitayama, T. (1986). Living and highly isotactic polymerization of methyl methacrylate by t-C_4H_9MgBr in toluene. *Polymer Journal*, *18*(12), 1037-1047.

Hazer, B., Hirao, A., & Volga, C. (1999). Reactions of anionic living polymers with bromomethyl-functionalized benzoyl peroxides. *Macromolecular Chemistry and Physics*, *200*(1), 71-76.

Henry, A. C., Tutt, T. J., Galloway, M., Davidson, Y. Y., McWhorter, C. S., Soper, S. A., & McCarley, R. L. (2000). Surface modification of poly(methyl methacrylate) used in the fabrication of microanalytical devices. *Analytical Chemistry*, *72*(21), 5331-5337.

Hirao, A., & Matsuo, A. (2003). Synthesis of chain-end-functionalized poly(methyl methacrylate)s with a definite number of benzyl bromide moieties and their application to star-branched polymers. *Macromolecules*, *36*(26), 9742-9751.

Hirao, A., Goseki, R., & Ishizone, T. (2014). Advances in living anionic polymerization: from functional monomers, polymerization systems, to macromolecular architectures. *Macromolecules*, *47*(6), 1883-1905.

Hirao, A., Matsuo, A., & Watanabe, T. (2005). Precise synthesis of dendrimer-like star-branched poly(methyl methacrylate)s up to seventh generation by an iterative divergent approach involving coupling and transformation reactions. *Macromolecules*, *38*(21), 8701-8711.

Hirao, A., Watanabe, T., Ishizu, K., Ree, M., Jin, S., Jin, K. S., Deffieux, A., Schappacher, M., & Carlotti, S. (2009). Precise synthesis and characterization of fourth-generation dendrimer-like star-branched poly(methyl methacrylate)s and block copolymers by iterative methodology based on living anionic polymerization. *Macromolecules*, *42*(3), 682-693.

Ho, C. C., Dai, C. A., & Su, W. F. (2009). High yield synthesis of diverse well-defined end-functionalized polymers by combination of anionic polymerization and "click" chemistry. *Journal of Applied Polymer Science*, *111*(3), 1571-1580.

Hsieh, H., & Quirk, R. P. (1996). *Anionic Polymerization: Principles and Practical Applications*. CRC Press.

Hu, H., & Nair, P. (1996). Electrical and optical properties of poly(methyl methacrylate) sheets coated with chemically deposited CuS thin films. *Surface and Coatings Technology*, *81*(2-3), 183-189.

Hu, W.-H., Huang, K.-W., & Kuo, S.-W. (2012). Heteronucleobase-functionalized benzoxazine: synthesis, thermal properties, and self-assembled structure formed through multiple hydrogen bonding interactions. *Polymer Chemistry*, *3*(6), 1546-1554.

Huang, Y., Kang, H., Li, G., Wang, C., Huang, Y., & Liu, R. (2013). Synthesis and photosensitivity of azobenzene functionalized hydroxypropylcellulose. *RSC Advances*, *3*(36), 15909-15916.

Hutchings, L. R., Narrainen, A. P., Eggleston, S. M., Clarke, N., & Thompson, R. L. (2006). Surface-active fluorocarbon end-functionalized polylactides. *Polymer*, *47*(24), 8116-8122.

Hutchings, L. R., Narrianen, A. P., Thompson, R. L., Clarke, N., & Ansari, I. (2008). Modifying and managing the surface properties of polymers. *Polymer International*, *57*(2), 163-170.

Hutchings, L. R., Sarih, N. M., & Thompson, R. L. (2011). Multi-end functionalised polymer additives synthesised by living anionic polymerisation—the impact of additive molecular structure upon surface properties. *Polymer Chemistry*, *2*(4), 851-861.

Illegal ads an eyesore in Taman Connaught. (2018). *New Straits Times*. https://www.nst.com.my/actionline/2018/03/350238/illegal-ads-eyesore-taman-connaught

Ishizone, T., Yoshimura, K., Hirao, A., & Nakahama, S. (1998). Controlled anionic polymerization of *tert*-butyl acrylate with diphenylmethyl anions in the presence of dialkylzinc. *Macromolecules*, *31*(25), 8706-8712.

Ishizone, T., Yoshimura, K., Yanase, E., & Nakahama, S. (1999). Controlled anionic polymerization of *tert*-butyl acrylate with diphenylmethylpotassium in the presence of triethylborane. *Macromolecules*, *32*(3), 955-957.

Ishizu, K., & Fukutomi, T. (1989). Synthesis of poly(methyl methacrylate) macromonomer. *Journal of Polymer Science Part A: Polymer Chemistry*, *27*(4), 1259-1266.

Järnström, J., Ihalainen, P., Backfolk, K., & Peltonen, J. (2008). Roughness of pigment coatings and its influence on gloss. *Applied Surface Science*, *254*(18), 5741-5749.

Jayasekara, R., Harding, I., Bowater, I., Christie, G., & Lonergan, G. T. (2004). Preparation, surface modification and characterisation of solution cast starch PVA blended films. *Polymer Testing*, *23*(1), 17-27.

Jeong, S. P., Renna, L. A., Boyle, C. J., Kwak, H. S., Harder, E., Damm, W., & Venkataraman, D. (2017). High energy density in azobenzene-based materials for photo-thermal batteries via controlled polymer architecture and polymer-solvent interactions. *Scientific Reports*, *7*(1), 1-12.

Jiang, W., Wang, G., He, Y., Wang, X., An, Y., Song, Y., & Jiang, L. (2005). Photo-switched wettability on an electrostatic self-assembly azobenzene monolayer. *Chemical Communications*, (28), 3550-3552.

Jiang, X., Wang, H., Chen, X., Li, X., Lei, L., Mu, J., Wang, G., & Zhang, S. (2010). A novel photoactive hyperbranched poly (aryl ether ketone) with azobenzene end groups for optical storage applications. *Reactive and Functional Polymers*, *70*(9), 699-705.

Jochum, F. D., Zur Borg, L., Roth, P. J., & Theato, P. (2009). Thermo-and light-responsive polymers containing photoswitchable azobenzene end groups. *Macromolecules*, *42*(20), 7854-7862.

Jog, P. V., & Gin, M. S. (2008). A light-gated synthetic ion channel. *Organic Letters*, *10*(17), 3693-3696.

Kaneta, M., Honda, T., Onda, K., & Han, M. (2017). Repeated photoswitching performance of azobenzenes adsorbed on gold surfaces: a balance between space, intermolecular interactions, and phase separation. *New Journal of Chemistry*, *41*(4), 1827-1833.

Katada, N., Sota, S., Morishita, N., Okumura, K., & Niwa, M. (2015). Relationship between activation energy and pre-exponential factor normalized by the number of Brønsted acid sites in cracking of short chain alkanes on zeolites. *Catalysis Science & Technology*, *5*(3), 1864-1869.

Kerajaan Negeri Selangor. (2015). *167,930 Iklan Haram Diturunkan MBSA*. https://www.selangor.gov.my/index.php/pages/view/1038

Kharandiuk, T., Hussien, E. J., Cameron, J., Petrina, R., Findlay, N. J., Naumov, R., . . . Goodlett, S. (2019). Noncovalent close contacts in fluorinated thiophene–phenylene–thiophene conjugated units: understanding the nature and dominance of O···H versus S···F and O···F interactions with respect to the control of polymer conformation. *Chemistry of Materials*, *31*(17), 7070-7079.

Kim, J.-H., Koo, E., Ju, S.-Y., & Jang, W.-D. (2015). Multimodal stimuli-responsive poly (2-isopropyl-2-oxazoline) with dual molecular logic gate operations. *Macromolecules*, *48*(14), 4951-4956.

Kim, J., Jung, H. Y., & Park, M. J. (2020). End-group chemistry and junction chemistry in polymer science: Past, present, and future. *Macromolecules*, *53*(3), 746-763.

Kimani, S. M., Hardman, S. J., Hutchings, L. R., Clarke, N., & Thompson, R. L. (2012). Synthesis and surface activity of high and low surface energy multi-end functional polybutadiene additives. *Soft Matter*, *8*(12), 3487-3496.

Kimani, S. M., Thompson, R. L., Hutchings, L. R., Clarke, N., Billah, S. R., Sakai, V. G., & Rogers, S. E. (2014). Multihydroxyl end functional polyethylenes: synthesis, bulk and interfacial properties of polymer surfactants. *Macromolecules*, *47*(6), 2062-2071.

Kinloch, A. (1980). The science of adhesion. *Journal of Materials Science*, *15*(9), 2141-2166.

Kitaura, T., & Kitayama, T. (2008). Anionic polymerization of (meth)acrylates with trialkylsilyl-protected lithium *N*-benzylamide. *Polymer Journal*, *40*(1), 37-45.

Kitaura, T., & Kitayama, T. (2013). Anionic polymerization of methyl methacrylate by difunctional lithium amide initiators with trialkylsilyl protection. *Polymer Journal*, *45*(10), 1013-1018.

Kitayama, T., Fujimoto, N., & Hatada, K. (1993, March). Kinetics and stereoregulation in the isotactic-specific and living polymerization of methyl methacrylate. In *Makromolekulare Chemie. Macromolecular Symposia* (Vol. 67, No. 1, pp. 137-146). Basel: Hüthig & Wepf Verlag.

Kitayama, T., Shinozaki, T., Sakamoto, T., Yamamoto, M., & Hatada, K. (1989). Living and highly syndiotactic polymerization of methyl methacrylate and other methacrylates by *tert*-butyllithiumtrialkylaluminium in toluene. *Die Makromolekulare Chemie: Macromolecular Chemistry and Physics*, *15*(S19891), 167-185.

Koberstein, J. T. (2004). Molecular design of functional polymer surfaces. *Journal of Polymer Science Part B: Polymer Physics*, *42*(16), 2942-2956.

Kohsaka, Y., & Kitayama, T. (2015). Precise anionic polymerization of methyl methacrylate: simultaneous control of molecular weight, stereoregularity and end-structure. *International Polymer Science and Technology*, *42*(10), 45-52.

Kohsaka, Y., Kurata, T., & Kitayama, T. (2013). End-functional stereoregular poly(methyl methacrylate) with clickable C=C bonds: facile synthesis and thiol–ene reaction. *Polymer Chemistry*, *4*(19), 5043-5047.

Kohsaka, Y., Kurata, T., Yamamoto, K., Ishihara, S., & Kitayama, T. (2015). Synthesis and post-polymerization reaction of end-clickable stereoregular polymethacrylates *via* termination of stereospecific living anionic polymerization. *Polymer Chemistry*, *6*(7), 1078-1087.

Kohsaka, Y., Yamamoto, K., & Kitayama, T. (2015). Stereoregular poly(methyl methacrylate) with double-clickable ω-end: synthesis and click reaction. *Polymer Chemistry*, *6*(19), 3601-3607.

Königsmann, H., Jüngling, S., & Müller, A. H. (2000). Metal-free anionic polymerization of methyl methacrylate in tetrahydrofuran using bis(triphenylphosphoranilydene)ammonium (PNP$^+$) as counterion. *Macromolecular Rapid Communications*, *21*(11), 758-763.

Kraft, R., Müller, A., Höcker, H., & Schulz, G. (1980). Kinetics of the anionic polymerization of methyl methacrylate in 1,2-dimethoxyethane. *Die Makromolekulare Chemie, Rapid Communications*, *1*(6), 363-368.

Kumar, G. S., & Neckers, D. (1989). Photochemistry of azobenzene-containing polymers. *Chemical Reviews*, *89*(8), 1915-1925.

Kuo, S. W., Huang, C. F., & Chang, F. C. (2001). Study of hydrogen-bonding strength in poly(ϵ-caprolactone) blends by DSC and FTIR. *Journal of Polymer Science Part B: Polymer Physics*, *39*(12), 1348-1359.

Kuo, S.-W., Wu, Y.-C., Wang, C.-F., & Jeong, K.-U. (2009). Preparing low-surface-energy polymer materials by minimizing intermolecular hydrogen-bonding interactions. *The Journal of Physical Chemistry C*, *113*(48), 20666-20673.

Kurusu, R. S., & Demarquette, N. R. (2017). Surface properties evolution in electrospun polymer blends by segregation of hydrophilic or amphiphilic molecules. *European Polymer Journal*, *89*, 129-137.

Kwei, T. (1984). The effect of hydrogen bonding on the glass transition temperatures of polymer mixtures. *Journal of Polymer Science: Polymer Letters Edition*, *22*(6), 307-313.

Landge, S. M., Tkatchouk, E., Benítez, D., Lanfranchi, D. A., Elhabiri, M., Goddard III, W. A., & Aprahamian, I. (2011). Isomerization mechanism in hydrazone-based rotary switches: lateral shift, rotation, or tautomerization? *Journal of the American Chemical Society*, *133*(25), 9812-9823.

Lazzari, M., Kitayama, T., Jancˇo, M., & Hatada, K. (2001). Synthesis of syndiotactic star poly(methyl methacrylate)s with controlled number of arms. *Macromolecules*, *34*(17), 5734-5736.

Lee, J. H., Jung, H. W., Kang, I.-K., & Lee, H. B. (1994). Cell behaviour on polymer surfaces with different functional groups. *Biomaterials*, *15*(9), 705-711.

Lee, L.-H., & Chen, W.-C. (2001). High-refractive-index thin films prepared from trialkoxysilane-capped poly(methyl methacrylate)−titania materials. *Chemistry of Materials*, *13*(3), 1137-1142.

Leonard, C., Halary, J., & Monnerie, L. (1985). Hydrogen bonding in PMMA-fluorinated polymer blends: FTi. r. investigations using ester model molecules. *Polymer*, *26*(10), 1507-1513.

Leyva, E., Medina, C., Moctezuma, E., & Leyva, S. (2004). Chemical oxidation of fluoroanilines to fluoroazobenzenes and fluorophenazines with potassium ferricyanide and potassium hydroxide. *Canadian Journal of Chemistry*, *82*(12), 1712-1715.

Li, R., Wu, G., Hao, Y., Peng, J., & Zhai, M. (2019). Radiation degradation or modification of poly(tetrafluoroethylene) and natural polymers. In *Radiation Technology for Advanced Materials* (pp. 141-182). Elsevier.

Li, Z., Chen, J., Zou, G., Zhang, T., Wei, D., Xu, X., . . . Zheng, A. (2019a). Anionic living polymerization of alkyl methacrylate at ambient temperature and its mechanism research. *Journal of Polymer Science Part A: Polymer Chemistry*, *57*(10), 1130-1139.

Li, Z., Chen, J., Zou, G., Zhang, T., Wei, D., Xu, X., . . . Zheng, A. (2019b). A controlled synthesis method of alkyl methacrylate block copolymers *via* living anionic polymerization at ambient temperature. *RSC Advances*, *9*(28), 16049-16056.

Lim, H. S., Han, J. T., Kwak, D., Jin, M., & Cho, K. (2006). Photoreversibly switchable superhydrophobic surface with erasable and rewritable pattern. *Journal of the American Chemical Society*, *128*(45), 14458-14459.

Ling, J., & Hogen-Esch, T. E. (2007). Alkylation and coupling of living poly(methyl methacrylate) ylides at ambient conditions. *Macromolecules*, *40*(16), 5706-5709.

Liu, J., Ni, P., Qiu, D., Hou, W., & Zhang, Q. (2007). Photochromism of liquid crystalline dendrimer with azobenzene terminal groups in solution. *Reactive and Functional Polymers*, *67*(5), 416-421.

Liu, J., Zhang, Q., Zhang, J., & Hou, W. (2005). Photochemical behaviours of star-like liquid crystal with azobenzene terminal groups. *Journal of Materials Science*, *40*(17), 4517-4521.

Lochmann, L., & Trekoval, J. (1981). The cleavage of β-ketoesters with sodium *tert*-butoxide. Reactivation of a pseudoterminated propagation centre in the anionic polymerization of methacrylates. *Die Makromolekulare Chemie: Macromolecular Chemistry and Physics*, *182*(7), 1951-1959.

Lochmann, L., Doskočilová, D., & Trekoval, J. (1977). Microstructure of poly(methyl methacrylate) prepared by anionic polymerization. Effects of alkali alkoxides. *Collection of Czechoslovak Chemical Communications*, *42*(4), 1355-1360.

Lochmann, L., Pospíšil, J., & Lim, D. (1966). On the interaction of organolithium compounds with sodium and potassium alkoxides. A new method for the synthesis of organosodium and organopotassium compounds. *Tetrahedron Letters*, *7*(2), 257-262.

Lochmann, L., Pospíšil, J., Vodňanský, J., Trekoval, J., & Lim, D. (1965). Interaction of alkyl lithium compounds with lithium alcoholates. *Collection of Czechoslovak Chemical Communications*, *30*(7), 2187-2195.

Lochmann, L., Rodová, M., Petránek, J., & Lím, D. (1974). Reactions of models of the growth center during anionic polymerization of methacrylate esters. *Journal of Polymer Science: Polymer Chemistry Edition*, *12*(10), 2295-2304.

Löhr, G., Müller, A., Warzelhan, V., & Schulz, G. (1974). Estimation of the rate constant of termination by the monomer in the anionic polymerization of methyl methacrylate. *Die Makromolekulare Chemie: Macromolecular Chemistry and Physics*, *175*(2), 497-505.

Long, T. E., Subramanian, R., Ward, T. C., & McGrath, J. E. (1986). Anionic synthesis and characterization of various poly(alkyl methacrylates). *American Chemical Society, Polymer Preprints, Division of Polymer Chemistry*, *27*(2), 258-260.

Ma, M., Hill, R. M., Lowery, J. L., Fridrikh, S. V., & Rutledge, G. C. (2005). Electrospun poly(styrene-*block*-dimethylsiloxane) block copolymer fibers exhibiting superhydrophobicity. *Langmuir*, *21*(12), 5549-5554.

Manah, N., Sulaiman, L., Azman, N., Abidin, Z. H. Z., Tajuddin, H. A., & Halim, N. A. (2019). Colour analysis of organic synthetic dye coating paint films consisting 4-hydroxycoumarin derivatives after exposed to UV-A. *Materials Research Express*, *6*(7), 076418.

Mani, D., & Arunan, E. (2013). The X–C⋯Y (X= O/F, Y= O/S/F/Cl/Br/N/P) 'carbon bond' and hydrophobic interactions. *Physical Chemistry Chemical Physics*, *15*(34), 14377-14383.

Manring, L. E. (1989). Thermal degradation of poly(methyl methacrylate). 2. Vinyl-terminated polymer. *Macromolecules*, *22*(6), 2673-2677.

Manring, L. E. (1991). Thermal degradation of poly(methyl methacrylate). 4. Random side-group scission. *Macromolecules*, *24*(11), 3304-3309.

Manring, L. E., Sogah, D. Y., & Cohen, G. M. (1989). Thermal degradation of poly(methyl methacrylate). 3. Polymer with head-to-head linkages. *Macromolecules*, *22*(12), 4652-4654.

Martínez-Ortega, L., Mira, A., Fernandez-Carvajal, A., Mateo, C. R., Mallavia, R., & Falco, A. (2019). Development of a new delivery system based on drug-loadable electrospun nanofibers for psoriasis treatment. *Pharmaceutics*, *11*(1), 14.

Matsuo, A., Watanabe, T., & Hirao, A. (2004). Synthesis of well-defined dendrimer-like branched polymers and block copolymer by the iterative approach involving coupling reaction of living anionic polymer and functionalization. *Macromolecules*, *37*(17), 6283-6290.

Matsuzaki, K., Nishida, Y., Kumahara, H., Miyabayashi, T., & Yasukawa, T. (1973). Polymerization of methyl methacrylate with alkyllithium in the presence of *N*, *N*, *N'*, *N'*-tetramethylalkylenediamines or ω-dimethylaminoalcohols as catalysts. *Die Makromolekulare Chemie: Macromolecular Chemistry and Physics*, *167*(1), 139-146.

Merino, E. (2011). Synthesis of azobenzenes: the coloured pieces of molecular materials. *Chemical Society Reviews*, *40*(7), 3835-3853.

Metwally, M. A., Bondock, S., El-Desouky, E., & Abdou, M. M. (2012). Synthesis, structure elucidation and application of some new azo disperse dyes derived from

4-hydroxycoumarin for dyeing polyester fabrics. *American Journal of Chemistry*, *2*, 347-354.

Min, M., Bang, G. S., Lee, H., & Yu, B.-C. (2010). A photoswitchable methylene-spaced fluorinated aryl azobenzene monolayer grafted on silicon. *Chemical Communications*, *46*(29), 5232-5234.

Mira, A., Mateo, C. R., Mallavia, R., & Falco, A. (2017). Poly(methyl vinyl ether-*alt*-maleic acid) and ethyl monoester as building polymers for drug-loadable electrospun nanofibers. *Scientific Reports*, *7*(1), 1-13.

Moradi Rufchahi, E. O., & Ghanadzadeh Gilani, A. (2019). Aryl and heteroaryl azo dyes derived from 6,8-dichloro-4-hydroxyquinolin-2(1H)-one: synthesis, characterisation, solvatochromism and spectroscopic properties. *Coloration Technology*, *135*(5), 391-406.

Morishima, Y., Tsuji, M., Kamachi, M., & Hatada, K. (1992). Photochromic isomerization of azobenzene moieties compartmentalized in hydrophobic microdomains in a microphase structure of amphiphilic polyelectrolytes. *Macromolecules*, *25*(17), 4406-4410.

Mossety-Leszczak, B., Wlodarska, M., Galina, H., & Bak, G. (2008). Comparing liquid crystalline properties of two epoxy compounds based on the same azoxy group. *Molecular Crystals and Liquid Crystals*, *490*(1), 52-66.

Nachtigall, O., Kördel, C., Urner, L. H., & Haag, R. (2014). Photoresponsive switches at surfaces based on supramolecular functionalization with azobenzene–oligoglycerol conjugates. *Angewandte Chemie International Edition*, *53*(36), 9669-9673.

Narrainen, A. P., Clarke, N., Eggleston, S. M., Hutchings, L. R., & Thompson, R. L. (2006). Surface adsorption of polar end-functionalised polystyrenes. *Soft Matter*, *2*(11), 981-985.

Narrainen, A. P., Hutchings, L. R., Ansari, I. A., Clarke, N., & Thompson, R. L. (2006). Novel multi end-functionalised polymers. Additives to modify polymer properties at surfaces and interfaces. *Soft Matter*, *2*(2), 126-128.

Narrainen, A. P., Hutchings, L. R., Ansari, I., Thompson, R. L., & Clarke, N. (2007). Multi-end-functionalized polymers: additives to modify polymer properties at surfaces and interfaces. *Macromolecules*, *40*(6), 1969-1980.

Nasir, K., Halim, N., Tajuddin, H., Arof, A., & Abidin, Z. (2013). The effect of PMMA on physical properties of dammar for coating paint application. *Pigment & Resin Technology*, *42*(2), 128-136.

O'connell, C., & Dollimore, D. (1999). Determination of the melting point using derivative thermogravimetry. *Instrumentation Science & Technology*, *27*(1), 13-21.

Oh, S.-K., Nakagawa, M., & Ichimura, K. (2002). Photocontrol of liquid motion on an azobenzene monolayer. *Journal of Materials Chemistry*, *12*(8), 2262-2269.

Paik, M. Y., Krishnan, S., You, F., Li, X., Hexemer, A., Ando, Y., Kang, S. H., Fischer, D. A., Kramer, E. J., & Ober, C. K. (2007). Surface organization, light-driven surface changes, and stability of semifluorinated azobenzene polymers. *Langmuir*, *23*(9), 5110-5119.

Pakula, C., Hanisch, C., Zaporojtchenko, V., Strunskus, T., Bornholdt, C., Zargarani, D., . . . Faupel, F. (2011). Optical switching behavior of azobenzene/PMMA blends with high chromophore concentration. *Journal of Materials Science*, *46*(8), 2488-2494.

Pan, S., Ni, M., Mu, B., Li, Q., Hu, X. Y., Lin, C., Chen, D., & Wang, L. (2015). Well-defined pillararene-based azobenzene liquid crystalline photoresponsive materials and their thin films with photomodulated surfaces. *Advanced Functional Materials*, *25*(23), 3571-3580.

Peptu, C., Harabagiu, V., Simionescu, B. C., Adamus, G., Kowalczuk, M., & Nunzi, J. M. (2009). Disperse red 1 end capped oligoesters. Synthesis by noncatalyzed ring opening oligomerization and structural characterization. *Journal of Polymer Science Part A: Polymer Chemistry*, *47*(2), 534-547.

Park, J., Moon, H. C., & Kim, J. K. (2013). Facile synthesis for well-defined A₂B miktoarm star copolymer of poly(3-hexylthiophene) and poly(methyl methacrylate) by the combination of anionic polymerization and click reaction. *Journal of Polymer Science Part A: Polymer Chemistry*, *51*(10), 2225-2232.

Patel, D. I., & Smalley, R. K. (1984). Thermolysis of aryl azides in phenyl isocyanate. *Journal of the Chemical Society, Perkin Transactions*, *1*, 2587-2590.

Pavlović, G., Racane, L., Čičak, H., & Tralić-Kulenović, V. (2009). The synthesis and structural study of two benzothiazolyl azo dyes: X-ray crystallographic and computational study of azo–hydrazone tautomerism. *Dyes and Pigments*, *83*(3), 354-362.

Pei, X., Fernandes, A., Mathy, B., Laloyaux, X., Nysten, B., Riant, O., & Jonas, A. M. (2011). Correlation between the structure and wettability of photoswitchable hydrophilic azobenzene monolayers on silicon. *Langmuir*, *27*(15), 9403-9412.

Piejko, K. E., & Höcker, H. (1982). Oligomeric side products in the anionic polymerization of methyl methacrylate in toluene. *Die Makromolekulare Chemie, Rapid Communications*, *3*(4), 243-247.

Pietzonka, T., & Seebach, D. (1993). The P4-phosphazene base as part of a new metal-free initiator system for the anionic polymerization of methyl methacrylate. *Angewandte Chemie International Edition in English*, *32*(5), 716-717.

Poutanen, M., Ikkala, O., & Priimagi, A. (2016). Structurally controlled dynamics in azobenzene-based supramolecular self-assemblies in solid state. *Macromolecules*, *49*(11), 4095-4101.

Quirk, R. P., & Zhu, L. F. (1990). Anionic synthesis of dimethylamino-functionalized polystyrenes and poly(methyl methacrylates) using 1-(4-dimethylaminophenyl)-1-phenylethylene. *British Polymer Journal*, *23*(1-2), 47-54.

Rau, H. (1990). Photoisomerization of azobenzenes. *Photochemistry and Photophysics*, *2*, 119-141.

Rezaei Kolahchi, A., Ajji, A., & Carreau, P. J. (2014). Surface morphology and properties of ternary polymer blends: effect of the migration of minor components. *The Journal of Physical Chemistry B*, *118*(23), 6316-6323.

Rezaeifard, A., Jafarpour, M., Rayati, S., & Shariati, R. (2009). The catalytic performance of Mn-tetraarylporphyrins in the highly selective oxidation of primary aromatic amines to azo compounds by Bu4NHSO5. *Dyes and Pigments*, *80*(1), 80-85.

Rodríguez-Hernández, J. (2016). Smart polymer surfaces. In *Industrial Applications for Intelligent Polymers and Coatings* (pp. 105-120). Springer.

Sarih, N. M. (2010). *Synthesis of Well-Defined Multi-End Functionalized Polymers via Living Anionic Polymerization* (Doctoral dissertation, Durham University).

Sasai, Y., Matsuzaki, N., Kondo, S.-i., & Kuzuya, M. (2008). Introduction of carboxyl group onto polystyrene surface using plasma techniques. *Surface and Coatings Technology*, *202*(22-23), 5724-5727.

Schattling, P., Jochum, F. D., & Theato, P. (2014). Multi-stimuli responsive polymers–the all-in-one talents. *Polymer Chemistry*, *5*(1), 25-36.

Schaub, T., Kellogg, G., Mayes, A., Kulasekere, R., Ankner, J., & Kaiser, H. (1996). Surface modification via chain end segregation in polymer blends. *Macromolecules*, *29*(11), 3982-3990.

Schlosser, M. (1967). Zur aktivierung lithiumorganischer reagenzien. *Journal of Organometallic Chemistry*, *8*(1), 9-16.

Schmohl, A., Khan, A., & Hess, P. (2004). Functionalization of oxidized silicon surfaces with methyl groups and their characterization. *Superlattices and Microstructures*, *36*(1-3), 113-121.

Schreiber, V. H. (1960). Über die abbruchsreaktionen bei der anionischen polymerisation von methylmethacrylat. *Die Makromolekulare Chemie: Macromolecular Chemistry and Physics*, *36*(1), 86-88.

Seo, H.-B., Yu, Y.-G., Chae, C.-G., Kim, M.-J., & Lee, J.-S. (2019). Synthesis of ultrahigh molecular weight bottlebrush block copolymers of ω-end-norbornyl polystyrene and polymethacrylate macromonomers. *Polymer*, *177*, 241-249.

Shanmugharaj, A., Yoon, J., Yang, W., & Ryu, S. H. (2013). Synthesis, characterization, and surface wettability properties of amine functionalized graphene oxide films with varying amine chain lengths. *Journal of Colloid and Interface Science*, *401*, 148-154.

Shaw, S. (1993). Epoxy resin adhesives. In *Chemistry and Technology of Epoxy Resins* (pp. 206-255). Springer.

Shawali, A. S., Harb, N. M., & Badahdah, K. O. (1985). A study of tautomerism in diazonium coupling products of 4-hydroxycoumarin. *Journal of Heterocyclic Chemistry*, *22*(5), 1397-1403.

Shi, Y., Yang, J., Zhao, J., Akiyama, H., & Yoshida, M. (2016). Photo-controllable coil-to-globule transition of single polymer molecules. *Polymer*, *97*, 309-313.

Shimomoto, H., Kanaoka, S., & Aoshima, S. (2012). Precise synthesis of end-functionalized thermosensitive poly (vinyl ether) s by living cationic polymerization. *Journal of Polymer Science Part A: Polymer Chemistry*, *50*(19), 4137-4144.

Shu, M.-z., Chen, B., Zou, B., Chen, F.-y., Zheng, A.-n., & Guan, Y. (2015). Transformation of the Counterion of Active Species and Anionic Block Copolymerization of PBMA-b-PMMA. *Acta Polymerica Sinica*, (7), 835-844.

Siewierski, L., Brittain, W., Petrash, S., & Foster, M. (1996). Photoresponsive monolayers containing in-chain azobenzene. *Langmuir*, *12*(24), 5838-5844.

Singh, L., Ludovice, P. J., & Henderson, C. L. (2003, June). Influence of film thickness, molecular weight, and substrate on the physical properties of photoresist polymer thin films. In *Advances in Resist Technology and Processing XX* (Vol. 5039, pp. 1008-1018). International Society for Optics and Photonics.

Song, X., Zhai, J., Wang, Y., & Jiang, L. (2006). Self-assembly of amino-functionalized monolayers on silicon surfaces and preparation of superhydrophobic surfaces based on alkanoic acid dual layers and surface roughening. *Journal of Colloid and Interface Science*, *298*(1), 267-273.

Sortino, S., Petralia, S., & Conoci, S. (2004). Monitoring photoswitching of azobenzene-based self-assembled monolayers on ultrathin platinum films by UV/Vis

spectroscopy in the transmission mode. *Journal of Materials Chemistry*, *14*(5), 811-813.

Southward, R., Lindsay, C., Didier, Y., McGrail, P., & Hourston, D. (1998). Nitroaryl and aminoaryl end-functionalized polymethylmethacrylate via living anionic polymerization: synthesis and stability. In. *ACS Symposium Series* (Vol. 696, pp. 291-303). ACS Publications.

Srinivasa, G., Abiraj, K., & Gowda, D. C. (2003). The synthesis of azo compounds from nitro compounds using lead and triethylammonium formate. *Tetrahedron Letters*, *44*(31), 5835-5837.

Stumpel, J. E., Broer, D. J., & Schenning, A. P. (2014). Stimuli-responsive photonic polymer coatings. *Chemical Communications*, *50*(100), 15839-15848.

Su, X., & Aprahamian, I. (2014). Hydrazone-based switches, metallo-assemblies and sensors. *Chemical Society Reviews*, *43*(6), 1963-1981.

Subramanian, R., Allen, R. D., McGrath, J. E., & Ward, T. C. (1985, January). Tacticity and thermal-analysis of some novel polymethyl-methacrylate (PMMA) homopolymers. In *Abstracts of Papers of the American Chemical Society* (Vol. 190, No. SEP, pp. 62-POY). 1155 16th St, NW, Washington, DC 20036: Amer Chemical Soc.

Sun, S., Liang, S., Xu, W. C., Xu, G., & Wu, S. (2019). Photoresponsive polymers with multi-azobenzene groups. *Polymer Chemistry*, *10*(32), 4389-4401.

Szwarc, M. (1956). 'Living' polymers. *Nature*, *178*(4543), 1168-1169.

Szwarc, M., Levy, M., & Milkovich, R. (1956). Polymerization initiated by electron transfer to monomer. A new method of formation of block polymers[1]. *Journal of the American Chemical Society*, *78*(11), 2656-2657.

Taborelli, M., Eng, L., Descouts, P., Ranieri, J., Bellamkonda, R., & Aebischer, P. (1995). Bovine serum albumin conformation on methyl and amine functionalized surfaces compared by scanning force microscopy. *Journal of Biomedical Materials Research*, *29*(6), 707-714.

Tamada, K., Nagasawa, J., Nakanishi, F., Abe, K., Ishida, T., Hara, M., & Knoll, W. (1998). Structure and growth of hexyl azobenzene thiol SAMs on Au(111). *Langmuir*, *14*(12), 3264-3271.

Tang, X., Liang, X., Gao, L., Fan, X., & Zhou, Q. (2010). Water-soluble triply-responsive homopolymers of N, N-dimethylaminoethyl methacrylate with a terminal azobenzene moiety. *Journal of Polymer Science Part A: Polymer Chemistry*, *48*(12), 2564-2570.

Theato, P. (2011). One is enough: Influencing polymer properties with a single chromophoric unit. *Angewandte Chemie International Edition*, *50*(26), 5804-5806.

Thompson, R. L., Hardman, S. J., Hutchings, L. R., Pillay Narrainen, A., & Dalgliesh, R. M. (2009). pH-Controlled polymer surface segregation. *Langmuir*, *25*(5), 3184-3188.

Thompson, R. L., Narrainen, A. P., Eggleston, S. M., Ansari, I. A., Hutchings, L. R., & Clarke, N. (2007). Recoverable surface modification using dendritically fluorocarbon-functionalized poly(methyl methacrylate). *Journal of Applied Polymer Science*, *105*(2), 623-628.

Tong, Z., Zhou, J., Huang, R., Zhou, J., Zhang, R., Zhuo, W., & Jiang, G. (2017). Dual-responsive supramolecular self-assembly of inclusion complex of an azobenzene-ended poly (ε-caprolactone) with a water-soluble pillar [6] arene and its application in controlled drug release. *Journal of Polymer Science Part A: Polymer Chemistry*, *55*(15), 2477-2482.

Toworfe, G., Composto, R., Shapiro, I., & Ducheyne, P. (2006). Nucleation and growth of calcium phosphate on amine-, carboxyl- and hydroxyl-silane self-assembled monolayers. *Biomaterials*, *27*(4), 631-642.

Trezza, T., & Krochta, J. (2001). Specular reflection, gloss, roughness and surface heterogeneity of biopolymer coatings. *Journal of Applied Polymer Science*, *79*(12), 2221-2229.

Usuki, N., Satoh, K., & Kamigaito, M. (2017a). Synthesis of isotactic-*block*-syndiotactic poly(methyl methacrylate) via stereospecific living anionic polymerizations in combination with metal-halogen exchange, halogenation, and click reactions. *Polymers*, *9*(12), 723.

Usuki, N., Satoh, K., & Kamigaito, M. (2017b). Synthesis of syndiotactic macrocyclic poly(methyl methacrylate) via transformation of the growing terminal in stereospecific anionic polymerization. *Macromolecular Chemistry and Physics*, *218*(12), 1700041.

Varshney, S. K., Hautekeer, J., Fayt, R., Jérôme, R., & Teyssié, P. (1990). Anionic polymerization of (meth)acrylic monomers. 4. Effect of lithium salts as ligands on the "living" polymerization of methyl methacrylate using monofunctional initiators. *Macromolecules*, *23*(10), 2618-2622.

Varshney, S. K., Jacobs, C., Hautekeer, J. P., Bayard, P., Jerome, R., Fayt, R., & Teyssie, P. (1991). Anionic polymerization of acrylic monomers. 6. Synthesis, characterization, and modification of poly(methyl methacrylate)-poly(*tert*-butyl acrylate) di-and triblock copolymers. *Macromolecules*, *24*(18), 4997-5000.

Varshney, S. K., Jerome, R., Bayard, P., Jacobs, C., Fayt, R., & Teyssie, P. (1992). Anionic polymerization of (meth)acrylic monomers. 7. Macrocyclic crown ethers as promoters of the living polymerization of methyl methacrylate using monofunctional initiators. *Macromolecules*, *25*(18), 4457-4463.

Viguier, M., Collet, A., & Schué, F. (1982). Homogeneous polymerization of methyl methacrylate initiated by potassium salts of methanol and *t*-butyl alcohol in the presence of cryptand [222]. *Polymer Journal*, *14*(2), 137-141.

Viguier, M., Collet, A., Schue, F., & Mula, B. (1987). Recent advances in anionic polymerization. *Elsevier*, *New York*, *NY*, 249.

Wang, C.-G., Koyama, Y., Uchida, S., & Takata, T. (2014). Synthesis of highly reactive polymer nitrile *N*-oxides for effective solvent-free grafting. *ACS Macro Letters*, *3*(3), 286-290.

Wang, J.-S., Jerome, R., Bayard, P., Baylac, L., Patin, M., & Teyssie, P. (1994). Anionic Polymerization of Acrylic Monomers. 15. Living anionic copolymerization of mixtures of methyl methacrylate and *tert*-butyl acrylate as promoted by dibenzo-18-crown-6. *Macromolecules*, *27*(16), 4615-4620.

Wang, T. L., Hwang, W. S., & Yeh, M. H. (2007). Preparation, properties, and anticorrosion application of poly(methyl methacrylate)/montmorillonite nanocomposites coating on brass via solution polymerization. *Journal of Applied Polymer Science*, *104*(6), 4135-4143.

Wang, X., Yang, Y., Gao, P., Yang, F., Shen, H., Guo, H., & Wu, D. (2015). Synthesis, self-assembly, and photoresponsive behavior of tadpole-shaped azobenzene polymers. *ACS Macro Letters*, *4*(12), 1321-1326.

Wang, Z., Han, E., & Ke, W. (2006). Effect of acrylic polymer and nanocomposite with nano-SiO_2 on thermal degradation and fire resistance of APP–DPER–MEL coating. *Polymer Degradation and Stability*, *91*(9), 1937-1947.

Warner, W., Dimov, D., Hogen-Esch, T., Juengling, S., & Warzelhan, V. (1999). Phosphor ylide-mediated polymerization of methyl methacrylate at elevated temperatures. *Polymer Preprints (USA)*, *40*(1), 74-75.

Warzelhan, V., Höcker, H., & Schulz, G. (1978). Kinetic studies of the anionic polymerization of methyl methacrylate in tetrahydrofuran with Na^+ as counter ion, using monofunctional initiators. *Die Makromolekulare Chemie: Macromolecular Chemistry and Physics*, *179*(9), 2221-2240.

Watanabe, T., Tsunoda, Y., Matsuo, A., Sugiyama, K., & Hirao, A. (2006, July). Synthesis of dendrimer-like star-branched poly(methyl methacrylate)s of generations consisting of four branched polymer chains at each junction by iterative methodology involving coupling and transformation reactions.

In *Macromolecular Symposia* (Vol. 240, No. 1, pp. 23-30). Weinheim: WILEY-VCH Verlag.

Wen, Y., Yi, W., Meng, L., Feng, M., Jiang, G., Yuan, W., Zhang, Y., Gao, H., Jiang, L., & Song, Y. (2005). Photochemical-controlled switching based on azobenzene monolayer modified silicon (111) surface. *The Journal of Physical Chemistry B*, *109*(30), 14465-14468.

Wenzel, R. N. (1936). Resistance of solid surfaces to wetting by water. *Industrial & Engineering Chemistry*, *28*(8), 988-994.

Wiles, D., & Bywater, S. (1962). The butyllithium-initiated polymerization of methyl methacrylate. *Polymer*, *3*, 175-185.

Wiles, D., & Bywater, S. (1964). The butyllithium-Initiated polymerization of methyl methacrylate. III. Effect of lithium alkoxides[1]. *The Journal of Physical Chemistry*, *68*(7), 1983-1987.

Xia, F., Zhu, Y., Feng, L., & Jiang, L. (2009). Smart responsive surfaces switching reversibly between super-hydrophobicity and super-hydrophilicity. *Soft Matter*, *5*(2), 275-281.

Xie, T., Kao, W., Sun, L., Wang, J., Dai, G., & Li, Z. (2020). Preparation and characterization of self-matting waterborne polymer–an overview. *Progress in Organic Coatings*, *142*, 105569.

Xue, X., Yang, J., Huang, W., Yang, H., & Jiang, B. (2015). Synthesis of hyperbranched poly (ε-caprolactone) containing terminal azobenzene structure via combined ring-opening polymerization and "click" chemistry. *Polymers*, *7*(7), 1248-1268.

Xue, X., Zhu, J., Zhang, Z., Cheng, Z., Tu, Y., & Zhu, X. (2010). Synthesis and characterization of azobenzene-functionalized poly (styrene)-b-poly (vinyl acetate) via the combination of RAFT and "click" chemistry. *Polymer*, *51*(14), 3083-3090.

Ya, Q., Dong, X.-Z., Chen, W.-Q., & Duan, X.-M. (2008). The synthesis of aminoazobenzenes and the effect of intermolecular hydrogen bonding on their photoisomerization. *Dyes and Pigments*, *79*(2), 159-165.

Yager, K. G., & Barrett, C. J. (2006). Novel photo-switching using azobenzene functional materials. *Journal of Photochemistry and Photobiology A: Chemistry*, *182*(3), 250-261.

Yang, C.-F., Wang, H.-C., & Su, C.-C. (2017). Enhancing the compatibility of poly(1, 4-butylene adipate) and phenoxy resin in blends. *Materials*, *10*(7), 692.

Yang, H., He, Y., Wu, Z., Miao, J., Yang, F., & Lu, Z. (2018). Fabrication of a superhydrophobic and high-glossy copper coating on aluminum substrates. *Applied Surface Science*, *433*, 1192-1196.

Yazdanbakhsh, M., Ghanadzadeh, A., & Moradi, E. (2007). Synthesis of some new azo dyes derived from 4-hydroxy coumarin and spectrometric determination of their acidic dissociation constants. *Journal of Molecular Liquids*, *136*(1-2), 165-168.

Yoo, H.-S., Watanabe, T., & Hirao, A. (2009). Precise synthesis of dendrimer-like star-branched polystyrenes and block copolymers composed of polystyrene and poly(methyl methacrylate) segments by an iterative methodology using living anionic polymerization. *Macromolecules*, *42*(13), 4558-4570.

Yordanov, D., Deneva, V., Georgiev, A., Vassilev, N., Vala, M., Zhivkov, I., & Antonov, L. (2020). 4-OH coumarin based rotary switches: Tautomeric state and effect of the stator. *Dyes and Pigments*, *184*, 108861.

Young, T. (1805). III. An essay on the cohesion of fluids. *Philosophical Transactions of the Royal Society of London*, *95*, 65-87.

Yuan, C., Ouyang, M., & Koberstein, J. T. (1999). Effects of low-energy end groups on the dewetting dynamics of poly(styrene) films on poly(methyl methacrylate) substrates. *Macromolecules*, *32*(7), 2329-2333.

Zagala, A. P., & Hogen-Esch, T. E. (1996). Living anionic polymerization of methyl methacrylate at ambient temperatures in the presence of the tetraphenylphosphonium cation. *Macromolecules*, *29*(8), 3038-3039.

Zha, R. H., Vantomme, G., Berrocal, J. A., Gosens, R., de Waal, B., Meskers, S., & Meijer, E. (2018). Photoswitchable nanomaterials based on hierarchically organized siloxane oligomers. *Advanced Functional Materials*, *28*(1), 1703952.

Zhang, C. Z., Zhu, J., Lu, C., Lu, G.-Y., & Cui, Y. (2009). Relationship between optical nonlinearities of H-shaped chromophores and electronegativities of their substituent groups. *Materials Chemistry and Physics*, *114*(2-3), 515-517.

Zhang, C., & Jiao, N. (2010). Copper-catalyzed aerobic oxidative dehydrogenative coupling of anilines leading to aromatic azo compounds using dioxygen as an oxidant. *Angewandte Chemie*, *122*(35), 6310-6313.

Zhang, T., Zheng, A., Zou, G., Wei, D., Xu, X., & Guan, Y. (2019). Initiating Mechanism of the Anionic Polymerization of Methacrylates with *t*-BuOK and the Synthesis of ABA Type Triblock Copolymers. *Macromolecular Chemistry and Physics*, *220*(24), 1900390.

Zhang, X., Wen, Y., Li, Y., Li, G., Du, S., Guo, H., Yang, L., Jiang, L., Gao, H., & Song, Y. (2008). Molecularly controlled modulation of conductance on azobenzene

monolayer-modified silicon surfaces. *The Journal of Physical Chemistry C*, *112*(22), 8288-8293.

Zhao, G.-J., & Han, K.-L. (2012). Hydrogen bonding in the electronic excited state. *Accounts of Chemical Research*, *45*(3), 404-413.

Zheng, A., Su, L., Li, Z., Zou, G., Xu, X., & Guan, Y. (2017). Synthesis of poly(*n*-hexyl methacrylate)-*b*-poly(methyl methacrylate) *via* anionic polymerization with *t*-BuOK as the initiator at ambient temperature. *RSC Advances*, *7*(85), 53996-54001.

Zheng, L.-Q., Yang, S., Lan, J., Gyr, L., Goubert, G., Qian, H., . . . Zenobi, R. (2019). Solution phase and surface photoisomerization of a hydrazone switch with a long thermal half-life. *Journal of the American Chemical Society*, *141*(44), 17637-17645.

Zou, G., Zheng, A., Wei, D., Li, Z., Su, L., Zhang, T., Xu, X., & Guan, Y. (2018). Synthesis of block copolymers of 2-ethylhexyl methacrylate, *n*-hexyl methacrylate and methyl methacrylate *via* anionic polymerization at ambient temperature. *Chinese Journal of Chemistry*, *36*(10), 934-938.

Zundel, T., Teyssié, P., & Jérôme, R. (1998a). New ligands for the living high-molecular-weight anionic (co)polymerization of acrylates in toluene at 0 °C.[1,2] 3. Ligation of *sec*-butyllithium by lithium silanolates. *Macromolecules*, *31*(17), 5577-5581.

Zundel, T., Teyssié, P., & Jérôme, R. (1998b). New ligands for the living isotactic anionic polymerization of methyl methacrylate in toluene at 0 °C. 1. Ligation of butyllithium by lithium silanolates. *Macromolecules*, *31*(8), 2433-2439.

Zvonkina, I. J. (2016). Adhesion of polymer coatings: principles and evaluation. In *Industrial Applications for Intelligent Polymers and Coatings* (pp. 605-617). Springer.